The University of Hull

Advanced biomedical applications of cell clusteroids based on aqueous two-phase Pickering emulsion systems

Being a Thesis submitted for the Degree of Doctor of Philosophy
in the University of Hull
by

Anheng Wang
BSc(Shenyang Normal University,China, 2015)

Sep 2022

Acknowledgements

I want to thank my academic supervisor, Professor Vesselin Paunov. I really appreciate his careful and professional supervision, which allowed me to gain an in-depth understanding of an area that I was not familiar with. It has been a real pleasure having you as my primary supervisor. I would also show my great respect to my second supervisor, Dr Leigh Madden, who provided careful and thorough support during my whole PhD study. I would also like to thank Dr Tommy Horozov for their advice and feedback during my PhD. I am grateful to SEM technician Tim Dunstan for his assistance with SEM/TEM sample preparation, cryostat training and flow cytometry training. I would also like to thank Paunov group members for their advices and selfless help, especially Dr Paul Weldrick and Dr Bongkot Ngamsom. Finally, I would like to thank my girlfriend and my mom for their long-lasting company during these three years. Without their help, I would definitely not finish my PhD happily and successfully.

Publications, Posters and Presentations

The work contained within this thesis has given rise to the following publications, posters and presentations and qualifications.

The publisher's The Royal Society of Chemistry (RSC), American Chemical Society (ACS) and Multidisciplinary Digital Publishing Institute (MDPI) in which the research in this thesis has been published, allow the full reproduction of articles in a thesis provided the correct acknowledgement is given with the reproduced material. The acknowledgement to these publishers is given at the appropriate chapters in this thesis.

Publications:

1) Wang A, Madden L A, Paunov V N. Advanced biomedical applications based on emerging 3D cell culturing platforms. Journal of Materials Chemistry B, 2020, 8(46): 10487-10501.**Chapter 1**

2) Wang A, Madden L A, Paunov V N. High-throughput fabrication of h epatic cell clusteroids with enhanced growth and functionality for tissue engineering applications[J]. Materials Advances, 2020, 1(8): 3022-3032.**Chapter 2**

3) Wang A, Madden L A, Paunov V N. Fabrication of Angiogenic Sprouting Coculture of Cell Clusteroids Using an Aqueous Two-Phase Pickering Emulsion System 2022 5 (4), 1804-1816 **Chapter 3**

4) Wang A, Madden L A, Paunov V N. Vascularized Co-culture Clusteroids of Primary Endothelial and HepG2 Cells Based on Aqueous Two-Phase Pickering Emulsions. Bioengineering 2022, 9(3), 126 **Chapter 4**

5) Wang A, Weldrick P J, Madden L A, et al. Biofilm-Infected Human Clusteroid Three-Dimensional Coculture Platform to Replace Animal Models in Testing Antimicrobial Nanotechnologies. ACS Applied Materials & Interfaces, 2021, 13(19): 22182-22194.2) **Chapter 5**

6) Wang A, Weldrick P J, Madden L A, et al. Enhanced clearing of Candida biofilms on 3D Urothelial cell *in-vitro* model by lysozyme-functionalized Fluconazole-loaded shellacnanoparticles. Biomaterials science, Biomater. Sci., 2021,9, 6927-6939 **Chapter 6**

7) Weldrick P J, Wang A, Paunov V N,et al.

Emerging Nanotechnologies for Targeting Antimicrobial Resistance.,
Nanoscale, 14(11), 4018-4041.

Presentations

1) 1st Eurasian International Workshop on Antimicrobial and Biosensing Nanotechnologies 14th & 15th May 2021 Keynote speaker

Topic：Biofilm-Infected Human Clusteroid Three-Dimensional Coculture Platform to Replace Animal Models in Testing Antimicrobial Nanotechnologies

Abstract:

The development of *in vitro* models for advancing the research of cell biology and cell physiology is of great importance to the fields of biotechnology, cancer study, drug testing, toxicity study. The emerging field includes tissue engineering and regenerative medicine will benefit from the models in a great way. Traditional mammalian two-dimensional (2D) methods cells culture encountered its limitations, and it is recently agreed that the three-dimensional (3D) cell culture features the *in vivo* environment more similarly owing to the increased cell-cell interactions and complex architecture like natural organ and tissue. In Chapter 1, we review the methods of generating 3D multicellular cell models on their merits and disadvantages. The assays that were mostly utilized to characterize the function of spheroids were also discussed. The application of 3D cell models has advanced the basic cell sciences, especially in understanding tumour biology, cancer drug discovery and cancer metastasis. Another potential down-stream application of the 3D cell models is that they could be utilized as basic building blocks for tissue constructs. In brief, emerging technologies aiming to generate and assess spheroids are pushing their application and wider their utilizations in drug testing and tissue engineering.

Chapter 2 describes the design and optimization of methods for encapsulating and generating the clusteroids of Hep-G2. The discontinuous and separated phases were selected from bio-compatible PEO and DEX, and the stabilizer was made from food-grade whey protein particles. It was due in part to the spontaneous partitioning of the cells to the DEX phase within the DEX droplets that the cells were easily captured. The experiment showed that a number of different parameters could be adjusted in order to ensure that the cell clusteroids were adequately encapsulated and generated by varying the ratio of DEX:PEO. With our method, we were able to show that a very large number of individual cell clusteroids could be produced. In addition, we utilized FDA assays to assess the viability of the clusteroids collected after the preparation procedures in order to demonstrate that they remain highly viable after the treatment. In Chapter 3, we demonstrated how to apply our ATPS based 3D cell culture method to the co-culture level. As a result, these two types of cells were able to coexist in a single droplet and be compacted into clusteroids during coculture. Hep-G2/ECV 304 cells collected in co-culture were both carcinoma cells, which would require the presence of blood vessels as the clusteroids grew larger. A simple change in the initial

cell ratio added to the DEX phase proved that the cell ratios of two types of cells within co-cultured clusteroids were variable. We found that using carcinoma cell lines in vitro to produce vascularized co-culture clusteroids could be a facile procedure. Chapter 4 examined the feasibility of co-culturing human liver cells with primary endothelial lines that are capable of angiogenesis by using w/w Pickering emulsion. A primary endothelial cell line could provide a better simulation of angiogenesis because it emulates the in vivo environment. The primary cells showed no repulsion to the carcinoma cell linesAngiogenesis proteins were less abundant in HUVECs than in ECVs (Chapter 3). As a VEGF pump, Hep-G2 cells were used in the co-culture model to stimulate the angiogenesis of HUVEC cells by releasing VEGF. This model could be an ideal for investigating drug toxicology and other applications related to tissue engineering.

Chapter 5 aimed to find a suitable application for the massive amount of the clusteroids collected from w/w Pickering emulsion. We generated a dense layer of 3D keratinocytes clusteroids to simulate skin *in vitro*. The *S. aureus* and *P. aeruginosa* could form biofilm on the clusteroids layer without breaking the structure of the 3D cell interactions. We further designed a nanotherapeutics based on antibiotic encapsulated Carbopol NPs, surface functionalised with a protease- alcalase. In comparison with non-coated ciprofloxacin and alcalase, this nanocarrier demonstrated a significant increase in antibacterial activity. In the clusteroids model, such nanoparticles did not pose a significant threat, and the clusteroids could continue to proliferate despite the presence of such nanoparticles. Moreover, this work showed that 3D cell clusteroids could have the potential to be used in further biomedical applications in the future.

Chapter 6 aim to broaden the application of the clusteroids layer to simulate the urinary track infection, which is commonly seen and tricky to solve in nosocomial infection. The aim of chapter 6 was to develop a 3D urothelial cell clusteroids model that mimicked the inner cell wall of the bladder infected with *C.albicans* biofilm. Using Fluconazole-loaded shellac nanotherapeutics in conjunction with a cationic enzyme Lysozyme to functionalize the Fluconazole nanocarriers, we made it possible to remove fungal biofilms from 3D urothelial *c*lusteroids.An extensive array of fungal biofilm infections, or bacterial infections, could be mimicked using a protocol such as this by changing the species of cellular type and pathogen type of the organism.

Content

Glossary

μm	Micrometre
μM	Micromolar
μL	Microlitre
μg	Microgram
λ	Wavelength
wt%	Weight percentage
w/v%	Weight per volume percentage
nm	Nanometre
min	Minute
h	Hour
g	Acceleration due to gravity
°C	Centigrade degree

List of abbreviations

2D	Two dimensional
3D	Three dimensional
ABX	Ciprofloxacin
ATPS	Aqueous two phases system
C. albicans	Candida albicans
CF	Cystic fibrosis
CFSE	Carboxyfluorescein succinimidyl ester
CFU	Colony forming Unit
CLSM	Confocal laser scanning microscopy
CMFDA	5-chloromethylfluorescein diacetate
DAPI	4′,6-Diamidino-2-phenylindole Dihydrochloride
DEX	Dextran
DMEM	Dulbecco's Modified Eagle Medium
DPPIV	Dipeptidyl Peptidase IV
ECM	Extracellular microenvironment

ECs	Endothelial cells (
ECV 304	Human urinary bladder carcinoma
EMEM	Eagle's minimal essential medium
EPS	Extracellular polymeric substance
FBS	Fetal bovine serum
FDA	Fluorescein diacetate
FITC	Fluorescein isothiocyanate
HaCaT	Human epidermal keratinocyte line
Hep-G2	Hepatoma G2
HIF	Hypoxia-inducible factor
HUVEC	Human Umbilical Vein Endothelial Cells
IGFBP	Insulin-like growth factor-binding protein
MCS	Multicellular spheroids
MHA	Mueller Hinton Agar
MHB	Mueller Hinton broth
MMP	Metalloproteinases
MTT	3-(4,5-dimethylthiazol-2-yl)-2,5-Diphenyltetrazolium bromide
NPs	Nanoparticles
P. aeruginosa	*Pseudomonas aeruginosa*
PBS	Phosphate-buffered saline
PEO	Poly(ethylene oxide)
RPM	Revolutions per minute
S. aureus	*Staphylococcus aureus*
SD	Standard Deviation
SEM	Scanning electron microscopy
TCB	The binodal curve
TEM	Transmission electron microscope
TIMP	Metallopeptidase inhibitor
TLL	Tie-line length
tPA	Tissue plasminogen activator

uPA	Urokinase
VEGF	Vascular endothelial growth factor
WP	Whey protein

1. Chapter1

1.1 Literature review

Microneedle-based, non-scaffold-based "Kenzan" bioprinters, which do not require scaffolds, have provided a scaffold-free, laboratory-friendly bioprinter with high throughput. This approach would allow the fusion of spheroids into cellular aggregates without the need for scaffolds, as well as the direct synthesis of the extracellular matrix. Spheroids can be manipulated with great robustness via this breakthrough in bioprinting techniques. Bio-engineering of tissues and organs has been made possible by this novel technology. In addition, manufacturing spheroids requires higher standards due to higher requirements, especially with regard to yield. The use of spheroids provides researchers with the ability to achieve a larger yield with a controlled size and composition of the cell clusters. Several techniques for the production of spheroid cultures are not discussed herein. Others have also provided impressive comprehensive reviews. To broaden the scope of the applicability of spheroids in biomedical research, we concentrate on the development of multicellular spheroids without scaffolds, particularly ATPS(aqueous two phases system)-based techniques that have been developed recently, as well as the applications of high-throughput spheroids.

1.2 The 3D cell model

After the first conception of a 3D(three-dimensional) cell model was introduced, spheroid models have attracted numerous researchers worldwide, focusing on clinical and biomedical problems. The utilization of the spheroids ranges from pharmacology to disease pathophysiology, and could be the ultimate answer for tissue regeneration.[1,2] Compared to classic two-dimensional(2D) cell culture, 3D cell cultures could better replicate the extracellular microenvironment(ECM) and the *in vivo* related growth factors and signalling cascades.[3,4] As the understanding about the fabrication and maintenance of 3D cell models have been more-in-depth, the experiments in translational medicine has been a plethora in studying the possibility implanting the spheroids into animals *in vivo* to investigate tissue regeneration.[5] Cell spheroids, also known as multicellular spheroids (MCS), are the simplest *in vitro* model of solid tumours. The generation of MCS are due to the inherent property of a wide range of cells, especially cancer cells. The non-adherent surface of hydrogel (3D matrix) would facilitate the self-assembly of the compact spheroid. Spheroids of

different sizes ranging from a few tens of micrometres to a millimetre scale can conveniently be generated.[6]

Spheroids exhibit 3D morphology similar to avascular tumours, with closer cell-cell adhesions, non-uniform concentrations of soluble factors, hypoxic, dormant, slow-cycling, and acidic environments in the extracellular space and low oxygen tension in the core.[1] In addition, the use of spheroids gives researchers a good opportunity to study the interaction of cancerous cells with tumour stroma and intra-cellular signals related to the tumour proliferation, angiogenesis, invasion, and resistance to drugs with regards to tumour stroma, as well as physical interactions between cancer cells and tumour stroma.[7,8] Since spheroids are inherently suitable to a wide range of tumour biology researches, even though they are a relatively simple model.

For cancer biology applications, spheroids are being increasingly used as surrogate tumour models because of their advantageous features. There has been a more than a decade of incubation in this field, and numerous proof-of-concept studies have been conducted, yet it is still in its infancy. Bioprinters are currently stagnating as a result of the technology's early success: the first ones, and the majority, were 3D printers that were modified for layer-by-layer dispersing biomaterials. Its energy-intensive nature and scaffold dependence make it difficult to use for biological applications (inkjet, micro-extrusion, or laser-assisted). A gentler, scaffold-free bio-assembling method may be more appropriate for the future of bioprinting. Further, in the simple drug testing arena, spheroids cannot be produced with scaffold-based techniques due to their inherently low yield. Recently, it was discovered that spheroids could be used as building blocks for tissue formation, however, at low yields, a lack of bricks makes it hard to build a “wall”.

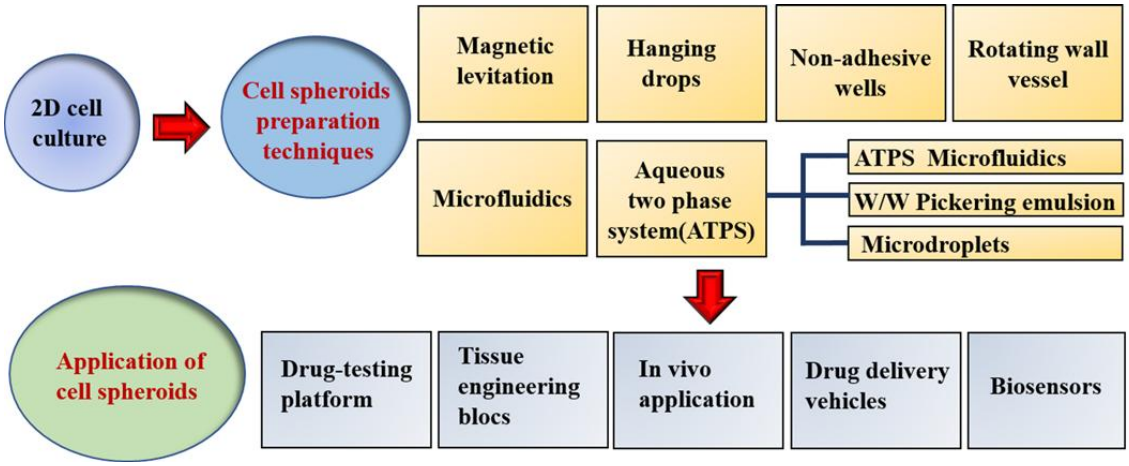

Scheme 1.1 Preparation techniques and various applications of cell spheroids.

1.3 Purpose of the work

The advent of a microneedles-based spheroid assembly (also known as the Kenzan spheroid assembly) and subsequent launch in Japan of a bioprinter that is based on this method has been a breakthrough in making it possible to directly and precisely print spheroids.[9] Through this method, spheroids can be fused into cellular aggregates and extracellular matrix is synthesized, improving both structural stability and robustness. Tissues and organs can be bioengineered with this new technology. While higher demands are placed on spheroids for better performance, especially in terms of yield, this has raised the requirements for manufacturing methods of spheroids as well. In recent years, researchers have developed various scaffold-free techniques that may be used to achieve high yields of spheroids with controlled sizing and chemical-physical characteristics. One of these methods, using gravity-enforced self-assembly, involves growing spheroids using hanging drops. [13] A tissue culture plate's inside lid is pipetted with small amounts of cell suspension (20 - 30μL) to create spheroids. Because of surface tension, drops remain stuck to the lid when the lid is inverted. A single spheroid is formed as a result of gravity settling and concentrating the cells at the bottom of the drop.[6, 14] In addition to primary cells, carcinoma cell lines have also been used to form spheroids using this method.[8, 15, 16] The formation of heterotypic spheroids can be achieved by co-culturing or even tri-culturing different cell types. As a result of adjusting the density of cells within each droplet of the spheroid, the size and composition of the spheroid can be controlled. A

single array of hanging drops can produce up to 384 spheroids per second, enabling high throughput production of spheroids.[13] A large quantity of uniform spheroids can, however, be produced in one go using this method.

Table 1.1 Current methods for the preparation of cell spheroids.

Method	Advantages	Disadvantages	References
Hanging drop	Fast spheroid formation Co-culture, Easy to monitor	Labour intensive, Low yield Special equipment needed	6，8，13-16
Non-adhesive wells	Inexpensive, Easy to handle	Variation in size/shape, Low yield	10，17-22
Rotating wall vessel	Mass production Long term culture, Co-culture	Special equipment needed Variation in size/shape, High shear force	23-26
Micro-fluidics	High yield, Good size control Easy to monitor	Special equipment needed Labour intensive	9，27-30
Magnetic levitation	Formation of complex Shapes Good size control, Co-culture	Low yield Special equipment needed	31-34
Aqueous two-phase System (ATPS)	Ultra-high yield Co-culture	High shear force	48-63

1.4 The hanging drop method

Gravity promotes self-assembly in spheroids produced by the hanging drop method.[13] Cell suspensions are pipetted into tissue culture plates in small volumes (20 - 30 µL) to make spheroids. Because of surface tension, the drops remain attached to the lid even when the lid is inverted. During the centrifugal force of gravity, the cells settle to the bottom of the drop and concentrate at its core, which creates one spheroid.[6, 14] It has also been possible to form spheroids using carcinoma cell lines as well as primary cells.[8, 15, 16] The creation of heterotypic spheroids can be accomplished by co-culturing different cell types, or even by tri-culturing cells. In each droplet, the density of the cells determines the size and composition of the spheroid. It has been established that hanging drop method can create spheroids in a high throughput manner, producing up to 384 spheroids in a single array of spheroids using this method.[13] However, a large quantity of uniform spheroids can be difficult to produce with this method.

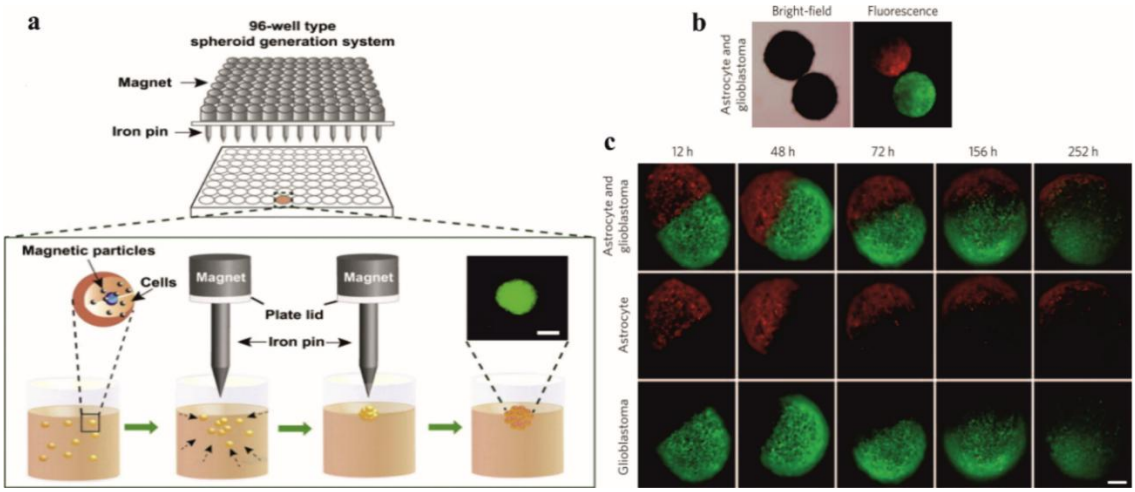

Figure 1. 1 (a) A schematic showing the spheroid generation platform using magnetic nanoparticles and iron pins.[35] Reprinted with permission from Ref. 35; Copyright 2013 Elsevier. Magnetic (b); bright-field and fluorescence images of human glioblastoma cells (green; GFP-expressing cells) and normal human astrocytes (red; mCherry-labelled) cultured separately and then magnetically guided together; (c) Confrontation between human glioblastoma cells and normal astrocytes monitored for different times.[31] Reprinted with permission from Ref. 31; Copyright 2015 Springer Nature. The scale bar is 200 µm.

1.5 Non-adhesive wells

It is known that certain specialist 96-well tissue culture plates and regular bacteriological-type Petri dishes made of non-adhesive plastic are suitable for generating MCS because of their non-adhesive properties.[17-21] This protocol has been widely used in a different type of spheroid culture. Alternatively, culture ware can be made non- adhesive for cells by coating with agarose thin films,[17] hydrophobic polymers, including poly(2-hydroxyethyl methacrylate) (PHEMA),[22] or poly-N-p-vinylbenzyl-D-lactonamide.[10] The culture parameters for optimal cell aggregation as well as uniform size and shape of spheroid are influenced by factors such as cell type, seeding density, medium composition, and the presence of static or stirring culture conditions.[10] As a result of the coating film's inaccuracy, the spheroids produced by this method usually have a broad size distribution. Consequently, the spheroids characteristics can be difficult to control, which may lead to an unpredictable result.

1.6 Rotating wall vessel

In a rotating wall vessel, cells are kept suspended and can aggregate into spheroids in the presence of microgravity.[23] In this protocol, cells in a suspension are rotated gradually around an x-axis in an artificial rotating wall vessel, which ensures that the cells fall freely at all times. Initially, rotation is very slow (~15 RPMs), but as spheroids begin to form and the mass of the aggregates increase, rotation is increased to keep the aggregates in suspension (~25 RPMs).[24-26] This method has been used to form spheroids from primary cells and many cell lines. Different cell types can be co-cultured to form heterotypic spheroids.[23-26] Perfusion, which impacts differentiation, is useful for controlling longer-term culture conditions. A low-shear environment is used for the production of aggregates. As a result of the rotation of the spheroid during culture, it is quite difficult to monitor the spheroid while it is in culture, and as a result, there is a low yield and variable size to be found.

1.7 Micro-fluidics based methods

Microfluidics uses microchannel networks to channel cells through microchambers where they are partitioned and exposed to micro-rotational flow.[27]. It can be used on primary cells, cell lines, and multiple cell types coculture.[9, 16, 19, 27] As many microfluidic platforms are equipped with biosensors for real-time imaging and monitoring of the system, microfluidic devices are making it possible for scientists to produce size-controlled spheroids for high-throughput analysis on a small scale.[28]

Additionally, fluid shear stress and soluble factors around the spheroids can be tightly controlled by the perfusion system.[16,23] The method has also been shown to be highly efficient for drug testing and co-culture of spheroids by using this method.[13,27,29,30] Microfluidics-based methods have the advantage of being able to precisely measure the size of the formed cell spheroids and have high yield, which is easily adjustable by changing the structure. Although microfluidics techniques can be used to produce large quantities of tissue engineering cell spheroids, their capacity for large-scale production is limited.

1.8 Magnetic levitation

Using bioinorganic hydrogels containing bacteriophage (phage) and magnetic iron oxide (MIO, Fe_3O_4, magnetite) together with gold nanoparticles self-assemble, this methodology is potentially adapted to high-throughput / high content screening.[31] (**Figure 1.1**). There is also the possibility of using substances as poly-L-lysine on the particles in order to encourage the cells to attach to the nanoparticles as well. Magnetic nanoparticles are then incorporated into cells through the use of this bacteriophage-based hydrogel.[32-34] The cells containing nanoparticles levitate, aggregate, and form large MCSs around 500 μm in diameter when magnetic forces are applied through magnets placed on top of tissue culture dishes. Furthermore, the magnetic forces induced by this technology cause cells to cluster into shapes dictated by their magnetic fields. By applying varying magnetic forces to the sphere, this technique is able to control its size and form and further stimulate cells to adhere together and form dense tissues.[31-33] Depending on the downstream application, the presence of magnetic particles may pose problems.

1.9 Aqueous two-phase system (ATPS)

At the time of its discovery, the ATPS was accidentally discovered by Martinus Willem Beijerinck while mixing aqueous solutions of starch and gelatin together. However, its application was furthered by Per-Ke Albertsson, who discovered a number of uses for it.[36-38] A variety of components can be mixed with water to form these systems.[39-41] There has been a rapid growth in interest in ATPS based on polymer-salt aqueous systems (e.g., phosphate, sulphate, or citrate) as these techniques offer advantages over conventional extraction methods. Especially valuable for biomolecule purification and concentration experiments, they are inexpensive, environmentally friendly, and able to run continuously.[42, 43] Due to the

presence of water in both phases of ATPS, biomolecules are easily separated from polymers, while polymers are stabilized, while other liquid-liquid extraction methods could damage biological products due to the stress of process conditions and organic solvents.[42]

Usually, biphasic systems consist of two polymers (e.g., polyethene glycol and dextran or phosphate, sulphate or citrate) or a polymer and a salt (e.g., phosphate). In practice, there are few cases in which solutions containing polymers are miscible, since this property of polymers sometimes results in the formation of two phases in the solution. Incompatibilities may also be observed when a polymer is mixed with an ionic salt of high strength. Due to steric exclusion, polymers form large aggregates and separate into two phases. The same exclusion phenomenon is observed when polymer - salt ATPS absorbs a large amount of water. **Figure 1. 2** illustrates an example of a phase diagram, which is similar to a fingerprint for a system under specific conditions (such as temperature and pH), which shows ATPS' potential working area. As a result, it provides information about the concentrations of components in two phases, their concentration in the bottom phase, and their concentration in the top phase.[43, 45] This diagram shows a binary curve (TCB), which divides the concentration area of components. This curve splits the concentrations which form two immiscible aqueous phases (above the binodal curve) from those that make one phase (below the binodal curve). There is a TB line in the diagrams connecting two nodes that lie on the binodal curve; it connects two nodes that lie on the binodal curve. Because all potential systems are on the same tie line (**Figure 1. 2A**), their equilibrium compositions at top phase and bottom phase are identical. Because all potential systems are on the same tie line (**Figure 1. 2A**), their equilibrium compositions at the top phase and bottom phase are identical. Binodal's critical point is indicated by C, and at this point, both phases are theoretically equal in volume. A zero value for the tie-line length (TLL) is found at point C. It is important to mention that the units of tie line length and component concentration are the same.

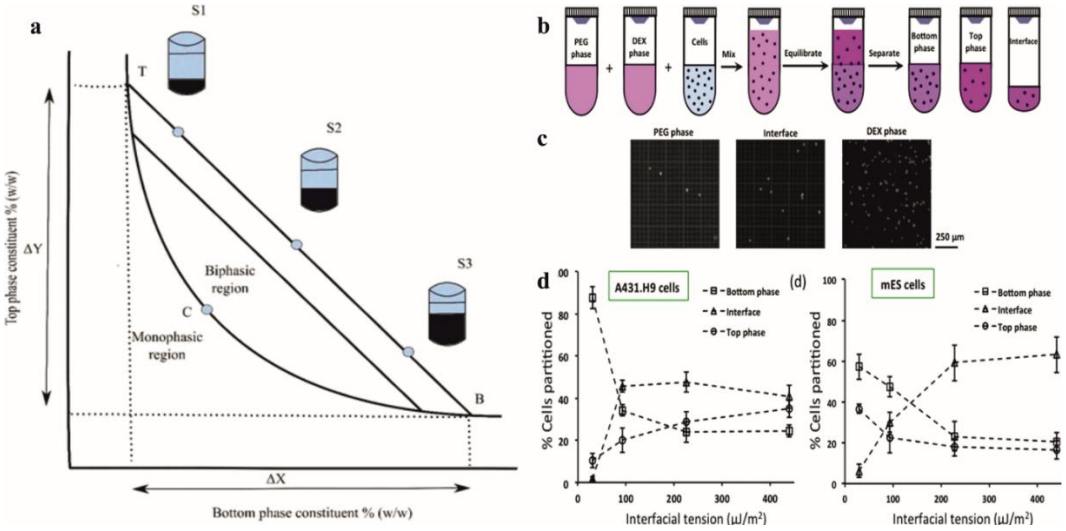

Figure 1. 2 (a) Schematic representation of the phase diagram. Concentrations above the binodal curve (TCB) forms aqueous two-phase system clashes[41] (b) Schematic of cell partition experiments with aqueous two-phase systems, (c) images of A431.H9 cells recovered from the top phase, interface, and bottom phase of the 5.0% PEG–6.4% DEX two-phase system and loaded on a hemo-cytometer counting, (d) percent of A431.H9 cells partitioned to each of the two bulk phases and their interface in four two-phase systems is shown vs interfacial tension.[44] Reprinted with permission from ref. 44. Copyright 2015 American Chemical Society.

1.9.1 Cell partition in ATPS

The spontaneous partitioning of cells in ATPS is one of the key advantages of generating cell spheroids.[44] Some studies have reported cell partitioning behavior. At present, researchers have devised different models to understand how cells partition in ATPS.[46, 47] Liquid-liquid mixtures do not have a good comprehensive theory. The work done by Atefi and co-workers has demonstrated that the interfacial tension between the two immiscible phases could influence the partition of cells, e.g. increasing the interfacial tension could cause cell accumulation at the interface (**Figure 1. 2b,c,d**).[44] Iqbal et al. showed that the partition behavior of cells is influenced by electrochemical factors, hydrophobicity, biospecific affinity, molecular weight, and conformation. In the presence of higher interfacial tension, cells accumulate and partition towards the interfacial region between two aqueous phases. In ATPS, the surface properties further modulate partitioning based on their differences in partitioning behavior and minimum free energy modeling.

1.10 ATPS based techniques to generate cell spheroid

1.10.1 Microfluidic devices

Microfluidic devices can be used to control the droplets' size to shrink, burst, or grow.[48, 49] Aqueous two-phase microfluidic devices have been optimized for generating spheroids based on these controls.[50-53] Polymeric ATPS is used to confine cells within a nanolitre-volume aqueous drop immersed within a second phase of immersion aqueous solution to form spheroid structures spontaneously. Due to the cell's strong partition to dextran in such a system, polyethene (PE) and dextran (DEX) are commonly used bio-available ATPS. An ATPS consisting of DEX and PEG has been reported to prepare a cell-laden microgel using microfluidic devices to overcome the ultra-low interfacial tension between the DEX and PEG solutions, which involved a periodically-changing injection force.[50,52] It is possible to change the injection conditions in order to control the diameter of the droplets.

A microfluidic droplet approach has recently been proposed by Tomasi et al. for sequentially modulating three-dimensional spheroids culture conditions, enabling complex protocols, such as co-culture, hydrogel encapsulation, and drug tests.[100]

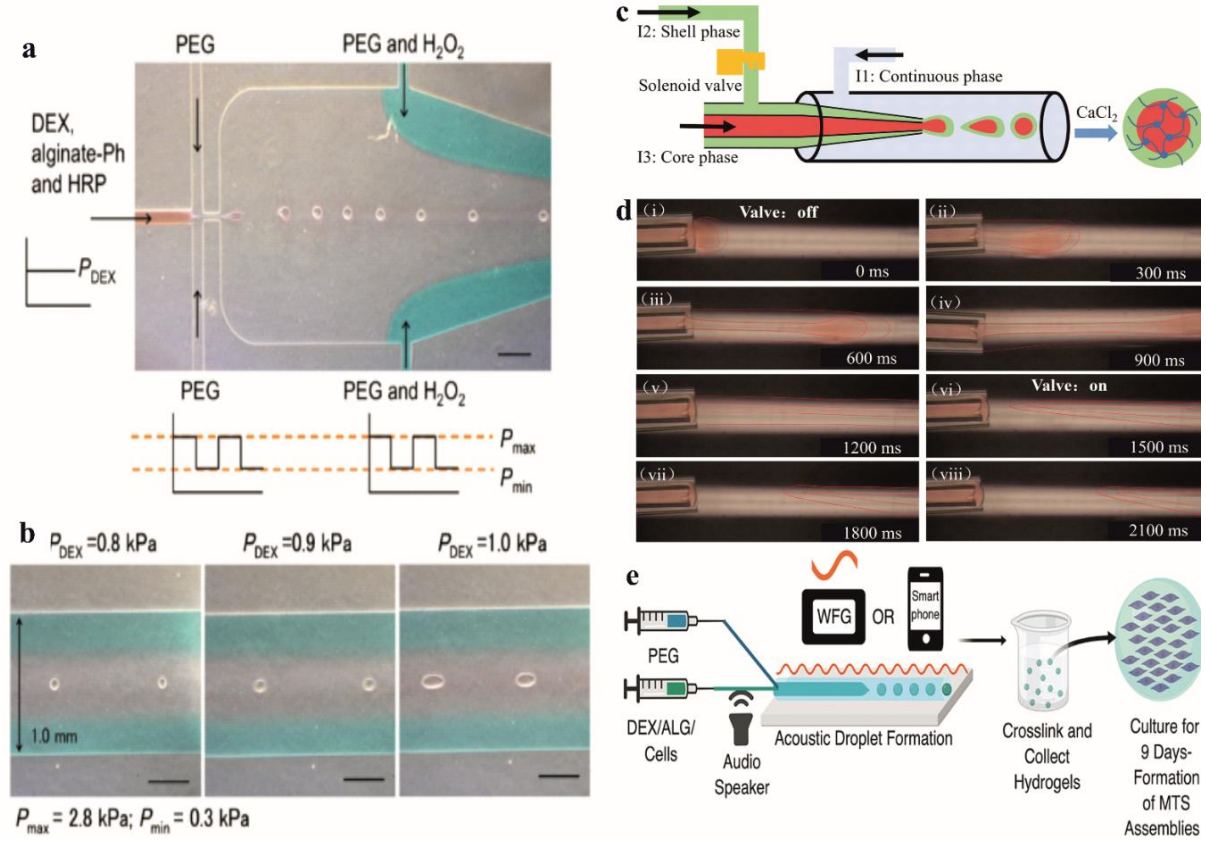

Figure 1.3 (a) Production of microgel using DEX/PEG-based ATPS in microfluidic devices.[50] Reprinted with permission from ref. [50]. Copyright 2017 Springer Nature; (b) Morphology of pre-gelated droplets passing through the narrowest channels in the downstream of the microfluidic device. (c) Schematic of the all-aqueous-phase microfluidic system for the fabrication of core−shell capsules. (d) The actual fabrication process of core−shell capsules with the help of a solenoid valve.[54] Reprinted with permission from ref. 54. Copyright 2019 American Chemical Society; (e) Acousto-fluidic device workflow for forming spherical hydrogels with encapsulated cells.[52] Reprinted with permission from ref. 52. Copyright 2019 American Chemical Society.

By using this platform, single-cell data can be collected time-resolved, which enables the discovery of a dynamic response regulated at the spheroid level. By using asymmetric anchor designs, we achieve a qualitative change in the functionality of the microfluidic approach for many biological applications, including sue engineering, immunotherapy modeling, and understanding host-pathogen interactions. Using this

chip, we are able to observe quantitatively the dynamics of drugs impinging on tumour spheroids due to the combination of precise control of single spheroids and high-density spheroids in this chip. It is also important to emphasize that Cristaldi et al. have introduced a method for detecting the droplet speed from a free-falling sample into a specifically conceived flow channel, which could provide valuable information about cell spheroids, such as their density, size and weight.[101] The method relies on measuring the droplet speed from the edge of the flow channel. As a result of this device, cell spheroids ranging in diameter from 20m to 200m can be measured. The crosslinking reagents horseradish peroxidase (HRP) and H_2O_2 could also be dissolved in DEX and PEG solutions, respectively, at concentrations suitable for gelation of the resulting droplets (**Figure 1. 3a,b**). Viability and growth potential were high among the cells encapsulated in the microgel. Depending on the concentration of gelatine derivatives incorporated into the microgel, the microgel was able to promote cell adhesion. In addition, a shell-core structure has been designed for a microfluidic device that can handle all aqueous phases. A gelation process was used to maintain the structure and induce the growth of spheroids by encapsulating the cells in the core phase (**Figure 1. 3c,d).** A microfluidic device designed by De Lora et al. can generate an ATPS into multicellular tumour spheroids (MTS) template droplets using an acoustic modulation from an amplified waveform generator or even a smartphone (**Figure 1. 3e**).

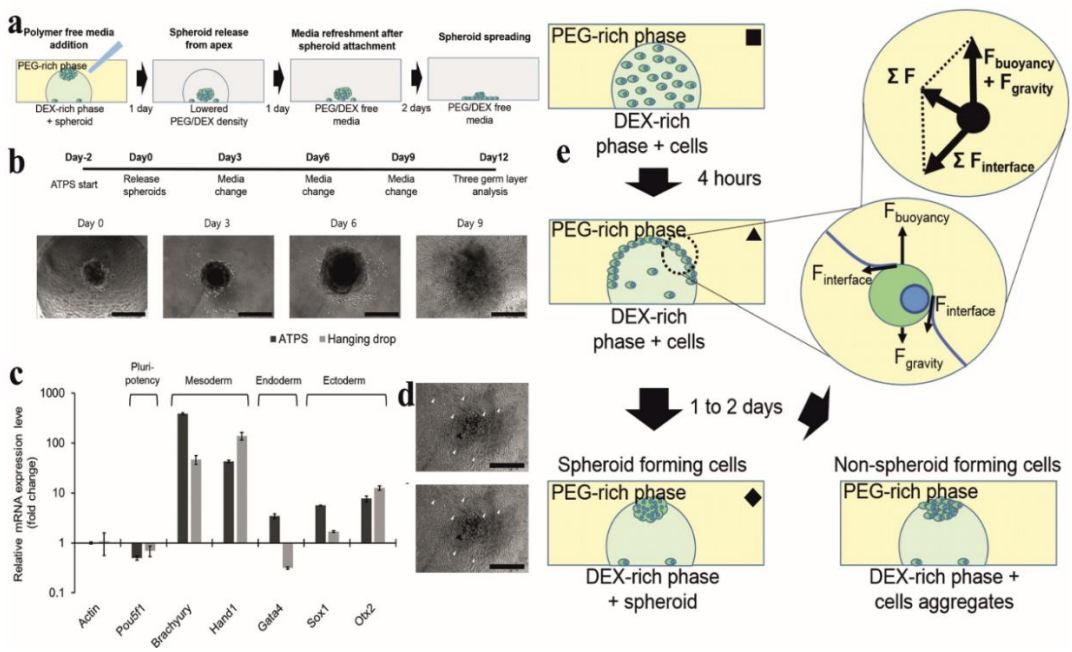

Figure 1.4 (A) Adding PEG/DEX-free fresh medium decreases the density of the DEX-in-PEG ATPS pattern; therefore floating spheroids settled. (B) EB formation and cardiac differentiation using DEX-in-PEG ATPS pattern. (C) Representative images of day 12 EBs. (D) qPCR analysis of representative three germ layer lineage markers. (E) Schematic model of ATPS spheroid formation.[55]

1.10.2 Microdroplet method

Cells accumulate at the apex of the ATPS and increase contact with each other as a result of gravity and cell partition behavior.[55-57] The alteration of the buoyancy force effect by altering the concentration of the two phases helps accumulate the cells at the apex. Following 4 hours of culture in the system, the DEX drop meniscus and most of the cells were trapped at the phase interface. During this state, trapped cells experience surface tension and buoyancy forces as a result of density differences. Due to DEX's positive interaction with cell membranes, DEX-rich phases have a greater contact angle with cells than PEG-rich phases.[44, 47] Surface forces are exerted in a tangential direction to the contact point due to the formation of this contact angle. Hence, a free body diagram can be used to illustrate the main forces. When these forces interact, a trapped cell travels down the phase interface until it reaches the apex of the DEX drop meniscus, where balance is achieved (**Figure 1. 4e**). As a result of pattern formation, most of the cells form either a tight cell spheroid or a loose cell

aggregate at the apex of the DEX drop on day one or two. This method is technically suitable for all sorts of cells due to the fact that it allows the density of the two phases to be adjusted easily by varying the DEX/PEO phase concentration. This method was not suitable for certain cells, such as HepG2, which prefer to form aggregates rather than spheroids, underlining the importance of carefully identifying and selecting cells. It depends on the cell characteristics whether the DEX drops form tight or loose cell aggregates and spheroids at the apex. This method is technically suitable for all types of cells due to the ability to adjust the density of the two phases by varying the DEX/PEO phase concentration. This method, however, did not work for several cells, such as HepG2, which tended to form aggregates rather than spheroids, highlighting the importance of carefully identifying and selecting cells for spheroids.

However, spheroids can be monitored easily with this method. A more important factor was that spheroid density and size could be easily controlled (**Figure 1. 4a-d**). A long-term culture led to spheroids with a diameter of 400 mm after nine days. Moreover, these spheroids were significantly more functional than monolayer cultures in terms of RNA expression. PEG droplets containing DEX droplets can also be pipetted directly into PEG phase as another ATPS droplet-based method. Spheroids form within 24 hours once the cells are confined in DEX droplets (**Figure 1. 4 a-d**). The spheroid's density can be controlled easily using this method, allowing the size of the spheroids to be modified. Moreover, the ATPS system facilitates monitoring and various testing on this platform.

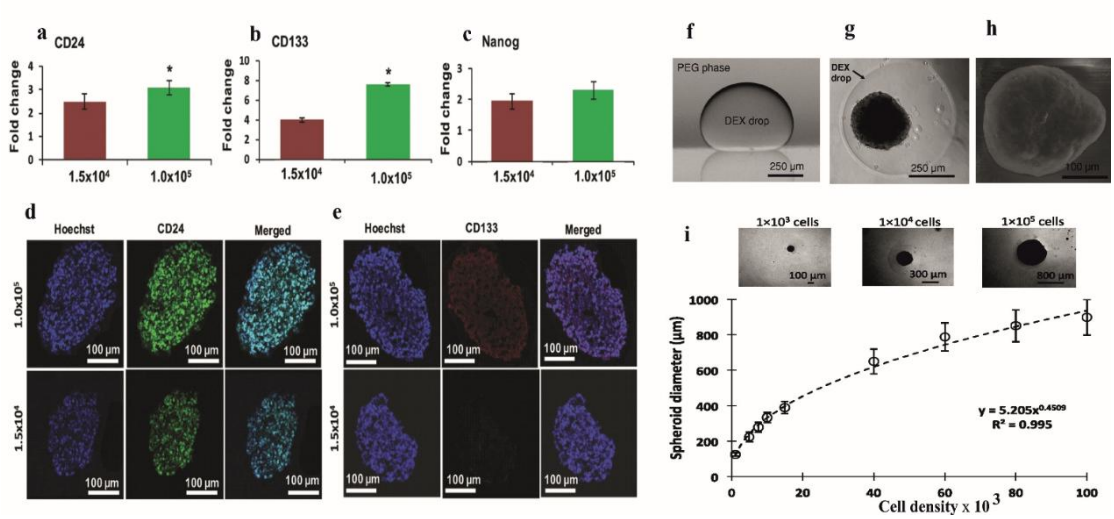

Figure 1. 5 (a) Side view of a DEX phase drop in the immersion PEG phase formed on a glass surface using equilibrated phases from an ATPS with initial composition of 6.4%(w/w) DEX and 5%(w/w) PEG. (b) A top-view of A431.H9 skin cancer cell spheroid formed with a cell density of 1×10^4 cells at 24 h. (c) Scanning electron microscope (SEM) image of A431.H9 cells after one week of incubation. (d) Spheroids generated using a wide range of density of cells.[57] Reproduced from ref. 56 with permission from copyright 2014 John Wiley and Sons. q-PCR analysis of expression of (e) CD24, (f) CD133, and (g) Nanog in ATPS spheroids of MDA-MB-157 cells normalized against mRNA levels of a monolayer of cells. Largest cryosections of 1.5×10^4 and 1.0×10^5 cell density spheroids immune-stained for cancer stem cell markers (h) CD24 (green) and (i) CD133(red).[56] Reproduced from ref. 58 with permission from copyright 2016 John Wiley and Sons.

1.10.3 Water-in-water Pickering emulsions

Such techniques could first confine the cells within emulsion droplets and then increase the concentration of constant phase to impose osmotic pressure to fabricate spheroid in a very short time[62,63] The Dextran (DEX) phase was more attractive to the cells than the poly(ethylene oxide) (PEO) phases, resulting in their encapsulation in the emulsion drops. Clusteroids were formed when cells interacted strongly with emulsion's droplets, which facilitated cell-cell interactions. Alginate gel was used to simulate the generation of real tissue from the clusteroids collected. In comparison with 2D monolayer culture, the area of albumin linked to cell proliferation was reinforced. It may be possible to extend the w/w emulsion platform to tissue

generation and drug testing using this methodology. Cells can be harvested in high yields without harming their viability with this technique. A limited number of types of cells were found to be workable in this technique, and further investigation of the details of the formed spheroids, such as RNA expression, protein expression, and enzyme expression, is needed.

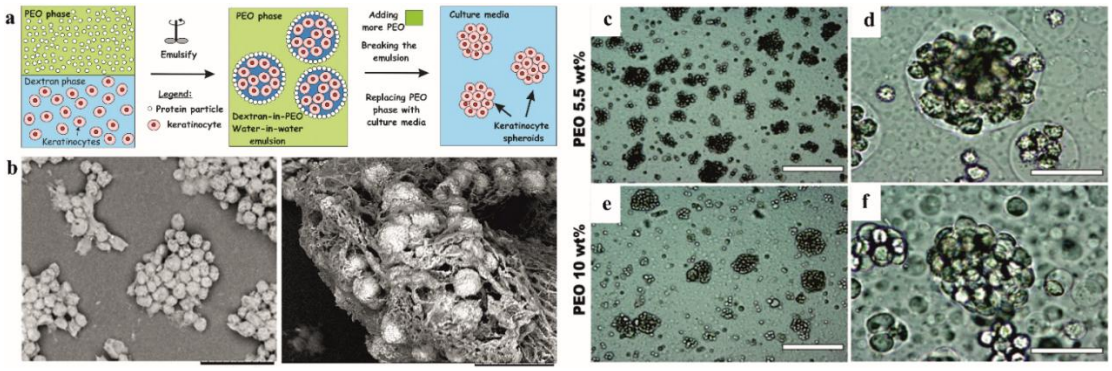

Figure 1. 6 Schematic model of spheroid formation in water-in-water Pickering emulsion (a) Schematics of our high-throughput method for preparation of keratinocyte cell spheroid (b). SEM images of a sample of HaCaT cell clusteroids after being removed from the medium.63 Optical microscopy images of (C,D,E) HaCaT cell droplets (5.5 wt% PEO/5.5 wt% Dextran) and (F,G,H) HaCaT cell clusteroids (10 wt% PEO/5.5 wt% Dextran) stabilized by 2 wt% WP particles. Here the cell and DEX volume fraction were, ϕHaCaT = 0.15 and ϕDEX = 0.25, respectively.

1.11 Co-culture spheroids

Spheroids with an outer layer of cells between 200 and 300 μm may form a necrotic core because nutrients and oxygen cannot penetrate the outer layer. The simulation of *in vivo* environments can be quite limited by single-cell spheroid systems. The reliability of spheroid models was therefore improved by co-cultures or tri-cultures. Tissue engineering has shown that co-culture can be an effective strategy for maintaining phenotypic characteristics *in vitro*.[15, 27, 51, 64-66] Generally, the results of co-cultures can be predicted by the types of cells used and how the co-cultures are performed. The liver-specific functions of different cells have been influenced in different ways by co-culturing with hepatocytes, such as endothelial cells (ECs), human adult keratinocytes (HaCaT), mesenchymal stem cells, etc.[5, 66-71] An ECs layer

and an ECM are sandwiched between hepatocytes in co-culture/tri-culture spheroids, followed by self-sorting of ECs. Through the formation of vascularization, the ECs could allow the spheroids to grow over the oxygen limitation.

[72] In this regard, ECs make an ideal co-culture partner with hepatocytes. A couple of other factors may influence hepatocyte fate, such as the pattern of co-culture, such as 3D or 2D culture as well as contact or non-contact culture. Regulatory pathways in the liver are mediated both by direct cellular communication via gap junctions and by paracrine mechanisms.[102,103] It is important to note that actual cell microenvironments do not only include the metabolism, and metastatic potential of a single cell, but also several types of cells, as well as scaffold structures that assist the cells in growing. Co-culturing or tri-culturing spheroids can enhance the accuracy of drug testing and transplantation by adding complexity and reliability.

1.12 Utilization of spheroids

1.12.1 Drug testing platform

For simulating tumour complexity *in vitro*, tumour globules have been used.[69, 73] Molecular studies of tumor-mesenchymal cell interactions have used mixed ellipsoids, which produce cells with an increased cell shape, structure, and gene expression profile.[74] In co-cultured hepatic cancer cells with fibroblasts, the cells demonstrate an invasive phenotype, which leads to the development of tissues more similar to primary hepatic cancer tissues.[67,69] Tumor cells are more resistant to chemotherapy and radiotherapy when endothelial cells are present in three dimensions, which allows study of their angiogenic and metastatic potential.[75, 76] A monolayer of cells has an IC50 of 100 times higher than a globular cell. Paclitaxel and cisplatin, for example, have an IC50 of 100 times higher.

Antibodies, enzymes, proteins, and immunotoxins showed similar results.[36, 77] There are many reasons for this result, including poor drug penetration, hypoxia, proliferation, intercellular contact, and different gene expression at different locations in the spheroids, just like in tumours. A radiolabelled drug such as doxorubicin has been used in fluorescence or autoradiography measurements on tumour spheroids to determine the three-dimensional penetrability of anthracyclines.[104] It is possible to predict individual tumours' response to different treatment regimens using 3D models built from human cells that have the potential to perform high-throughput and high-content screening.

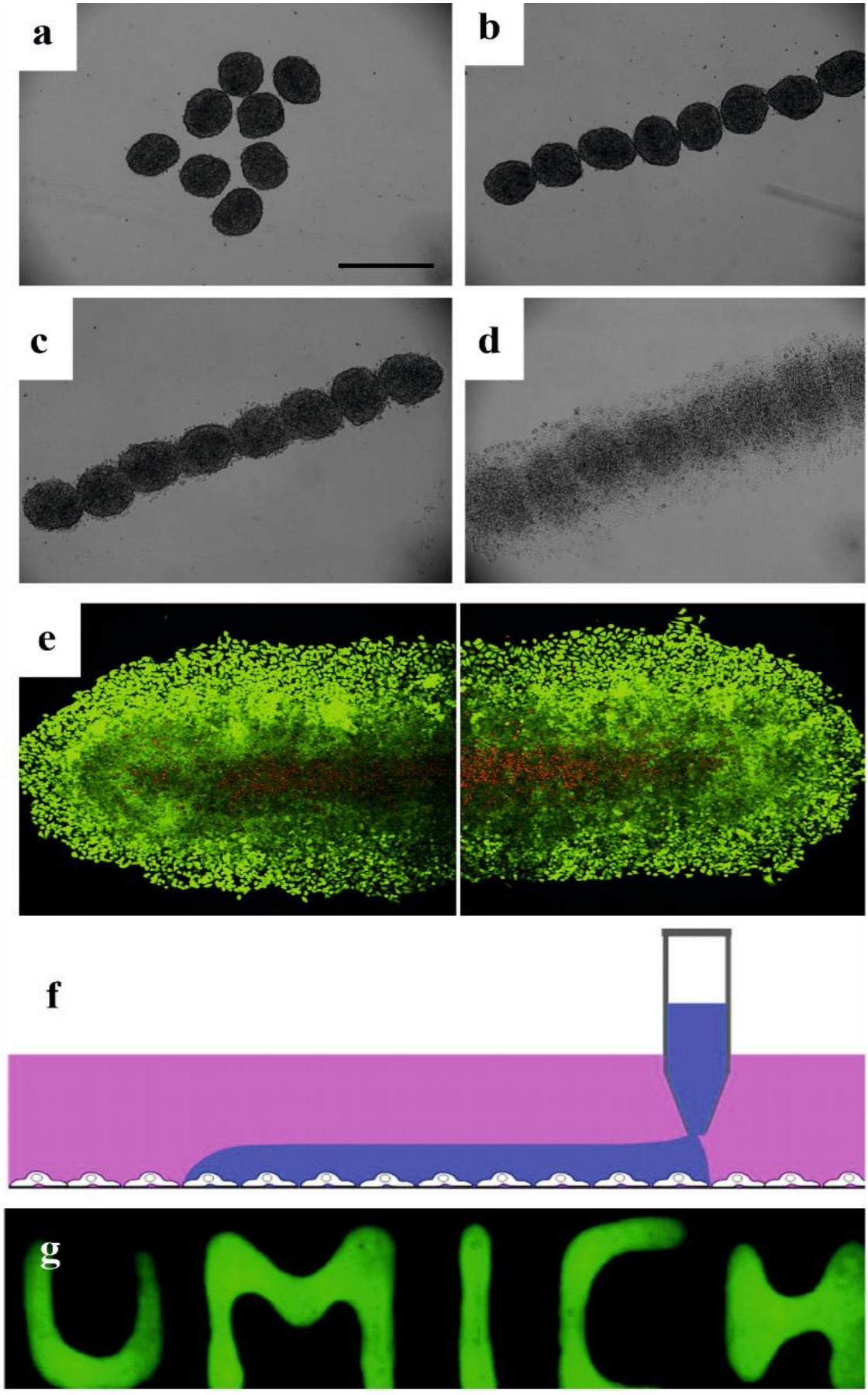
a
b
c
d
e
f
g
UMICH

Figure 1.7 Magnetic patterning of HeLa multicellular spheroids. (A) Random distribution of magnetic HeLa spheroids without any applied magnetic field. 3-day-old spheroids were used. Scale bar represents 500 mm. (B) Magnetic HeLa spheroids were patterned with an applied magnetic field within a few seconds. (C) The patterned magnetic HeLa spheroids start to fuse after 3 h. (D) Fusion and growth of the patterned magnetic HeLa spheroids after 18 h. (E) Live/dead stain of the fused tissue construct formed by the patterned magnetic HeLa spheroids after 48 h of culture. Viable cells are green, while non-viable cells are red. Scale bar represents 250 mm.[32] Reprinted with permission from ref.32. Copyright 2010 Elsevier; (F) Schematics of cell printing on a cell monolayer in user-defined shapes. Cell suspension in the DEX phase is printed onto an existing cell layer by continuous dispensing from the pipette tip.[58] Reprinted with permission from ref. 58. Copyright 2019 Springer Nature.

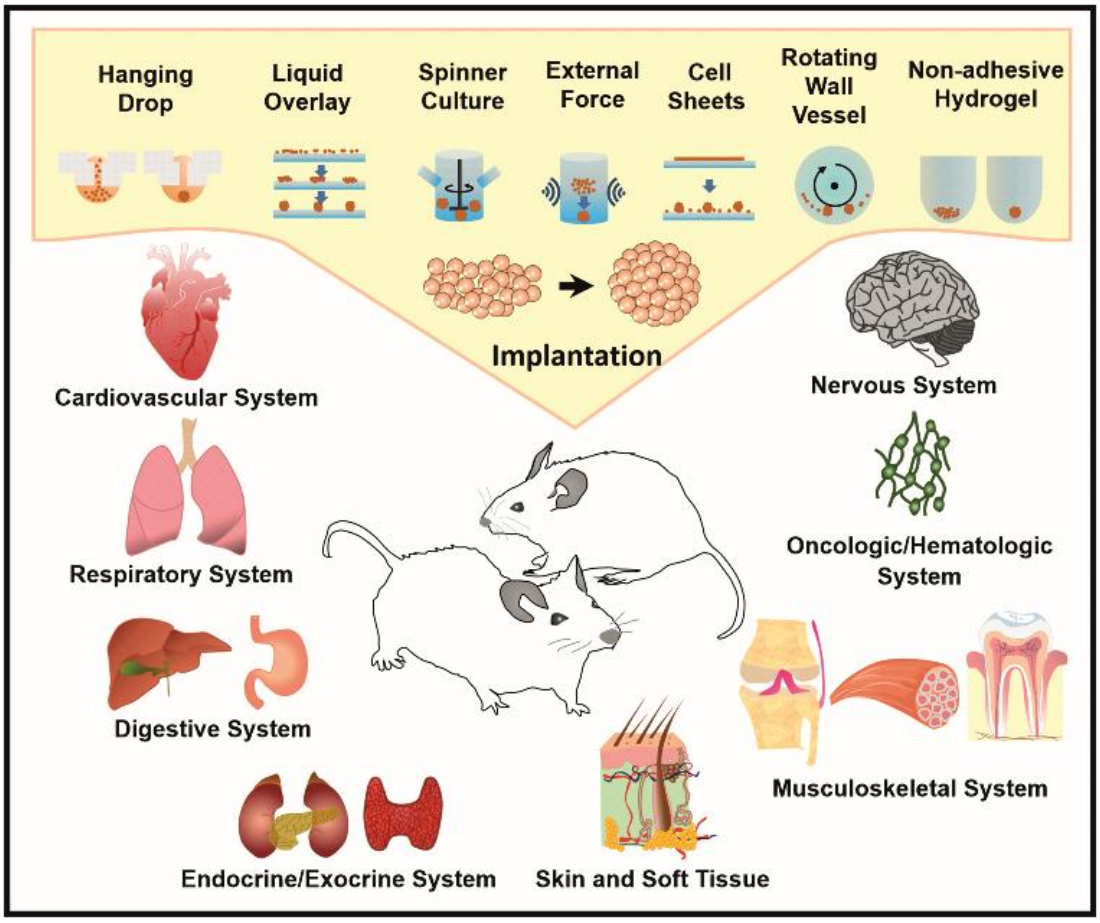

Figure 1. 8 *In vivo* therapeutic applications of cell spheroids: Spheroid formation methods and organ systems for potential clinical applications.[94]. Reprinted with permission from ref. 94. Copyright 2018 Elsevier.

1.12.2 Tissue engineering blocks

It is currently difficult to fabricate large tissues with high densities of living cells *in vitro* in the field of tissue engineering.

Similarly, nutrient delivery limits spheroid diameters to 200 - 400 μm. A capillary-like network was developed by using endothelial cells to break through the size limitations of the cell spheroids.[8, 66, 78-80] Spheroids with clinical success are usually relatively thin tissues (2 mm) where oxygen, nutrients, and metabolic waste are transported via simple diffusion, which is essential to cell viability. A larger vascularized tissue could be formed after fusing the 'endothelialized' spheroids to address vascular integration with the host's system.[68,81-83] It is crucial to pre-vascularize the implants before implanting them.[20, 84-86] Spheroids are being used as building blocks to try and fabricate organs *in vitro* in the emerging field of bioprinting and biofabrication. A layer-by-layer printing of living cells and an ECM material is done using bio-printers that are adapted from inkjet printing and rapid prototyping technologies.[9,78] In spheroid culture, magnetic levitation is attractive because it provides an easy method for controlling fusion between spheroids (**Figure 1. 7a- e**). There was no difficulty in modulating magnetic spheroids into various shapes.[31,32,85,87] ATPS-based spheroid fabrication is also an emerging technique that provides excellent direct bioprinting results. Due to ATPS' bioavailability, the system can be utilized as a kind of bio-ink to construct tissues fast (**Figure 1. 7f**).[35, 58,88,89]

1.12.3 *In vivo* applications

In the future, spheroids will be used for tissue engineering and regeneration as well as to address a wide range of clinical and biomedical problems (**Figure 1. 8**). The three-dimensional extracellular microenvironment, so-called growth factors, and its signaling cascades are more easily reproduced in spheroids than in traditional two-dimensional culture. Translational studies investigating *in vivo* implantation of spheroids into various animal models of tissue regeneration have been conducted as knowledge about the preparation and maintenance of spheroids has improved. The spheroid transplant has been utilized in almost all the human systems including cardiovascular system,[90] digestive system,[91] musculoskeletal system,[92] and skin.[63,93] There is limited published data on tissue engineering using spheroids *in vivo*. As far

as *in vivo* applications are concerned, spheroids seem to present an unexplored potential.

1.12.4 Delivery vehicles

Since Mesenchymal stem cells (MSCs) possess tumour-tropic qualities, they have been increasingly used to treat cancer. Nevertheless, MSC-based cancer therapy has limited options due to short retention and limited payload options. A hybrid spheroid/nanomedicine system comprising MSC spheroid entrapping drug-loaded nanocomposite, to address these limitations has been reported (**Figure 1. 9**).[95] MSC tumour tropism was enhanced by spheroid formulations, and therapeutic payloads could also be loaded more easily. Active drug delivery was performed using this system to specifically target glioblastoma cells for drug delivery. The engineered MSC and nanocomposite provided an effective method of delivering a combination of proteins as well as chemotherapeutic drugs. In a heterotopic glioblastoma murine model, the hybrid spheroids showed higher nanocomposite retention than single MSC approaches, leading to enhanced tumor inhibition. In order to advance targeted combinational cancer therapy, the spheroid system incorporates the merits of cell-mediated and nanoparticle-mediated drug delivery with the tumour-homing qualities of MSC.

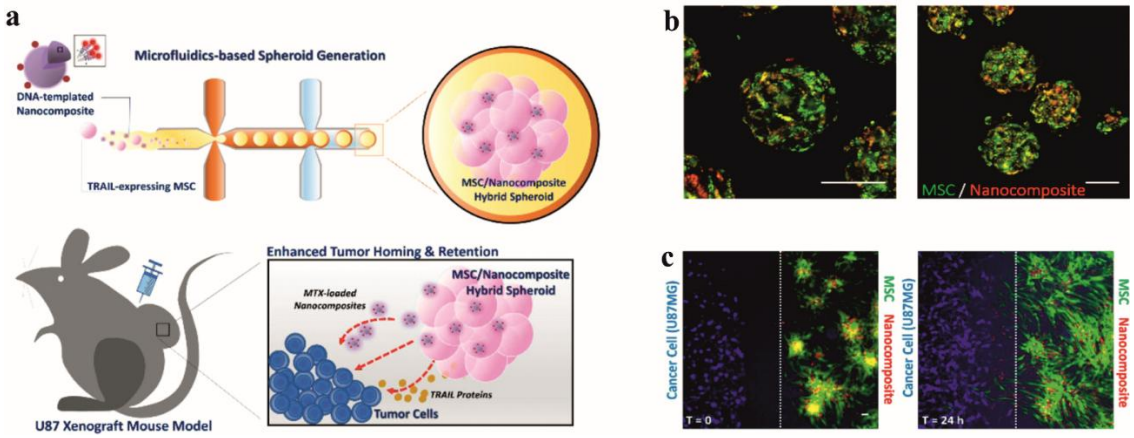

Figure 1. 9 The design and properties of MSC/DNA-templated nanocomposite hybrid spheroid for GBM therapy. (A) Schematic illustration of the hybrid spheroid system. (B) Comparison of the *in vitro* tumour homing property between single and spheroid-formulated MSCs. (C) Representative confocal images of the hybrid spheroids. (D) *In vitro* tumour homing of the hybrid spheroids. Scale bar = 50 μm.[96] Reprinted with permission from ref. 96. Copyright 2019 American Chemical Society;

1.12.5 Biosensors

Increasingly complex cell architectural structures have prompted the need for simple and reliable viability assays that are suitable for *in vivo*-like pharmacotoxicological experiments. Developing a 3D spheroidal culture format viability/cytotoxicity *in vitro* electrochemical sensor is a challenging task. Biosensors have recently been developed to measure cell viability/toxicity in living cells by electrochemically monitoring the enzymatic activity of non-specific esterases via the hydrolysis of 1-naphthyl acetate into 1-naphthol.[96] Based on this enzyme-based biosensor, it is convenient to measure the viability of both 2D and 3D cell culture formats and provide more dynamic data for drug/toxicity screening. It is also possible to generate measurable analytical signals from molecular recognition at the cellular and molecular levels through another type of biosensor.[97,98] Biosensors developed by Elisa and colleagues contain immobilized spheroids of human cell lines producing red- and green-emitting luciferase under the control of the NFB pathway and a constitutive promoter, respectively. In contrast to identifying single constituents of a sample, the 3D cell biosensor can assess the toxicity and inflammatory effects of the sample as a whole.[99] In addition, the use of engineered cell lines could result in spheroids with a wide range of bioactive biomarkers, including liver toxicity, genotoxicity, and oxidative stress responses.

1.13 Conclusions

In vitro models can be developed using MCS culture techniques to simulate many aspects of *in vivo* conditions. By understanding MCS's complex structure, we are able to better understand interactions between cells and between cells and matrix. It is also possible to perform basic research in cancer biology using MCS simulations of the microenvironment in *vivo*, and also provide opportunities for pharmacological research *in vitro*, and for the culture of 3D functional tissues *in vitro*. It is difficult, however, to implement such a compelling concept. In the MCS structure, the number of cells limited the further expansion of spheroids, resulting in higher initial cell density required for spheroids to form. The second problem with traditional methods is their low level of repeatability and quality assurance. There is also a third reason why existing methods of MCS differ from those *in vivo*, which can cause different affects on the cellular behaviour. Cell migration between MCS cannot be achieved

with current methods. The development of spheroids *in vitro* is difficult due to a lack of heterogeneous cell-cell interactions, tissue interactions with the extracellular matrix, and cellular signalling pathways. Consequently, gene expression profiles, protein content, and enzyme content are important for demonstrating the correlation between real tissues and MCS. In addition, low yield also greatly hinders the study of MCS. Over the past decade, there has been a substantial development of methods for fabricating MCSs *in vitro*. ATPS systems are considered promising because they produce controlled uniform-size MCSs and restore cellular morphology and functionality by restoring the complex matrix-cell interactions. MCSs can develop their extracellular matrices, which are crucial to their functions, under the physical stress present in the ATPS system. MCSs can be fabricated in a controlled uniform-size environment using chambers or droplets from the ATPS. At last, researchers are able to use ATPS microspheres for a wider range of applications, including tissue engineering and toxicological tests, thanks to the higher yields available from ATPS. By altering the osmotic pressure for MCS formation and growth, this approach is also capable of tuning the microenvironment to mimic the conditions *in vivo*. By improving techniques like ATPS or magnetic levitation, the breakthrough of size and yield control of MCSs opens the way for *in vivo* applications, making this an important area of research for regenerative medicine and other clinical applications. The challenge of forming MCSs in relevant physiological micro- and macro-environments is addressed by more elegant designs for spheroids culture systems, such as co-culture and tri-culture systems.

1.14 Aims of the thesis

As seen above, the first chapter provides a general introduction overviewing the 3D cell culture protocols and various applications. The utilization of the 3D cell culture platform in tissue engineering applications are of magnificent potential. The comparatively low yield rate restraints the application of the advanced 3D cell culture models in biomaterials and tissue engineering application. This thesis focuses on development of a high-throughput 3D culture protocol and assess its possibility to be used in tissue engineering applications. The 3D culture models were generated using an aqueous two phases system, water-in-water Pickering emulsion. The 3D co-culture models with angiogenesis potential were also carefully introduced in the thesis. The skin and urinary 3D cell culture models were used as *in vitro* models to simulate the

formation and removal process of the biofilm. Each following chapter provides an introduction and aims, and includes the methods, results, discussion, and conclusions.

The research in **chapter 2** investigates the new protocol to generate the 3D cell clusteroids, which use a water-in-water Pickering emulsion to encapsulate the living cells for improved attachment. The emulsions were stabilized by biocompatible whey protein particles and the two phases were Dextran and poly ethylene oxide (PEO). The goal was to find the best whey protein features (Size, zeta potential) to stabilize the DEX/PEO water-in-water emulsions with optimal ratio. The cell numbers that were encapsulated in the emulsions were also systematically characterized. The aim was to prove that the cells could be condensed into densely packed clusteroids with high viability and improved functionality.

Chapter 3 advances the 3D cell clusteroids generated by the ATPS system into Co-culture level. The Hepatic cancer cells were co-culture with ECV304 bladder cancer cell lines which also exhibits endothelial cells features. The two kinds of cells were homogenously dispersed in the Dextran phase prior to the emulsion fabrication. The aim was to prove that the two kinds of cells could co-exist and interact in the droplets to form a co-cultured cell clusteroids. Another purpose of the chapter was to prove that the ECV304 cells could functionalize the Hepatic cells using the co-culture pattern, which would trigger the production of angiogenesis proteins and boost the functionality of the cells to a great extent.

Chapter 4 aimed to examine either the co-culture models could be expanded to primary cells levels. The efforts of utilising primary cells to vascularize the hepatic cells lines were that they commonly are more fragile *in vitro*. But the primary cells would better mimic the *in vivo* environments. We utilize the widely used primary endothelial cells line, Human umbilical vein endothelial cells to vascularize the Hep-G2 cells in the 3D cell clusteroids model and prove if this could be effectively generated. The co-cultured Hep-G2/HUVEC 3D clusteroids showed high viability and high functionality in producing Hepatic related markers like urea and albumin. The angiogenesis proteome array proved that the HUVEC cells could self-regulate in the 3D clusteroids and vascularized the 3D clusteroids. The 3D co-cultured clusteroids could form sprouts into the Matrigel which are key features of the *in vitro* vascularization.

Chapter 5 explores the application of the 3D cell clusteroids in simulating the bacterial biofilm infection and testing nano-therapeutics' efficiency *in vitro* to replace the animal models. The 2D cells were widely used to mimic the bacterial infection process but the monolayer cell culture is commonly way too fragile when applying the pathogens. The densely packed 3D cells would be ideal models in simulating such things. We firstly prove that the ATPS system could also be applied to the Keratinocytes on generating 3D cell clusteroids. We designed the antibiotic (Ciprofloxacin) encapsulated NPs(Carbopol), surface functionalised with a protease (Alcalase) which could be used to selectively target the cationic bacterial biofilms using electrical forces. The 3D cultured clusteroids models were co-cultured with bacterial (*Pseudomonas aeruginosa* and *Staphylococcus aureus*) to track the biofilm formation process on the clusteroids layer. The removal process of the biofilm using the nanoparticles were also carefully characterized. The NPs showed minor influence on the clusteroids viability.

Chapter 6 aims to further examine that would the 3D cell/Biofilm co-culture models could be used to tolerate the hard-to-treat fungal infection that commonly happened in urinary track caused by the implanted apparatus. We firstly generate the 3D clusteroids using ECV 304 human bladder cancer cells lines. The ECV304 cell clusteroids were robust and proliferated fast. We designed and fabricated the Fluconazole loaded -Lysozyme functionalized -Shellac nanoparticles at adequate concentration. The final aim was to examine the *Candida albicans* infection process and the effect of the nanoparticles. The cytotoxic effects of these NP formulations against the cell clusteroids

The thesis concludes in Chapter 7 with a summary of the project's findings, identifying areas deemed prudent for further study.

1.15 Ethical statement

There are no ethical implications in the project for public health and safety. The human cells used HaCaT, a spontaneously transformed aneuploid immortal keratinocyte cell line from adult human skin, HepG2(human liver cancer cell line), ECV 304(Human bladder cancer cell line), HUVEC(human primary endothelial cell line) in this study are derived from a commercially available and well-characterised depository, ATCC or the European Collection of Authenticated Cell Cultures

(ECACC) at Public Health England, 85011430, respectively. This does not require the cell lines to be regulated by the Human Tissue Act 2004.

The chronic wound bacterial isolates were provided by the Hull Royal Hospital Pathology department and have been fully anonymised with no patient data collected. *Staphylococcus aureus subsp. aureus* Rosenbach (ATCC® 29213™), *Pseudomonas aeruginosa* (Schroeter) Migula (ATCC® 27853™), *Staphylococcus epidermidis* (Winslow and Winslow) Evans (ATCC® 35984™), *Candida. albicans* (Robin) Berkhout (ATCC® MYA-2876) were purchased from ATCC and are commercially available from a well-characterised depository.

1.16 References

1. L. G. Griffith and M. A. Swartz, *Nat. Rev. Mol. Cell Biol.*, 2006, **7**, 211-224.
2. LI.D, Iku.S, Nemoto.K, Nature, 2003,**424**,870-872.
3. K. L. Schmeichel and M. J. Bissell, *J. Cell. Sci.*, 2003, **116**, 2377-2388.
4. M. Simian and M. J. Bissell, *J. Cell. Biol.*, 2017, **216**, 31-40.
5. J. A. Kyffin, P. Sharma, J. Leedale, H. E. Colley, C. Murdoch, A. L. Harding, P. Mistry and S. D. Webb, *Toxicol. In Vitro*, 2019, **55**, 160-172.
6. Y. C. Tung, A. Y. Hsiao, S. G. Allen, Y. S. Torisawa, M. Ho and S. Takayama, *Analyst*, 2011, **136**, 473-478.
7. J. Fukuda, A. Khademhosseini, Y. Yeo, X. Yang, J. Yeh, G. Eng, J. Blumling, C. F. Wang, D. S. Kohane and R. Langer, *Biomaterials*, 2006, **27**, 5259-5267.
8. N.E. Timmins, S. Dietmair and L.K. Nielsen, *Angiogenesis*, 2004, 97-103.
9. N. I. Moldovan, N. Hibino and K. Nakayama, *Tissue Eng. Part B Rev.*, 2017, **23**, 237-244.
10. R. Z. Lin and H. Y. Chang, *Biotechnol. J.*, 2008, **3**, 1172-1184.
11. T. M. Achilli, J. Meyer and J. R. Morgan, *Expert Opin. Biol. Ther.*, 2012, **12**, 1347-1360.
12. X. Cui, Y. Hartanto and H. Zhang, *J. Roy. Soc. Interf.*, 2017, **14**, 1-15.
13. A. Y. Hsiao, Y. C. Tung, X. Qu, L. R. Patel, K. J. Pienta and S. Takayama, *Biotechnol. Bioeng.*, 2012, **109**, 1293-1304.
14. Y. Wang and J. Wang, *Analyst*, 2014, **139**, 2449-2458.
15. R. Foty, *J. Vis. Exp.*, 2011, DOI: 10.3791/2720.

16. O. Frey, P. M. Misun, D. A. Fluri, J. G. Hengstler and A. Hierlemann, *Nat. Commun.*, 2014, **5**, 4250.

17. K. M. Burleson, R. C. Casey, K. M. Skubitz, S. E. Pambuccian, T. R. Oegema, Jr. and A. P. Skubitz, *Gynecol. Oncol.*, 2004, **93**, 170-181.

18. Y. Sakai and K. Nakazawa, *Acta Biomater.*, 2007, **3**, 1033-1040.

19. A. N. Mehesz, J. Brown, Z. Hajdu, W. Beaver, J. V. da Silva, R. P. Visconti, R. R. Markwald and V. Mironov, *Biofabrication*, 2011, **3**, 025002.

20. V. Beachley, V. Kasyanov, A. Nagy-Mehesz, R. Norris, I. Ozolanta, M. Kalejs, P. Stradins, L. Baptista, K. da Silva, J. Grainjero, X. Wen and V. Mironov, *J. Tissue Eng.*, 2014, **5**, 2041731414556561.

21. E. C. Costa, D. de Melo-Diogo, A. F. Moreira, M. P. Carvalho and I. J. Correia, *Biotechnol. J.*, 2018, **13**, 1700417.

22. M. M. Capeling, M. Czerwinski, S. Huang, Y. H. Tsai, A. Wu, M. S. Nagy, B. Juliar, N. Sundaram, Y. Song, W. M. Han, S. Takayama, E. Alsberg, A. J. Garcia, M. Helmrath, A. J. Putnam and J. R. Spence, *Stem Cell Reports*, 2019, **12**, 381-394.

23. H. Ota, R. Yamamoto, K. Deguchi, Y. Tanaka, Y. Kazoe, Y. Sato and N. Miki, *Sensors and Actuators B: Chemical*, 2010, **147**, 359-365.

24. T. G. Hammond and J. M. Hammond, *Am. J. Physiol. Renal Physiol.*, 2001, **281**, F12-25.

25. M. Krüger, S. Kopp, M. Wehland, J. Bauer, S. Baatout, M. Moreels, M. Egli, T. J. Corydon, M. Infanger and D. Grimm, *Acta Astronautica.*, 2019, **159**, 267-272.

26. T. T. Chang and M. Hughes-Fulford, *Am. J. Physiol. Renal Physiol.*, 2009, **15**, 559-567.

27. H. F. Chan, Y. Zhang and K. W. Leong, *Small*, 2016, **12**, 2720-2730.

28. K. Ziolkowska, A. Stelmachowska, R. Kwapiszewski, M. Chudy, A. Dybko and Z. Brzozka, *Biosens. Bioelectron.*, 2013, **40**, 68-74.

29. L. Y. Wu, D. Di Carlo and L. P. Lee, *Biomed Microdevices*, 2008, **10**, 197-202.

30. H. Ota and N. Miki, *Sensors and Actuators A: Physical*, 2011, **169**, 266-273.

31. G. R. Souza, J. R. Molina, R. M. Raphael, M. G. Ozawa, D. J. Stark, C. S. Levin, L. F. Bronk, J. S. Ananta, J. Mandelin, M. M. Georgescu, J. A. Bankson, J. G. Gelovani, T. C. Killian, W. Arap and R. Pasqualini, *Nat. Nanotechnol.*, 2010, **5**, 291-296.

32. V. H. Ho, K. H. Muller, A. Barcza, R. Chen and N. K. Slater, *Biomaterials*, 2010, **31**, 3095-3102.

33. R. Z. Lin, W. C. Chu, C. C. Chiang, C. H. Lai and H. Y. Chang, *Tissue Eng. Part C Methods*, 2008, **14**, 197-205.

34. Lewis, N. S., Lewis, E. E., Mullin, M., Wheadon, H., Dalby, M. J., & Berry, C. C. 2017., 8, 2041731417704428.

35. J. A. Kim, J. H. Choi, M. Kim, W. J. Rhee, B. Son, H. K. Jung and T. H. Park, *Biomaterials*, 2013, **34**, 8555-8563.

36. S. Lemmo, E. Atefi, G. D. Luker and H. Tavana, *Cell Mol. Bioeng.*, 2014, **7**, 344-354.

37. S. Singh and H. Tavana, *Front. Chem.*, 2018, **6**, 379.1-7

38. B. P. Binks and H. Shi, *Langmuir*, 2019, **35**, 4046-4057.

39. B. T. Nguyen, T. Nicolai and L. Benyahia, *Langmuir*, 2013, **29**, 10658-10664.

40. H. Shin, C. Han, J. M. Labuz, J. Kim, J. Kim, S. Cho, Y. S. Gho, S. Takayama and J. Park, *Sci. Rep.*, 2015, **5**, 13103.

41. H. Sakuta, T. Fujimoto, Y. Yamana, Y. Hoda, K. Tsumoto and K. Yoshikawa, *Front. Hem.* 2019, **7**, 44.

42. J. Benavides, O. Aguilar, B. H. Lapizco-Encinas and M. Rito-Palomares, *Chem. Engin. & Technol.,* 2008, **31**, 838-845.

43. V. Ramakrishnan, L. C. Goveas, N. Suralikerimath, C. Jampani, P. M. Halami and B. Narayan, *Biocatal. Agricult. Biotechnol.*, 2016, **6**, 19-27.

44. E. Atefi, R. Joshi, J. A. Mann, Jr. and H. Tavana, *ACS Appl. Mater. Interf.*, 2015, **7**, 21305-21314.

45. S. P. M. Ventura, R. L. F. de Barros, J. M. de Pinho Barbosa, C. M. F. Soares, Á. S. Lima and J. A. P. Coutinho, *Green Chem.*, 2012, **14**, 734–740.

46. M. Rito-Palomares, *J.Chromatogr.B Analyt Technol. Biomed. Life Sci.*, 2004, **807**, 3-11.

47. J. M. Cabral, *Adv. Biochem. Eng. Biotechnol.*, 2007, **106**, 151-171.

48. B. U. Moon, D. K. Hwang and S. S. Tsai, *Lab Chip*, 2016, **16**, 2601-2608.

49. S. Álvaro, G. Marín, S. Vincent, Á. G. Marín, W. V. Hoeve, P. García-sánchez, N. Convine, A. Rosser-james, M. Tyler, K. Bandoo, L. Warncke, A. Lee and V. Vogel, *Lab on a Chip*, 2013, **15**, 4491-4498.

50. Y. Liu, N. O. Nambu and M. Taya, *Biomed. Microdevices*, 2017, **19**, 55.

51. D. Lee and C. Cha, Pharmaceutics, 2018, 10, 229.

52. J. A. De Lora, F. A. Fencl, A. D. Y. Macias Gonzalez, A. Bandegi, R. Foudazi, G. P. Lopez, A. P. Shreve and N. J. Carroll, *ACS Appl. Bio Mater.*, 2019, **2**, 4097-4105.

53. S. L. Ham, E. Atefi, D. Fyffe and H. Tavana, *J. Vis. Exp.*, 2015, DOI: 10.3791/52754, e52754.

54. K. Zhu, Y. Yu, Y. Cheng, C. Tian, G. Zhao and Y. Zhao, *ACS Appl. Mater. Interf.*, 2019, **11**, 4826-4832.

55. C. Han, S. Takayama and J. Park, *Sci.Rep.*, 2015, **5**, 11891.

56. E. Atefi, S. Lemmo, D. Fyffe, G. D. Luker and H. Tavana, *Adv. Funct. Mater.*, 2014, **24**, 6509-6515.

57. Ham SL, Joshi R, Luker GD, Tavana H. Adv Healthc Mater. 2016;**5**:2788-2798.

58. Tavana, Hossein, Andreja Jovic, Bobak Mosadegh, Queenie A. Y. Lee, X-F Liu, K. E. Luker, G. D. Luker, Stephen J Weiss and Shuichi Takayama. Nature Mater.2009,8,736-741

59. G. Balakrishnan, T. Nicolai, L. Benyahia and D. Durand, *Langmuir*, 2012, **28**, 5921-5926.

60. L.-H. Xue, C.-Y. Xie, S.-X. Meng, R.-X. Bai, X. Yang, Y. Wang, S. Wang, B. P. Binks, T. Guo and T. Meng, *ACS Macro Lett.*, 2017, **6**, 679-683.

61. P. Singh, B. Medronho, M. G. Miguel and J. Esquena, *Food Hydrocolloids*, 2018, **75**, 41-50.

62. A. A. K. Das, B. W. Filby, D. A. Geddes, D. Legrande and V. N. Paunov, *Mater. Horiz.*, 2017, **4**, 1196-1200.

63. S. B. G. Celik, S. R. Dominici, B. W. Filby, A. A. K. Das, L. A. Madden and V. N. Paunov, *Biomimetics*, 2019, **4**, 50.

64. H. F. Lu, K. N. Chua, P. C. Zhang, W. S. Lim, S. Ramakrishna, K. W. Leong and H. Q. Mao, *Acta Biomater.*, 2005, **1**, 399-410.

65. A. Y. Hsiao, Y. S. Torisawa, Y. C. Tung, S. Sud, R. S. Taichman, K. J. Pienta and S. Takayama, *Biomaterials*, 2009, **30**, 3020-3027.

66. X. Yang, X. Wang, X. Huang, R. Hang, X. Zhang and B. Tang, *J. Mater. Sci. Mater. Med.*, 2017, **28**, 139.

67. J. Liu, L. A. Kuznetsova, G. O. Edwards, J. Xu, M. Ma, W. M. Purcell, S. K. Jackson and W. T. Coakley, *J. Cell. Biochem.*, 2007, **102**, 1180-1189.

68. K. Ohashi, T. Yokoyama, M. Yamato, H. Kuge, H. Kanehiro, M. Tsutsumi, T. Amanuma, H. Iwata, J. Yang, T. Okano and Y. Nakajima, *Nat. Med.*, 2007, **13**, 880-885.

69. S. C. Ramaiahgari, M. W. den Braver, B. Herpers, V. Terpstra, J. N. Commandeur, B. van de Water and L. S. Price, *Arch. Toxicol.*, 2014, **88**, 1083-1095.

70. A. C. Y. Chua, A. Ananthanarayanan, J. J. Y. Ong, J. Y. Wong, A. Yip, N. H. Singh, Y. Qu, L. Dembele, M. McMillian, R. Ubalee, S. Davidson, A. Tungtaeng, R. Imerbsin, K. Gupta, C. Andolina, F. Lee, S. W. T. K, F. Nosten, B. Russell, A. Lange, T. T. Diagana, L. Renia, B. K. S. Yeung, H. Yu and P. Bifani, *Biomaterials*, 2019, **216**, 119221.

71. J. Gu, X. Shi, Y. Zhang, X. Chu, H. Hang and Y. Ding, *Hepatol. Res.*, 2009, **39**, 398-407.

72. A. M. Laib, A. Bartol, A. Alajati, T. Korff, H. Weber and H. G. Augustin, *Nature Protocols*, 2009, **4**, 1202-1215.

73. G. Mehta, A. Y. Hsiao, M. Ingram, G. D. Luker and S. Takayama, *J. Control Release*, 2012, **164**, 192-204.

74. T. Rodrigues, B. Kundu, J. Silva-Correia, S. C. Kundu, J. M. Oliveira, R. L. Reis and V. M. Correlo, *Pharmacol. Ther.*, 2018, **184**, 201-211.

75. M. Upreti, A. Jamshidi-Parsian, N. A. Koonce, J. S. Webber, S. K. Sharma, A. A. Asea, M. J. Mader and R. J. Griffin, *Transl. Oncol.*, 2011, **4**, 365-376.

76. J. Debnath and J. S. Brugge, *Nat. Rev. Cancer*, 2005, **5**, 675-688.

77. G. M. Thurber, M. M. Schmidt and K. D. Wittrup, *Adv. Drug Deliv. Rev.*, 2008, **60**, 1421-1434.

78. X. Ma, X. Qu, W. Zhu, Y. S. Li, S. Yuan, H. Zhang, J. Liu, P. Wang, C. S. Lai, F. Zanella, G. S. Feng, F. Sheikh, S. Chien and S. Chen, *Proc. Natl. Acad. Sci. U S A*, 2016, **113**, 2206-2211.

79. G. Lazzari, V. Nicolas, M. Matsusaki, M. Akashi, P. Couvreur and S. Mura, *Acta Biomater.*, 2018, **78**, 296-307.

80. T. R. Olsen, B. Mattix, M. Casco, A. Herbst, C. Williams, A. Tarasidis, D. Simionescu, R. P. Visconti and F. Alexis, *Acta* Biomater., 2015, **13**, 188-198.

81. A. C. Daquinag, G. R. Souza and M. G. Kolonin, Tissue Eng. Part C Methods, 2013, **19**, 336-344.

82. A. Alajati, A. M. Laib, H. Weber, A. M. Boos, A. Bartol, K. Ikenberg, T. Korff, H. Zentgraf, C. Obodozie, R. Graeser, S. Christian, G. Finkenzeller, G. B. Stark, M. Heroult and H. G. Augustin, Nat. Meth., 2008, **5**, 439-445.

83. A. A. Chen, D. K. Thomas, L. L. Ong, R. E. Schwartz, T. R. Golub and S. N. Bhatia, Proc. Natl. Acad. Sci. U S A, 2011, 108, 11842-11847.

84. A. P. Rago, D. M. Dean and J. R. Morgan, *Biotechnol. Bioeng*., 2009, **102**, 1231-1241.

85. B. M. Mattix, T. R. Olsen, M. Casco, L. Reese, J. T. Poole, J. Zhang, R. P. Visconti, A. Simionescu, D. T. Simionescu and F. Alexis, *Biomaterials*, 2014, **35**, 949-960.

86. M. W. Laschke and M. D. Menger, Trends Biotechnol., 2017, **35**, 133-144.

87. R. F. Fakhrullin, A. I. Zamaleeva, R. T. Minullina, S. A. Konnova and V. N. Paunov, *Chem. Soc. Rev*, 2012, **41**, 4189-4206.

88. R. Agarwal, K.R. Ko, P.F. Gratzer and J. P. Frampton, *MRS Advances*, 2017, **2**, 2443-2449.

89. Gopinathan, J., Noh, I. Recent trends in bioinks for 3D printing. *Biomater Res.,* 2018,**22**, 11

90. R. Noguchi, K. Nakayama, M. Itoh, K. Kamohara, K. Furukawa, J. I. Oyama, K. Node and S. Morita, *J.Heart Lung Transplant*, 2016, **35**, 137-145.

91. J. Bierwolf, T. Volz, M. Lutgehetmann, L. Allweiss, K. Riecken, M. Warlich, B. Fehse, J. C. Kalff, M. Dandri and J. M. Pollok, *Tissue Eng. Part A*, 2016, **22**, 742-753.

92. Y. Yamaguchi, J. Ohno, A. Sato, H. Kido and T. Fukushima, *BMC Biotechnol*., 2014, **14**, 105.1-10.

93. N. Lebonvallet, N. Boulais, C. Le Gall, U. Pereira, D. Gauche, E. Gobin, J. O. Pers, C. Jeanmaire, L. Danoux, G. Pauly and L. Misery, *Exp. Dermatol*., 2012, **21**, 156-158.

94. C. S. Ong, X. Zhou, J. Han, C. Y. Huang, A. Nashed, S. Khatri, G. Mattson, T. Fukunishi, H. Zhang and N. Hibino, *Biotechnol. Adv*., 2018, **36**, 494-505.

95. S. Suryaprakash, Y. H. Lao, H. Y. Cho, M. Li, H. Y. Ji, D. Shao, H. Hu, C. H. Quek, D. Huang, R. L. Mintz, J. R. Bago, S. D. Hingtgen, K. B. Lee and K. W. Leong, *Nano Lett*., 2019, **19**, 1701-1705.

96. E. Flampouri, S. Imar, O. C. K and B. Singh, ACS Sens., 2019, **4**, 660-669.

97. W. He, S. Yuan, W. H. Zhong, M. A. Siddikee and C. C. Dai, Appl. *Microbiol. Biotechnol*., 2016, **100**, 1109-1119.

98. G. Thouand, Anal. Bioanal. Chem., 2018, **410**, 1189-1190.

99. E. Michelini, M. M. Calabretta, L. Cevenini, A. Lopreside, T. Southworth, D. M. Fontaine, P. Simoni, B. R. Branchini and A. Roda, *Biosens. Bioelectron*., 2019, **123**, 269-277.

100. R.F.-X. Tomasi, S. Sart, T. Champetier, C.N. Baroud, *Cell Rep*., 2020, **31**, 107670.1-13.

101. D.A. Cristaldi, A. Sargenti, S.Bonetti, F. Musmeci, C. Delprete, F. Bacchi, S. Pasqua, C. Cavallo, L. Bonsi, F. Alviano, D. Gazzola and S. Santi, *Micromachines*, 2020, **11**, 465.1-13.

102. Vinken M, Vanhaecke T, Papeleu P, et al. *Cellular signalling*, 2006, **18**,592-600.

103. Hervé, J. C., & Derangeon, M.. Cell and tissue research, 2013,**352**, 21-31.

104. Liu, F., Tan, G., Li, J., Dong, X., Krissansen, G. W., & Sun, X. *Cancer science*, 2007,98, 1381-1387.

2. Chapter2. High-throughput fabrication of hepatic cell clusteroids with enhanced proliferation and functionality

2.1 Abstract:

Basic biological research and therapeutics development can benefit from growing cells as three-dimensional (3D) clusters. The complexity, complication, and expense of 3D cultures, however, are often greater than that of two-dimensional (2D) cultures. In the current state of tissue spheroids production, complex materials are required, tedious facilities must be used, and the process is not scalable. We report a novel inexpensive and up-scalable method for the preparation of large quantities of viable cell clusters (clusteroids) of hepatocytes (Hep-G2). An aqueous two-phase system (ATPS) based on dextran drops and polyethylene oxide particles stabilized with whey protein particles has a high throughput potential for producing water-in-water (w/w) Pickering emulsions. Hep-G2 cell clusteroids were synthesized rapidly using this system. To begin with, the interfacial tension of the aqueous phase is used in this experiment to wrap the cells into compartments, and subsequently to shrink the droplets by adjusting the balance of ATPS, resulting in spherical clustering of the cells. As the 3D clusteroids formed within the Pickering emulsion droplets, cell-cell adhesion was strongly promoted. Once the emulsion had been diluted with culture media, they were collected. Cell proliferation and function of hepatic clusteroids under the same conditions were evaluated by incorporating them into an alginate hydrogel. As we found, the clusteroid-based tissues had higher levels of urea and albumin production than those with individual cells, both of which are associated with hepatocyte cell function. In addition to tissue generation, this methodology could potentially be used to prepare large quantities of organoids for drug tests and to replace animal models in drug development

2.2 Introduction

In addition to metabolizing and excreting numerous xenobiotics, the liver processes a number of environmental pollutants. It is also possible for some of these xenobiotics to cause liver injury during detoxification.[1] A robust system for xenobiotic assessment is needed, especially in the early stages of research and development, to support a variety of

industries, such as pharmaceuticals, agrochemicals, industrial chemicals, and consumer products.[2] With about 21% of drug attrition attributed to toxicity during development, adverse drug reactions are a significant hindrance to the improvement of novel therapeutics.[3] ADRs are a major cause of liver injury and are responsible for up to 7% of hospital admissions. Druginduced liver injury (DILI), one of the most common forms of ADRs, is the main reason for the withdrawal of drugs from the market.[3–5] These reactions are complicated and often require interactions between the multiplex of parenchymal hepatocytes and non-parenchymal cells such as stellate cells (SCs), Kupffer cells (KCs), liver sinusoidal endothelial cells (LSECs), etc. A wide range of symptoms characterize DILI, including impaired mitochondrial function, chronic inflammation, apoptosis, necrosis, and microvesicular steatosis and cholestasis.[6] The pharmaceutical industry is highly interested in *in vitro* liver models capable of predicting potentially adverse liver manifestations.[7] Various surgical options have been explored to increase the number of livers available for transplant, including split liver transplants and partial liver transplants from living relatives.[8] However, despite these advances in surgery and improved allocation of organs, organ shortages persist, making liver transplantation alone unlikely to meet the growing need. As an alternative to organ transplantation, cell-based therapies have long demonstrated promise. 3D cell models are available to biomedical researchers today in several forms. Organotypic explants are newly dissected tissues preserved *in vitro* and closely resemble native tissues.[9] Biomedical research fields have used tissue explants for decades and they will likely not be replaced by other 3D culture models anytime soon. In addition to difficult specimen acquisition and ethical approval, such a model faces several major challenges. The size of tissue explants is typically several millimetres, which hinders nutrient transport to central regions. As a practical alternative to tissue explants and drug testing platforms, a 3D culture model that is easy to prepare and on a scale of 100-500 μm would be useful. It is common practice to use hanging-drop culture and 3D culturing in microwells in order to control the size of individual spheroids.[10-12] For forming similar sized tissue spheres, alternative techniques use microrotational flow and the magneto-Archimedes effect.[13,14] Cellosome production methods could also be used for the large-scale production of desired spheroids using current techniques.[15,16] A number of natural biopolymers have been successfully used to

encapsulate cells in such structures, including alginate, pectin, agarose, and chitosan.[17] Currently, most approaches for creating cell spheroids cannot be used to engineer tissues since they require large-scale production. There is a need for a reliable and affordable technology that can produce spheroid in high quantities quickly and cheaply. Aqueous two-phase systems (ATPS) have previously been used to make tumouroids, mainly by distributing dextran-rich drops (DEX) and tumour cells to a polyethylene glycol rich aqueous medium (PEG). [12,18,19] These DEX drops contain isolated tumour cells that have been cultured into individual globules and tested for their response to drug therapy.[12,20–22] Compared to globules cultured in 2D, this technique has been found to produce higher levels of chemotherapeutic drug resistance.[19] Although tumor spheroids have been successfully produced in the past to study drug efficacy, this study created large spheroids that would have a necrotic core and proliferating cells. These methods are not scalable in tissue engineering (TE) applications when producing large numbers of cell spheroids because of technical limitations. As a result of trapping human embryonic kidney cells (HEK293) in w/w Pickering emulsion droplets, Das et al. have successfully produced tissue globules from human embryonic kidney cells (HEK293).[23,24] Pickering emulsions are formed by mixing equal parts of oil and water. The cells are divided efficiently into droplets within the emulsion. To accomplish this, the interfacial tensions in the aqueous DEX phase in the droplets, where proteins partition preferentially, are employed to separate the cells into compartments, then the droplets are shrunk by changing the osmotic balance between the two aqueous phases (ATP), resulting in more spherical cells. These are collected after the break down of the w/w emulsion by subsequent dilution with a growth media. Intending to generate cell clusters with enhanced function, we developed further the method of Das et al.and Celik et al., for the preparation of hepatocyte cell clusters (clusteroids) using w/w Pickering emulsions as templates and explored their formulation in suitable hydrogel matrix for 3D tissue engineering of the liver graft. [23,24] For the production of hepatocyte spheroids, three-dimensional cultures of human adult hepatocytes (Hep-G2) were used. A blueprint for growing liver cells from patients and fabricating autologous cell clusteroids could be developed using this methodology. Specifically, this work examines the materials and techniques for determining the average size of clusteroids of hepatocytes formed out of

emulsion drop templates. This technique is capable of producing large quantities of viable hepatocyte clusteroids. The clusteroids that we have been able to fabricate by our Pickering emulsion templating in conjunction with our w/w Pickering emulsion techniques enable the hepatic cells to grow at a faster rate, resulting in higher albumin and urea production as well.

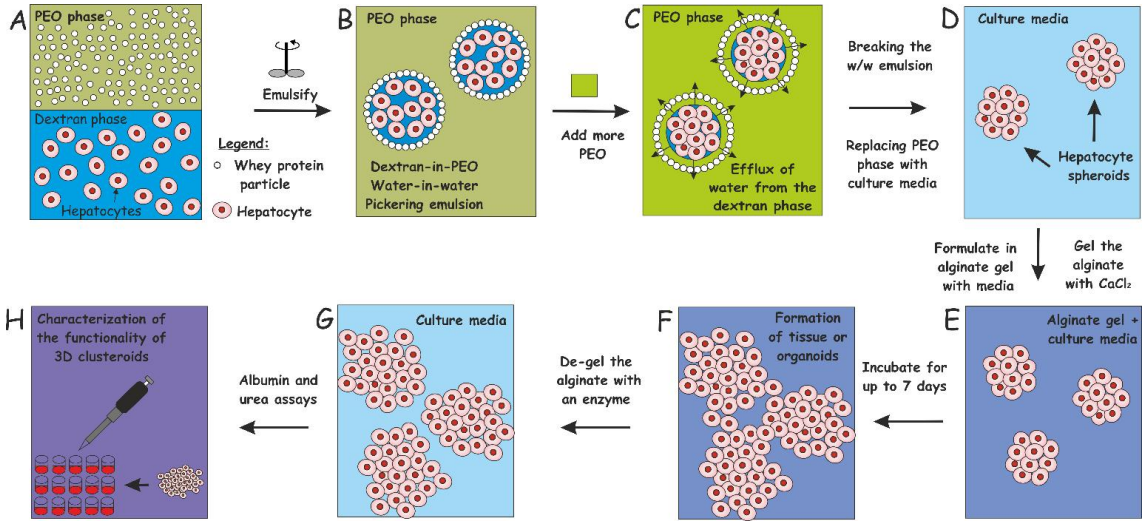

Figure 2.1 Schematics of our high-throughput method for the preparation of hepatocyte cell spheroids (A-D) and 3D tissues culturing (D-F) with characterization (G–H). The hepatocyte cells are encapsulated in a dextran-PEO water-in-water emulsion template stabilized by 2 wt% whey protein (WP) particles. The continuous phase is PEO 5.5wt% and the dispersed phase is composed of cells encapsulated in 5.5% dextran droplets. Upon emulsification, the cells prefer the discontinuous dextran phase, which allows their encapsulation. Adding a more concentrated PEO phase causes osmotic shrinking of the cell-rich dextran drops, whose interfacial tension packs the cells into tissue spheroids. The latter are isolated by breaking the emulsion by dilution with culture media.

2.3 Materials and methods

2.3.1 Materials

Deionized water purified by reverse osmosis and ion exchange using a Milli-Q water system (Millipore) was used in all our studies. Dextran (MW 500 kDa) and PEO (MW

200 kDa) were both purchased from Sigma-Aldrich. Whey protein was sourced from No1. Supplements, Suffolk, UK. Fluorescein diacetate (FDA, 98%) and sodium alginate and Cornings Transwells polyester membrane cell culture inserts (12 mm, 12 well plates) were purchased from Sigma-Aldrich, UK. Sodium chloride (99.8%) and calcium chloride were purchased from Fisher Scientific. Eagle's Modified Eagle Medium (EMEM) and Trypsin–EDTA were sourced from Gibcos, Fisher Scientific. NUNC Cell culture 24-well plates were purchased from Thermo Fisher Scientific. Urea and albumin ELISA kit were purchased from Sigma-Aldrich. Fetal bovine serum (FBS, Labtech, Heathfield, UK) 0.25% Trypsin–EDTA (1X, Lonza). Alginate lyase was purchased from Sigma Aldrich. All other chemicals were of analytical grade.

2.3.2 Method

2.3.2.1 2D Hep-G2 cell culture

Hep-G2 cell line culture was purchased from Public Health England (PHE, Culture collection 85011430 Hep G2) cultured from growing cells. The cells were cultured in EMEM media supplemented with 10% FBS and placed in an incubator (37 ^{o}C, 5% CO_2) After reaching 80% confluence, Hep-G2 cells were carefully washed with phosphate buffer saline (PBS, Labtech, UK) for 10 s and then incubated with 0.25% Trypsin–EDTA (1X, Lonza, UK), which allowed us to detach the cells from their support after 5 min. Its action was neutralized by adding complete EMEM medium before centrifugation at 400 g for 4 min. After resuspension in fresh medium, the Hep-G2 cells were reseeded in tissue culture flasks (Sarstedt, UK).

2.3.2.2 Preparation of whey protein (WP) particles

Whey protein powder was dissolved in water at a concentration of 2 wt% for 2 h under agitation. The solution was placed at 4^{o}C for 12 h to fully hydrate the whey protein. Then, the solution was centrifuged at 10800 g for 1 h and the supernatant was collected. A solution of 300 mM NaCl was prepared and mixed with an equal volume of WP solution. The pH was adjusted to the required value by drop-wise addition of filtered 0.5 M HCl aqueous solution. After heating the WP/NaCl solution in an oil bath at 85^{o}C for 15 min, it was left to cool at 4^{o}C. This precipitation process produced WP particles, which were used in our protocol as stabilizers for the waterin-water Pickering emulsions.

2.3.2.3 Production of hepatic cell clusteroids

The cell clusteroid fabrication process was somewhat similar to the procedure described in ref. [23] and [24]. Briefly, PEO aqueous solution (5.5 wt%) was prepared by dissolving PEO into the heat-treated solution of WP, which constituted the continuous phase of the water-in-water emulsion. Centrifugation of the PEO solution was done beforehand at 5000 g for 7 min to remove the silica nanoparticles from the PEO solution, which have been added by the manufacturer. A solution of 5.5 wt% dextran (in total) in EMEM complete medium under sterile conditions was used as a disperse phase (DEX phase) together with the Hep-G2 cells. The DEX phase with the hepatocytes formed different volume fractions with respect to the DEX/PEO w/w emulsion. To form the latter, the DEX phase was mixed with the pelleted cells and then was transferred to the WP/NaCl/ PEO solution, and gently homogenized using two pumps with a BD Microlancet 3, 6 or 12 needles (21G 12, internal diameter 0.512 mm) and a BD Plastipak™ syringe of 5 mL using two pumps (BD biosciences, Wokingham, UK). The w/w emulsion was prepared using PEO and DEX phases at various volume fractions of the two phases. The emulsion was further mixed with an aliquot of PEO solution of higher concentration (14 wt% PEO) to reach a total concentration of 10% in order to osmotically squeeze the DEX droplets with the cells into densely packed clusteroids. The cell clusters were left in the emulsion for 2 h to achieve better cell–cell adhesion and stick together. The emulsion would then be broken down by adding ten times higher volume of EMEM medium, and the cell clusteroids were settled by gravity driven sedimentation.[25]

2.3.2.4 3D hepatocyte clusteroids culture

An aqueous solution of 2 wt% sodium alginate was prepared and then sterilized in an autoclave. EMEM complete medium was mixed with the 2 wt% sodium alginate solution at different volumes to vary the gelling agent overall concentration. Hep-G2 cell clusteroids were then carefully resuspended in this solution and seeded on 24-well tissue culture plates. The addition of 2 wt% $CaCl_2$ (aq) allowed the crosslinking of the alginate chains in the media and formation of a hydrogel. After 2 min of incubation, the $CaCl_2$ solution was carefully pipetted out without compromising the integrity of the hydrogel–clusteroid composite and the wells were topped up with EMEM medium. The $Ca2^+$ ions were used for the crosslinking of the alginate hydrogel. The excess $CaCl_2$ solution was

removed after the hydrogel formation. The crosslinking process takes no longer than 2 min which had a very marginal impact on the embedded cells.

2.3.2.5 Optical microscopy

The microstructure of w/w Pickering emulsion at different fDEX ratios and the resulting clusteroids at different forms were first analyzed using a fluorescence microscope (Olympus BX51), and samples were observed under various water immersion objectives at ambient temperature (25 ^{o}C). Briefly, 30 mL dispersions were shifted and spread onto the hollow glass slide, which was then enclosed by the glass cover.

2.3.2.6 WP particle size distribution measurement

The WP particle size was measured after diluting (100) the samples with purified water to an appropriate particle concentration using the Zetasizer Nano ZS (Malvern Instruments Ltd., Malvern, Worcestershire, UK) and Malvern MasterSizer 3000. All measurements were carried out at room temperature and the reported results were the averages of three readings.

2.3.2.7 Cell viability assay

Cell clusteroids were treated with a 5 g L^{-1} solution of fluorescein diacetate (FDA, from Sigma-Aldrich) in acetone (10 mL of solution per 1 mL of the dispersion of re-suspended clusteroids) to evaluate cell viability. After 10 min of incubation at room temperature in the dark, the sample was observed using an Olympus BX-51 fluorescence microscope (Olympus) with a DP70 digital camera and FITC fluorescence filter set. FDA is known to diffuse through cell membranes and only viable cells are able to hydrolyze non-fluorescent FDA internally to fluorescein by intracellular esterases. Since fluorescein dissociates in water, its crossing of the cell membranes is hindered by its ionic charge, which results in the accumulation of the fluorescent by-product inside the intact cells.[23,24] This indicates that the cell membranes are intact and the cells are viable.

2.3.2.8 Urea and albumin production assays

Analyses based on diacetylmonoxime and acid- and heat-catalyzed condensation of urea with diacetylmonoxime were carried out to determine the levels of urea in the samples. Based on the manufacturer's protocol, 100 mL of the cell culture medium was collected, homogenized with the urea assay buffer, and then analyzed. After de-gelling

the sample, albumin was tested because alginate gel might interfere with albumin readings.[41] In brief, each well was incubated at 37°C for 30 min after adding 1 mL of 5 mg mL1 alginate lyase. Based on the manufacturer's instructions, the ELISA method was used to measure albumin content in the degelled media. Horseradish peroxidase was used to detect the peroxidase and the substrate used to detect it was 3,3,5,5-tetramethylbenzidine to detect the peroxidase. A Synergy HT plate reader was used to calculate absorbance (450 nm) and a standard curve was used to quantify values. The samples were taken 72 hours after the initial seeding of the cells in a 2D culture. To achieve optimal growth in 3D cultures, the culture media must be changed every day, so 24 h cumulative albumin secretion was measured at days 1, 2, 3, 4, 5, 6 and 7.

2.3.2.9 Cryo-SEM imaging

The morphology of the clusteroids was revealed by cryo-scanning electron microscopy (Cryo-SEM). After the aqueous solution was evaporated, patches of fixed cell clusteroids were prepared for Cryo-SEM imaging. As part of this study, aliquots of 1 mL of the Hep-G2 cell clusteroids were deposited on dry Aclart sheets (Agar Scientific Ltd, Essex, UK) or poly-lysine coated glass coverslips, and then treated with 2% glutaraldehyde for 1 h, washed multiple times with Mill-Q water, and then dried at critical point. The samples were then imaged using a Cryo-scanning electron microscope SEM (ZEISS EVO 60 EPSEM).

2.3.2.10 Crystal Violet staining

The 96-well plates were stained with Crystal Violet (CV) by adding 130 mL to each cell. The 96-well plates were then incubated for 30 min at room temperature and then rinsed 3 times by gentle submersion in water and allowed to dry overnight. After the wells were fully dried, the CV was solubilised by adding 125 mL from a stock solution of 30% acetic acid in deionized water to each cell in the 96-well plates. The solubilised CV solution was then transferred to new 96-well plates and absorbance readings were taken using the Bio-Tek Synergy HT Multi-Detection Microplate Reader at 550 nm. The 30% stock solution of acetic acid was used as a blank. The absorbance readings were then normalised.

2.3.2.11 Statistical analysis

Comparisons were made using unpaired t-tests or analysis of variance as appropriate with significance set at $p < 0.05$.

2.4 Results and discussion

2.4.1.1.1 WP particle characterization

It was previously demonstrated that emulsions containing preheated and aggregated proteins were more stable than those containing native proteins.[26–28] It makes proteins aggregate at the interface between continuous and dispersed aqueous phases, making them stronger adsorbers. The whey protein particles are a biocompatible stabilizer of the w/w Pickering emulsions. These molecules play a crucial role in preventing DEX droplets dispersed in the PEO phase from coalescing, which causes emulsion breakdown. Due to poor emulsion stability and an absence of protein particles, phase separation occurs very quickly.[24,28,29] This results in poorly reproducible results without a particle stabilizer. We were able to handle the cell-loaded emulsions over the selected time interval with the Pickering emulsions in the presence of the whey protein particles, thereby producing cell clusteroids with reproducible average sizes. The size of droplets has been found to increase with the radius of protein particles over 85 nm.[28] Using our methodology, we produced WP particles that were characterized before being used to stabilize w/w Pickering emulsions. **Figure 2.2** shows the typical particle size distribution of WP particles at different pH values. The WP particles were most homogeneous at pH 6.18, with an average particle size of 130 nm. As a result, pH 6.18 was chosen for preparing WP particles for the following experiments. Our experiments tested DEX-in-PEO emulsions without WP particle stabilizers and found that none were stable. In a study conducted by Balakrishnan et al., DEX/PEO aqueous two phase system with other protein particles without encapsulated cells has been thoroughly investigated.[33] There is a high level of stability with these systems and they can last for days. This study is not applicable to water-in-water Pickering emulsions devoid of cells since their behavior differs from those containing cells.

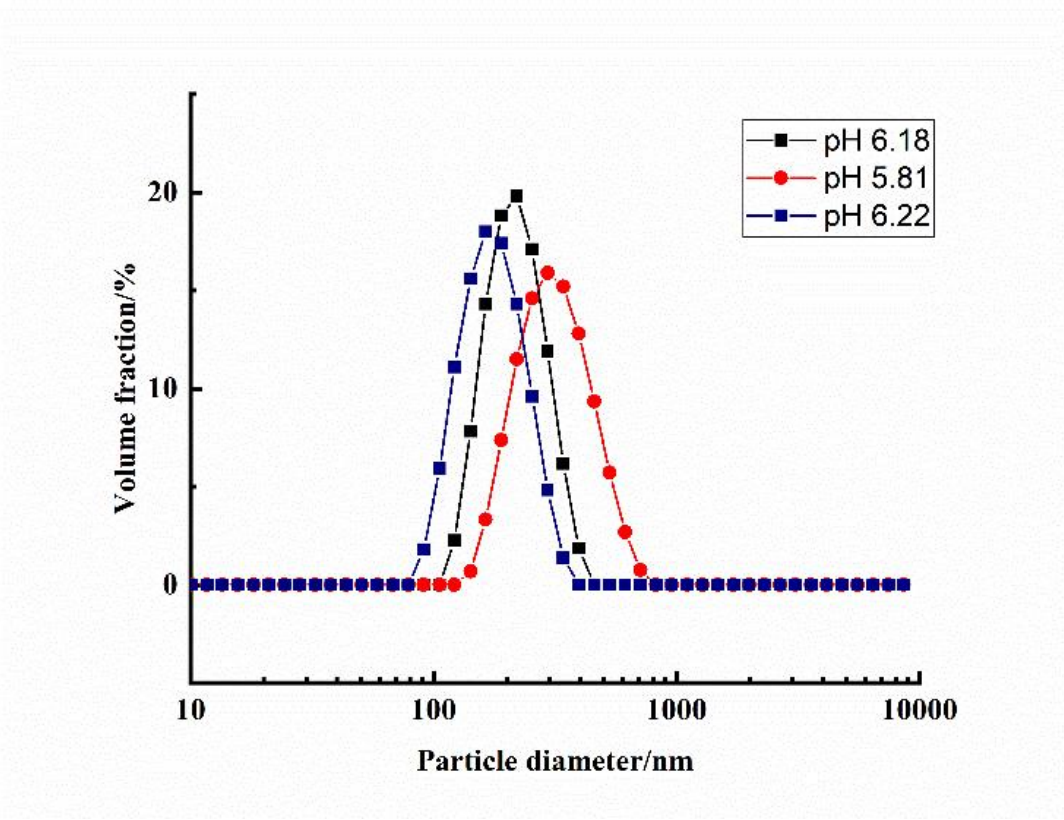

Figure 2.2 The distribution of the hydrodynamic diameter of the produced WP particles at different pH.

2.4.2 Water-in-water emulsion characterization

In order to control the size of the DEX droplets, Pickering w/w emulsions of different volume fractions of the DEX phase were produced: f = 0.1, 0.11, 0.125, 0.14, 0.17, 0.2, 0.25, 0.33 and 0.5. The images shown in **Figure 2. 3** demonstrate that the variation of the DEX phase volume has a strong impact on the emulsion droplet size. The average size of the DEX emulsion droplets with fDEX = 0.5 was about 80 μm, with a sharp decrease to μm when the fDEX decreased to 0.14. After the shrinking stage, the DEX droplets (without any cells) had a similar size distribution around 5 μm at any f ratio, which demonstrates the strong effect of the osmotic pressure driven by the addition of high concentration PEO solution (**Figure 2. 4**). Hence, decreasing the volume fraction of the DEX phase resulted in smaller DEX droplets with the decreased capacity for encapsulating a lower number of cells. The microscopy observation of DEX droplets shown in **Figure 2. 3**, showed that the water-in-water emulsions contain a higher drop

size with φDEX = 0.2 and 0.17. Consequently, φDEX = 0.2 was selected for use in our production of hepatocyte clusteroids in this research.

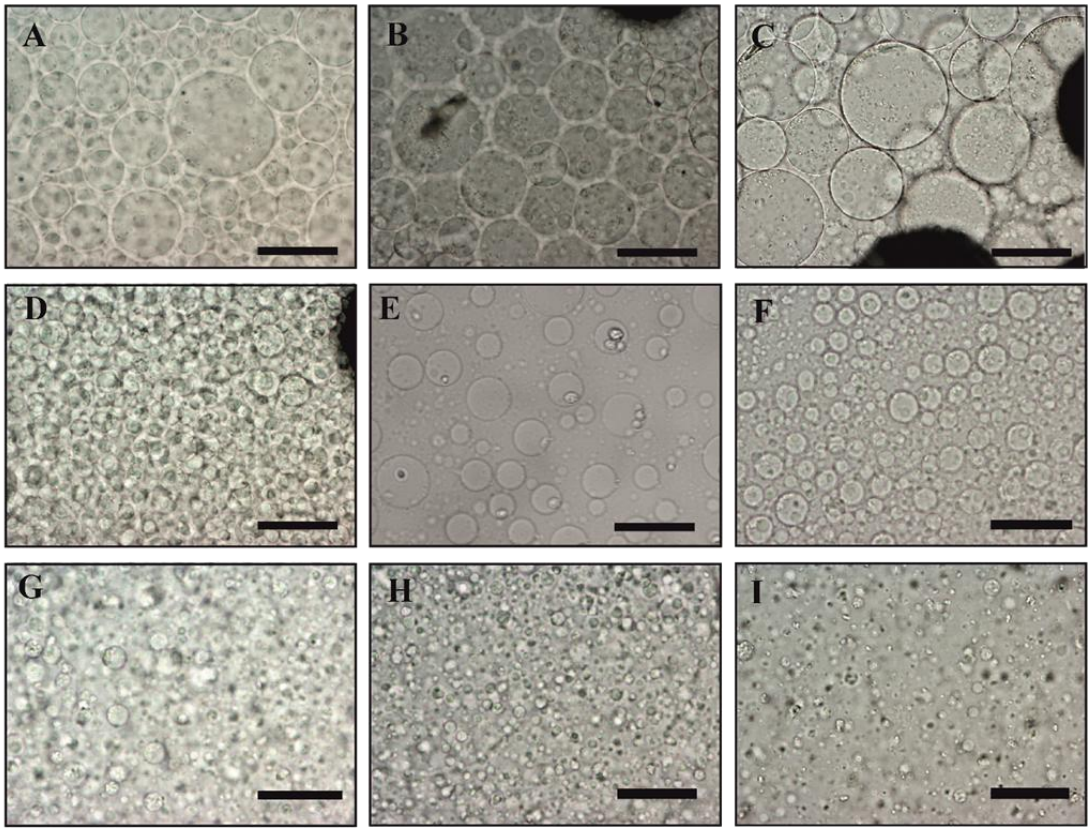

Figure 2.3 Optical microscopy images of a DEX/PEO water-in-water Pickering emulsion (PEO 5.5wt% and DEX 5.5 wt%). (A) ϕ_{DEX} = 0.5, (B) ϕ_{DEX} = 0.33, (c) ϕ_{DEX} = 0.25, (c) ϕ_{DEX} = 0.2 (c), ϕ_{DEX} = 0.17 (c), ϕ_{DEX} = 0.14, ϕ_{DEX} = 0.125, ϕ_{DEX} = 0.11 and ϕ_{DEX} = 0.1, stabilized by 2wt% WP particles at pH 6.18. Scale bars are 100 μm.

2.4.3 Effect of the hepatic cells' encapsulation on the average drop size of the w/w Pickering emulsion

DEX droplet sizes were controlled by using Pickering w/w emulsions with different volumes of the DEX phase: f = 0.1, 0.11, 0.125, 0.14, 0.17, 0.2, 0.25, 0.33 and 0.5. The images shown in **Figure 2. 3** and Figure 2. 4 demonstrate that the variation of the DEX phase volume has a strong impact on the emulsion droplet size. In DEX emulsion droplets with φDEX = 0.5, the average size was 80 μm, decreasing to 5 μm at φDEX = 0.14. In DEX emulsion droplets with φDEX = 0.05, the average size was 80 mm, decreasing to 5 μm at φDEX = 0.14, demonstrating how the osmotic pressure generated

by the addition of a high concentration PEO solution greatly influenced the droplet size. As a consequence, DEX droplets were smaller and had a reduced capacity for encapsulating cells when the volume fraction of the DEX phase was decreased. The microscopy observation of DEX droplets shown in **Figure 2. 3**, showed that the water-in-water emulsions contain a higher drop size with φDEX = 0.2 and 0.17. Consequently, φDEX = 0.2 was selected for use in our production of hepatocyte clusteroids in this research.

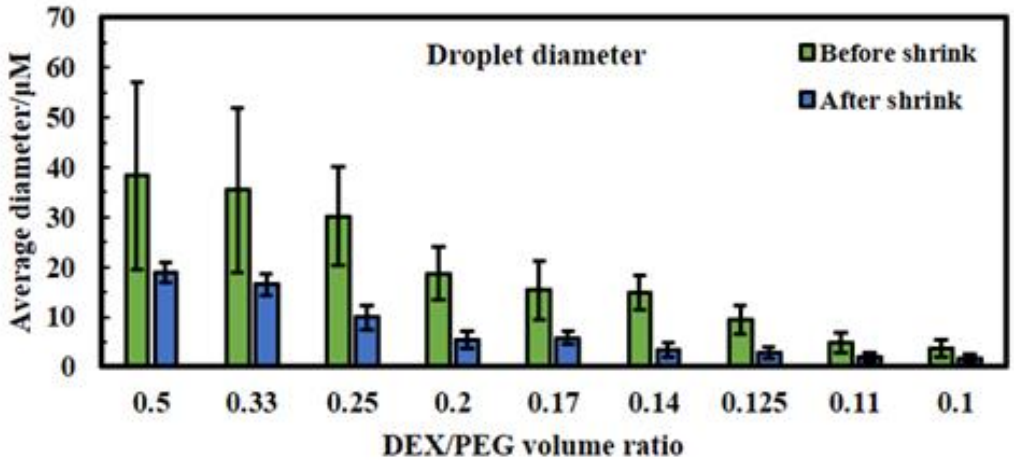

Figure 2.4 Average DEX droplet diameter for the DEX/PEO Pickering emulsion produced from WP/NaCl 300 mM solution at pH 6.18, 5.5wt% PEO/5.5wt% dextran for varying volume fractions of the DEX phase (average of 200–300 individual drops) (A) Before shrinking (B) After shrinking. The data were obtained by optical microscopy measurements of the DEX droplets for each micrograph with Image J software. (Student's t-Test, NS:).

2.4.4 Cell clusteroid formation in DEX-in-PEO emulsions

Research on cancer has recently gained increased interest in three-dimensional cultures of tumour cells. Drug discovery can be facilitated by these spheroids as they mimic various properties of solid tumours and are a useful model for drug discovery.[11,29–31] Celik et al. have studied the effect of DEX/PEO volume fraction on the size of the

HaCaT cell spheroid. [23] In the APTS system, the size of the spheroid depends both on DEX/PEO ratio and on cell concentration. As such phase diagrams are complex, and spheroid size varies with cell type and concentration, scanning the entire range of parameters was not practical. Moreover, the clusteroid's size is affected by osmotic shrinking, i.e. by adding concentrated PEO. Therefore, we adopted the optimized protocol by Celik et al.[23] Currently, this work focuses on demonstrating the enhanced functionality of clusteroids prepared with hepatic cells. We used the ATPS system made with PEO (MW 35 kDa)-DEX (MW 500 kDa) solutions to demonstrate the efficiency of the cell encapsulation. The Hep-G2 cells were suspended in PEG phase solution, and the solution was dispersed and mixed with the suspension. The collected clusteroids were imaged using the microscope, as shown in **Figure2.5-2.7**, and seems compatible in structure and relatively uniform in size, at about 20 μm. By compacting the cells, the osmotic pressure also helps them adhere to one another better and form clusteroids. A w/w emulsion incubated with Hep-G2 cells allows them to form compact clusteroids within one hour. We then examined spheroid formation with each of the four two phases solutions after 1 hour. The longer-term culture was then tested for viability. Initially, the FDA live/dead assay was used to test the viability of the hepatic cell spheroids and single cells before they were added to the gel. It can be seen from **Figure 2.8** that the viability of the individual (single) cell, as well as the viability of the clusteroids, is the same. As a result, our preparation method has no effect on the viability of cells within the clusteroids. Based on these results, combined with those of water-in-water emulsion, it appears that DEX drop shrinking concentrations of 0.2 and 10% PEO are appropriate for preparing clusteroids of Hep-G2 cells. The following study was conducted using this composition

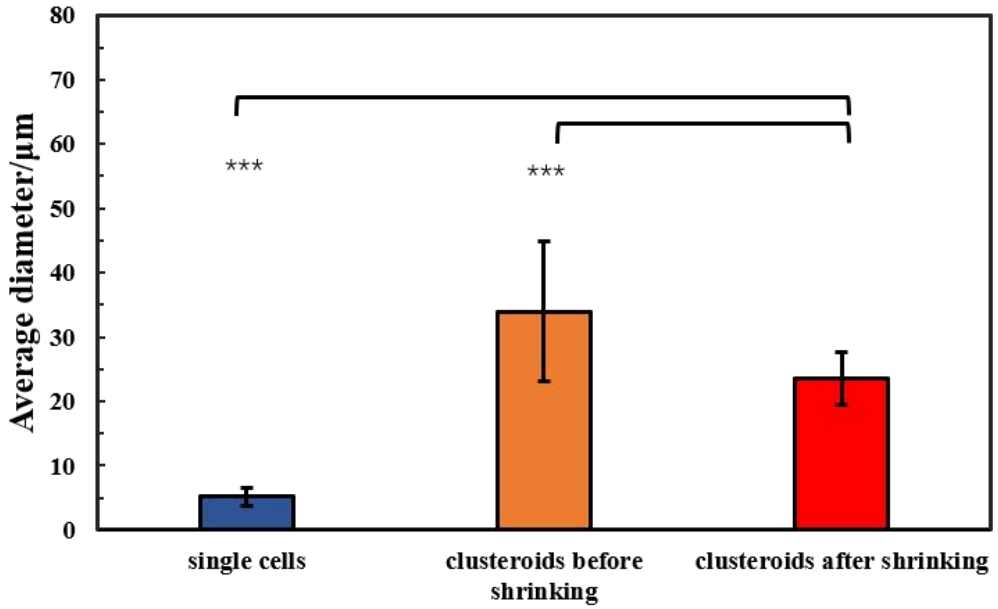

Figure 2.5 Average diameter of Hep-G2 cell clusteroids and drops with encapsulated cells(average of 100–200 individual clusteroids). The data were obtained by optical microscopy measurements of clusteroids for each micrograph with ImageJ Software (Student's t-Test, NS: Non-significant, **p<0.01, ***p < 0.001).

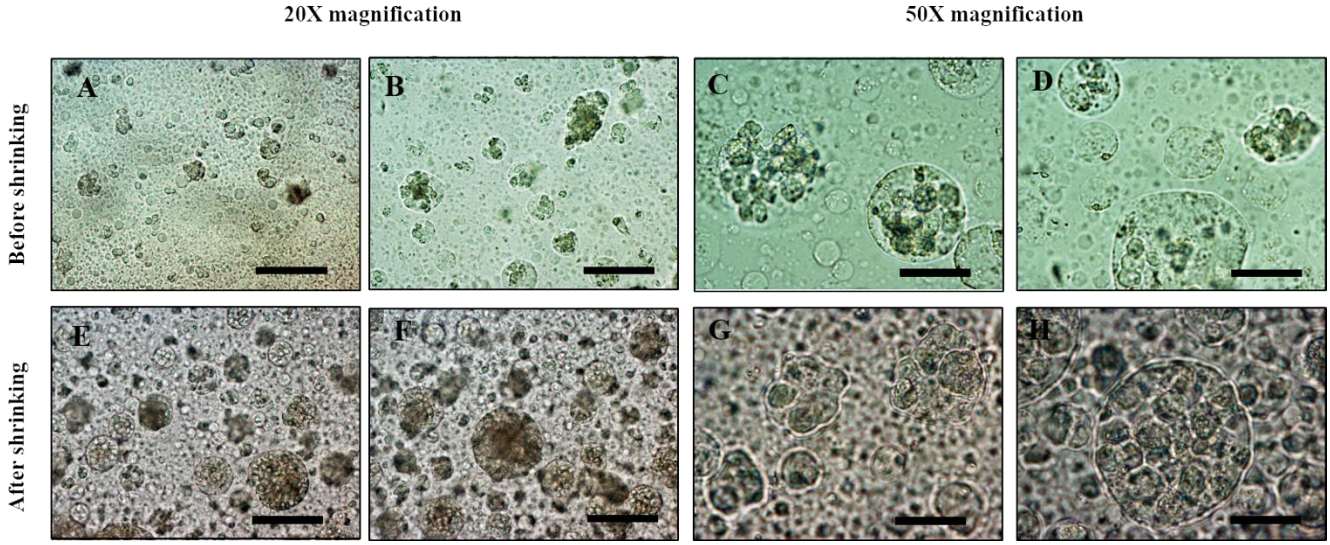

Figure 2.6 Optical microscopy images of (A, B, C, D) Hep-G2 cell-loaded droplets (before shrinkage) and (E, F, G, H) Hep-G2 cell clusteroids obtained (after shrinkage of the DEX phase). The initial w/w emulsion was stabilized by 2 wt% WP particles with 5.5 wt% PEO/5.5 wt% Dextran. Here the DEX volume fraction was $\phi_{DEX} = 0.2$. Scale bars are 50 µm for (A, B, E, F). The bar of (C, D, G, H) is 50µm

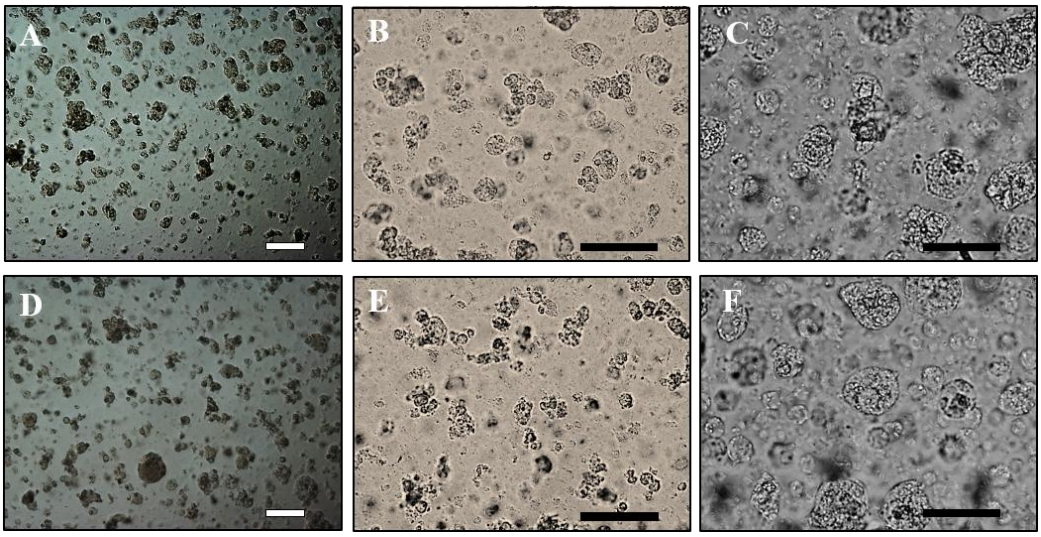

Figure 2.7. Optical microscopy images of Hep-G2 cell droplets encapsulated in the DEX/PEO water-in-water emulsions after shrinkage stabilized by 2 wt% WP particles at different magnification. Scale bars are (A,B,D,E) 100 μm and (C,F) 50μm.

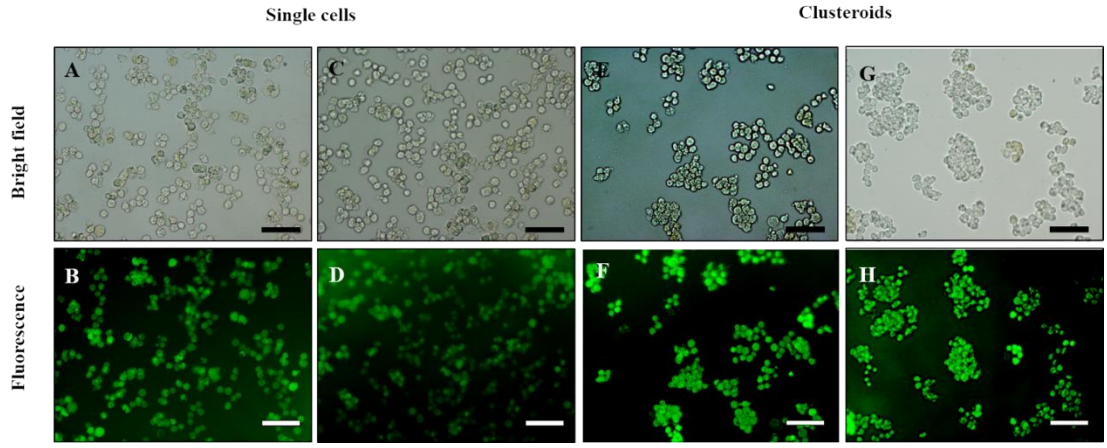

Figure 2.8. (A, C) Optical bright-field microscopy images and (B, D) fluorescence microscopy images of single Hep-G2 cells after being treated with FDA live/dead assay. (E, G) Optical bright-field images and (F, H) fluorescence microscope images (F, H) of Hep-g2 cell clusteroids treated with 1 mM FDA. FDA treatment was done after the cell clusteroids fabrication. The green fluorescence indicates that both the Hep-G2 cells preserve their viability during the clusteroids fabrication process (**Figure 1**). The scale bar is 100 μm.

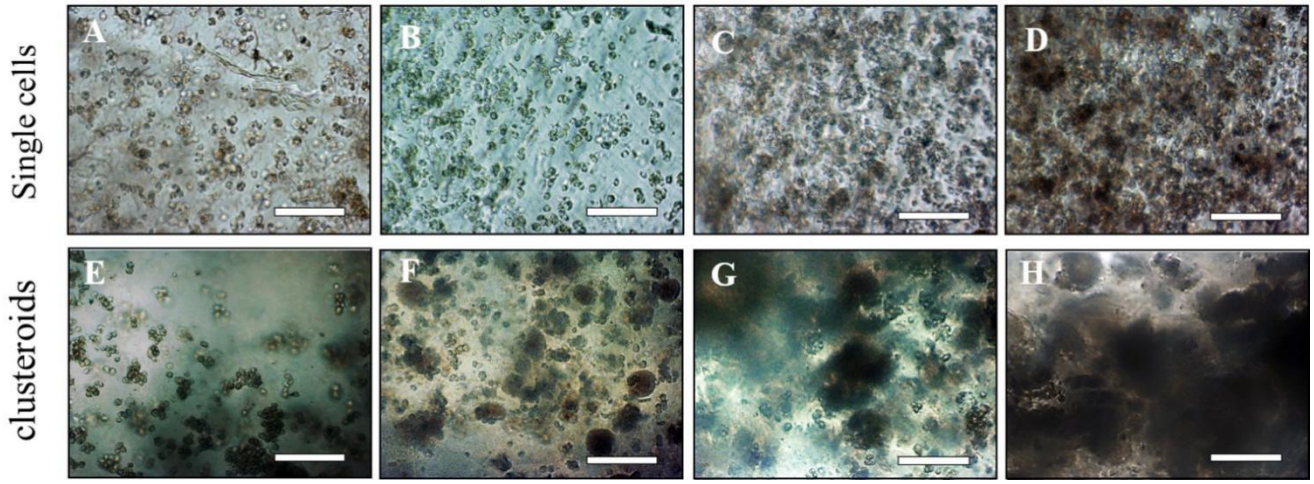

Figure 2.9. Bright-field optical microscope images of (A, B, C, D) monolayer cultured single Hep-G2 cells (E, F, G, H) Hep-G2 clusteroids isolated by a dilution of the DEX/PEO emulsion by a factor 3 with EMEM medium and incorporated with 1 wt% sodium alginate in EMEM media followed by cross-linking with 1M CaCl_2. The Hep-G2 cells clusteroids were cultured in the alginate film for seven days under EMEM media and images were taken from each well to determine the average clusteroids size. Scale bars are 100 μm

2.4.5 Hepatic clusteroid growth during long-term culture

The assay was tested for compatibility with longer-term culture. Within 50 mL DEX drops immersed in the PEO phase, clusteroids of $1x10^6$ to $1x10^5$ mL1 were generated, and then they were injected into alginate hydrogel fortified with 1 M $CaCl_2$. In each condition, 12 replicates were set up, which is half of a 24-well plate. The growth medium was added to the wells every 24 hours after the old medium was removed after growing the clusteroids within each well for 24 hours. In this way, clusteroids removed each day's urea and albumin from the culture without accumulating it. Clusteroids were imaged every other day. **Figure 2.9** contains images showing that after three days of their growth, the cells change from a cluster of individual cells to thicker, globular structures. A five-day culture of clusteroids allowed them to make contact with neighbouring clustered cells by percolating through the hydrogel. We were unable to further monitor the clusteroids' diameter beyond seven days due to the percolation of the hepatocyte clusteroids and the formation of a denser clusteroids layer (see **Figure 2.9**). As shown in **Figure 2.9**, the growing mode of single cells and clustered cells is completely different. It is not possible to form a cluster or spheroid in the individual cells as they proliferated individually.[47] We observed, however, that the clusteroids in the alginate gels grew into a compact tissue structure. Alginate hydrogel does not provide an appropriate environment for clusteroid

formation, as evident from the results.

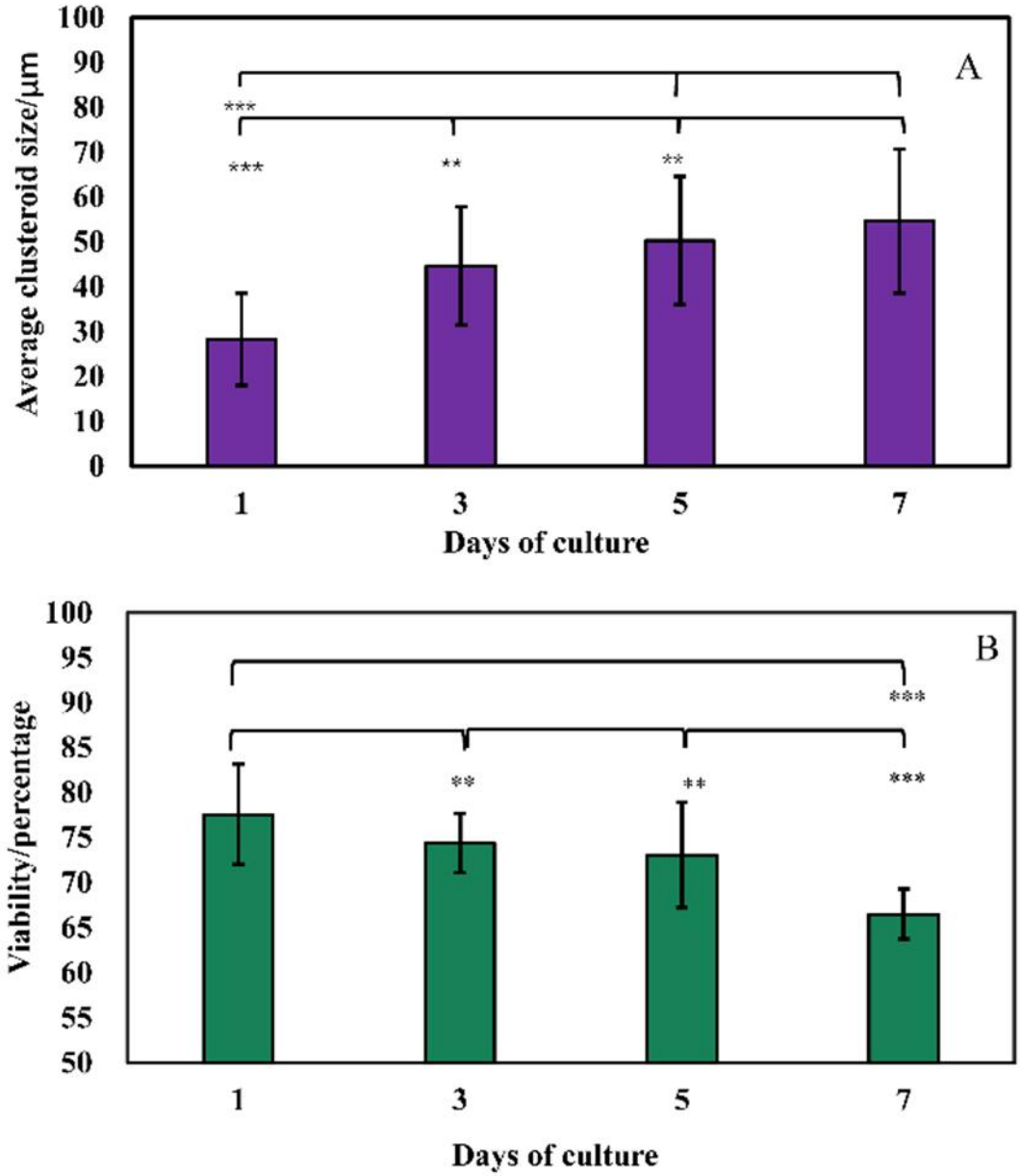

Figure 2.10. Evolution of the Hep-G2 clusteroids embedded in a hydrogel composed at different days of culture. (A) The spheroid size vs. time and (B) viability vs. time. Measurements of the clusteroids were made every day with ImageJ software by taking the average of the vertical and horizontal diameter of 500 clusteroids in each well. (**p < 0.01,***p< 0.001)

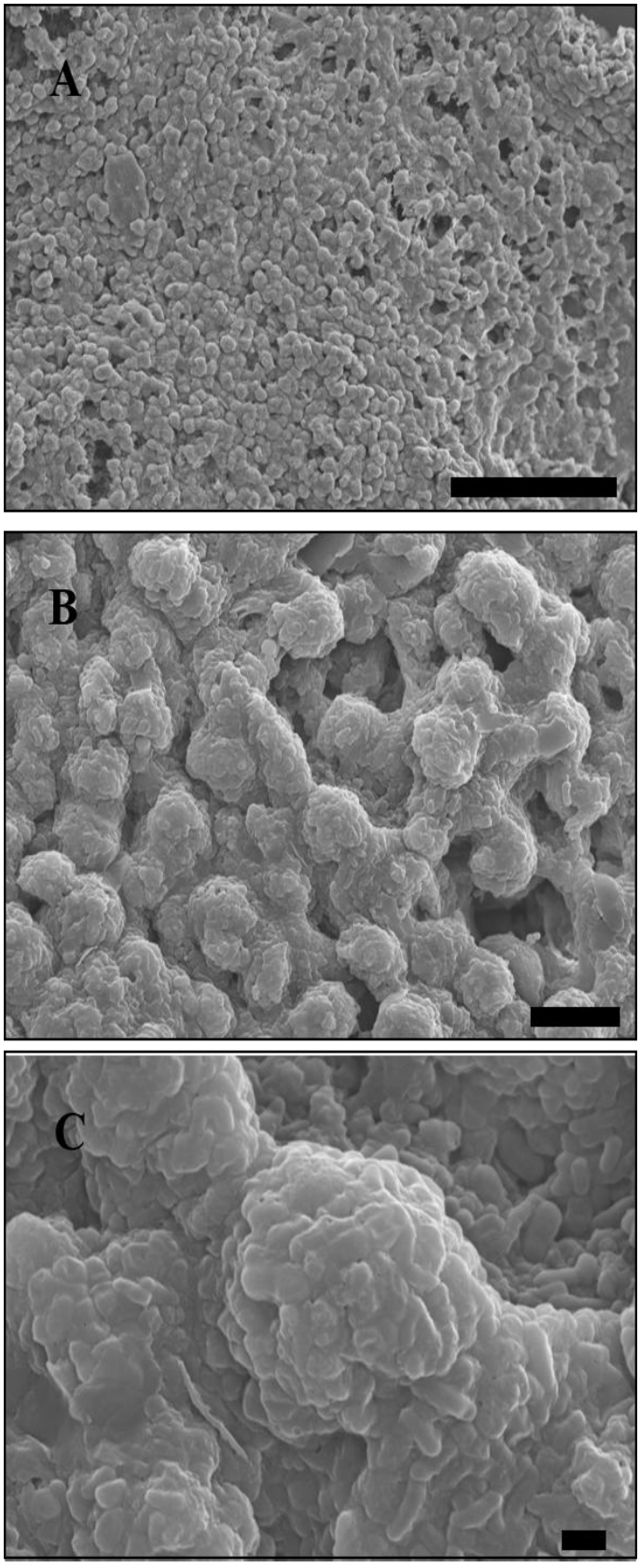
A
B
C

Figure 2.11 SEM images of a sample of Hep-G2 cell clusteroids encapsulated in the sodium alginate gels after 7 days culture, deposited on a glass substrate and freeze-dried before imaging. (A–C) Images correspond to different resolutions. Note that the size of the clusteroids of cells is slightly lower than the original cell clusteroids due to shrinkage. The bars are (A) 100 μm; (B) 10 μm; (C) 1 μm.

By directing Pickering emulsion droplets onto embedded cells, clusteroids form in our experiments. The result shows that our technique is capable of making clustered cells proliferate around the initial core in a pattern similar to how they would do naturally. The clusteroids' size was measured manually using ImageJ software as the cell clusteroids continued growing in the seven-day culture (**Figure 2.10A**). After the first three days when the clusteroids grew rapidly, the size of the cells increased slowly to 55 μm after the fourth day, possibly because more cells were necessary to enlarge the clusteroids. Our goal was to use the clusteroids produced here in tissue engineering applications that require high yields of clusteroids rather than an absolute homogeneity of their size in order to get the best results. In a drug test, the uniformity of the clusteroids is crucial because it allows their use of them to be more effective. As part of the growth monitoring procedure, clusteroids with a lower cell count of $1x10^5$ mL were additionally placed in alginate gel for observation of how the individual clusteroids grew. Adding 5 mg mL alginate lyase solution to a sample of alginate gel enabled viability studies to be conducted on clusteroids. In order to assess the viability of the cells within the clusteroids on various days, we performed a viability assessment test. The cells' viability decreased over a few days of culture, from 78% to 65% (**Figure 2.10B**). In the case of clusters that become progressively larger, necrotic cores may be formed as the clusters become progressively larger. **Figure 2. 11** shows the microscopical observations of the FDA-treated clusteroids at various stages after various treatments were applied. One can see from **Figure 2. 12,** that after 3 days of culture in a hydrogel, the cell clusteroids became dense and compact. It is possible for a single clusteroid of Hep-G2 to reach up to 80 μm in length after seven days of culture. These images show a variety of resolutions of SEM images taken after freeze-drying samples of such grafts. Clusteroids have clustered in the hydrogel matrix and have begun to spread out and percolate through the gel. This process

led to the formation of integral tissues over the course of seven days. A relatively uniform size was observed among the cell clusteroids. Tissue engineering applications favor dense clusteroids because they form a dense layer.

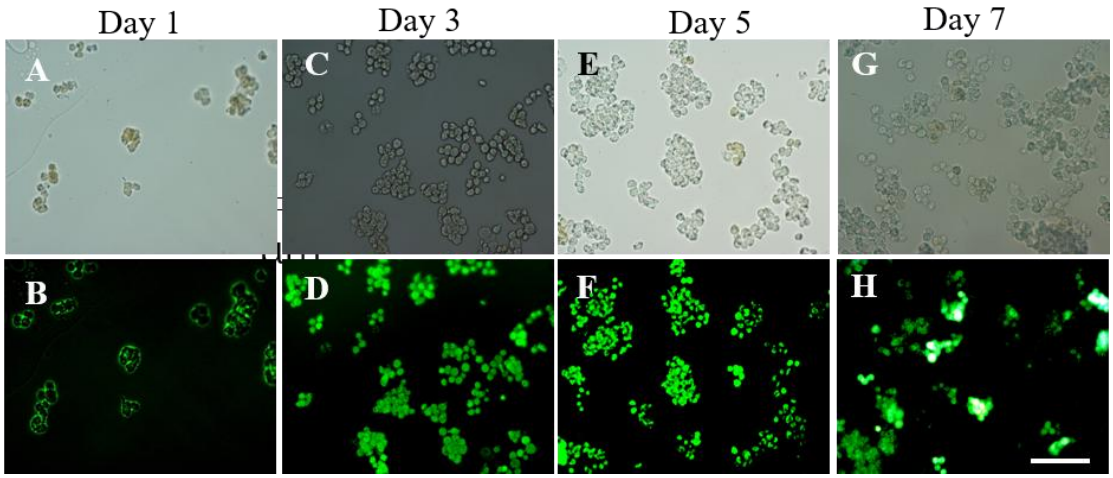

Figure 2.11.(A, C,E,G) Optical bright-field images and (B, D,F,H) fluorescence microscope images of Hep-G2 clusteroids after being treated with FDA live/dead assay after various days of culture. (The fluorescence indicates that both the Hep-G2 cells preserve their viability during the clusteroids fabrication process. The scale bar is 100 μm.

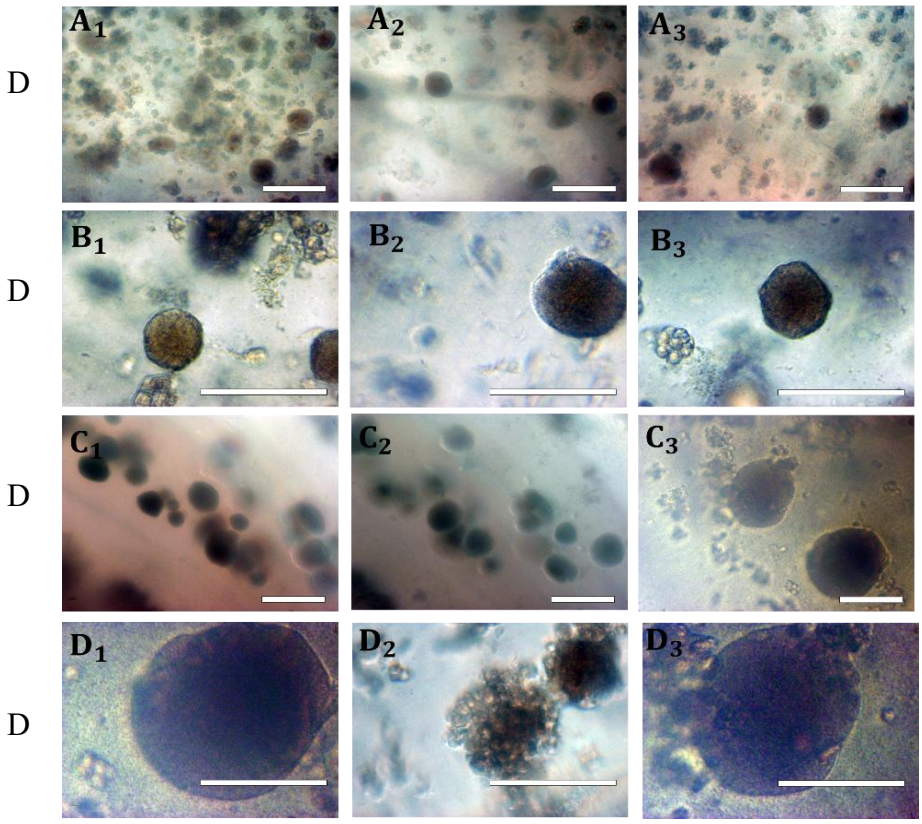

Figure 2.12. Bright-field optical microscope images of (A, B, C, D) 3D cultured Hep-G2 clusteroids isolated by a dilution of the DEX/PEO emulsion by a factor 3 with EMEM medium and incorporated with 1 wt% sodium alginate in EMEM media followed by cross-linking with 1M $CaCl_2$. The Hep-G2 cells clusteroids were cultured in the alginate film for seven days under EMEM media and images were taken from each well to determine the average clusteroids size. Scale bars are 100 µm

2.4.6 Cell clusteroids liver-specific functionality

Cell polarity and ECM signalling have been shown to promote liver-specific functions such as albumin secretion and metabolic enzyme expression.[32] To study the liver-specific functions of the clustered Hep-G2 cells, albumin secretion and urea synthesis by 1×10^6 of HepG2 cells pre-clustered in clusteroids, cultured in series of 1 wt% sodium alginate gel, were quantified. Urea synthesis was quantified over 7 days of culture. **Figure 2.13A** shows the amount of albumin secreted into the medium per day in each well after fixed number of days of accumulation. A trend was found for cells

cultured with gels: the albumin secretion increases with longer culturing. In alginate gel cultured with single cells, albumin secretion was slightly higher than the gels encapsulated with clustered cells at day 1. The result shown in **Figure 2.14** could also demonstrate that the albumin production increased for every 24 h in culture. On day 10, the amount of albumin secreted by Hep-G2 clustered cells was approximately three times higher than that of similar number of individual Hep-G2 cells. The result suggests that albumin secretion of the cells is improved in clusteroids. Urea synthesis is another important liver-specific function of Hep-G2 cells. The urea production profile of the cells was similar to that for albumin secretion. As shown in **Figure 2. 13B**, after 7 days of culture, urea synthesis by the accumulation of both the individual cells and clusteroids increases with time, but the urea production per day was continuously decreasing for the seven days as shown in **Figure 2. 14**. This could be attributed to the reduction of mesothelial cells with the cell proliferation, which accounts for urea production.[2] In addition, the urea synthesis rate by the clusteroids was two times higher than the single cells, confirming again that the introduction of clusteroids enhances the liver-specific functions of the Hep-G2 cells. The result indicates that the cell–cell interactions in these clusteroids benefit their high level of liver-specific functions as revealed in **Fig. 13**.

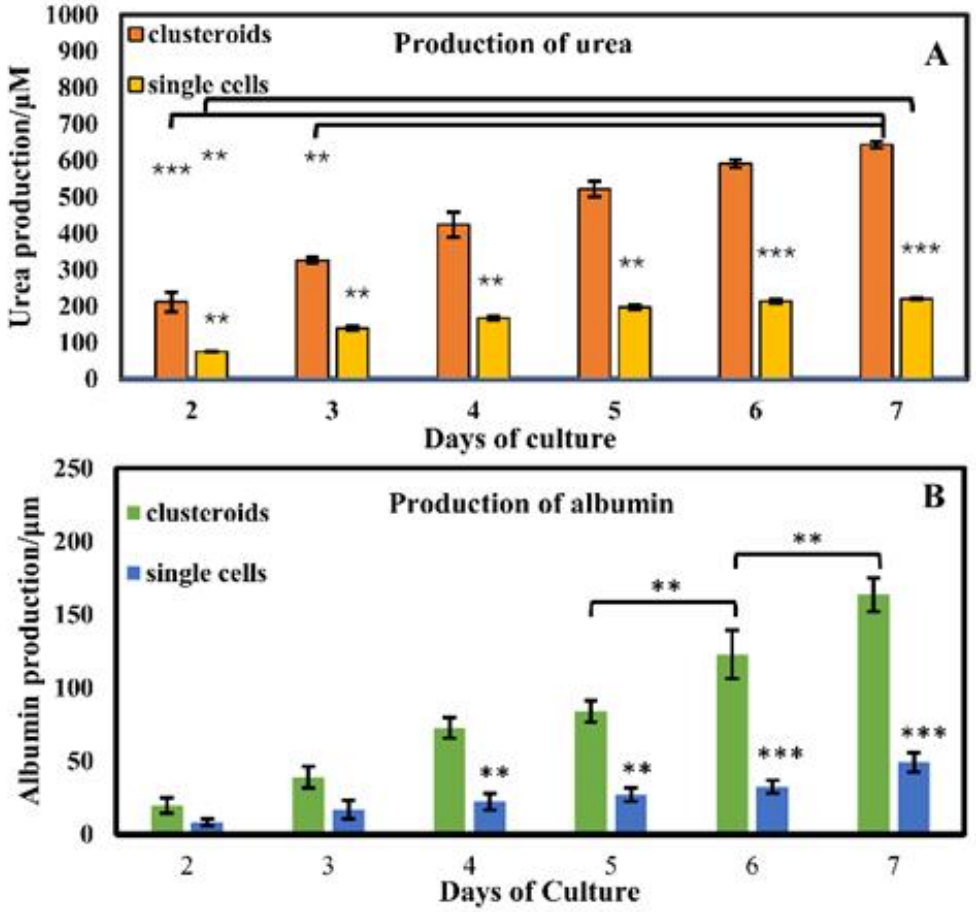

Figure 2.13 (A) Urea synthesis and (B) Albumin secretion by Hep-G2 cells in blend gels as a function of culture time by accumulation. Data are shown as mean ± standard

deviation from two samples. The superscript letters represent significant difference

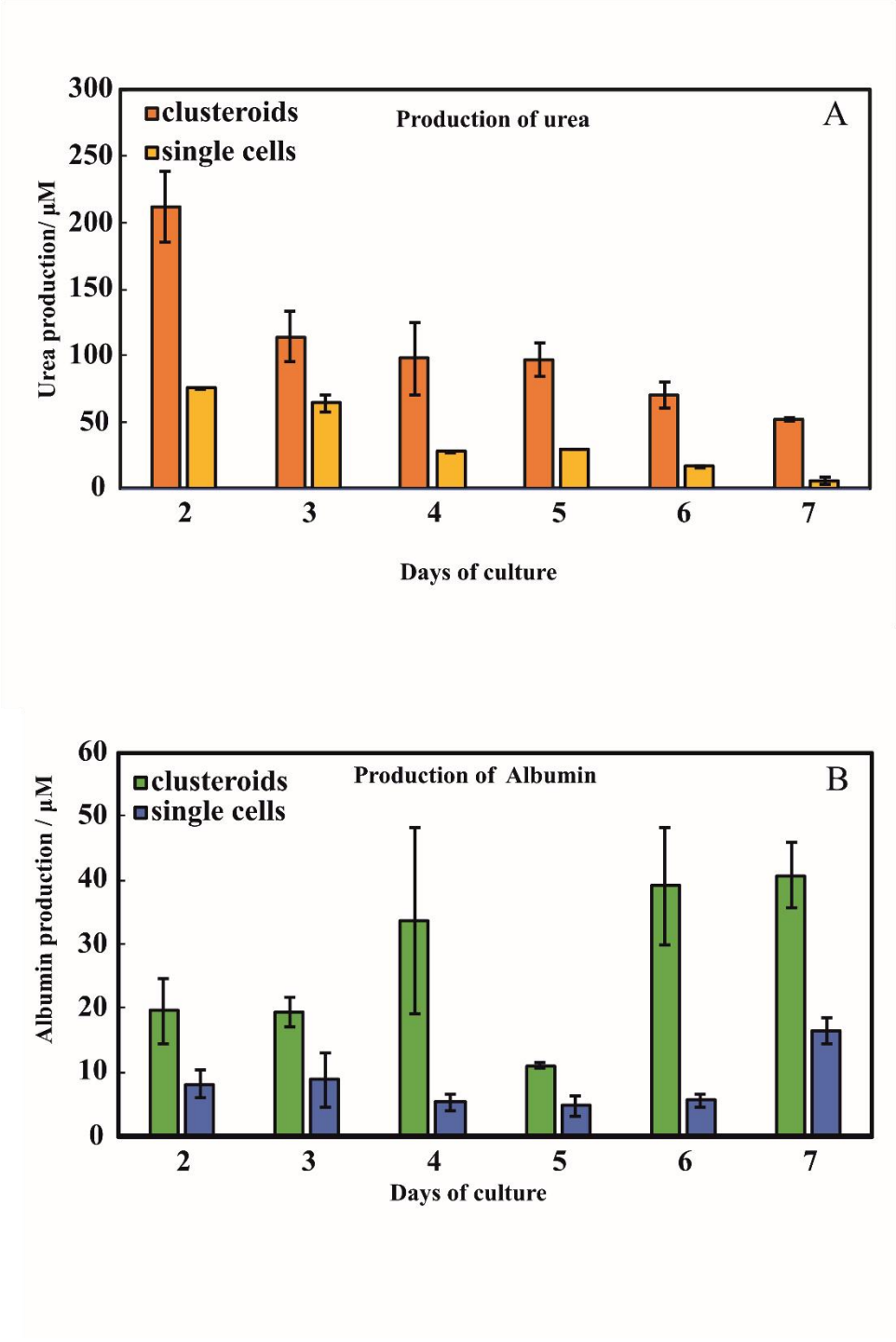

Figure 2.14. (A) Albumin secretion and (B) urea synthesis by Hep-G2 cells in blend gels as a function of culture time by days. Data are shown as mean ± standard deviation from two samples. The superscript letters represent significant difference between groups.

between groups (**p < 0.01, ***p< 0.001).

2.5 Conclusions

A 3D model of solid tumor cells as spheroids can be a useful tool to provide an *in vitro* model that is equivalent to the physiological behaviour of solid tumours, which, along with its physiological relevance, can be used to test for the identification of potent anti-cancer drugs. Although spheroids are often recognized as superior for high throughput screening, spheroids are underutilized in these applications due to their limitations in preparation techniques. The use of immiscible aqueous solutions of two biopolymers, dextran and PEO, for the culture of hepatic tumour cells (Hep-G2) in 3D has been demonstrated in this study. Using PEO solution as an osmotic pressure source, we demonstrate that Pickering emulsion droplets are capable of encapsulating cells and facilitating the aggregation and formation of compact cell spheroids by increasing Pickering emulsion osmotic pressure in the continuous phase. In order to achieve this, more PEO was added to the continuous phase after the emulsion had been formed. By dilution with culture media, cell clusters were obtained from DEX drops after osmotic shrinkage with PEO. It is possible, through this method, to create tissue-like structures in 24-well plates that are able to provide thousands of spheroids, thereby allowing further biochemical measurements to be conducted in situ, using plate readers, in order to assess cell responses. Under the same conditions, we incorporated single cells and followed their growth over a course of up to 7 days in alginate gel. Hepatocytes' liver-specific functions were greatly enhanced by the formation of cell clusteroids. Tissue engineering applications can benefit from this configuration since the same number of cells can grow faster, as well as efficient high throughput screening applications or further drug testing platforms. Hepatic cells can be cultured in 3D without the need for special plates, devices, or facilities so that a wide range of applications can be met in tissue engineering and drug library screening.

2.6 References

1 X. Gu and J. E. Manautou, Expert Rev. *Mol. Med*., 2012, **14**, e4.

2 J. A. Kyffin, P. Sharma, J. Leedale, H. E. Colley, C. Murdoch, A. L. Harding, P. Mistry and S. D. Webb, *Toxicol. In Vitro*, 2019, **55**, 160–172.

3 N. G. McDowell, R. A. Fisher, C. Xu, J. C. Domec, T. Holtta, D. S. Mackay, J. S. Sperry, A. Boutz, L. Dickman, N. Gehres, J. M. Limousin, A. Macalady, J. Martinez-Vilalta, M. Mencuccini, J. A. Plaut, J. Ogee, R. E. Pangle, D. P. Rasse, M. G. Ryan, S. Sevanto, R. H. Waring, A. P. Williams, E. A. Yepez and W. T. Pockman, *New Phytol*., 2013, **200**, 304–321.

4 M. Eichelbaum, M. Ingelman-Sundberg and W. E. Evans, Annu. Rev. Med., 2006, 57, 119–137. 5 K. M. Lee, D. Kang, M. L. Clapper, M. Ingelman-Sundberg, M. Ono-Kihara, C. Kiyohara, S. Min, Q. Lan, L. Le Marchand, P. Lin, M. L. Lung, H. Pinarbasi, P. Pisani, P. Srivatanakul, A. Seow, H. Sugimura, S. Tokudome, J. Yokota and E. Taioli, Cancer Epidemiol., *Biomarkers Prev.*, 2008, **17**, 1120–1126.

6 L. Yuan and N. Kaplowitz, Clin. *Liver Dis.*, 2013, **17**, 507–518.

7 S. Blach, S. Zeuzem and M. Manns, *Lancet Gastroenterol. Hepatol.*, 2017, **2**, 161–176.

8 D. Azoulay, D. Castaing, R. Adam, E. Savier, V. Delvart, V. Karam, B. Y. Ming, M. Dannaoui, J. Krissat and H. Bismuth, *Ann. Surg.*, 2001, **233**, 565–574.

9 N. Lebonvallet, N. Boulais, C. Le Gall, U. Pereira, D. Gauche, E. Gobin, J. O. Pers, C. Jeanmaire, L. Danoux, G. Pauly and L. Misery, *Exp. Dermatol*., 2012, **21**, 156–158.

10 E. Nicholas, S. D. Timmins and L. K. Nilesen, *Angiogenesis,* 2004, **7**, 97–103.

11 Y. C. Tung, A. Y. Hsiao, S. G. Allen, Y. S. Torisawa, M. Ho and S. Takayama, *Analyst*, 2011, **136**, 473–478.

12 E. Atefi, S. Lemmo, D. Fyffe, G. D. Luker and H. Tavana, *Adv. Funct. Mater.*, 2014, **24**, 6509–6515.

13 H. Ota, R. Yamamoto, K. Deguchi, Y. Tanaka, Y. Kazoe, Y. Sato and N. Miki, *Sens. Actuators*, B, 2010, **147**, 359–365.

14 G. R. Souza, J. R. Molina, R. M. Raphael, M. G. Ozawa, D. J. Stark, C. S. Levin, L. F. Bronk, J. S. Ananta, J. Mandelin, M. M. Georgescu, J. A. Bankson, J. G. Gelovani, T. C. Killian, W. Arap and R. Pasqualini, *Nat. Nanotechnol*., 2010, **5**, 291–296.

15 M.-L. Brandy, O. J. Cayre, R. F. Fakhrullin, O. D. Velev and V. N. Paunov, *Soft Matter*, 2010, **6**, 3494–3498.

16 R. F. Fakhrullin, M.-L. Brandy, O. J. Cayre, O. D. Velev and V. N. Paunov, *Phys. Chem. Chem. Phys*., 2010, **12**, 11912–11922.

17 L. Gasperini, J. F. Mano and R. L. Reis, *J. R. Soc., Interface*, 2014, **11**, 20140817.

18 E. Atefi, R. Joshi, J. A. Mann and H. Tavana, *ACS Appl. Mater. Interfaces*, 2015, **7**, 21305–21314.

19 S. Singh and H. Tavana, *Front. Chem*., 2018, **6**, 379.

20 S. Lemmo, E. Atefi, G. D. Luker and H. Tavana, *Cell. Mol. Bioeng*., 2014, **7**, 344–354.

21 S. L. Ham, E. Atefi, D. Fyffe and H. Tavana, *J. Vis. Exp*., 2015, **98**, e52754.

22 P. Shahi Thakuri, S. L. Ham, G. D. Luker and H. Tavana, *Mol. Pharm*., 2016, **13**, 3724–3735. 23 S. B. G. Celik, S. R. Dominici, B. W. Filby, A. A. K. Das, L. A. Madden and V. N. Paunov, *Biomimetics*, 2019, **4**, 50.

24 A. A. K. Das, B. W. Filby, D. A. Geddes, D. Legrande and V. N. Paunov, *Mater. Horiz*., 2017, **4**, 1196–1200.

25 C. Han, S. Takayama and J. Park, *Sci. Rep*., 2015, **5**, 11891.

26 B. P. Binks and H. Shi, *Langmuir*, 2019, **35**, 4046–4057.

27 N. Chatsisvili, A. P. Philipse, B. Loppinet and R. H. Tromp, *Food Hydrocolloids*, 2017, 65, 17–23.

28 B. T. Nguyen, T. Nicolai and L. Benyahia, *Langmuir*, 2013, **29**, 10658–10664.

29 J. Fukuda, A. Khademhosseini, Y. Yeo, X. Yang, J. Yeh, G. Eng, J. Blumling, C. F. Wang, D. S. Kohane and R. Langer, *Biomaterials*, 2006, **27**, 5259–5267.

30 Y. Wang and J. Wang, *Analyst*, 2014, **139**, 2449–2458.

31 Y. Li and E. Kumacheva, *Sci. Adv*., 2018, **4**, 1–11.

32 S. C. Ramaiahgari, M. W. den Braver, B. Herpers, V. Terpstra, J. N. Commandeur, B. van de Water and L. S. Price, Arch. *Toxicol*., 2014, **88**, 1083–1095.

33 G. Balakrishnan, T. Nicolai, L. Benyahia and D. Durand, *Langmuir*, 2012, **28**, 5921–5926.

34. Wang, A., Madden, L. A., & Paunov, V. N. (2020). High-throughput fabrication of hepatic cell clusteroids with enhanced growth and functionality for tissue engineering applications. *Materials Advances*, *1,***8**, 3022-3032.

3. Chapter 3

Fabrication of Angiogenic Sprouting Coculture of Cell Clusteroids Using an Aqueous Two-Phase Pickering Emulsion System

3.1 Abstract:

A growing interest in tumour cell spheroids and 3D cell cultures has been generated during the past decade due to their relative ease of production and potential applications for biomedical research. Personalized cancer treatment and tissue engineering applications have been possible with 3D tumour models to date. A central part of an artificial construct cannot survive without adequate oxygen and nutrients without vascularization. There remains a significant hurdle in their wider practical application due to the formation of a necrotic core within *in vitro* 3D cell models. This study proposes a rapid formation protocol based on the use of water-in-water (w/w) Pickering emulsion template to produce phenotypically endothelial/hepatic coculture cell clusteroids (ECV304/Hep-G2) capable of angiogenic activity. We developed an aqueous two-phase Pickering emulsion template based on dextran/poly (ethylene oxide) aqueous system stabilized by whey protein particles. To achieve optimum performance, it is possible to manipulate the initial cell proportion in the coculture clusteroids. The cocultured pattern of the endothelial/hepatic cells could significantly promote the production of angiogenesis-related proteins. We have demonstrated that cocultured clusteroids can stimulate the sprouting of cells in a 1:2 ratio of HepG2/ECV304, without the addition of vascular endothelial growth factor (VEGF) or other angiogenesis inducers. With coculture clusteroids, angiogenesis gene production, urea levels, insulin-like growth factor-binding protein levels, and CD34 levels were enhanced, indicating angiogenesis progress. We developed aqueous Pickering emulsion templates that provided a convenient method to vascularize a target cell type in 3D cell coculture without the requirement for additional stimuli. These templates could potentially be used with both

cell lines and biopsy tissues, extending the downstream application capabilities of clusteroids.

3.2 Introduction

In comparison to 2D cell cultures, 3D cell cultures aim to simulate the *in vivo* environment by constricting cells into densely packed aggregates. This enhances cell-to-cell interaction.[1,2] The popularity of 3D cell culture models has increased recently because they help achieve levels of cell differentiation and tissue organization that are impossible in conventional 2D cultures.[3,4] An ethical review and sophisticated operation are generally required for the most commonly used animal models.[5] The lack of animal experiments provides a poor foundation for clinical trials in part due to this.[6] In the past decade, 3D cell culture models have attracted interest because of their high availability and precise mimicry of real-life environments. Based on the fabrication methods, spheroids and organoids are the most commonly discussed 3D cell culture models.[7] There are a number of factors which are causing the use of cell spheroids as a model of preclinical assessment of various drugs and therapeutics with regards to their biological performance.[8,9] Spheroids have recently been applied to tissue engineering applications, where they can be used as building blocks for constructing scaled artificial organs *in vitro*. [10–12] Several kinds of organs, including skin, bone, and others, may be replaced or repaired with artificial tissue. It should be noted, however, that the reconstruction of living organs utilizing 3D cell cultured models still faces significant interference, particularly at the interfaces between different species of cells. During spheroids' proliferation, spatial and temporal gradients of chemicals and oxygen play a crucial role.[13] The absence of a vascular system results in necrotic cores inside cell spheroids composed of nonendothelial cells. Before spheroids can be systematically used, they must have a high intracellular vascularization level, as the cores of these artificial constructs cannot survive longer periods of cultivation without this tubular network. There are several growth factors that initiate the process of angiogenesis, including vascular endothelial growth factor (VEGF).[14,15] As a result, endothelial cells are transformed from their resting state into activated tip cells.[16] After releasing matrix metalloproteinases (MMPs), the tip cells degrade the extracellular matrix and migrate

into surrounding tissues or the extracellular matrix (ECM). [17,18] Capillary buds and sprouts form as a result of the proliferation of endothelial stalk cells, which gradually move toward the angiogenic stimulus.[19] After the sprouts have formed a lumen, they interconnect with each other to form new vessels that have been perfused with blood.[20] Coculture of endothelial cells with other cell types results in spontaneous formation of vascular-like networks. Endothelial sprouting (angiogenesis) occurs.[21–23] Recently, Correa de Sampaio et al.[47] reported a 3D model of the sprouting coculture of fibroblast and endothelial cells. The hanging drop method is an approach for generating composite vascularized spheroids that involves coculture of fibroblasts with human umbilical vein endothelial cells (HUVECs).[24] The fibroblasts are thought to impose a signal of vascularization upon the Endothelial cell lines(E.Cs), causing them to establish a vascular network spontaneously in the coculture spheroids. Coculture with E.Cs also stimulated vascularization in mesenchymal stem cells and a number of tumor cells.[25–27] A low yield rate or high labor costs were associated with the microfluidic devices or extracellular matrixes used for coculturing vascularized spheroids, which limited their practical application. Atefi et al.,[28] Lemmo et al.,[29] and Das et al.[30] described the development of a high throughput production method for an aqueous two-phase system (ATPS) using 3D cell clusteroids as Pickering emulsions stabilized with β-lactoglobulin. There have been a number of follow-up reports since the method was introduced, which indicate that the clusteroids generated in this way are more functional and are more productive.[31–33] Using Pickering emulsion as a template, a process utilizing water-in-water (w/w) Pickering emulsion may meet the demands of high throughput and cell co-culture at the same time. The three-dimensional cell clusteroids collected differ from classical spheroids in that they are more porous and do not have necrotic cores as the media is capable of freely diffusing into the cores. There has never been a report on the use of this w/w Pickering emulsion system for coculturing cell lines. The purpose of this study was to systematically generate and characterize cocultured Hep-G2/ECV304 clusteroids using the Pickering emulsion w/w as a template (see **Figure 3.1**). A proof of principle study was conducted on vascularized cocultured clusteroids derived from the cocultured HepG2 cells and ECV-304 cells. It is generally possible to switch the cell types between any cell line or primary cell culture. A significant increase in angiogenesis was observed in

cocultured clusteroids compared with single clusteroids, as reported below. After embedding the coculture clusteroids in a sodium alginate hydrogel matrix, we found that they could spontaneously sprout, especially when the cell ratio was 1:2 between Hep-G2/ECV304. Considering the high yields and reproducibility of the method, it would be an ideal platform for tissue engineering and advanced drug testing. In addition to enhancing the applications of coculture clusteroids, this new facile platform can improve the process of manufacturing them.

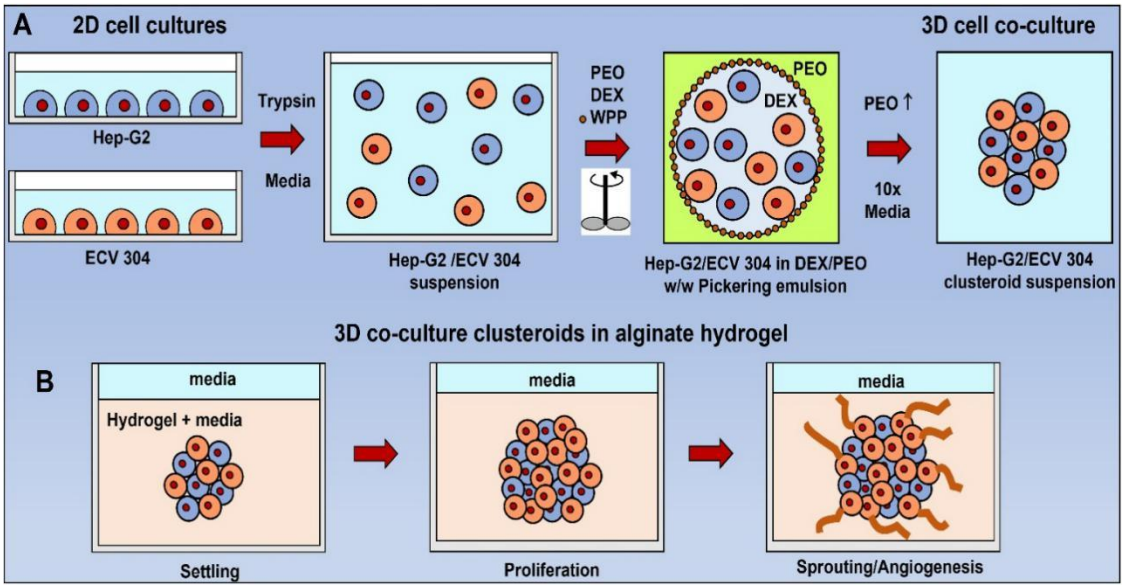

Figure 3.1 (A) Schematics of the high throughput preparation method of 3D co-culture clusteroids from 2D cell cultures of Hep-G2 and ECV 304 but using aqueous two-phase systems in a Pickering emulsion template. (B) The evolution of the prepared 3D co-culture Hep-G2/ECV 304 clusteroids in ECM hydrogel matrix resulting into spontaneous angiogenesis and sprouting. No sprouting occurs in the single cell type clusteroids.

3.3 Experimental section

3.3.1 Materials

CellTracker™ Green CMFDA Dye, CFSE far-red, CFSE green fluorescence dye are both purchased from NUNC Cell culture 24-well plates were sourced from Thermo Fisher Scientific (U.K.). Dextran(DEX) (MW 500 kDa) and polyethylene oxide(PEO) (MW 200 kDa) were purchased from Sigma-Aldrich, U.K. Sodium chloride (99.8%) and calcium chloride, Dulbecco's Modified Eagle Medium, and Trypsin-EDTA were sourced from Fisher Scientific (U.K.). Media supplements were fetal bovine serum (10% v/v, Labtech, Heathfield, U.K.) and 0.25% Trypsin-EDTA (1X, Lonza). The ECV 304 and Hep-G2 cell line were purchased from ECACC cell collection. Urea analysis kit was obtained from Sigma Aldrich (Saint Louis, USA). The MMP-2 ELISA kit was sourced from GE healthcare (Amersham, U.K.), the IGFBP ELISA kit and angiogenesis array kit were sourced from the Bio-techne (Abingdon, U.K.). The urea kit was provided by Sigma-Aldrich, U.K. Whey protein was kindly provided by No1. Supplements(Suffolk,UK).Deionized water was purified by MilliQ water system (Millipore). All the other chemicals are of analytical grade.

3.3.2 Method

3.3.2.1 ECV 304 and Hep-G2 monolayer cell culture

The human ECV 304 is believed to be a T24 derivative (urinary bladder carcinoma), which was believed to originate from endothelial cells obtained from the umbilical vein of a healthy donor.[33] The ECV 304 cell line contains many important characteristics of endothelial cells. The immortalized nature of this cell makes it a valuable model to set an initial model for endothelial vascularization.[33] The ECV 304 and Hep-G2 cell lines were cultured in DMEM and EMEM mediums supplemented with 10 % Foetal Bovine Serum, respectively. Both types of cells were cultured in T75 easYFlask (Thermo Fisher Scientific, U.K.) at 37 ^{o}C supplemented 5 % CO_2. The medium was discarded when the cells reached a confluency of 80% before the cells

were rinsed with phosphate buffer saline (PBS, Lonza, U.K.) twice to remove the excessive medium. The cells were then detached from the flasks using 0.25 wt% trypsin solution and passage in 1:8 (ECV304) and 1:4 (Hep-G2). The trypsinization was stopped by mixing the trypsin solution with a proper complete medium (either DMEM or EMEM), and the cells were collected by centrifugation at 400 × g for 4 min.

3.3.2.2 Production of 3D ECV 304,Hep-G2 monolayer and co-cultured clusteroids.

The method of generating individual Hep-G2 and ECV 304 3D clusteroids was modified from the protocol introduced by Das et al. [30] The protocol is on the basis of all aqueous phase systems, water-in-water Pickering emulsion. Briefly, the 22wt% PEO and 11 wt% Dextran(DEX) solutions were obtained by dispersing a properly weighted amount of PEO and dextran powders in deionized water. The solution needs to be magnetically stirred overnight to achieve proper solubilization. The solutions were then autoclaved (121 ºC, 15 min) to obtain a sterile solution. An equal volume of the 22 wt% PEO solution 1wt% heat-treated whey protein particle suspension (WP) was then mixed. The whey protein particles suspension was filter-sterilized prior to the mixing to avoid contamination. Then the 11 wt% PEO/WP or DEX solutions were mixed with an equal amount of DMEM/EMEM(50:50) medium supplemented with 10% FBS to obtain 5.5 wt% PEO/Medium/WP and DEX/Medium solutions. The DMEM/EMEM (50:50) medium supplemented with 10% FBS was treated as a complete medium for the co-culture clusteroids in the following experiments. The 5.5 wt% DEX solution was utilized as the dispersed phase for both Hep-G2 and ECV 304 cells as the cells have a better affiliation to DEX compared to PEO. The cells were harvested using trypsin, and a fixed ammount of cells (either Hep-G2, ECV 304, or mixed cell types at different ratios) were collected and resuspended in the 50μL DEX/Medium solution. The emulsification of the w/w Pickering emulsions was achieved by gentle pumping using a syringe (BD Plastipak™ syringe) fitted with a needle (BD Microlance™ 12 needle, B.D. biosciences, Wokingham, U.K.). The DEX/PEO Pickering emulsions encapsulated with cells were compressed to allow the formation of clusteroids by adding higher condensed PEO/DMEM solution(11wt%) to reach a final PEO concentration of 8 wt%. The transportation of water from the DEX drops to the PEO phase would shrink the DEX drops along with the

encapsulated cells. The cells were incubated in the emulsions overnight to allow the clusteroids formation, which would accumulate at the interface between DEX/PEO. 10×fold complete medium was used to break the emulsion, and the clusteroids were collected.

3.3.2.3 Long term growth of the spheroids in sodium alginate gels

The support of an ECM in the formation of endothelial networking, especially the cell sprouts in the angiogenesis process *in vitro,* is essential. Here we use sodium alginate as an ECM to support the growth of the clusteroids. The 3wt% sodium alginate was suspended in PBS with magnetic agitation followed by autoclaving. The 3wt% sodium alginate gels were mixed with an equal volume of complete medium supplemented with 10% FBS to reach a final concentration of 1.5wt%. After the formation of the clusteroids, the 100μL of the individual cell-typed clusteroid or the co-culture clusteroids were seeded in 400μL 1.5wt% sodium alginate and fortified using 500μL 1wt% calcium chloride in 24 wells plate. The culture was incubated with 500μL complete media supplemented with 10% FBS at 37^{o}C with 5% CO_2.

3.3.2.4 Bright field, fluorescence, and Confocal microscopy observations

The visualization of the microstructure of the clusteroids encapsulated in the emulsion template was achieved using bright field optical microscopy supplemented with a fluorescence burner (Olympus BX-51). 20 μL samples were observed using various immersion objectives on a concave slide under various immersion objectives. 4′,6-diamidino-2-phenylindole (DAPI), or CFSE far-red were used as the fluorescence dye on the Hep-G2 cells, and CFSE green was used for ECV 304 cells. For tracking of the long-term proliferation of the co-culture clusteroids, CFSE far-red and CFSE green were used for Hep-G2 and ECV304, respectively. CFSE would permeate into cells and bind to their interior by the succinimidyl group, which would be trackable after the cell splits (Generally within 14 days). The observation of the various clusteroids was also carried out using a confocal laser scanning microscope (CLSM, Zeiss LSM710). Z-stacking images were taken to generate a 3D view of the individual clusteroids and clusteroids film. The CLSM imaging was produced on precise mode.

3.3.2.5 Spheroid sprouts analysis

To generate the sprouts, a low serum medium was employed. Unlike the medium introduced in the long-term culturing of the clusteroids, the complete medium was supplemented with 2wt% FBS to stimulate the formation of sprouts. The 100μL of co-

cultured or single-cell clusteroids were gently pipetted into 400µL of the 1.5wt% alginate gel before solidifying by the 500µL of 1wt% calcium chloride. The cultures were incubated with 500µL complete media supplemented with 2wt% FBS at 37°C with 5% CO_2. The spheroids sprouts were analyzed by WimSprout assay (Wimasis image analysis, Córdoba, Spain) and the 20 longest sprouts from the clusteroids were measured on their size to calculate the degree of angiogenesis.

3.3.2.6 Urea, MMP-2, and IGFBP Elisa kit

500µL of the 3D clusteroids culture's supernatant was collected at different days of culture. Urea concentration in the samples was quantified using a colorimetric endpoint assay based on acid- and heat-catalyzed condensation of Urea with diacetylmonoxime (Sigma Aldrich, St Louis, USA). The clusteroids supernatant was brought to a final volume of 50µL with Urea Assay Buffer and shifted to a pre-coated 96 well flasks. 50µL of the appropriate reaction mix was added to each of the wells. The flask was incubated for 60 minutes at 37 °C with horizontal shaking, protected from light during the incubation. The absorbance was measured at 570 nm (A570).

MMP-2 was quantified following the manufacturers' instructions. For the IGFBP ELISA duoset, 100µL of capture antibody was incubated in 96 well plates overnight at room temperature to allow proper coating. The capture antibody was discarded, and the 96 well plates was rinsed with 400µL wash buffer three times using an automatice washer. Plates were blocked by adding 300 µL of reagent diluent to each well and incubated at room temperature for a minimum of 1 hour. 100µL of clusteroids supernatant was added to each well and incubated for 2 hours. 100µL of detection antibody, Streptavidin-HRP, and substrate solution was added in order, with a washing procedure between each step. 50µL of stop solution was added last to each well. The optical density of each well was determined immediately using a microplate reader set to 450 nm

3.3.2.7 SEM Image of the clusteroids

The clusteroids were taken out from the sodium alginate gel using 1wt% alginate lyase, which would enzymatically degrade the gel. The clusteroids were then rinsed twice with deionized water to remove excessive sodium alginate and medium. The clusteroids were then fixed in a 1wt% glutaraldehyde solution for two hours at

ambient temperature. The clusteroids were then left air-dried overnight before being imaged with Zeiss smart SEM software (Zeiss Evo-60 S.E.M., Germany).

3.3.2.8 Angiogenesis array kit

These experiments were performed according to the Human Angiogenesis Antibody Array series 1000 (Bio-techne) guidelines. To evaluate the production of angiogenesis-related genes, 1mL of conditioned media were obtained from the 3D co-cultured clusteroids (Hep-G2:ECV304=1:1), Hep-G2 clusteroids, and ECV304 clusteroids embedded in the 1.5wt% sodium alginate gel. Array membranes were incubated overnight with the 1mL conditioned media at room temperature with gentle shaking. The medium was discarded, and the membranes were washed with washing buffer (5 min, four times) and washing buffer II (5 min, two times), an array antibody cocktail, and a horseradish peroxidase-conjugated streptavidin antibody was incubated with the membranes for two h. Membranes were detected using 1X detection buffers C and D, and the array was exposed for 200s using a chemiluminescence system (ATTO, WSE 6100 LuminoGraph I). Blot spot intensity was calculated using GelAnalyzer 19.1 (www.gelanalyzer.com). Relative expression levels in each group were determined using the algorithm mentioned in the manufacturer's protocol.

3.4 Results and discussion

3.4.1 Cell clusteroid formation in DEX-in-PEO emulsions

A number of *in vitro* drug testing procedures have used 3D cell culture in the past few decades. Three-dimensional spheroids are being increasingly utilized as building blocks to form complex tissues using the 3D cell model. *Ex vivo* simulations of spheroids are capable of simulating high levels of gene and cytokine expression.[2]

This study was conducted using an aqueous two phase system (ATPS), which contains three phases: dextran phase, per phase, and whey protein particles. It has been reported that the formation of clusteroids in several cell lines is strongly correlated with the proportion of DEX/PEO in the volume fraction.[33] Cells could be encapsulated and condensed into clusteroids in a short period of time by changing the volume fraction and ratio between the two phases (**Figure 3.1**). In order to conduct the experiment, the overall cell concentration was first set to 10^6 cells per mL, followed by suspension in the 5.5 wt% DEX/Medium solution, and then mixing with 5.5 wt% PEO/WP/Medium solution at a variety of cell ratios (Hep-G2:ECV304). After the w/w emulsion has been formed with compressed cells encapsulated in a w/w emulsion under the influence of gravity, the Dextran phase precipitates under the effect of gravity, since this phase has a higher density than PEO at any concentration (**Figure 3.2**A). In contrast, clusteroids cannot form spontaneously in complete medium when the two types of cells are dispersed (**Figure 3.3**). According to the volume of the emulsion fractions, the precipitation process generally took several hours (**Figure 3.2**B). During the precipitation process, the cells were sufficiently concentrated in the dextran droplets to form stable clusteroids within them and are able to accumulate on the interface between the DEX and PEO since their density is between 5.5wt% Dextran and 8wt% PEO (**Figure 3.2**C). [32] The clusteroids would not come into contact with the plastic surface in this manner.

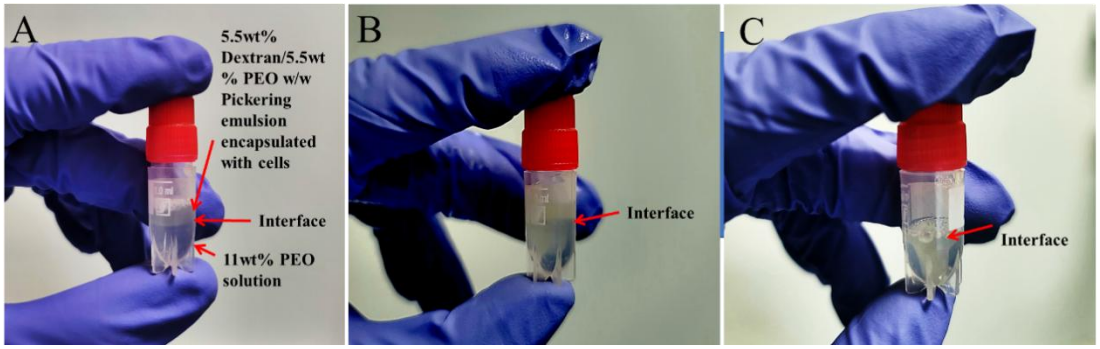

Figure 3.2 A: Clusteroids formation in the w/w Pickering emulsion template before shrinked by higher concentrated PEO solution. B: Starting point of the Sediment of the Dextran phase encapsulated with cells and the shrinking process. C: Finishing point of the sediment ediment of the Dextran phase encapsulated with cells

and the shrinking process.

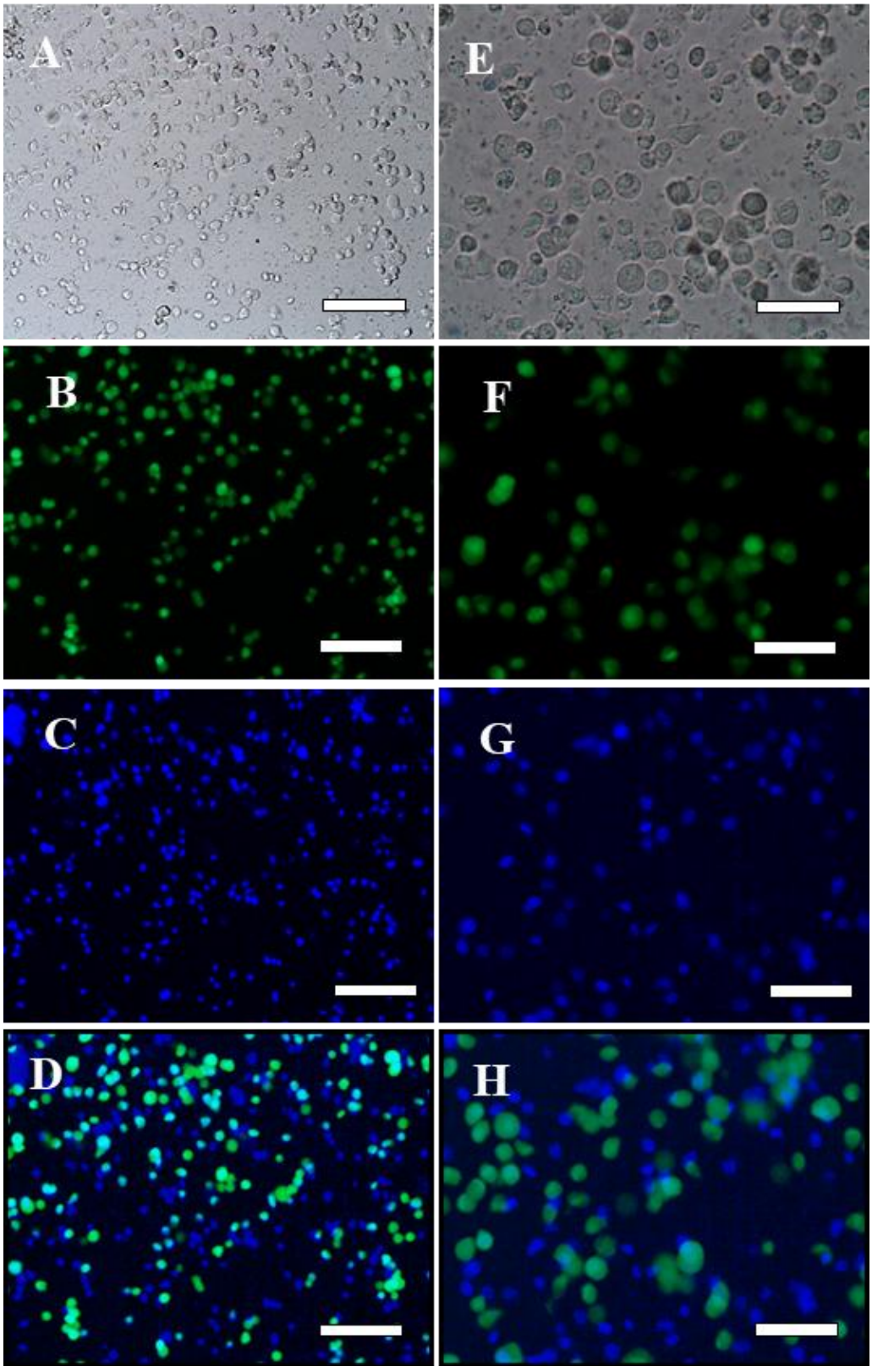

Figure 3.3. Observation of the co-culture cells in complete medium set at bright-field (A,E) ,CFSE far red (B,F), DAPI(C,G) and Dual Fluorescence (D,H) for imaging. The bar is 100μm for A-D and 50μm for E-H.

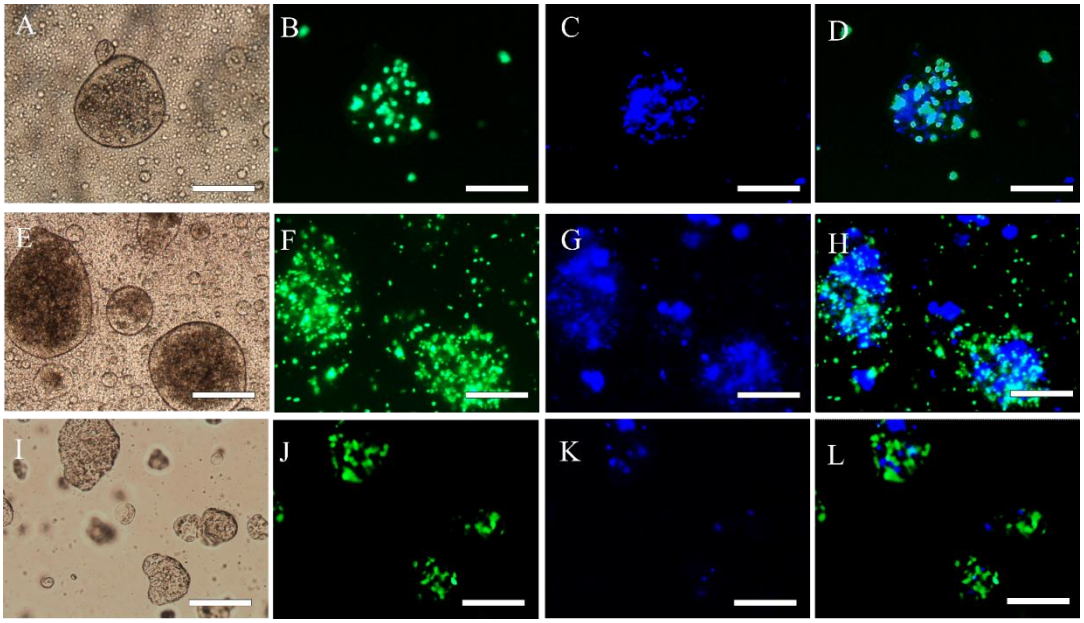

Figure 3.4. Bright-field (A, E, I) and fluorescence microscope observation of mixed Hep-G2/ECV 304 (cell ratio=1:1) cells encapsulated by 5.5 wt% DEX in 5.5 wt% PEO emulsions before (A-H) and after shrinking by 11 wt% PEO (I-L) set at FITC (B, F, J), DAPI (C, G, K) and Dual fluorescence (D, H, L) channels. The Hep-G2 cells and ECV 304 cells were pre-stained with DAPI and CMFDA, respectively. The bar is 100 μm for (A-D) and (I-L). The bar for (E-H) is 50 μm.

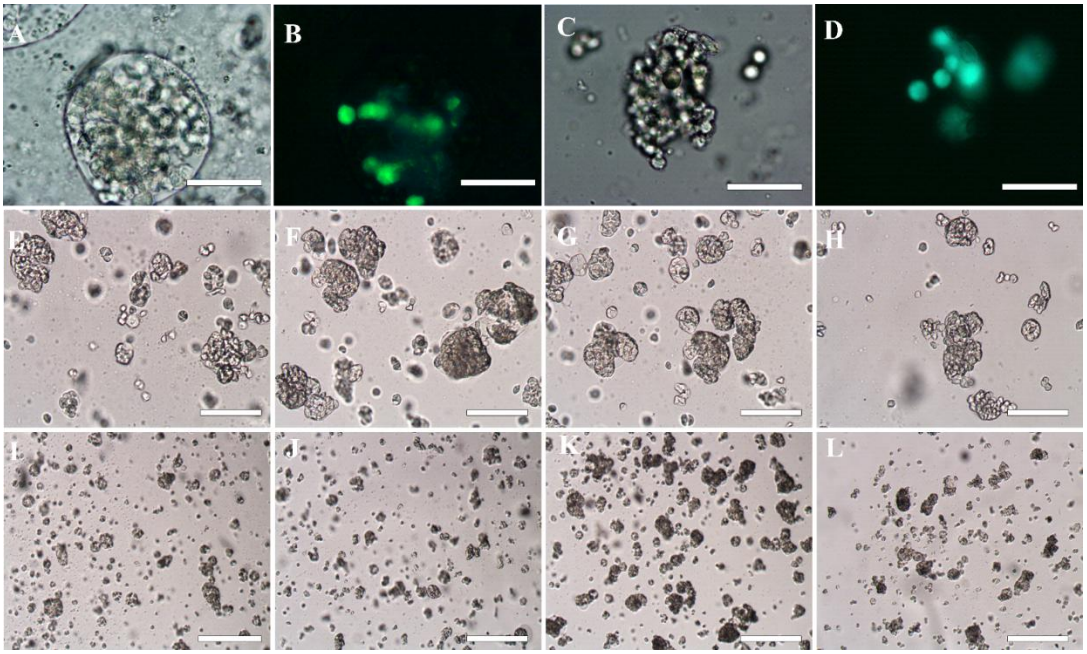

Figure 3.5 Brightfield and fluorescence microscopy images on the co-cultured clusteroids with Hep-G2:ECV304 ratio of 1:1 in the emulsion droplets (A, B) and flow state (C, D). The ECV 304 cells were solely stained to show their location within the clusteroids. Brightfield microscopy images of the collected co-culture clusteroids from the DEX/PEO w/w Pickering emulsion template with different Hep-G2/ECV cells ratio: (E, L) 1:1, (F, J) 2:1, (G, K) 5:1, (H, L) 10:1. The bar is 50 μm for (A-D), 100 μm for (E-H) and 200 μm for (I-L).

As a preliminary evaluation of the efficacy of cell encapsulation, we used a fluorescence microscope to observe the cells. A DAPI stain was used on Hep-G2 cells and a CMFDA stain on ECV304 cells for observation purposes. The figure demonstrates that the two types of cells coexist harmoniously at a cell ratio of 1:1 in multiple droplets with similar cell numbers prior to shrinking (**Figure 3. 4A-H**). Spheroids were compressed successfully without affecting the cell ratio by the shrinking process. There was structural compatibility among the compressed clusteroids, as well as homogeneity in terms of their size (**Figure 3.4H-K, Figure 3.5A, B, E, F**). Dextran droplets encapsulated with cells are squeezed by the osmotic pressure, which promotes the interaction between cells. A notable point is that no previous report has mentioned the possibility of co-culture of cells in ATPS. High-throughput fabrication of co-cultured cell clusteroids can be achieved using Pickering aqueous two-phase emulsion templates. A further examination of the compatibility of

the clusteroids obtained in a flow state further strengthened the importance the obtained results. A 10 x complete medium was used to break down the emulsion droplets. Observations were then made on the clusteroids suspension. There was no evidence that the strutrue of the co-cultured clusteroids would be remained without the presence of an emulsion template (**Figure 3.5C, D, G, H**). A clear distinction could be made between the two kinds of cells due to their self-sorting behavior. In **Figure 3.5I-P**, the clusteroids' average diameter decreases slightly when the ratio of

cells is changed since Hep-G2 cells have a larger size (**Figure 3.5I-P**).

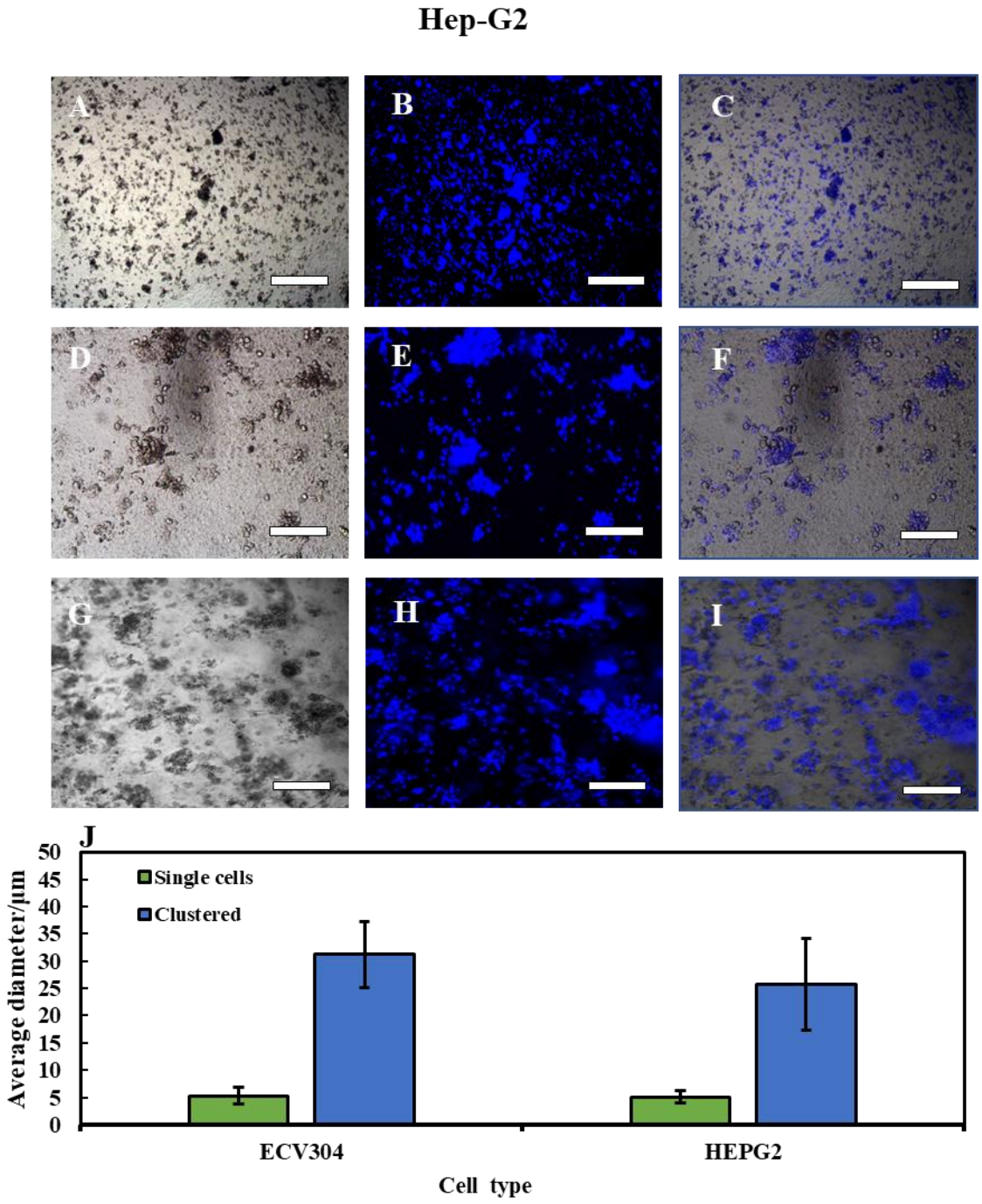

Figure 3.6. Observation of the HepG2 clusteroids in different forms : A-F: flow state in complete medium, G-I:clusteroids in the 1.5wt% alginate gel,. The filters were set at bright-field (A, D, G) , DAPI(B, E, H) and Dual Fluorescence (C, F,I) for imaging. K is the average diameter of the various forms of ECV304 and Hep-G2 cells. The bar is 200μm for A-C and 100 for D-J.

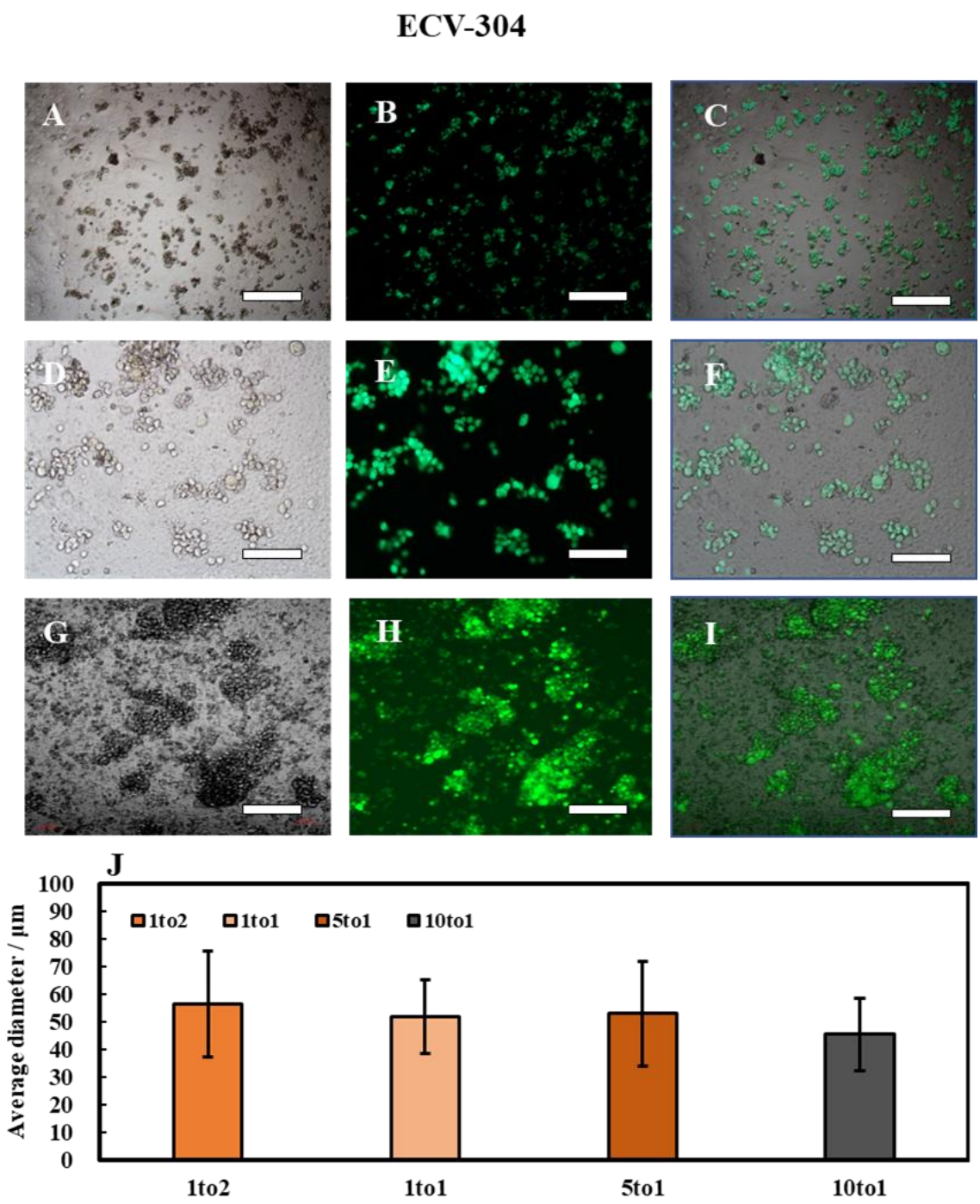

Figure 3.7. Observation of the ECV304 clusteroids in different forms: A-F: flow state in complete medium, G-J:clusteroids in the 1.5wt% alginate gel,. The filters were set at bright-field (A, D, G) , DAPI(B, E, H) and Dual Fluorescence (C, F, I) for imaging. J is the average diameter of the co-cultured clusteroids at different cell ratio. The bar is 200μm for A-C and 100 for D-I.

We also used Image-J to measure the size of the two kinds of clusteroids, as well as the morphology of the Hep-G2 and ECV304 clusteroids under a fluorescence microscope. Aqueous emulsion templates have previously been used by our group to produce different kinds of cell clusteroids. This study was conducted to determine whether this method can be effectively used in mass production (**Figure 3.13(6)A-J**, **Figure 3.14(7) A-J**). Compared to Hep-G2, the size of ECV304 is slightly bigger than the Hep-G2, of about 5.00, therefore there are more clusteroids formed with ECV304 compared to Hep-G2.

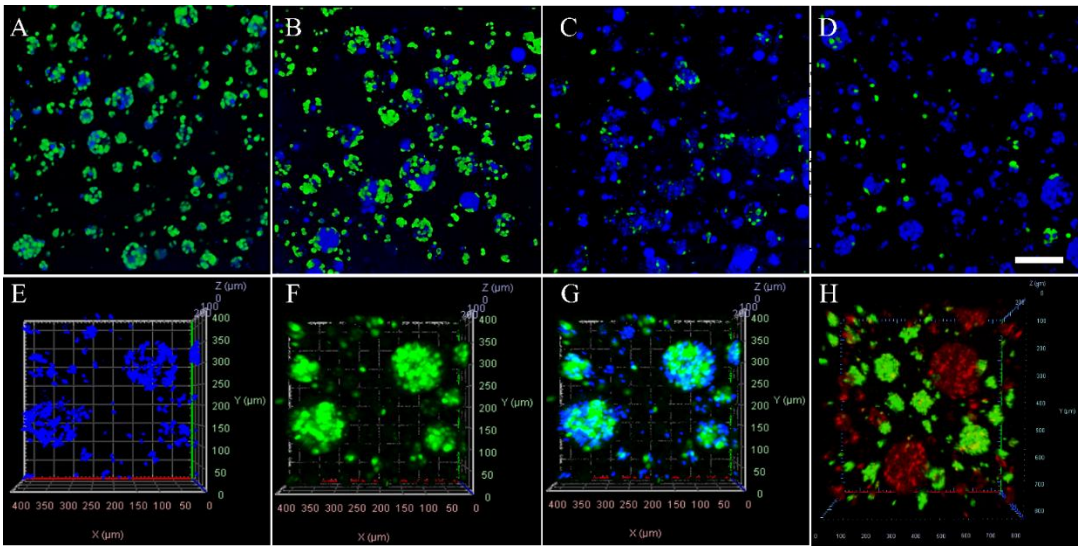

Figure 3.8. A-B: Confocal microscopy observations of co-cultured clusteroids at different Hep-G2/ECV cells ratio: (A) 1:1, (B) 2:1, (C) 5:1, (D) 10:1. (E-F) 3D Z-stacked image of E-G co-cultured Hep-G2/ECV 304 clusteroids at a cell ratio of 1:1 set at different fluorescence channels-FITC (F), DAPI (E) and Dual fluorescence (G) (H) 3D Z-stacked image of the mixture of individual Hep-G2 and ECV 304 clusteroids at a cell ratio of 1:1. In (A-D), the Hep-G2 cells and ECV 304 cells were pre-stained with DAPI and CMFDA, respectively. For distinguishing the different patterns, the Hep-G2 cells were stained with CFSE far-red, and the ECV 304 cells were stained with CFSE green in (H). The bar is 100μm for (A-D). The box size is 400×400 μm for (E-G) and 800×800 μm for (H).

Confocal microscopy was used to further evaluate the co-culture pattern of clusteroids. As can be seen in **Figure 3.8A-D**, its proportion in the clusteroids of Hep-G2/ECV304 corresponds to the ratio of cell types suspended in every droplet, which is in agreement with the proportion of each type within a droplet. Hep-G2 proportion

decreased from 68m to 45m, decreasing the clusteroids' size. The individual or clustered cell size of ECV304 is larger in comparison to the result in **Figure 3.6**, **3.7** It was evident from the 3D Z-stacked images that were shown in **Figure 3.4E-G** that the two kinds of cells self-organized into integral clusteroids by co-culturing Hep-G2/ECV 304 with a cell ratio of 1:1. Through these images, it was attainable to see that the two kinds of cells self-organized into integral clusteroids through different fluorescence channels. To demonstrate that Hep-G2 and ECV 304 clusteroids did not migrate together to form co-cultured clusteroids, **Figure 3.8H** illustrates the 3D Z-stacked image of a mixture of individual clusteroids at a 1:1 cell ratio. The use of the W/W emulsion template enabled the production of co-cultured clusteroids with different cell ratios by varying the initial cell proportion.

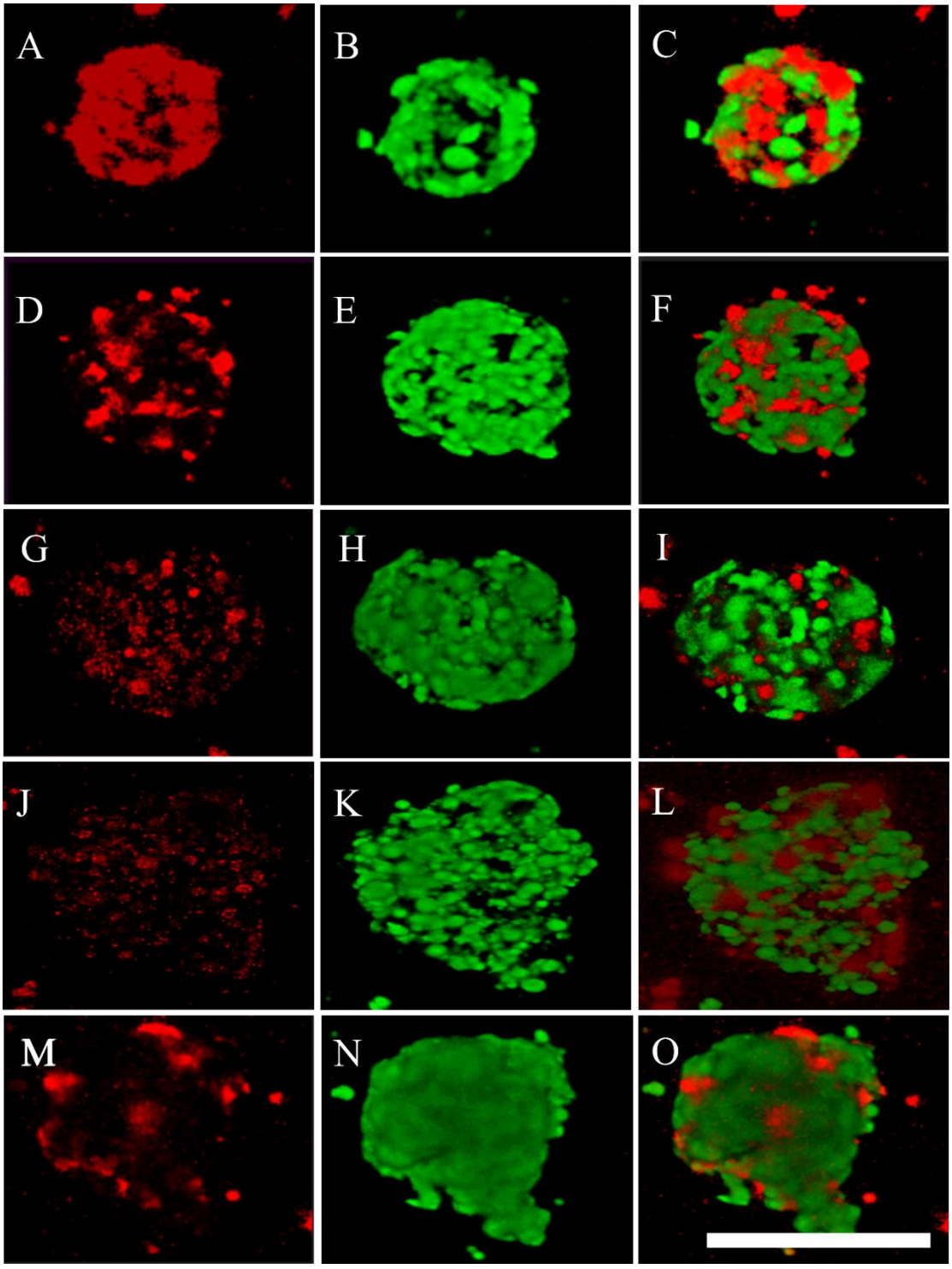

Figure 3.9. 3D Z-stacked CLSM images of co-cultured Hep-G2/ECV 304 clusteroids at a cell ratio of 1:1 after different days of culture: (A-C) day 1, (D-F) day 3, (G-I) day 5, (J-L) day 11, (M-O) day 14. The filters were set at CFSE far red (A, D, G, J, M), FITC,(B, E, H, K, N) and Dual Fluorescence (FITC/TRITC) (C, F, I, L, O) channels for imaging. The bar is 100 μm. The Hep-G2 cells were stained with CFSE far-red, and the ECV 304 cells were stained with CFSE green.

3.4.2 Long term proliferation of the co-cultured cell clusteroids in sodium alginate gel

Vesselized cell clusters are frequently used for tissue engineering and drug testing purposes. [34,35] These two purposes require different numbers of clusters of cells in order to be effective, and the requirements for each are different. Cell clusteroids were adjusted to have the appropriate concentration in the gel to suit the downstream application that was to be performed.For the layered cell formation, we transferred 1×10^6 cells/mL into 24-well microplates, and over 20×10^5 cells/mL for the single clusteroid observation. After mixing the cells with sodium alginate gels, a fixed amount of co-cultured clusteroids was transferred into a 96-well microplate. The calcium chloride-solidified substrate allows clusteroids to propagate in three dimensions for a very long time. For 14 days, fluorescence microscopes monitored the proliferation of Hep-G2 and ECV 304 clusteroids, which were labelled with generational dyes. There is a strong likelihood that the single clusteroid would proliferate gradually as shown in the **Figure 3. 9**where there is a 1:1 ratio between Hep-G2 and ECV 304. Co-cultured clusteroids dominated by green signals after day 5 since the ECV 304 cells grew at a significantly faster pace than the Hep-G2 cells and we observed a pronounced increase in green signals after day 5 as well. When the ECV 304 was cultured in monolayer, it was possible to split the cells into 16 in just one passage (**Figure 3.9**). Generally, following 14 days of proliferation, the proportion of Hep-G2 cells was equal to that of the ECV 304 cell, with an increase in the Hep-G2 cell ratio (5:1) (**Figure 3.9**). Increasing the cell concentration (1×10^6) to facilitate fusion between clusteroids was important for production of the clusteroids layer (**Figure 3.10**).

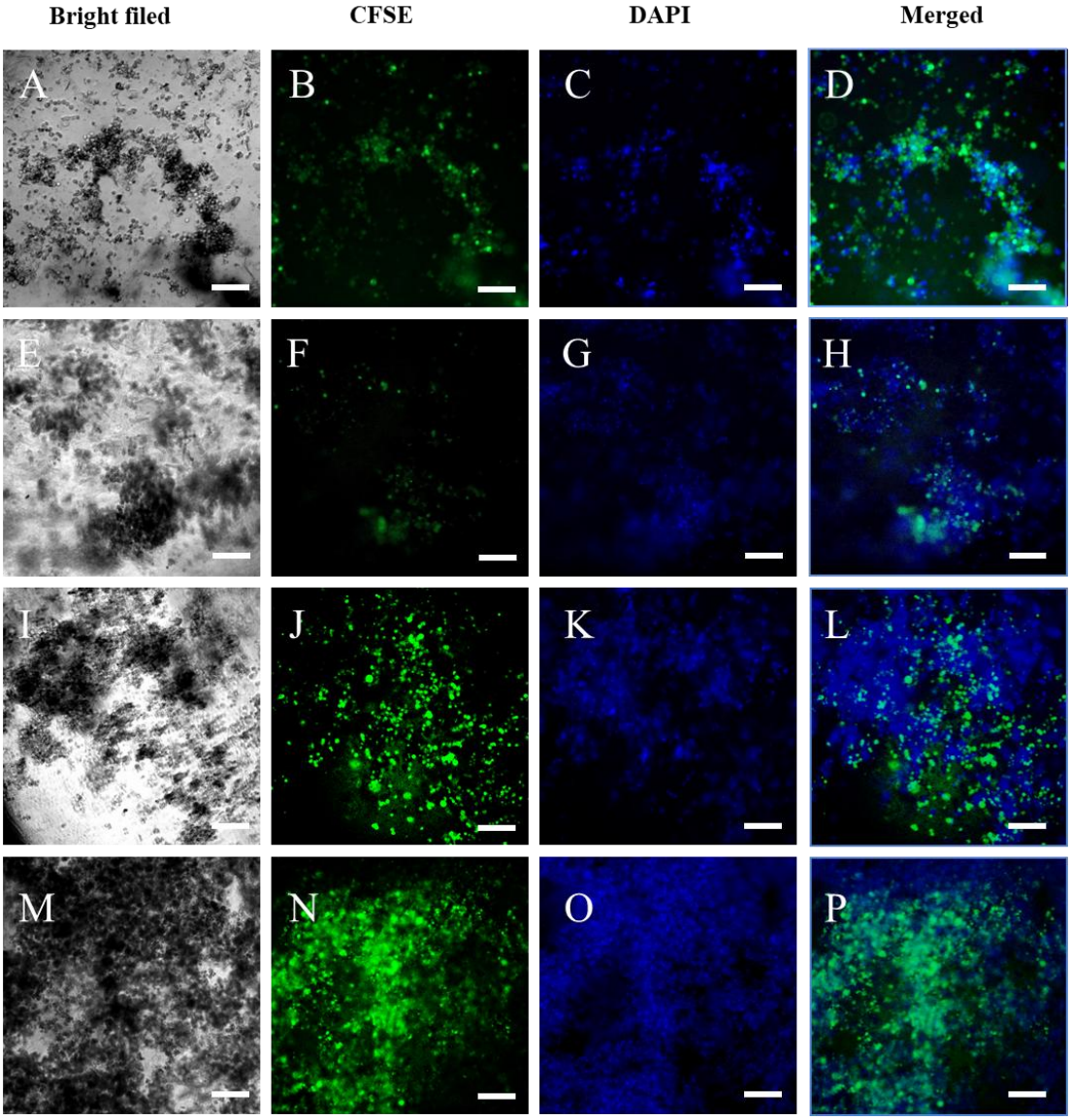

Figure 3.10. Observation of the co-culture spheroid growth in 1wt% sodium alginate gel at different days of culture: A-D: day 1, E-H: day 3, I-L: day 5 M-P: day 7. The filters were set at bright-field (A,E,I,M) ,CMFDA (B,F, J,N), DAPI(C,G,K,O) and Dual Fluorescence (D,H,L,D) for imaging. The bar is 100μm.

It takes a long time before the clusteroids are able to reach their appropriate interfaces because they proliferate. At a 1:1 ratio of Hep-G2:ECV304, it is also obvious that ECV304 dominates the proliferation of the larger number of cell clusteroids. A tissue-like 3D compacted layer formed after the individual clusteroids grew to fill the space between them. Observations of the layered formation tracking on the clusteroids suggest just the same layout on the confocal scale. Green fluorescent signals controlled clusteroids and proliferation of ECV304 cells (**Figure**

3.11). In summary, these results indicate that we can benefit from our Pickering emulsion template in terms of preparing both individual Hep-G2/ECV304 cells or many co-cultured cells at different ratios with the aim of testing drugs or engineering tissues for use in tissue engineering or tissue testing applications. This method is proven to be superior based on morphological characterization. Several tests were performed to ensure that our co-culturing method clearly and reproducibly enhances cell-to-cell contact.

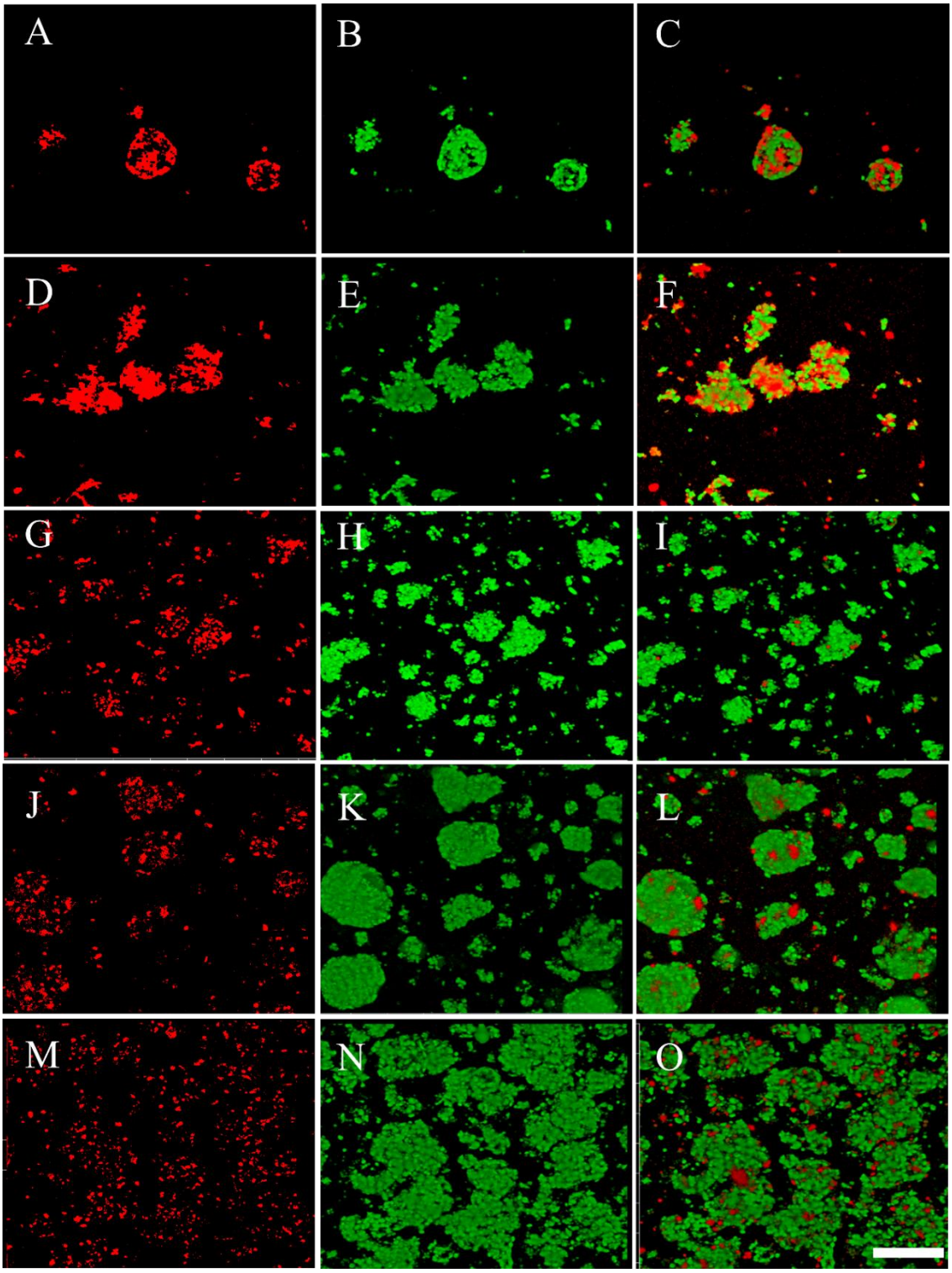

Figure 3.11. CLSM images of the proliferation of co-cultured Hep-G2/ECV 304 clusteroids at a cell ratio of 1:1 after different days of culture in 1wt% sodium alginate gel: (A-C) day 1, (D-F) day 3, (C-I) day 5, (J-L) day 11, (M-O) day 14. The filters were set at CFSE far-red/Fluorescein dual channels imaging.The Hep-G2 cells were

stained with CFSE far-red, and the ECV 304 cells were stained with CFSE green. The bar is 100μm.

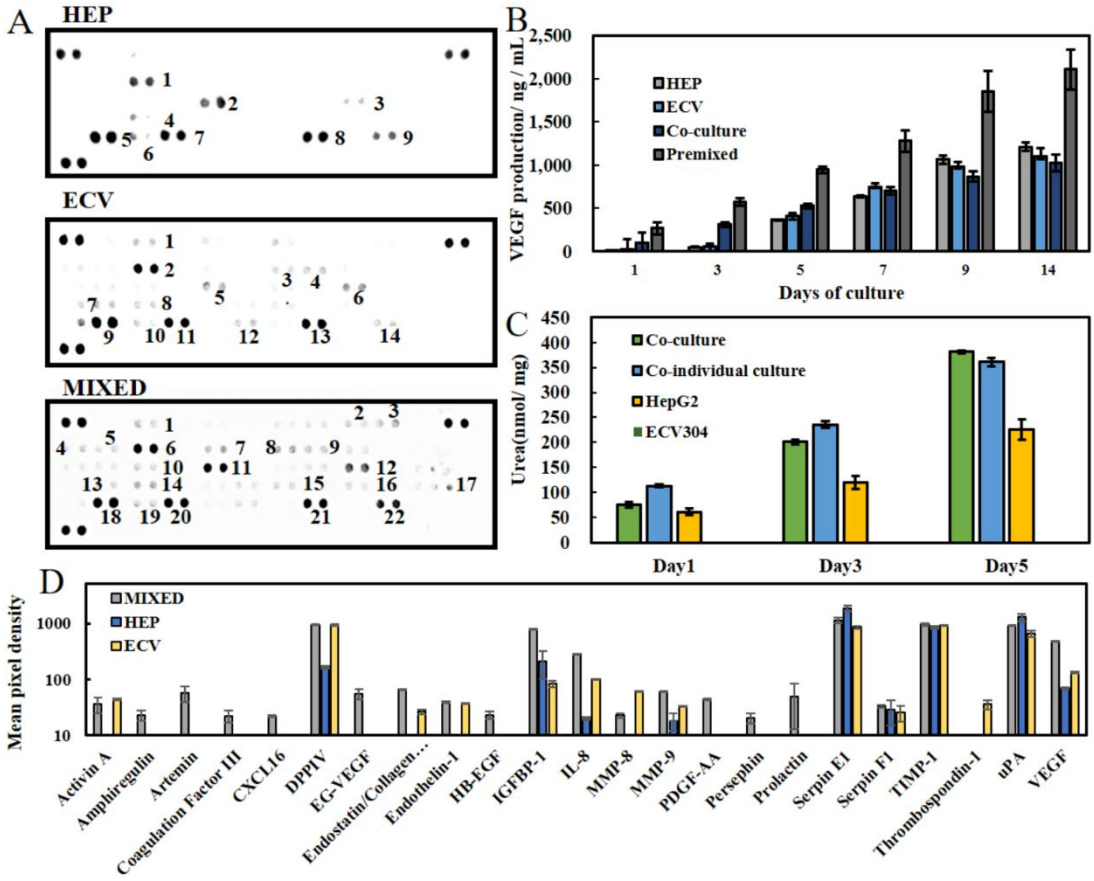

Figure 3.12 (A) Angiogenesis array membrane of individual Hep-G2 clusteroids, ECV 304 clusteroids, and the co-culture clusteroids at a cell ratio of 1:1 after 14 days of proliferation in the gel. The initial cell number were 1×10^6 for all. (B) VEGF production of the Hep-G2 clusteroids, ECV 304 clusteroids, simple mixing of individual Hep-G2 and ECV 304 clusteroids, and the co-culture clusteroids at a cell ratio of 1:1. (C) Urea production of Hep-G2 clusteroids, ECV 304 clusteroids, and the co-culture clusteroids at a cell ratio of 1:1 after 7 days of proliferation in the gel. The initial cell number were 1×10^6 for all. (D) Angiogenesis-related protein production in the individual Hep-G2 clusteroids, ECV 304 clusteroids, and the co-culture clusteroids at a cell ratio of 1:1 after 14 days of proliferation.

3.4.3 Production of angiogenic factors by co-cultured clusteroids

We were interested in determining if either of the clusteroids would vascularize in a co-culture pattern by co-culturing ECV304 and Hep-G2. To perform a cocktail antibody array for the detection of angiogenesis in clusteroids, we collected the

supernatant from the clusteroids cultures. The production of various genes implicated in angiogenesis was compared between the co-cultured clusteroids and the individual clusteroids of ECV304 and Hep-G2. Several angiogenesis-related genes were induced in co-culture patterns, as shown by **Figure 3.12A**. **Figure 3.13** shows the specific genes detected in the three types of clusteroids. Angiogenesis and anti-angiogenesis features of these genes are shown in **Figure 3.14**. Comparing the cultures to the ECV304 and HEP-G2 clusteroids, it was clearly evident that there had been a significant rise in the expression of IGFBP-1, IL-8, and VEGF when compared to the control cultures (**Figure 3.12D**). It has been found that seven genes can only be detected in the clusteroids co-cultured with other clusteroids. These genes include Activin A, Amphiregulin, Artemin, and Human Basic EGF, all of which are believed to be pro-angiogenic (**Figure 3.13**). Serpin-F1, Serpin-E1, and TIMP-1 production levels were not enhanced. The Serpin-E1 is known to be a potential inhibitor of tissue plasminogen activator (tPA) as well as urokinase (uPA).[36] Angiogenesis is negatively regulated by serine proteases (Serpin E1, Serpin F1).[37] The encoded protein is secreted and strongly inhibits angiogenesis. The TIMP production was also highly connected to the inhibition of angiogenesis by serving as natural inhibitors of the matrix metalloproteinases (MMPs). [38] In summary, the angiogenesis array suggests that both the co-cultured platform and the HEP-G2 clusteroids demonstrated that seven pro-angiogenesis-related proteins were released on the co-cultured platform, seven proteins that were not found on either ECV304 or HEP-G2. There was no increased production of TIMP, Serpin-F1, or Serpin-E1 anti-angiogenesis proteins. Blood vessel formation may also be influenced by the imbalance of anti- and proangiogenic proteins.

+)	Activin A
(+)	Amphiregulin
(+)	Artemin
(+)	Coagulation Factor III
(+)	CXCL16
(+)	DPPIV
(+)	EG-VEGF
(+)	Endostatin/Collagen XVIII
(+)	Endothelin-1
(+)	HB-EGF
(+)	IGFBP-1
(+)	IL-8
(+)	MMP-8
(+)	MMP-9
(+)	PDGF-AA
(+)	Persephin
(+)	Prolactin
(-)	Serpin E1
(-)	Serpin F1
(-)	TIMP-1
(+)	uPA
(+)	VEGF

Figure 3.13. The effect of the Angiogenesis-related genes on the vascularization precess. (+) represents that they are pro-angiogenesis and vice versa.

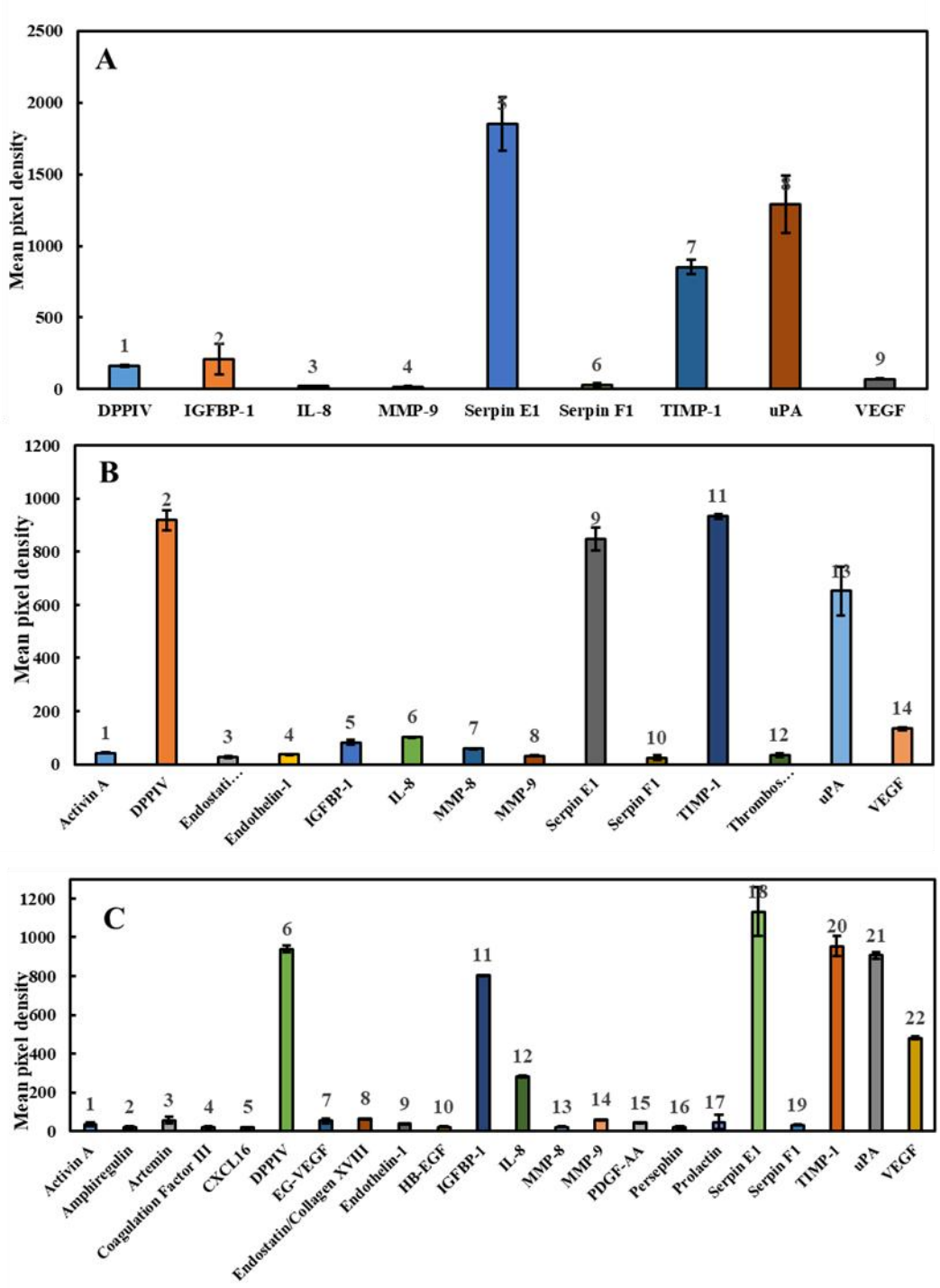

Figure 3.14. Angiogenesis-related protein production in the A: individual Hep-G2 clusteroids, B: ECV 304 clusteroids, and the C:co-culture clusteroids at a cell ratio of 1:1 after 14 days of proliferation.

The angiogenesis kit was verified through the use of several ELISA kits, including VEGF, IGFBP-1, MMP-2, and Urea assays. Angiogenesis-related cytokines such as VEGF are frequently discussed because they act as stimulators on the *in vitro*

vascularization of spheroid structures.[39,40] Over the course of 14 days of culture, we tested four patterns of clusteroids for VEGF production. A comparison between **Figure 3.12B** and **Figure 3.12C** illustrates that the co-cultured pattern produced two-fold more than the other three. As can be seen in **Figure 3.12D**, this result corresponds to the result that can be seen in **Figure 3.12D.** Another major function of Hep-G2 related to nitrogen-containing compounds is the metabolism of Urea, which is the main nitrogen-containing substance in the urine of mammals and plays an essential role in the metabolism of nitrogen-containing compounds by animals. In the early stages of cell co-culture, the production of Urea was low on day2, most probably because the cells had yet to adapt to the culture conditions (**Figure 3.12E**). As compared to the other patterns, the production on day 7 has been outperforming the other patterns on a massive scale.

3.4.4 Endothelial cell sprouting

In primary cultured endothelial cells, the spheroid-based sprouting assay has been demonstrated to be a reliable and robust method for analyzing the effects of genetic alterations or pharmacological compounds on the formation of capillary-like tubes. In most cases, Matrigel is used as the ECM. We performed the sprouts assay on sodium alginate gel. Angiogenesis extent can be determined by the length of the sprouts on spheroids. The work we performed in our study has shown that when the ratio of Hep-G2:ECV304 was 1:2, the clusteroids may form sprouts into the sodium alginate gel under the same conditions (**Figure 3.15A-D**). There may be a unique interaction between cells that results in the different cell ratio necessary for sprouts to form. There were no capillary structures that could be formed by the individual clusteroids of Hep-G2 or ECV304 cells. It is usually necessary to add VEGF externally to encourage sprouting when conducting the 3D endothelial cell sprout assay. Here, we generated sprouts without adding any exogenous substances by co-culturing carcinoma cells with ECV304 cells. By irritating the ECV304 cells with VEGF, Hep-G2 could drive sprouting.[41] The clusteroids, however, did not continue to stretch the existing sprouts after the spheroids sprouted to about 10m on day 3 (**Figure 3.15F**). Matrix metalloproteinases are comprised of a number of proteins including the MMP-2 protein. It plays an important role in assisting in the breakdown of ECM, both in normal physiological processes like the development of embryos, reproduction, and tissue remodelling, as well as in diseases such as arthritis and

metastasis. [42] When clusteroids sprout into the extracellular matrix, MMP-2 plays a crucial role.[43] As a result of co-culturing clusteroids with ECV304 and Hep-G2, MMP-2 production was slightly higher after 14 days as compared to the individual clusteroids (**Figure 3. 15E**). The sprouts may have stopped expanding after 3 days of culture, or it may be related to the fact that the sprouts are declining in size(**Figure 3.16**). There have been earlier reports demonstrating that spheroids cultured with carcinoma cells or E.C.s produced sprouts without the addition of VEGF, similar to those that were observed in the culture of carcinoma cells and E.C.s. [44,45] In a co-culture pattern, the sprouting ability of the E.C.s could, however, clearly be retained.[44] SEM imaging revealed that the clusteroids in the co-cultured clusteroids were observed to have several tail-like structures (**Figure 3. 16**C), which was not observed in the individual clusteroids (**Figures 3. 17A, B**).

.

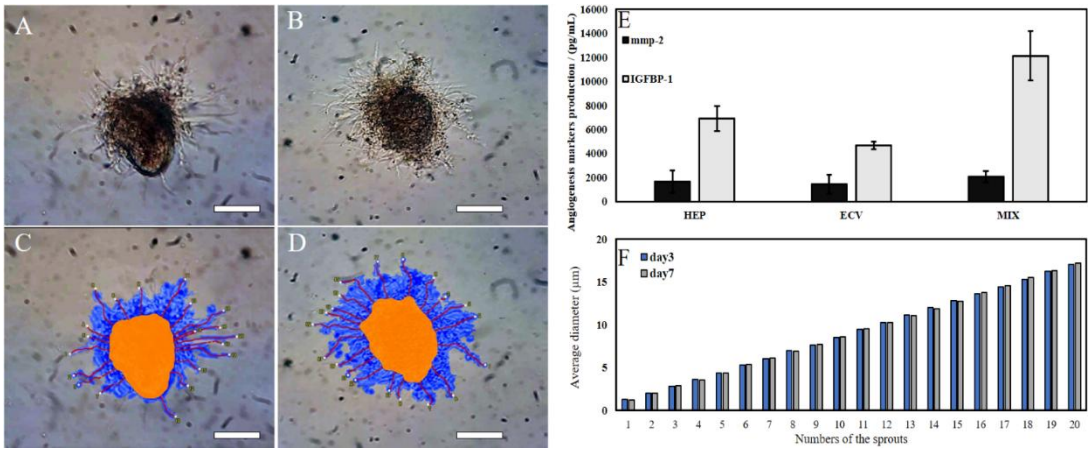

Figure 3. 15. Bright field observation (A, B) and the corresponding Wimasprouts analysis (C, D) of the co-culture clusteroids at a cell ratio of 1:2 (Hep-G2 : ECV 304) after 3 days of culture in 1wt% sodium alginate gel. (E) MMP-2 and IGFBP-1 production of the individual Hep-G2 clusteroids, ECV 304 clusteroids, and the co-culture clusteroids at a cell ratio of 1:1 after 14 days of proliferation in the gel (The initial cell number were 1×10^6 for all). (F) The length of the sprouts in (C, D).

The bar is 50 μm.

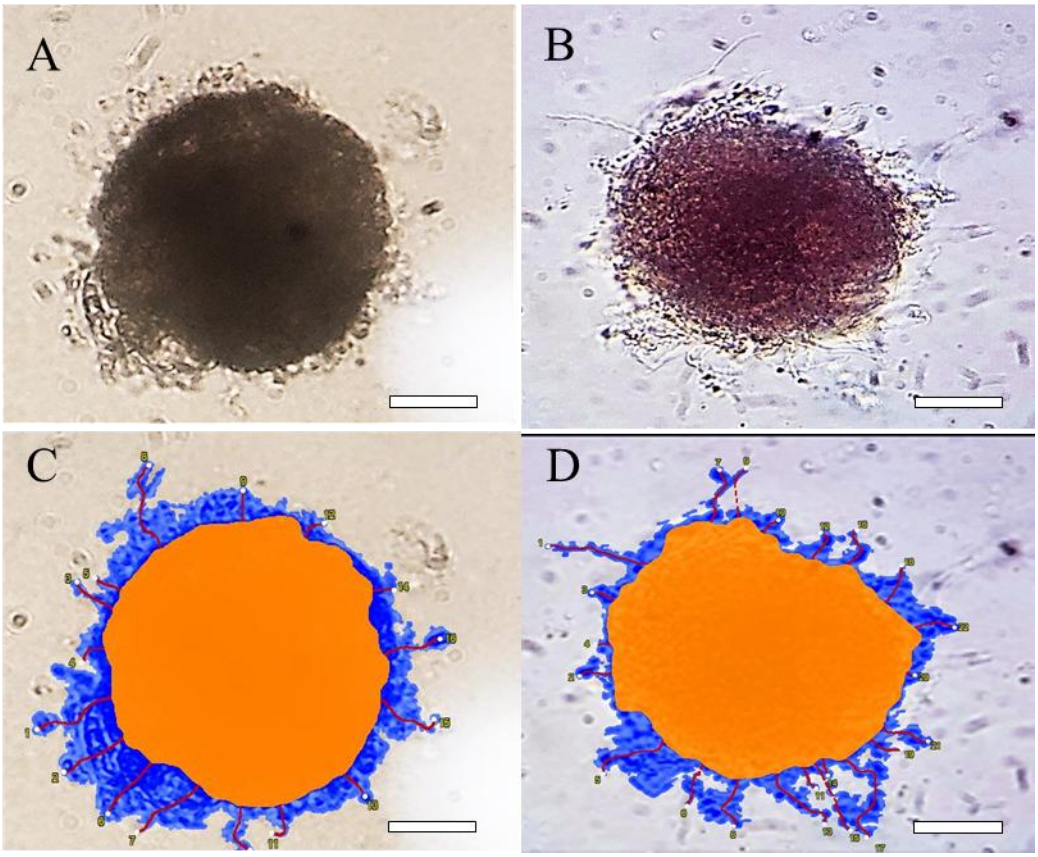

Figure 3.16. Bright field observation(A, B) and the corresponding Wimasprouts analysis (C, D) of the co-culture clusteroids at a cell ratio of 1:2(Hep-G2:ECV 304) after 3 days of culture in 1wt% sodium alginate gel. The bar is 50μm.

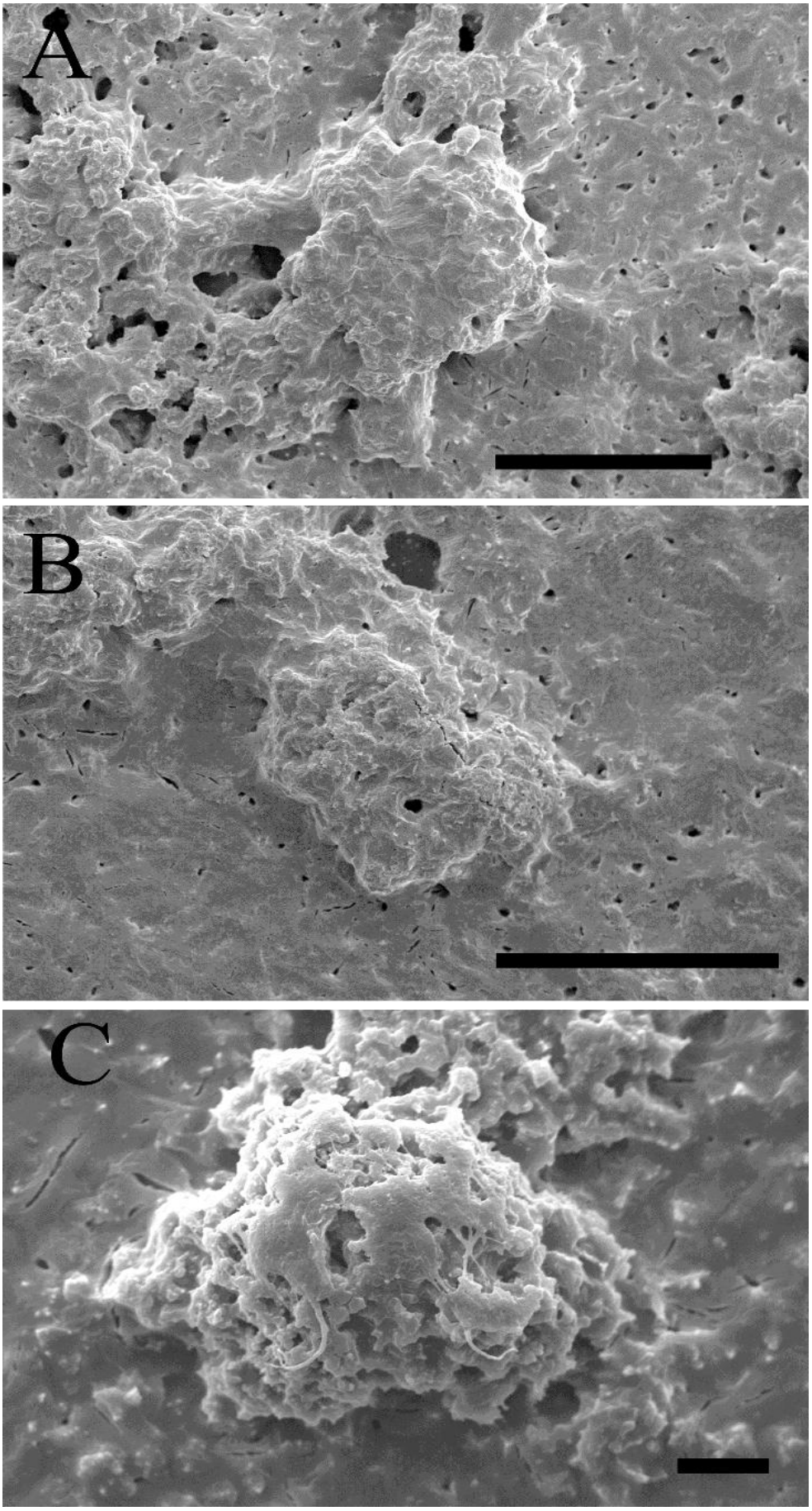
A
B
C

Figure 3. 17. SEM observation of the (A) single cell type Hep-G2 clusteroids, (B) single cell type ECV 304 clusteroids, (C) Co-culture of Hep-G2 : ECV 304 clusteroids at a ratio of 1:1. The bar is 100μm for A,B and 10μm for C.

As far as immunostaining is concerned, immunohistochemistry (IHC) is the most common application of immunostaining. By exploiting the principle of antibodies binding specifically to antigens in biological tissues, this approach involves the process of selectively identifying antigens (proteins) in cells of a tissue section based on the fact that antibodies are known to bind to antigens in biological tissues. It has been shown that ECV304 cells cultured on collagen I are strongly positive for CD34, weakly positive for CD31, and negative for von Willebrand factor. In this study, the endothelial phenotype of cocultured clusteroids was evaluated using an immunofluorescent staining for CD34 and endothelial cell surface markers. In vitro, CD34 selects endothelial cells with a tip cell phenotype. CD34 is a highly glycosylated transmembrane cell surface glycoprotein, expressed by a hematopoietic stem and progenitor and on the luminal cell membrane of quiescent endothelial cells of small blood vessels and lymdphatics.46 CD34 was detected in a single cocultured clusteroid and the cocultured clusteroid layer (**Figure 3.18**). Cocultured clusteroids showed a clear tubule network, which was further illustrated by CD34 staining within the cocultured clusteroids, providing a slight hint as to whether or not the cocultured clusteroids formed their own blood vessels. Angiogenic behavior of cancer cells in vivo has the potential to be studied in detail by using primary cell lines or biopsy tissue so as to understand the precise interaction between the endothelial cells and the carcinoma cells in vivo. These coculture models should be tested for adhesion junction proteins like VE-cadherin and cytoskeletal proteins.

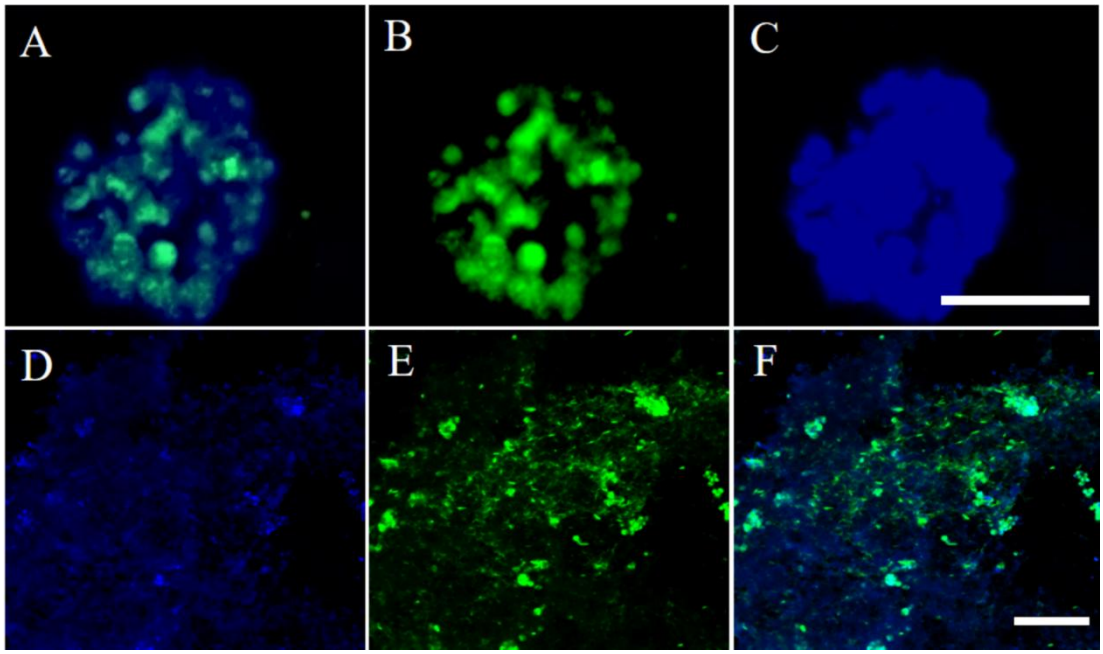

Figure 3.18 Confocal observation of the Co-culture of Hep-G2 clusteroids and ECV 304 clusteroids at a ratio of 1:1 with CD34-FITC conjugated labeling on individual clusteroid (A-C) and (D-F) formed layer of clusteroids. The bar is 200 μm for (D-F).

3.5 Conclusions

In this study, we developed a facile and efficient method of producing a three-dimensional coculture of Hep-G2/ECV304 clusteroids by combining mixed cell types Hep-G2. With whey protein particles stabilized by Pickering emulsion droplets, clusteroids with various cell ratios could be cocultured. Using fluorescence microscopy and confocal microscopy as well as the long-term tracking of the co-cultured clusteroids, we were able to accomplish the objective successfully. Several cell types were characterized as well as the role that large amounts of the clusteroids cocultured in one cell type were played in the proliferation pattern. The cocultured clusteroids sprouted into sodium alginate hydrogel ECM when the ratio of two cell types (Hep-G2/ECV304) was changed to 1:2. It has been found that the cocultured clusteroid pattern significantly increases the production of various angiogenesis genes in a manner that is similar to angiogenesis. The enhanced production of VEGF, urea, and IGFBP also indicated the angiogenesis progress triggered by the coculture pattern. Immunohistochemistry assays also revealed the presence of a marker that is associated with angiogenesis, known as CD34. Researchers can fabricate a variety of

cocultured and conceivably tricultured clusteroids using this coculturing platform. It was possible to replace the cell lines used in our experiments with any other cell lines or primary cell cultures as needed. The aim of this work is to resolve the lack of a simple-to-handle, high-throughput method to produce vascularized 3D clusteroids in vitro, which are expected to be used in numerous applications including drug testing, tissue engineering, and cell biology.

3.6 Reference

1. Wang, A.; Madden, L. A.; Paunov, V. N. *J. Mater. Chem. B Mater. Biol. Med,.* 2020, **8** , 10487–10501.

2. Ravi, M.; Paramesh, V.; Kaviya, S. R.; Anuradha, E.; Solomon, F. D. P. *J. Cell. Physiol,.* 2015, 230 (1), 16–26.

3. Jensen, C.; Teng, Y. *Front. Mol. Biosci,.* 2020, **7**, 33.

4. Fontoura, J. C.; Viezzer, C.; Dos Santos, F. G.; Ligabue, R. A.; Weinlich, R.; Puga, R. D.; Antonow, D.; Severino, P.; Bonorino, C. *Mater. Sci. Eng. C Mater. Biol,. Appl*. 2020, **107** , 110264.

5. Andersen, M. L.; Winter, L. M. F. *An. Acad. Bras. Cienc*. 2019, **91** (suppl 1), e20170238.

6. Varga, O. E.; Hansen, A. K.; Sandøe, P.; Olsson, I. A. S. *Altern. Lab. Anim,.* 2010, **38** (3), 245–248.

7. Gilazieva, Z.; Ponomarev, A.; Rutland, C.; Rizvanov, A.; Solovyeva, V. *Cancers (Basel),.* 2020, **12** , 2727.

8. Guillaume, L.; Rigal, L.; Fehrenbach, J.; Severac, C.; Ducommun, B.; Lobjois, V. *Sci. Rep,.* 2019, **9**, 6597.

9. Hirschhaeuser, F.; Menne, H.; Dittfeld, C.; West, J.; Mueller-Klieser, W.; Kunz-Schughart, L. A. *J. Biotechnol,.* 2010, **148**, 3–15.

10. Mironov, V.; Visconti, R. P.; Kasyanov, V.; Forgacs, G.; Drake, C. J.; Markwald, R. R. *Biomaterials,.* 2009, **30** , 2164–2174.

11. Mattix, B.; Olsen, T. R.; Gu, Y.; Casco, M.; Herbst, A.; Simionescu, D. T.; Visconti, R. P.; Kornev, K. G.; Alexis, F. *Acta Biomater,.* 2014, **10**, 623–629.

12. Kim, E. M.; Lee, Y. B.; Kim, S.-J.; Park, J.; Lee, J.; Kim, S. W.; Park, H.; Shin, H. *Acta Biomater,.* 2019, **100**, 158–172.

13. Mukomoto, R.; Nashimoto, Y.; Terai, T.; Imaizumi, T.; Hiramoto, K.; Ino, K.; Yokokawa, R.; Miura, T.; Shiku, H. *Analyst,.* 2020, **145** , 6342–6348.

14. Folkman, J.; Haudenschild, C. *Nature,.* 1980, 288 (5791), 551–556.

15. Carmeliet, P. *Oncology*,.2005, **69**, 4–10.

16. Benedito, R.; Roca, C.; Sörensen, I.; Adams, S.; Gossler, A.; Fruttiger, M.; Adams, R. H. *Cell*,. 2009, **137**, 1124–1135.

17. Karagiannis, E. D.; Popel, A. S. *J. Theor. Biol,.* 2006, **238**, 124–145.

18. Yana, I.; Sagara, H.; Takaki, S.; Takatsu, K.; Nakamura, K.; Nakao, K.; Katsuki, M.; Taniguchi, S.-I.; Aoki, T.; Sato, H.; Weiss, S. J.; Seiki, M. *J. Cell Sci,.* 2007, **120**, 1607–1614.

19. Vandekeere, S.; Dewerchin, M.; Carmeliet, P. *Microcirculation,.* 2015, **22** (7), 509–517.

20. Shamloo, A.; Heilshorn, S. C. *Lab Chip,.* 2010, **10**, 3061–3068.

21. Twardowski, R. L.; Black, L. D., III. Ann. *Biomed. Eng,.* 2014, **42**, 1074–1084.

22. Wirz, W.; Antoine, M.; Tag, C. G.; Gressner, A. M.; Korff, T.; Hellerbrand, C.; Kiefer, P. *Differentiation,.* 2008, **76**, 784–794.

23. Pfisterer, L.; Korff, T. *In Methods in Molecular Biology*,. 2016; pp 167–177.

24. Timmins, N.; Dietmair, S.; Nielsen, L. *Angiogenesis,.* 2004, **7**, 97–103.

25. Shah, S.; Lee, H.; Park, Y. H.; Jeon, E.; Chung, H. K.; Lee, E. S.; Shim, J. H.; Kang, K.-T. *J. Vis. Exp,.* 2019, **151**, e60032.

26. Correa de Sampaio, P.; Auslaender, D.; Krubasik, D.; Failla, A. V.; Skepper, J. N.; Murphy, G.; English, W. R. *PLoS One,.* 2012, **7**, e30753.

27. Nashimoto, Y.; Okada, R.; Hanada, S.; Arima, Y.; Nishiyama, K.; Miura, T.; Yokokawa, R. *Biomaterials,.* 2020, **229**, 119547.

28. Atefi, E.; Lemmo, S.; Fyffe, D.; Luker, G. D.; Tavana, H. *Adv. Funct. Mater*,. 2014, **24** , 6509–6515.

29. Lemmo, S.; Atefi, E.; Luker, G. D.; Tavana, H. *Cell Mol Bioeng,.*2014, **7**, 344–354.

30. Das, A. A. K.; Filby, B. W.; Geddes, D. A.; Legrande, D.; Paunov, V. N. *Mater. Horiz,.* 2017, **4**, 1196–1200.

31. Wang, A.; Weldrick, P. J.; Madden, L. A.; Paunov, V. N. *ACS Appl. Mater. Interfaces,.* 2021, **13**, 22182–22194.

32. Wang, A.; Weldrick, P. J.; Madden, L. A.; Paunov, V. N. *Biomater. Sci,.* 2021, **9**, 6927–6939.

33. Xiong, W.-C.; Simon, S. ECV304 Cells: *J. Biol. Chem,.* 2011, ***286*** , le21.

34. Kim, S.; Kim, E. M.; Yamamoto, M.; Park, H.; Shin, H. *Adv. Healthc. Mater,.* 2020, **9** , 2000608.

35. Laschke, M. W.; Menger, M. D. *Biotechnol. Adv,.* 2017, **35** , 782–791.

36. Fortenberry, Y. M. Plasminogen *Expert Opin. Ther. Pat,.* 2013, **23**, 801–815.

37. Ratushnyy, A.; Ezdakova, M.; Yakubets, D.; Buravkova, L. *Stem Cells Dev,.* 2018, **27**, 831–837.

38. Ito, A.; Sato, T.; Iga, T.; Mori, Y. *FEBS Lett,.* 1990, **269**, 93–95.

39. Pepper, M. S.; Mandriota, S. J.; Jeltsch, M.; Kumar, V.; Alitalo, K. . *J. Cell. Physiol,.* 1998, **177**, 439–452.

40. van Nieuw Amerongen, G. P.; Koolwijk, P.; Versteilen, A.; van Hinsbergh, V. W. M. *Arterioscler. Thromb. Vasc. Biol,.* 2003, **23**, 211–217.

41. Fujimoto, A.; Onodera, H.; Mori, A.; Nagayama, S.; Yonenaga, Y.; Tachibana, *T. Cancer Res,.* 2005, ***65***, 268–269.

42. Rundhaug, J. E. *J. Cell. Mol. Med,.* 2005, **9** , 267–285.

43. Sang, Q. X. *Cell Res,.* 1998, **8**, 171–177.

44. Kunz-Schughart, L. A.; Schroeder, J. A.; Wondrak, M.; van Rey, F.; Lehle, K.; Hofstaedter, F.; Wheatley, D. N. *Am. J. Physiol. Cell Physiol,.* 2006, **290** , C1385–C1398.

45. Wenger, A.; Kowalewski, N.; Stahl, A.; Mehlhorn, A. T.; Schmal, H.; Stark, G. B.; Finkenzeller, G. *Cells Tissues Organs,.* 2005, **181** , 80–88.

46. Fujimoto, A.; Onodera, H.; Mori, A.; Nagayama, S.; Yonenaga, Y.; Tachibana, *T. Cancer Res,.* 2005, **65** , 268–269.

47. Siemerink, M. J.; Klaassen, I.; Vogels, I. M. C.; Griffioen, A. W.; *Angiogenesis,.*2012, **15** , 151–163.

4. Chapter 4

Vascularized Co-Culture Clusteroids of Primary Endothelial and Hep-G2 Cells Based on Aqueous Two-Phase Pickering Emulsions

4.1 Abstract

Due to its availability and relatively mature biochemical properties, three-dimensional cell culture has been extensively used in biomedical applications. *In vitro* models require a higher level of detail than 3D cell culture models based on hydrogels or different scaffolds. As oxygen permeation is impaired in the absence of blood vessels, necrotic core formation interferes with the use of 3D cell cultures *ex vivo*. Using a water-in-water (w/w) Pickering emulsions template, we report a simple method for forming co-cultured 3D clusteroids of angiogenic HUVEC and Hep-G2 cells. By manipulating the proportion of cells, we were able to stimulate the production of various angiogenic proteins markers in the co-cultured clusteroids. Without the exogenous addition of Vascular Endothelial Growth Factor (VEGF) or other angiogenesis inducers, HUVEC cells form endothelial cell sprouts in Matrigel in the presence of Hep-G2 cells and their byproducts. Cell co-culture spheroids may also be produced by this method with ease using other types of cells.It can be used in drug testing and tissue engineering applications as well as for the fabrication of 3D co-culture models using w/w Pickering emulsion templates.

4.2 Introduction

For the creation of 3D cell culture models, non-adhesive flasks, hydrogels, or microfluidic devices are used to aggregate the cells into densely packed spheroid.[1-3] Since their introduction during the 20th century, 3D cell models have been widely utilized in the field of drug testing. [4,5] A significant advantage of these *in vitro* 3D models over animal models is that there are no sophisticated operations or strict ethical review requirements as there is with animal models. [6,7] Its availability and precise replica of real-life environments have attracted a significant amount of attention. A preclinical test of drugs can be conducted on 3D spheroids/organoids for the purpose of determining their release kinetics.[8-10] Scientists have been developing

organoids biobanks using patients' biopsy samples since the discovery of cancer organoids *in vitro*. By utilizing additive manufacturing methods and 3D cell culture platform, artificial organs can be generated *in vitro* using spheroids.[11,12] Many studies have demonstrated the effectiveness of spheroids for the repair or replacement of damaged skin or bones. There is still one Achilles' heel to 3D cell culture, and that is the formation of necrotic cores. Due to the spatiotemporal gradients of chemicals and oxygen in spheroids' proliferation, a necrotic core is inevitable in 3D non-endothelial cell spheroids.[13,14] Three-dimensional spheroids are still undergoing significant challenges in preclinical testing, including uniformity, reproducibility, yield, and method of assessment.[15] A critical step in performing longer-term experiments is to pre-vascularize the spheroids prior to applying them.

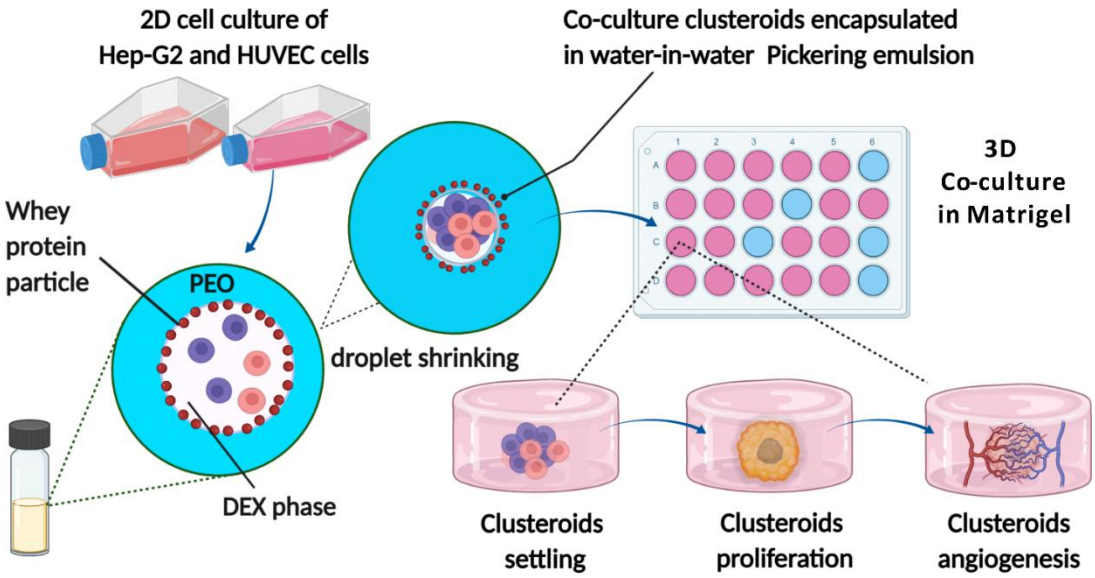

Figure 4.1. Schematic illustration of the HUVEC/Hep-G2 co-culture clusteroids in the w/w Pickering emulsion template and clusteroids angiogenesis. Created with BioRender.com.

In vivo, angiogenesis is mediated by several growth factors, especially VEGF. [15,16] A first step is to activate the Notch signaling pathway in order to transform resting endothelial cells into activated tip cells.[17] *In vitro*, metalloproteinases (MMPs) are released to stimulate the degrading and migration of cell endothelial cells. [18,19] In response to an angiogenic stimulus, endothelial stalk cells form capillary buds and sprouts.[20] A network of blood-perfused microvessels is

formed when the sprouts connect with each other and form a lumen. Several models of co-culture between endothelial cells and cancer cells have shown luminescent structures. [21-23] An endothelial growth factor pump could be formed by a cancer cell line that releases stimulatory factors to encourage endothelial cells to turn into capillary buds and sprouts. Microfluidic devices are typically used in co-cultures spheroids, which require specialized equipment and high costs of labor. It is difficult to achieve a high yield of spheroids using scaffolds or non-adhesive flasks-based technology. A convenient production method that could generate co-culture 3D cell models in a larger scale with low cost is required. A previously developed water-in-water Pickering emulsion template (ATPS) could be reused to facilitate high throughput co-culture of vascularized clusteroids using an aqueous two-phase system (ATPS).[24-26] After Poortinga et al.'s first report on Pickering water-in-water emulsions, the use of these emulsions is attracting increased attention.[27] Research has been conducted on a number of particles, including particles derived from dopamine, cellulose, and protein. [28-30] Biomedical and food applications are ideal for this emulsion system due to its low interfacial tension. [31]

In the present study, we demonstrate how human umbilical vein endothelial cells (HUVEC) can be used to vascularize the Hep-G2 cells upon co-culturing them using the w/w Pickering emulsion template. The Hep-G2 cell could be easily swapped to any other cell line or patient biopsy sample to study vascularization *in vitro*. we would prefer, in principle, for the co-cultured clusteroids to be a mix of any two cell types so that the model would function according to what it was intended to do. As compared to clusteroids cultured from single cells, the 3D co-cultured clusteroids exhibited a significant increase in angiogenesis. Coculture with Hep-G2 and HUVEC cells at a ratio of 5:1 led to spontaneous sprouting of clusteroids into Matrigel. With this simple platform, biomedical and tissue engineering applications for co-culture spheroids could be easily generated in a laboratory.

4.3 Materials and Methods

4.3.1 Materials

CFSE far-red, CFSE green fluorescence dye, easYFlasks and NUNC cell culture 24-well plates were purchased from Thermo Fisher Scientific (Loughborough, U.K.). Dextran (DEX) (MW 500 kDa) was purchased from Alfa Aesar (Heysham, Lancashire; United Kingdom.U.K), sodium chloride (99.8%) and calcium chloride,

Eagle's Modified Eagle Medium, and Trypsin-EDTA were sourced from Gibco (Loughborough,U.K.). Fetal bovine serum (FBS) was sourced from Labtech (Heathfield, U.K.), trypsin-EDTA was purchased from Lonza (U.K.). Endothelial cell culture medium was purchased from ATCC and HUVEC cell line was sourced from Promocell (Lutterworth,Leicestershire,U.K.) and Hep-G2 cell line was purchased from ECACC cell collection(Salisbury, U.K.). The MMP-2 ELISA kit was purchased from GE healthcare (Amersham, U.K.), the IGFBP, VEGF, IL-8 and HIF-α DuoSet ELISA kits and angiogenesis array kit (ARY007) were all purchased from Bio-Techne (Abingdon, U.K.). The 2 wt% gelatin suspension was sourced from Sigma Aldrich (Gillingham, U.K.) Matrigel was purchased from Corning (Flintshire, U.K.). Whey protein was sourced from No1. Supplements (Suffolk, UK). Deionized water was purified by using MilliQ reverse osmosis water purification system (Millipore). All the other chemicals were of analytical grade.

4.3.2 Method

4.3.2.1 HUVEC and Hep-G2 monolayer cell culture

The HUVEC and Hep-G2 cell lines were cultured in complete endothelial cell medium (ATCC, Manassas, Virginia,USA) or EMEM medium supplemented with 10 % FBS, respectively. The Hep-G2 cells were cultured in T75 easYFlask at 37°C with 5 % CO_2. The HUVEC cells were cultured in a T75 easYFlask precoated with 1 wt% gelatin suspension. The cells were passaged after they reached 80% confluency using 0.25 wt% trypsin solution and passaged in 1:4 for both cell lines.

4.3.2.2 HUVEC and Hep-G2 3D clusteroids culture

The fabrication of the co-culture clusteroids is based on aqueous phase-phase system, developed as a water-in-water Pickering emulsion. The clusteroids preparation method used here was adapted from Wang et al. as developed earlier by Wang et,al.[32]Briefly, a freshly prepared 22 wt% PEO(poly-ethylene oxide) and 11 wt% Dextran (DEX) solutions were sterilized by autoclaving (121°C, 15 min). Equal volume of the 22 wt% PEO solution 1 wt% heat-treated whey protein particle suspension (WPP) was thoroughly mixed using magnetic agitation to prepare a 11wt% PEO-0.5wt%WPP solution. WPP was then either UV sterilized or 0.45 μm filter-sterilized to avoid contamination. The 11wt% PEO-0.5wt%WPP solution was further mixed with equal volume of medium (EMEM/endothelial cell medium) to prepare the 5.5wt%PEO/0.25wt%WPP/Medium solution. The 11 wt% Dextran (DEX)

solution was also diluted using medium to generate 5.5wt% DEX/Medium solution. The cells were harvested by centrifugation, resuspended in DEX/culture medium and then mixed with PEO/culture medium solution using a syringe and needle. The generated w/w emulsion droplets were then shrunk by adding PEO solution of higher concentration in culture medium overnight to generate co-culture cell clusteroids. The initial cell ratio and cell concentration were adjusted using Trypan Blue counting.

4.3.2.3 Long term growth of the co-culture clusteroids in Matrigel

The support of an extracellular matrix (ECM) is essential in the formation of endothelial networking, especially the cell sprouts in the angiogenesis process *in vitro*. The most commonly used ECM for HUVEC is Matrigel. Here we utilized Matrigel to support the proliferation of the clusteroids. The Matrigel was kept frozen in ice to avoid polymerization before it was used. Matrigel was diluted in media (50/50 v/v EMEM/Endothelial cell growth medium) to 5 mg/mL before use. After the formation of the clusteroids, the clusteroids were centrifugated at 300×g for 4 min to collect them as a pellet. The pellet was then resuspended in 500 μL Matrigel and transferred to a 24-well plate. The initial cell number of the clusteroids in Matrigel was 1×10^5/mL. Matrigel was allowed to polymerize in the incubator at 37°C for 30 min. The culture was then topped up with 500 μL complete medium (supplemented with 10% FBS) and incubated at 37°C with 5% CO_2. For the individual cell clusteroids, either endothelial cell medium or EMEM medium was used. The 50/50 (v/v) Endothelial cell medium/EMEM medium was used for the co-culture clusteroids. The medium was replaced every 2 days.

4.3.2.4 Bright field, fluorescence, and confocal microscopy observations

Bright-field optical and fluorescence microscopy were employed to characterize the microstructure of the emulsions and encapsulated cell clusters using Olympus BX-51 Fluorescence microscope. CFSE and CFSE far-red were used as the fluorescence dyes to stain the Hep-G2 and HUVEC cells, respectively. These two dyes were also used for the longer-term tracking of clusteroids proliferation. The clusteroids were further characterized using a confocal laser scanning microscope (CLSM, Zeiss LSM710).

4.3.2.5 Spheroid sprouts analysis

The generation of the sprouts requires a low-serum medium. For this purpose, the co-cultured clusteroids medium was changed to complete endothelial

medium/EMEM medium supplemented with only 2 %v/v FBS. The clusteroids were also embedded in Matrigel with an initial cell concentration of 1×10^5 cells per mL in 24 well plates. The cultures were topped up with 500 µL complete medium (supplemented with 2 %v/v FBS) and incubated at 37°C with 5% CO_2. The clusteroids sprouts were analyzed by WimSprout assay (Wimasis image analysis, Córdoba, Spain) and the size of the 20 longest sprouts from the clusteroids were measured to estimate the degree of angiogenesis.

4.3.2.6 HIF-α, MMP-2, IGFBP, and VEGF ELISA

A 500 µL aliquot of the 3D clusteroids culture's supernatant was collected for testing at different days of culture (in days 1, 7, 14 and 21). MMP-2 was quantified following the manufacturers' instructions. The remaining ELISA kits were developmental antibody pairs (IL-8, IGFBP, HIF-α, and VEGF) used with appropriate ancillary reagents. For these, 100 µL of specified capture antibody was added to each well of the 96-well plates overnight at room temperature to coat the well. The plates were then rinsed three times with wash buffer using an automatic plate washer. Plates were blocked by adding 300 µL of reagent diluent to each well and incubated at room temperature for a minimum of 1 h. A 100 µL aliquot of the clusteroids supernatant was added to each well and incubated for 2 h. A 100 µL aliquot of the detection antibody, Streptavidin-HRP, and substrate solution were added in order, with incubation and washing between each step. Finally, an aliquot of 50 µL stop solution was added last to each well. The optical density of each well was determined immediately a wavelength of 450 nm by using a Syngery HT microplate reader.

4.3.2.7 SEM imaging of the clusteroids

The clusteroids were released from Matrigel after 21 days of culture using collagenase, which enzymatically degrades the gel. The clusteroids were then centrifuged and rinsed twice with PBS (Phosphate-buffered saline) to remove the excess of hydrogel and the medium. The clusteroids were then fixed in a 1 wt% glutaraldehyde solution for 2 h at ambient temperature and washed with deionized water, then air-dried overnight before being imaged with Zeiss smart SEM software (Zeiss Evo-60 S.E.M., Germany).

4.3.2.8 Angiogenesis array.

The angiogenesis-related protein markers produced in the 3D co-culture clusteroids were analyzed using the proteome profiler angiogenesis array kit

according to the manufacturers' instructions. A 1 mL aliquot of the conditioned media were obtained from the 3D clusteroids (Individual Hep-G2, individual HUVEC, and co-cultured clusteroids (Hep-G2: HUVEC=5:1) embedded in the 5 mg/mL Matrigel.

Array membranes were firstly blotted for 1 h. To reach the optimal sensitivity, the array was incubated overnight with the 1 mL of conditioned media at room temperature with gentle shaking. The membranes were carefully submerged in a wash buffer for 10 min with three repeats to remove non-attached protein. The array antibody cocktail and a horseradish peroxidase-conjugated streptavidin antibody were incubated with the membranes for another 12 h. Membranes were then mixed with 1X detection buffers. The membranes were then imaged using a Bio-Rad image system exposed for 200 s set at chemiluminescence blot (ATTO, WSE 6100 LuminoGraph I). The ChemiBlot intensity was calculated using GelAnalyzer 19.1 (www.gelanalyzer.com). Relative expression levels in each group were determined using the algorithm mentioned in the manufacturer's protocol.

4.3.2.9 Statistical analysis

In the experimental sections, three independent experiments were carried out to present the mean experiments ± SD (Standard Deviation). The comparation between two group were done using 2-tailed independent-sample t-tests. Statistical significance was defined as $p < 0.05$ or $P < 0.01$.

4.4 Results and discussion

4.4.1 Clusteroids culture in the w/w Pickering emulsion template

As a template, DEX/PEO Pickering emulsion stabilized with biocompatible WPP particles was used to encapsulate the cells and form clusteroids. Cells accumulate preferentially within the DEX phase of DEX/PEO ATPS in other studies. [32,33] DEX/PEO Pickering emulsion was used as a template in order to encapsulate the cells and form clusteroids as a result of stabilizing it with biocompatible WPP particles. As shown in other studies, the DEX phase of DEX/PEO ATPS accumulates cells predominately compared to the PEO phase.[24] As you can see in **Figure 4.1**, we have shown schematically how to generate a w/w emulsion template and how to apply it to the sample. As indicated in **Figure 4. 2**, we have set the initial cell concentration to 10^6 cells per mL (**Figure 4. 2**). It would be possible to increase the number of cells in

the clusteroids in order to produce clusteroids of larger size at the same other conditions. The clusteroids were formed by osmotically shrinking the DEX drops together with the cells after the w/w DEX/PEO emulsion had been formed. As osmotic equilibrium is restored between the DEX and PEO phases, the DEX droplets shrink due to redistributed water. After adhering to each other, the cell clusters are compacted by interfacial tension forces (**Figure 4.2(3)E-F**). Cells are more dense than DEX phase at 5.5 wt% and more dense than PEO phase at any concentration.[34] Using fluorescence microscopy, we observed the cell encapsulation efficiency for the first time.

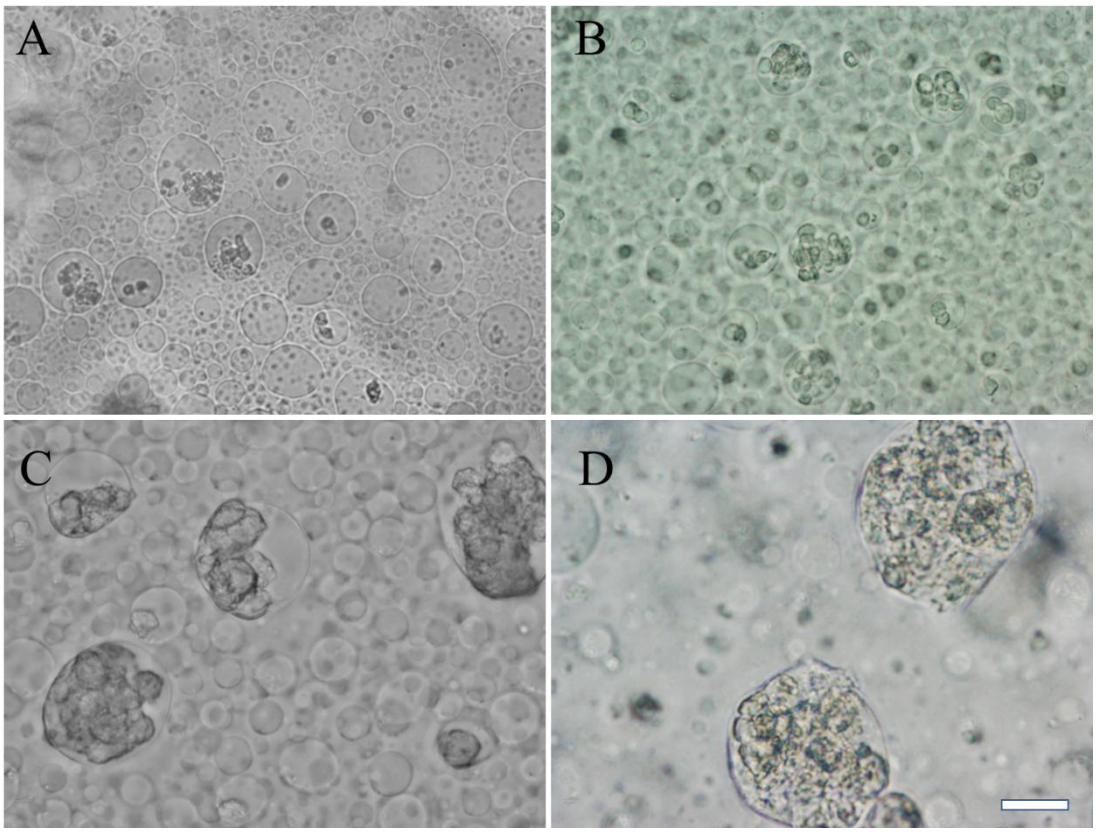

Figure 4.2. Different cell concentration of mixed HUVEC/Hep-G2 cells in 5.5wt% DEX/5.5wt% PEO w/w Pickering emulsion with different cell cocentration before shrinking:A:1×10^3/mL B:1×10^4/mL C:1×10^5 D: 1×10^6/mL. The bar is 100μm for A,B and 50μm for C,D.

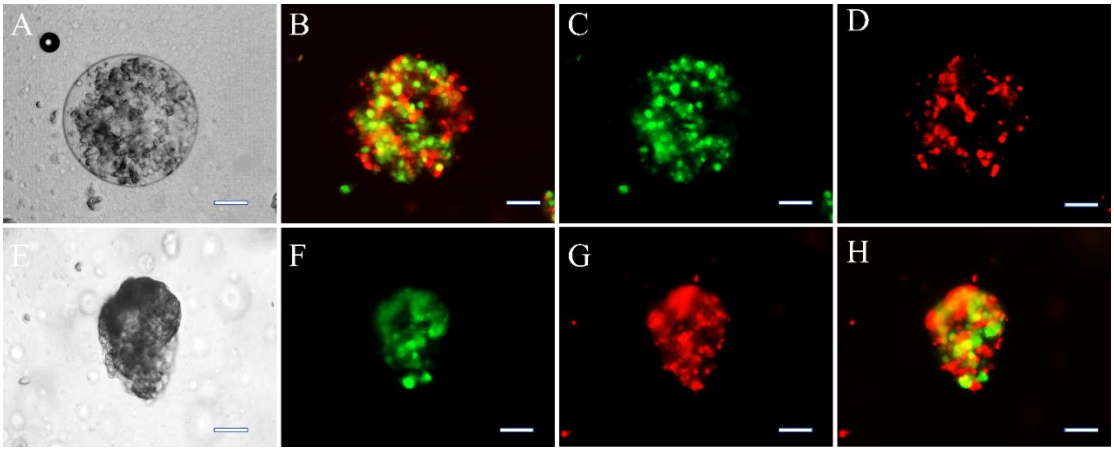

Figure 4.2. Bright-field (A, E) and fluorescence microscope observation of mixed Hep-G2/HUVEC (cell ratio=5:1) cells encapsulated by 5.5wt% DEX in 5.5wt% PEO emulsions before (A-D) and after shrinking by 11 wt% PEO (E-H) set at FITC (B, F), CFSE far red set at TRITC (C, G) and dual fluorescence FITC/TRITC channels (D, H). The clusteroids in the emulsions(A-D) and the clusteroids taken out from the emulsions(E-H) were taken for imaging immediately after their formation. The Hep-G2 cells and HUVEC cells were pre-stained with CFSE and CFSE far red, respectively. The bar is 50 μm.

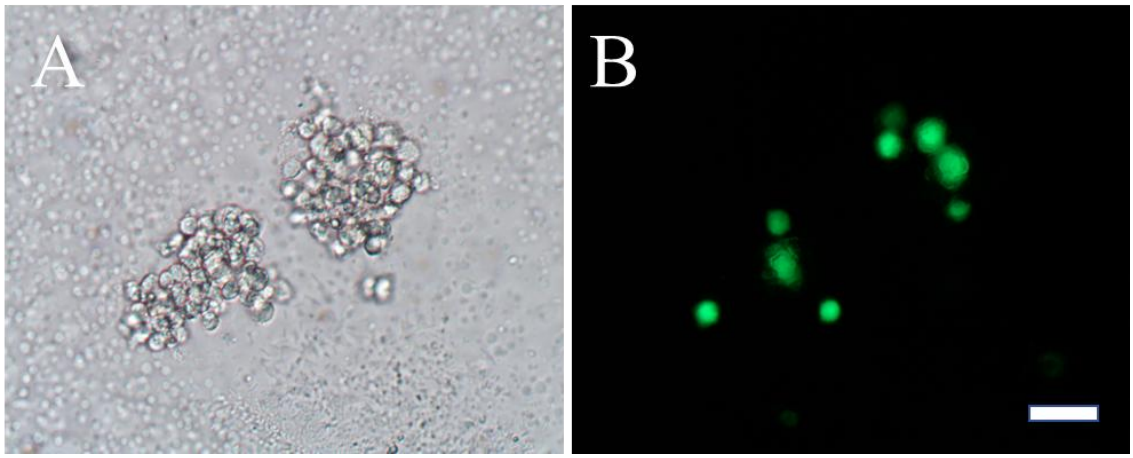

Figure 4.4. Bright field observation(A) and fluorescence microscopy observation(B) of the freshly collected Hep-G2/HUVEC co-culture clusteroids at a cell ratio of 5:1. The bar is 100μm.

A CFSE-labeled Hep-G2 cell and a CFSE-labeled HUVEC cell have been shown in the images above. As seen in **Figure 4.3A-D**, most of the cells are located in the DEX phase of the w/w emulsion, indicating that they are mainly located in the DEX phase of the w/w emulsion. This can be seen in **Figure 4.3E-H** where clusteroids are formed after the DEX drops are contracted by the higher concentration PEO solution. It may be seen that the extra space between the cells has been squeezed out, which allows the cells to be in close contact. There was an even distribution of both types of cells within the clusteroids. **Fig4. 4** illustrates the formation of individual clusteroids (Hep-G2, HUVEC) based on the adhesion of the single cells. Based on these results, Pickering emulsion systems w/w are highly efficient for preparing co-cultured cells in 3D. The cells within the clusteroids were monitored using confocal microscopy to see how they were arranged within the clusteroids in three dimensions (**Figure 4.5**). Observations of confocal microscopy were conducted using the resuspended mixed clusteroids after centrifugation and suspension in a complete medium. The structure of the clusteroids has been preserved after they have been removed from the emulsion template (**Figure 4.4**). Hep-G2:HUVEC ratio was compared with Hep-G2:HUVEC ratio (1:1 and 5:1).

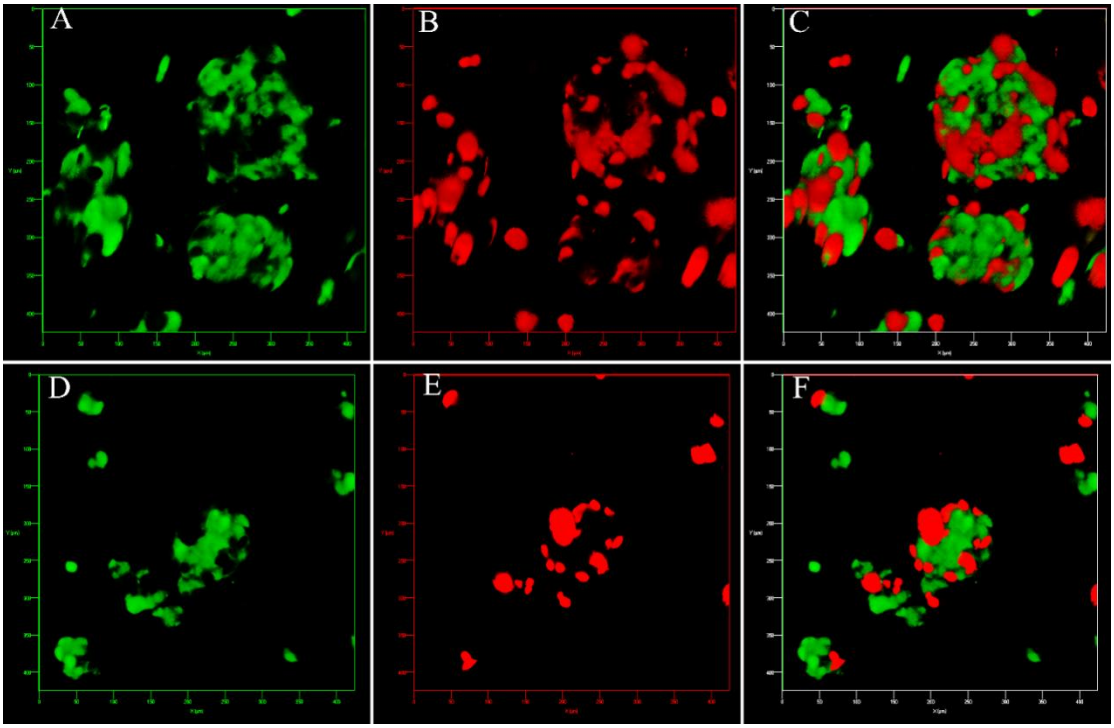

Figure 4.5. 3D Z-stacked image of co-cultured Hep-G2/HUVEC clusteroids at a cell ratio of: (A-C) 1:1 and D-F:5:1 set at different fluorescence channels: FITC (A,D), CFSE far red (B,E) and dual fluorescence (C,F) The box size is 400×400 μm.

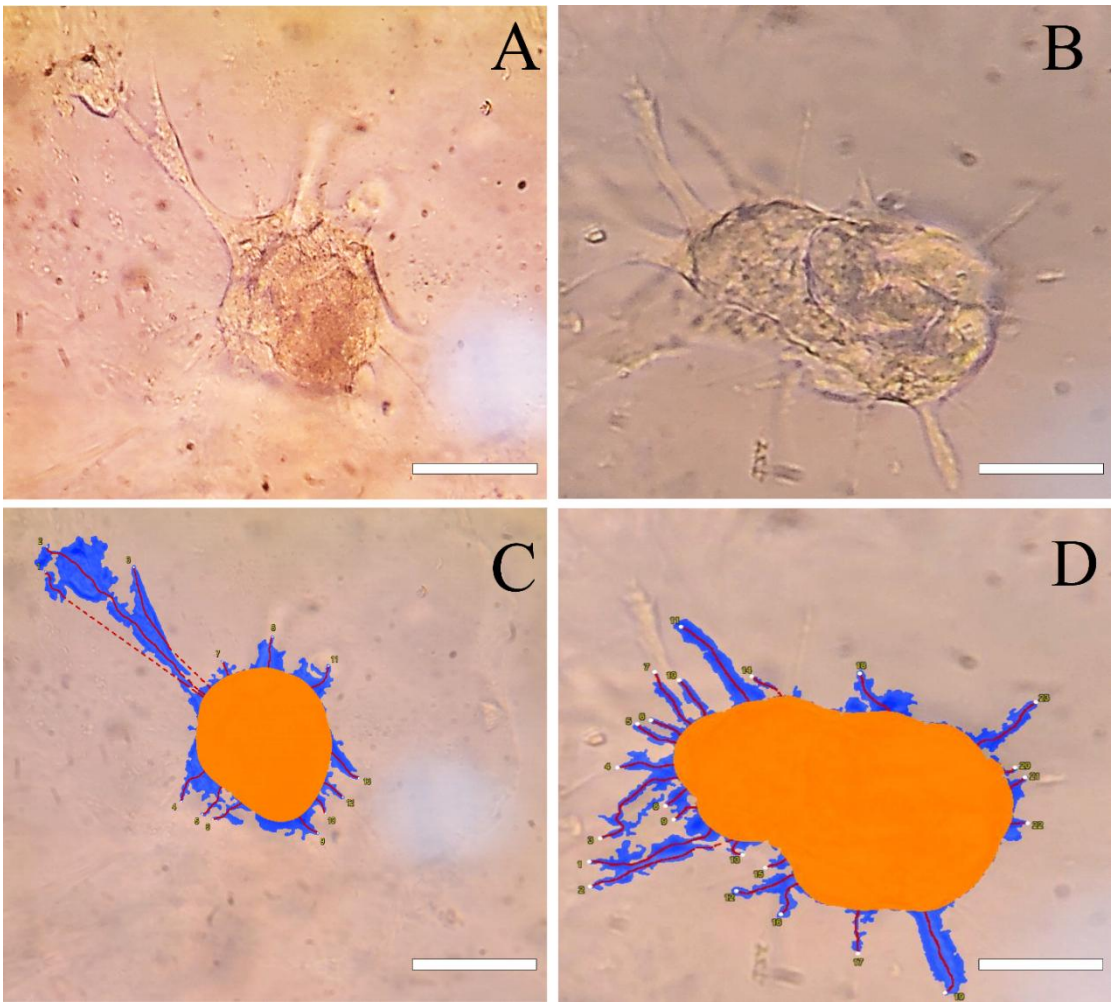

Figure 4.6. A-D:Bright field observation of the co-culture clusteroids sprouting after 7 days of culture a cell ratio of 5:1 (Hep-G2:HUVEC) in 5mg/mL Matrigel.The corresponding Wimasprouts analysis of A,B was shown in C,D. The bar is 50 μm.

Upon culturing the mixed clusteroids for a long period of time, neither of the cell ratios appeared to have a significant effect on the distribution of the cells. As we observed from an observation of the Hep-G2 clusteroids, the surface of the layers appeared to be smooth and exhibited a strong tendency to fusion (**Figure 4.6A**). There was evidence of neovascularization surrounding the clusteroids of HUVEC cells (**Figure 4.7B**). As a consequence of co-culture, the clusteroids displayed tail-like structures that appeared after a couple of days (**Figure 4.7C**).

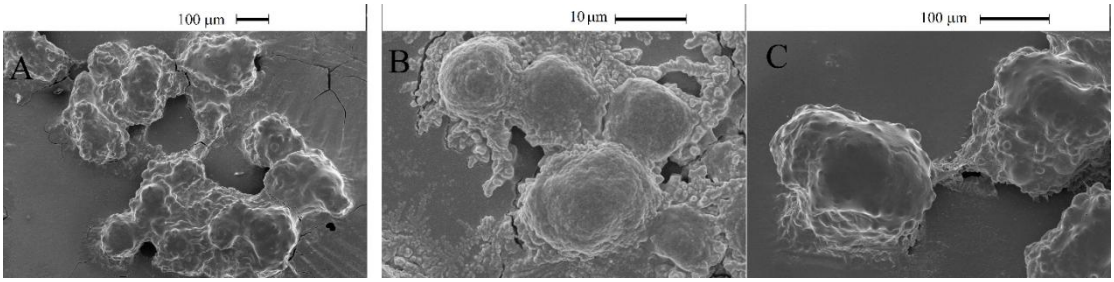

Figure 4.7. SEM observation of the A: Individual Hep-G2 clusteroids, B: Individual HUVEC clusteroids, C: Co-culture of Hep-G2 and HUVEC clusteroids at a cell ratio of 5:1. The cells were kept growing in the Matrigel before the gels were degraded.The scale bar is 100μm.

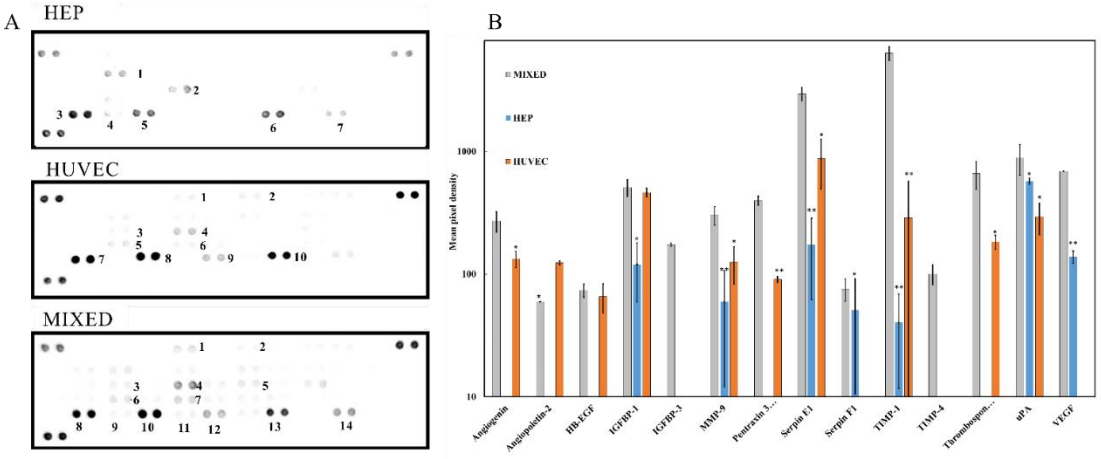

Figure 4.8. (A) Angiogenesis array membrane of individual Hep-G2 clusteroids, HUVEC clusteroids, and the co-culture Hep-G2/HUVEC clusteroids at a Hep-G2/HUVEC cell ratio of 5:1 after 21 days of proliferation in the Matrigel. The initial total cell number was 1×10^6 mL^{-1}. (B) Angiogenesis-related protein production in the individual Hep-G2 clusteroids, HUVEC clusteroids, and the co-culture Hep-G2/HUVEC clusteroids. Data were plotted as mean ± standard deviation of at least 3 independent experiments. Statistically significant differences between each region are denoted by * ($P<0.05$) or **($P<0.01$).

4.4.2 Production of angiogenic factors by the co-cultured clusteroids

In addition to microfluidic devices and scaffolds, hydrogels and scaffolds have been used in studies that use HUVEC and Hep-G2 cells in co-culture.[35-37] To obtain

better understanding which protein markers related to angiogenesis that has been produced in the clusteroids, the supernatant of these clusteroids embedded in the Matrigel was collected for analysis via a proteome angiogenesis array. The production of these markers in the co-cultured (HUVEC/Hep-G2) clusteroids and the individual Hep-G2 and HUVEC clusteroids was compared. Antibody cocktails are contained in the angiogenesis array. Angiogenesis-related proteins from 55 different species of humans were detected simultaneously in this study. A chemiluminescent detection reagent is used to visualize the captured proteins. A proportional amount of analyte is bound to produce a proportional signal. Based on the relative density of detected proteins compared to controls on the corners of each membrane, it was possible to easily compare the intensity of different detected proteins. Angiogenesis markers were produced more frequently by either HUVEC or Hep-G2 as shown in **Figure 4.8A**. It can be seen in **Figure 4.9** that these produced proteins influenced angiogenesis. As a result of the co-culturing of HUVEC/Hep-G2 clusteroids, levels of angiogenin, MMP-9, uPA, IGFBP and VEGF were greater when compared to the clusteroids of the two cell types cultured separately (**Figure 4.8B**). HUVEC/Hep-G2 clusteroids cocultured with TIMP-4 and IGFBP-3, which both promote angiogenesis, produced both proteins. Inhibition of angiogenesis by TIMP-1 is evidenced by decreased production of tissue plasminogen activator (tPA) and urokinase (uPA).[38]TIMP-1 would also block the production of matrix metalloproteinases (MMPs) as a result of its co-efficiency with the TIMP and uPA families. [39] Additionally, our study revealed that the HUVEC cell clusteroids were not capable of producing VEGF on their own. As a result of the co-cultured pattern, angiogenesis-related proteins are secreted at a higher level. There was some evidence that the two cell types (HUVEC and Hep-G2) were only able to exhibit certain characteristics in cell production when they were co-cultured together in a 3D format. As a result of the angiogenesis array, a glimpse into the secretion of these angiogenesis proteins was given to us as a result of the analysis. Several ELISA kits, including VEGF, IGFBP-1, MMP-2 and HIF-α, were used to investigate how these protein markers were produced over the course of 21 days. The most commonly used angiogenesis-related cytokine is VEGF, which induces endothelial cell vascularization *in vitro*.[40] By analyzing the supernatants of three kinds of cell clusteroids, we have been able to determine how much VEGF they produce.

(+)	Angiogenin
(+)	angiopoietin-2
(+)	HB-EGF
(+)	IGFBP-1
(+)	IGFBP-3
(+)	MMP-9
(+)	Pentraxin 3 (PTX3)
(-)	Serpin E1
(-)	Serpin F1
(-)	TIMP-1
(-)	TIMP-4
(+)	Thrombospondin-1
(+)	uPA
(+)	VEGF

Figure 4.9. The effect of the Angiogenesis-related genes on the vascularization precess. (+) represents that they are pro-angiogenesis and vice versa.

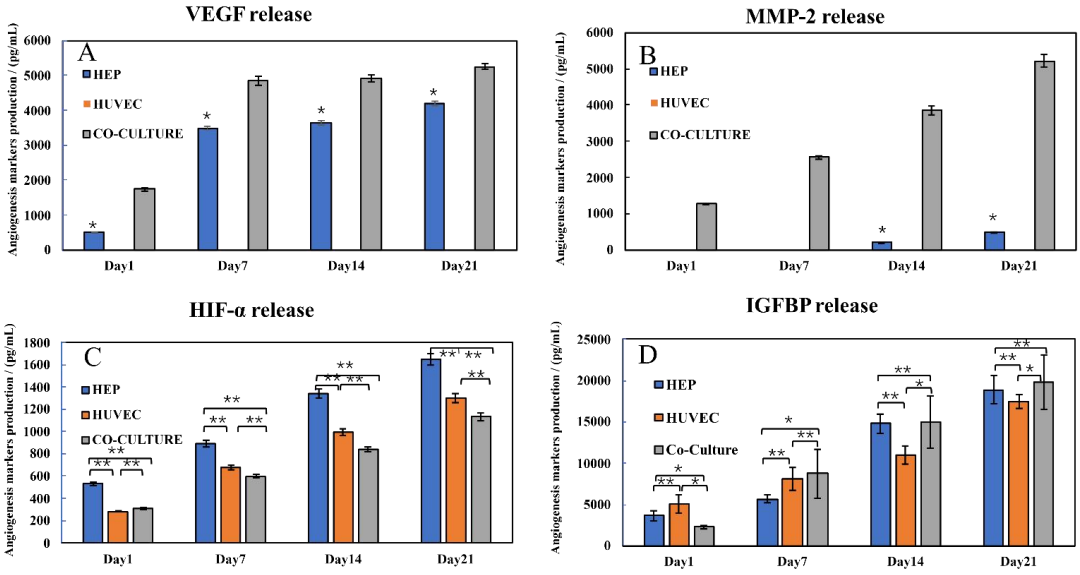

Figure 4.10: A: VEGF B: MMP-2 C: HIF-α and D: IGFBP-1 production of the individual Hep-G2 clusteroids, HUVEC clusteroids, and the co-culture clusteroids at a cell ratio of 5:1(Hep-G2: HUVEC) during 21 days of proliferation in the 5 mg mL^{-1} Matrigel. The initial total cell number was 1×10^{6} mL^{-1} for all three set. Data were plotted as mean ± standard deviation of at least 3 independent experiments. Statistically significant differences between each region are denoted by * ($P<0.05$) or **($P<0.01$).

On the other hand, the co-cultured clusteroids of Hep-G2 and HUVEC (**Figure 4.10A**) showed that VEGF was not detectable in the HUVEC clusteroids; however, the co-cultured clusteroids of Hep-G2 and HUVEC showed about 50% more VEGF than the individual clusteroids of Hep-G2. The results obtained from the proteome arrays also corresponded to what was determined from the proteome array results. As well as the MMP family of proteins, there is another important marker related to the sprouting of endothelial cells, which includes molecules that break down the extracellular matrix (ECM). Neither HUVEC nor the exogenous VEGF could induce MMP-2 production in the cells, which suggests that the HUVEC would not have been able to sprout into the ECM without the exogenous VEGF induction (**Figure 4.10B**). As a result of 14 days of culture, very little MMP-2 is produced by Hep-G2. Comparing co-culture models with Hep-G2 clusteroids, the co-culture models

produced five times more MMP-2 than the clusteroids grown on Hep-G2, indicating that MMP-2 may influence sprouting in the co-cultured models.

Angiogenesis was clearly evident in the co-cultured clusteroids after 21 days as evidenced by the production of MMP-2 and VEGF. Hypoxia is a condition in which oxygen availability in the cell decreases, and HIF-α responds to it. There has been some speculation that this substance could be a reverse indicator of the state of clusteroids with regards to vascularization. According to **Figure 4.10C**, on days 1 through 21, clusteroids co-cultured with each other produced the lowest level of HIF-α. It was inevitable that oxygen and nutrients would be difficult to reach the core cells due to the proliferation of the three kinds of clusteroids. It is therefore expected that HIF-α could be produced at a higher level. It is important to note that insulin-like growth factors (IGFs) are proteins that are closely related to insulin in terms of sequence. A cell's ability to communicate with its environment is largely dependent on the expression of IGFs. Several proteins known as IGF-binding proteins regulate the levels of IGF-1 and IGF-2. There are many mechanisms by which these proteins play a role in modulating IGF action in complex ways. This includes both inhibiting IGF action by preventing binding to the IGF-1 receptor as well as facilitating IGF action by aiding in its delivery and extending the half-life of IGF. Clusteroids produced IGFBP similarly to angiogenesis arrays in all three types. (**Figure 4.10D**).

IGFBP levels were highest in clusteroids that had been co-cultured for seven days. In the first seven days following transplantation, HUVEC produced a large amount of IGFBP. The self-sorting nature of co-cultured clusteroids may explain this result.

4.4.3 Endothelial cell sprouting

Primary cultured endothelial cells are grown on spheroid-based sprouts to examine gene expression and pharmacological compounds on capillary-like tube formation. [41, 42] Endothelial cell lines commonly use Matrigel as the ECM. An Engelbreth-Holm-Swarm (EHS) mouse sarcoma cell line secretes a solubilized basement membrane matrix, called Matrigel, that is manufactured by Corning Life Sciences (by Corning Life Sciences). Using 5 mg/mL Matrigel as a seeding medium, we co-cultured Hep-G2/HUVEC clusteroids and sprouted them in the medium. The exogenous VEGF or EGF is not required in the HUVEC sprouting assays, in contrast to the standard HUVEC spheroids sprouting assays. HUVEC sprouting can be

accomplished with the help of VEGF pumps that are provided by Hep-G2. As a measure of the degree of angiogenesis of the 3D cells culture, the length of the sprouting clusteroids was measured. A 5:1 cell ratio of His-G2/HUVEC clusteroids co-cultured for 7 days without VEGF (**Figure 4.6**) showed that sprouting could be easily observed without VEGF addition. There was no sprouting of Hep-G2 cells or HUVEC cells into the ECM as a result of the individual cells. (**Figure 4.11**). The results of this study suggest it may be necessary for sprouting behavior to be attributed to the unique cell-cell interactions observed. Based on the results obtained from the ELISA kit and angiogenesis array kit, this outcome could be explained by the results obtained from these kits. According to **Figure 4.12)**, each sprout measures a particular length. There was no evidence that HUVEC cells produced VEGF, which may stimulate the sprouting of endothelial cells. It is because it is a carcinoma that the Hep-G2 cells are capable of producing high levels of VEGF. It is therefore theoretically possible to induce angiogenesis and sprouting from the combination of endothelial cells and carcinoma cell lines. HUVEC cells may also be breaking down the ECM by producing MMP-2. Despite the fact that the Hep-G2 clusteroids secreted a small amount of MMP-2, the amount was limited. As a result of the activity of MMP-2, clusteroids sprout into the extracellular matrix.[43] A significant increase in MMP-2 production was observed within the co-cultured clusteroids after 21 days of culture, approximately five times greater than in the individual clusteroids of Hep-G2 (**Figure 4.10B**). There have been previous reports that have observed similar results when culturing carcinoma cells with endothelial cells spheroids without VEGF addition, i.e. the carcinoma cells would stimulate the spheroids to sprout without VEGF addition.[42] In the co-cultured clusteroids (**Figure 4.7C**), several tail-like structures can also be observed, which cannot be seen when the clusteroids are isolated (**Figure 4.7A, B**).[42,44] In this study, we are developing an *in vitro* model of 3D cell co-culture that can be used to investigate the possibility of angiogenesis. A version of this new model could be used in a variety of drug testing applications, particularly in those that attempt to prevent the formation of new blood vessels. This model could be used to test the effectiveness of anti-angiogenic and pro-angiogenic treatments. To demonstrate the integrity of clusteroids as well as structural changes during treatment, immunohistochemistry may be used to further characterize them.

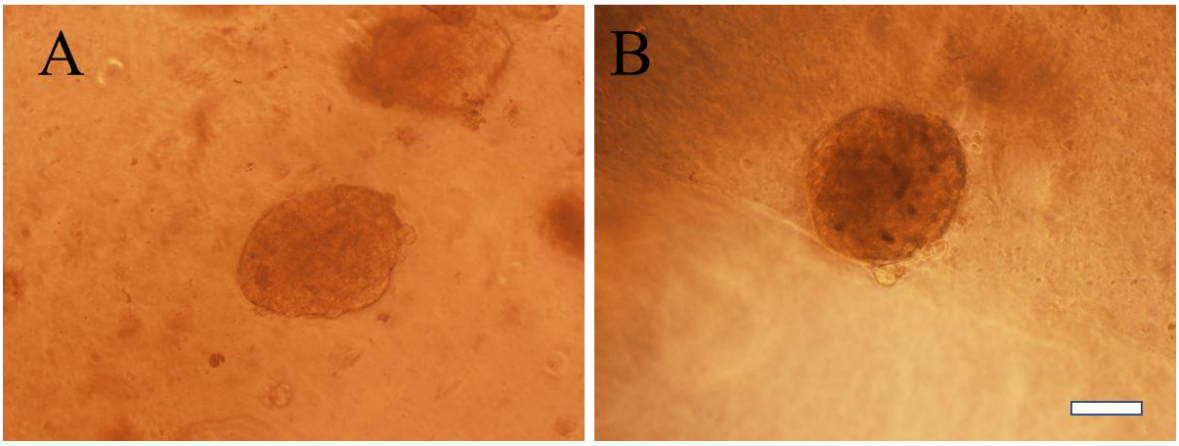

Figure 4.11. Bright field observation of the individual Hep-G2: A and B:HUVEC clusteroids in 5mg/mL matrigel after 21 days of culture in low serum medium. The bar is 50μm.

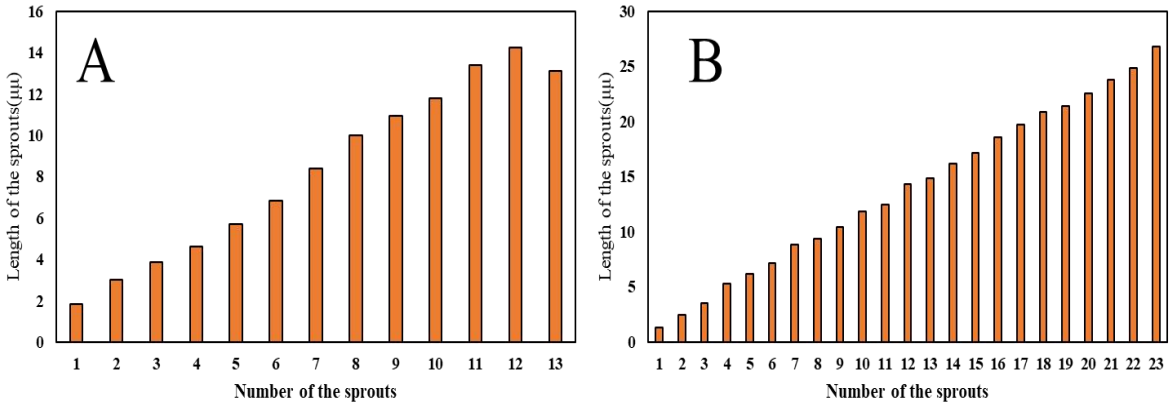

Figure 4.12. The length of the sprouts in **Figure 4.11**.

4.5 Conclusions

The purpose of this study is to demonstrate that a 3D platform of co-culture cell clusteroids of primary endothelial cells and hepatic tumor cells can have similar *in vitro* behavior as in *vivo*. Co-cultured clusteroids produced from ATPS could sprout into Matrigel when the cell ratio was adjusted to 1:2 (Hep-G2 : HUVEC), which approximated the real *in vivo* environment. The co-culture clusteroids produced a greater amount of angiogenesis proteins than the individual types of cells. It is possible to handle this approach without the use of expensive instruments or consumables. Ideally, cells could be substituted for any two kinds of cells except

those used for 3D cell vascularization. Additionally, this model could be used to investigate drug toxicology as well as other applications related to tissue engineering.

4.6 References

1. Laschke, M.W.; Menger, M.D. *Trends Biotechnol*,. 2017, **35**, 133–144.
2. Wang, A.; Madden, L.A.; Paunov, V.N. *J. Mater. Chem. B Mater. Biol. Med*. 2020, **8**, 10487–10501.
3. Santini, M.T.; Rainaldi, G. T. *Pathobiology,.* 1999, **67**, 148–157.
4. Friedrich, J.; Seidel, C.; Ebner, R.; Kunz-Schughart, L.A. S *Nat. Protoc,.* 2009, **4**, 309–324.
5. Tung, Y.-C.; Hsiao, A.Y.; Allen, S.G.; Torisawa, Y.-S.; Ho, M.; Takayama, S. *Analyst*,. 2011, **136**, 473–478.
6. Alini, M.; Eisenstein, S.M.; Ito, K.; Little, C.; Kettler, A.A.; Masuda, K.; Melrose, J.; Ralphs, J.; Stokes, I.; Wilke, H.*J. Eur. Spine J*,. 2008, **17**, 2–19.
7. Pasupuleti, M.K.; Molahally, S.S.; Salwaji, S. *J. Indian Soc. Periodontol,.* 2016, **20**, 360–368.
8. Glorioso, J.M.; Mao, S.A.; Rodysill, B.; Mounajjed, T.; Kremers, W.K.; Elgilani, F.; Hickey, R.D.; Haugaa, H.; Rose, C.F.; Amiot, B.; et al. *J. Hepato*l,. 2015, **63**, 388–398.
9. Li, M.; Izpisua Belmonte, J.C. N. Engl. *J. Med,.* 2019, **380**, 569–579, .
10. Shi, R.; Radulovich, N.; Ng, C.; Liu, N.; Notsuda, H.; Cabanero, M.; Martins-Filho, S.N.; Raghavan, V.; Li, Q.; Mer, A.S.; et al. *Clin. Cancer Res,.* 2020, **26**, 1162–1174.
11. Moldovan, N.I.; Hibino, N.; Nakayama, K. *Tissue Eng. Part B Rev,.* 2017, **23**, 237–244.
12. Bowser, D.A.; Moore, M.J. *Biofabrication,.* 2019, **12**, 015002.
13. Mukomoto, R.; Nashimoto, Y.; Terai, T.; Imaizumi, T.; Hiramoto, K.; Ino, K.; Yokokawa, R.; Miura, T.; Shiku, H. *Analyst,.* 2020, **145**, 6342–6348, .
14. Giverso, C.; Preziosi, L. I *Int. J. Non Linear Mech,.* 2019, **108**, 20–32.
15. Ferrara, N. *Nat. Rev. Cancer,.* 2002, **2**, 795–803.
16. Ferrara, N. *EXS,.* 2005, 209–231.
17. Blanco, R.; Gerhardt, H. *Cold Spring Harb. Perspect. Med*,. 2013, **3**, a006569.
18. Rundhaug, J.E. *J. Cell. Mol. Med,.* 2005, **9**, 267–285.

19. Sang, Q.X. *Cell Res*,. 1998, **8**, 171–177.

20. Gerhardt, H.; Betsholtz, C. *EXS*,. 2005, 3–15.

21. Devadas, D.; Moore, T.A.; Walji, N.; Young, E.W.K. *Biomicrofluidics,*. 2019, **13**, 064122

22. Patra, B.; Peng, Y.-S.; Peng, C.-C.; Liao, W.-H.; Chen, Y.-A.; Lin, K.-H.; Tung, Y.-C.; Lee, C.-H. *Biomicrofluidics*,.2014, **8**, 052109.

23. Ingthorsson, S.; Sigurdsson, V.; Fridriksdottir, A., Jr; Jonasson, J.G.; Kjartansson, J.; Magnusson, M.K.; Gudjonsson, T.*BMC Res,*. Notes 2010, **3**, 184.

24. Wang, A.; Madden, L.A.; Paunov, V.N.*Mater. Adv,*. 2020, **1**, 3022–3032, .

25. Wang, A.; Weldrick, P.J.; Madden, L.A.; Paunov, V.N. *Biomater. Sci,*. 2021, **9**, 6927–6939.

26. Wang, A.; Weldrick, P.J.; Madden, L.A.; Paunov, V.N. *ACS Appl. Mater. Interfaces*,.2021, **13**, 22182–22194.

27. Poortinga, A.T. Microcapsules from Self-Assembled Colloidal Particles *Langmuir*,. 2008, **24**, 1644–1647.

28. Zhang, J.; Hwang, J.; Antonietti, M.; Schmidt, B.V.K.J. Water-in-Water *Biomacromolecules*,. 2019, **20**, 204–211,

29. Nguyen, B.T.; Nicolai, T.; Benyahia, L. *Langmuir,*. 2013, **29**, 10658–10664.

30. Ben Ayed, E.; Cochereau, R.; Dechancé, C.; Capron, I.; Nicolai, T.; Benyahia, L. *Langmuir,*. 2018, **34**, 6887–6893,

31. Nicolai, T.; Murray, B. *Food Hydrocoll,*. 2017, **68**, 157–163,

32. Wang, A., Madden, L. A., & Paunov, V. N. (2022). *Bioengineering*,. *9,***3**, 126.

33. Han, C.; Takayama, S.; Park, J. *Sci. Rep,*. 2015, **5**, 11891.

34. Atefi, E.; Lemmo, S.; Fyffe, D.; Luker, G.D.; Tavana, H. *Adv. Funct. Mater,*. 2014, **24**, 6509–6515.

35. Atefi, E.; Joshi, R.; Mann, J.A., Jr; Tavana, H. *ACS Appl. Mater. Interfaces,*. 2015, **7**, 21305–21314.

36. Chiew, G.G.Y.; Fu, A.; Perng Low, K.; Qian Luo, K. *Sci. Rep*,. 2015, **5**, 10801.

37. Lasli, S.; Kim, H.-J.; Lee, K.; Suurmond, C.-A.E.; Goudie, M.; Bandaru, P.; Sun, W.; Zhang, S.; Zhang, N.; Ahadian, S.; et al. *Adv. Biosyst*,. 2019, **3**, e1900104.

38. Timmins, N.E.; Nielsen, L.K. Methods *Mol. Med*,. 2007, **140**, 141–151.

39. Handsley, M.M.; Edwards, D.R. Int. *J. Cancer,.* 2005, **115**, 849–860, .

40. Vizoso, F.J.; González, L.O.; Corte, M.D.; Rodríguez, J.C.; Vázquez, J.; Lamelas, M.L.; Junquera, S.; Merino, A.M.; García-Muñiz, J.L. Br. *J. Cancer,.*2007, **96**, 903–911.

41. Shibuya, M. *Struct. Funct*,.2001, **26**, 25–35.

42. Stahl, A.; Wu, X.; Wenger, A.; Klagsbrun, M.; Kurschat, P. *FEBS Lett,.* 2005, **579**, 5338–5342.

43. Pfisterer, L.; Korff, T. Methods Mol. Biol,. 2016, **1430**, 167–177.

44. Haas, T.L.; Davis, S.J.; Madri, J.A. T. *J. Biol. Chem,.* 1998, **273**, 3604–3610.

5. Chapter 5

A biofilm infected 3D human cell culture platform to replace animal models in testing antimicrobial nanotechnologies

5.1 Abstract:

There is an increasing concern among biomedical professionals regarding biofilm formation, which includes wound care, implant devices, as well as organ infections. In the presence of Biofilm, extracellular polymeric substance (EPS) could be produced, which could impair to the wound, and enable the wound to be more susceptible to the effects of anti-bacterial drugs, possibly resulting in Sepsis. In order to increase the penetration of traditional antibacterial drugs within biofilms, there has been a trend toward using nanocarrier-based delivery vehicles. *In vitro* skin models are not available that are capable of simulating the formation and clearance of biofilms i*n vivo*. It has been developed and tested herein a new 3D clusteroids/biofilm co-culture system that has been also used as a tool for measuring the clearance efficiency of biofilm with nanoparticle-based therapeutics based on NPs. The nanoparticles chosen for study were based on chitosan-based nanogels loaded with ciprofloxacin and then functionalized on the surface with alcalase to form formerly reported nanoparticles. We explored the antibacterial effect of the alcalase-coated ciprofloxacin-loaded nanogel carriers on clearing *Staphylococcus. aureus* and *Pseudomonas. aeruginosa* biofilms on our clusteroids/biofilm co-culture model. Biofilms made of clusteroids were successful at infecting and coating the clusteroids layer. When ciprofloxacin-loaded nanocarriers were combined with the appropriate concentration of bacteria, their antibacterial effect was significant. In conclusion, this study successfully demonstrated that our co-culture model can be used to evaluate the effectiveness of various nanoparticles in killing biofilms and that it can be used in a variety of applications. In addition to the potential for developing better antibacterial and disinfecting agents as a result of this 3D cell culture technique, it might also lead to the development of dental formulations for plaque reduction, wound dressings, anti-algal/anti-biofouling formulations, as well as new antifungal agents.

5.2 Introduction:

There is a major concern regarding biofilms in the fields of biomedicine, food and the environment. EPS (extracellular polymeric substance) is an extracellular polymer that gives bacteria a high level of resistance to antibiotics. Biofilms are multicellular colonies that are 3D-structured and adhere to the EPS, increasing their resistance to antibiotics[1] In general, biofilms are formed in a multi-staged process that involves the expression of polysaccharides, RNA, and DNA.[2] The enhanced structural strength caused by the cell-cell interaction attracts considerable interest on the biofilm formation mechanism.[3] Most of the human microbiota have been viewed as a complex eco-system of bacteria instead of a simple layer of coexisting bacteria for over 50 years since the first definition of biofilms in the late 1970s. [4] Bacterial biofilms represent a critical component indwelling tissues of various kinds which may become colonized with microorganisms. The first observation of biofilms, aggregated bacteria enclosed within a matrix of extracellular materials, was reported in the lungs of cystic fibrosis (CF) patients, a genetic disorder that often causes repeated lung infections.[5, 6] A 50 year research process has resulted in biofilms being detected in the majority of organs and implants within the human body, including kidney stones, urinary tract infections, vaginosis, chronic wounds and chronic infections. This knowledge has been confirmed with clinical trials.[7-9] Wounded healing is a major problem associated with biofilm. This is largely due to opportunistic pathogens including Staphlococcus, Pseudomonas, and Klebsiella genus.[5, 10] By inhibiting innate inflammatory pathways and resisting traditional therapies, the bacteria that cause EPS impair wound healing, potentially leading to sepsis.[11-14] There is a worldwide prevalence of bacterial invasion of wounds. As a result, millions of people suffer chronic wounds every year as a result of bacterial invasion. Microbial biofilms possess a number of inherent defence mechanisms, including a high level of tolerance to antibiotics, a high level of cell-to-cell interaction, and general resistance to host inflammatory cells, all of which make them extraordinarily durable components of diseases that do not heal.[5.15]

Biofilms on wounds have been the subject of numerous therapeutic developments until recently. There are a number of widely recognized methods for removing the psoriasis-like biofilm through the use of nanoparticles (NPs). A variety of nanomaterials are used to encapsulate antibacterial compounds, including Ag-Au

nanocomposite particles, CuONPs, Mg(OH) 2 nanoparticles, silica nanoparticles, and Au nanoparticles. [11, 16] According to Weldrick and colleagues, advanced materials using hydrolases, amylases, and proteases can be used to degrade biofilms. [16]

A new *in vivo* or *in vivo* model for mimicking biofilm formation and clearance is urgently needed because of the significant issues associated with biofilm formation on various tissues or implants. From microtiter plate assays to flow cells, these systems range from simple to sophisticated.[17-20] Due to the affordability, reproducibility, and ethical issues associated with animal experiments, *in vitro* models have become commonplace in biofilm biofilm research for antibacterial susceptibility screening. *In vitro* models, however, are not adequately replicated in *in vivo* settings as a result of a considerable amount of literature that has been published on them. Due to the complexity of preparation and the low rate of yield in *in vivo* biofilm tests, a 3D cell culture platform has not been investigated in previous research. In 2016, we developed a new technique for trapping keratinocytes and hepatocytes in Pickering emulsion droplets to produce tissue clusteroids (cell clusters).[21-23] Using w/w Pickering emulsions, a large number of spherical clusteroids are rapidly compressed through efficient encapsulation in the emulsion droplets. This study provided a straightforward method for producing dense layers of 3D keratinocyte clusteroids *in vitro*. The system could be used to investigate the co-culture of biofilms with cells *in vitro*. The aim of this investigation is to assess the feasibility of utilizing the ATPS-based technique to produce clusteroids for generation of an *in vitro* skin-like tissue. Using this tissue layer as a platform for drug delivery and testing, a biofilm was produced by co-culturing it with bacteria.

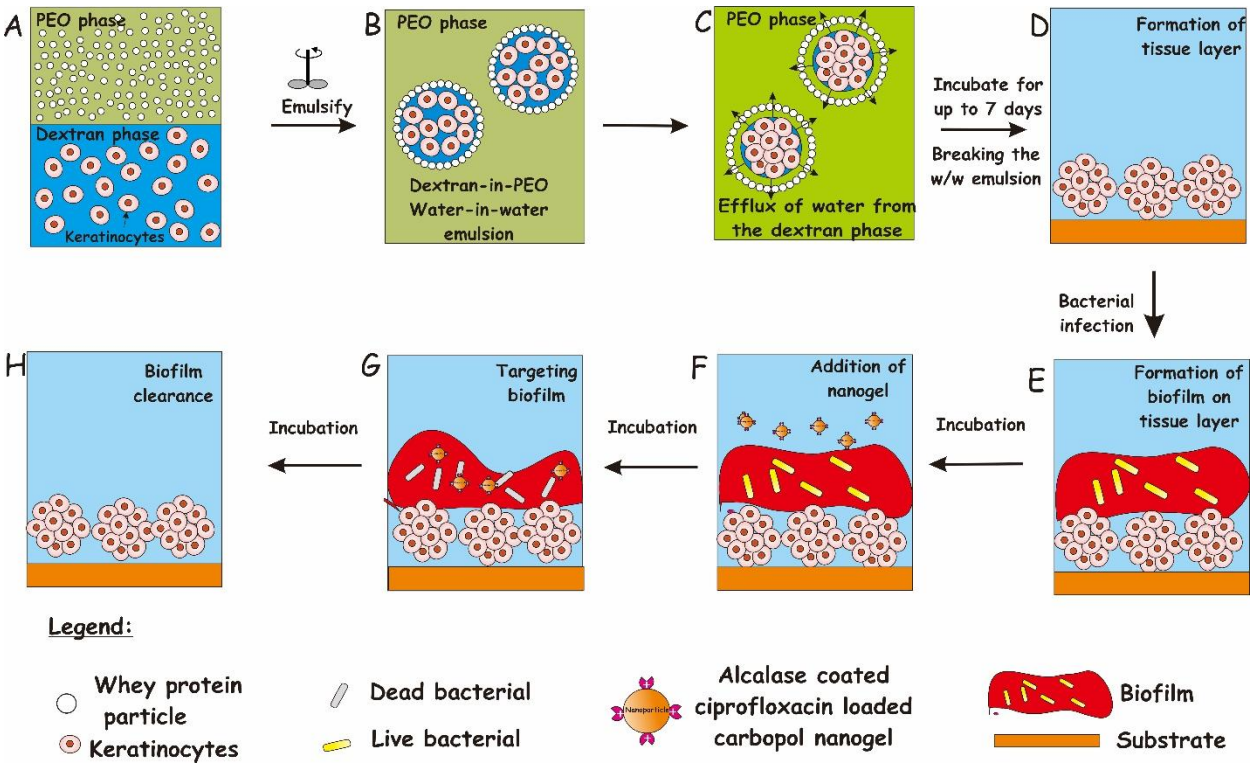

Figure 5.1. Schematic for the individual clusteroids formation and clusteroids layer formation :(A,B,C,D,E):The HaCaT cells were gently suspended in the 5.5wt% DEX in DMEM medium, the suspension was mixed with 5.5wt% PEO phase by 3 pumps. The DEX-in-PEO emulsion was then shrunk by adding a more concentrated PEO (11wt%) to facilitate cell-cell interaction and the clusteroids formation. HaCaT clusteroids were left in the emulsion for 2h to allow the clusteroids formation and the emulsion was broken down using ten-fold DMEM medium. Clusteroids were then collected and plotted in poly-L-lysine coated 96-well plate to proliferate over 7 days. and clusteroids/biofilm co-culture platform formation(C). Biofilm formation and clearance of the biofilm utilizing NPs was shown in (D,E,F,G,H,I).:After the formation of clusteroids layer, 20 µL normalized bacterial suspension(*S.aureus* or *P.aeruginosa*) was added to the clusteroids layer. Biofilm was formed after overnight incubation at 37oc with 5% CO2. 50µL of 0.2 wt% Carbopol-0.0032 wt% ciprofloxacin NPs-0.2 wt% Alcalase NPs was used for the biofilm clearance. The cultures were left in incubator for another 12h before assessing the clearance effect of the biofilm.

5.3 Material and method

5.3.1 Materials

Carbopol Aqua SF1 nanogel (30 wt% aqueous suspension) was purchased by Lubrizol, USA. The Bacteria used in this experiment were purchased from American Type culture collection and were and were, *Staphylococcus aureus subsp. aureus Rosenbach* (ATCC® 29213™) and *Pseudomonas aeruginosa* (Schroeter) Migula (ATCC® 27853™. De-ionized water purified Milli-Q water system (Millipore) was used in all our studies. Whey protein was bought from (No1. Supplements, Suffolk, UK). Sodium alginate, Corning® Transwell® polyester membrane cell culture inserts (96 well plates) and NUNC Cell culture 6-well plates were purchased from Thermo Fisher Scientific (UK). Dextran (MW 500 kDa) and PEO (MW 200 kDa) were purchased from Sigma-Aldrich, UK. Sodium chloride (99.8%) and calcium chloride, Dulbecco's Modified Eagle Medium and Trypsin-EDTA were sourced from Fisher Scientific (UK). Mueller-Hilton Broth (MHB), Mueller-Hilton Agar (MHA) were supplied by Oxoid, UK. Alcalase 2.4 L FG EC number; 3.4.21.62 was kindly provided by Novozymes, Denmark. Media supplements were fetal bovine serum (10% v/v, Labtech, Heathfield, UK) and 0.25% Trypsin-EDTA (1X, Lonza). An MTT colorimetric survival and proliferation kit (Millipore Corp, USA) was used for HaCaT cell viability experiments. The poly-L-lysine and alginate lyase was purchased from Sigma Aldrich. All other chemicals were of analytical grade.

5.3.2 Method

5.3.2.1 2D Keratinocytes Cell Culture

HaCaT cell line culture was kindly provided by the Skin Research Group at St James University Hospital at Leeds. The cells were cultured in DMEM (Gibco, UK) media supplemented with 10% fetal bovine serum (FBS) and incubated at 37 ◦C with 5% CO_2. The cells were passaged after reaching 70%-80% confluence. Cells were carefully washed with phosphate buffer saline (PBS, Labtech, UK) two times before adding 5ml 0.25% Trypsin-EDTA (1X, Lonza, UK). The cells were then incubated for 10minutes to detach the cells from the flasks. Trypsinization was neutralized by adding a DMEM medium before centrifugation at 400× g for 4 min to isolate the cell pellet. The HaCaT cells were reseeded at a ratio of 1:6 each passage.

5.3.2.2 Preparation of the Whey Protein (WP) Particles

The preparation of Whey protein particles was conducted followed by the method previously[21]. Briefly, the whey protein powder was weighted and suspended under agitation for 2h in an aqueous solution at a concentration of 2wt%. The WP solution was then hydrated at 4 º C overnight. To remove the insoluble substances obtained from the hydration, the solution was centrifugated at 8000×g for 40min. The supernatant was mixed in a proportion of 1:1 to 0.3M NaCl solution, followed by dropwise addition of 0.1mol/L HCL or NaCl to adjust the pH to 6.18. The heating process was carried out at 82 º C for 20 min followed by centrifugation at 8000×g to discard the sediment. The supernatant was used as WP solution in the following experiments.

5.3.2.3 Production of cell clusteroid and clusteroid layer

The preparation of clusteroids was slightly modified from the method introduced by Celik,et,al[23]. PEO aqueous solution (5.5 wt%) was prepared by dissolving an adequate amount of PEO into the heat-treated solution of WP to make the continuous phase. A solution of 5.5wt% dextran in DMEM complete medium under sterile conditions was used as a disperse phase. HaCaT cells were carefully suspended and normalized to adequate cell numbers ($1x10^6$/mL) in the DEX phase. To form the cell encapsulated emulsions, the DEX phase (with the cells) were transferred to the WP/ NaCl /PEO solution and gently homogenized using BD Microlance™3,6, or 12 needles (21G 12, internal diameter 0.512 mm) and a BD Plastipak™ syringe of 1 mL by six pumps (BD biosciences, Wokingham, UK). The emulsions were mixed with a higher concentrated PEO solution (14%wt) to a final concentration of 10%wt to compress the cells into densely packed clusteroids. The emulsions were left in the incubator for two hours to allow the formation of cell clusters. The emulsions were broken down by adding ten times DMEM complete medium and the clusteroids were collected from the sediment of the suspension. The viability of clusteroids after at different times in culture was measured microscopically after staining the cells with fluorescein diacetate (FDA), which stains viable cell cytoplasm green. To form 3D clusteroids that would be facile for the biofilm/clusteroids co-culture, clusteroids were collected and transferred to a 96 wells culture plate coated with poly-L-lysine instead of the alginate gel. The initial cell density of the clusteroids was standardized to 1×10^6 and a 7 days' duration was allowed for the formation of the clusteroids layer.

5.3.2.4 Bacterial culture and biofilm/clusteroids layers co-culture.

Frozen ATCC species (*Staphylococcus aureus* and *Pseudomonas aeruginosa*) were prepared onto MHA plates according to manufacturer's instructions. Overnight (O/N) cultures were prepared by incubating a single colony from the MHA stock plates into 10 mL of MHB for 16 hr at 37°C with 140 rpm shaking (Stuart Orbital Incubator S1500). For biofilm assays, O/N cultures were adjusted to 0.5 McFarland standard by diluting the O/N culture into 0.85 w/v% sterile saline until an optical density of 0.08-0.12 at 625 nm (1-2 × 10^8 CFU/mL) was obtained using a spectrophotometer (FLUO star Omega spectrophotometer, BMP Labtech). These adjusted bacterial saline suspensions were then diluted 1:150 into MHB to yield starting concentrations between 5 × 10^5 – 1 × 10^6 colony forming units per mL (CFU mL^{-1}). To visualize the bacterial under fluorescence and confocal microscope, the CFSE was used to dye the bacteria. CFSE is a fluorescent dye that is often used to track cells (e.g. during phagocytosis) or monitor cellular division. Its peak excitation is 494nm and emission at 521nm and is thus easily detectible by fluorescence microscopy or flow cytometry. To achieve the labelling, we firstly transferred 1 ml of bacterial suspension into a 1.5 mL tube and centrifuged at 4000xg for 5 minutes to obtain a cell pellet. The supernatant was discarded and pellet was resuspended in 2x CFSE working solution. The cells were then incubated at 37°C with shaking. CFSE labelled bacterial were collected by centrifugation and the pellet was resuspended in MHB and adjusted between 5 × 10^5 – 1 × 10^6 CFU/mL.

The co-culture of biofilm and clusteroid layer was achieved by adding 20µL of the either labelled or un-labelled bacterial suspensions to the each well contains the formed clusteroids layer supplemented with 200µL DMEM complete medium. The culture was left overnight (12h) in the incubator to form a biofilm.

5.3.2.5 Preparation of ciprofloxacin-loaded nanogel.

To date, various methods have been developed and introduced to produce the anti-bacterial NPs. We modified a commonly used preparation method REF HERE. Briefly, a 100 mL of 0.2 wt% aqueous dispersion of the Carbopol nanogel was prepared, this was then adjusted to pH 7.5 by dropwise addition of 0.25 M NaOH or 0.25M HCl solution with gentle agitation at 37 °C. For the estimation of NPs concentration, an aliquot of 0.0032 wt% ciprofloxacin hydrochloride aqueous dispersion was prepared by weighing 3.2 mg of the antibiotic (ABX = ciprofloxacin)

powder, diluting into 100 mL of de-ionized water and then warming to 37 °C. The 100 mL ABX solution was then added to the pH 7.5 nanogel dispersion and mixed for 30 min at 37 °C to allow the antibiotic cations to diffuse into and electrostatically bind in the cores of the swollen nanogel particles. The pH of the ABX–Carbopol solution was then reduced to pH 5.5 using droplets of 0.25 M HCl whilst being mixed for a further 30 min. The ABX–Carbopol suspension was then centrifuged at 6000g for 15 min, and the supernatant was removed and retained for encapsulation efficiency analysis. The pellet was washed three times with deionized water and re-dispersed into 100 mL of deionized water. The pH was then increased to 7.5 by gradually adding droplets of 0.25 M NaOH and the solution was gently stirred overnight. The final ABX–Carbopol nanogel solution were normalized to pH 5.5 using acetate buffer solution.

5.3.2.6 Coating of the ciprofloxacin encapsulated Carbopol NPs with Alcalase 2.4 L FG

A 0.2 wt% solution of Alcalase L FG 2.4 was created by diluting 0.6 mL of the stock liquid enzyme solution and diluting with Milli-Q water to a final volume of 100 mL. The 0.2 wt% Alcalase solution was sonicated for 15 minutes to prevent aggregation. 25 mL of the 0.2 wt% Carbopol Aqua SF1 suspension and 25 mL of the 0.6 wt% Alcalase L FG 2.4 solution were mixed together for 30 min at pH 5.5 with constant stirring to allow the enzyme to electrostatically bind to the Carbopol NPs. After mixing the suspension was centrifuged at 6000g for 15 min and the pellet was washed three times with deionized water and then dispersed into 50 mL of fresh deionized water. Droplets of acetate buffer solution were added to maintain the dispersion at pH 5.5. The particle size and zeta potential distribution of the Carbopol-Alcalase NPs were measured using a Malvern Zetasizer. Prior to measurement, and the use of the nanogels in treatments, the 0.2 wt% Carbopol-0.2 wt% Alcalase dispersion was sonicated for 5 minutes to remove aggregates and diluted into deionized water to the appropriate concentration.

5.3.2.7 Characterization of free Alcalase, Alcalase-nanogel and Alcalase-coated Ciprofloxacin-loaded nanogel.

All hydrodynamic diameter and zeta potential measurements were performed using a Malvern Zetasizer Nano ZS. The isoelectric point of Alcalase L FG 2.4; 10

mL of 0.02 wt% aqueous solution Alcalase aliquots were created at a range of pH 5 to 12 using droplets of either 0.25 M HCl or 0.25 M NaOH. Afterwards, the aliquots were sonicated for 15 min. 1 mL of each aliquot was added to a quartz cuvette and the zeta potential measured using a ZEN1002 dip cell at a refractive index of 1.45 and absorption of 0.001 as per Malvern Instruments protein refractive index manual. Measurements were performed at 25^{o}C and data represented as the mean of 3 repeats.

5.3.2.8 Biofilm viability after NP-Ciprofloxacin treatment

An overnight bacterial culture was adjusted to 1 × 10^5 CFU/mL in saline and 20 μL of this culture was added as a unit to each well contains clusteroids layer. The sample was then incubated for 24 hours at 37^{o}C to generate biofilm. 0.1 mL of Milli-Q water was considered as the control. 0.2 wt% Carbopol, 0.2 wt% Alcalase 2.4 L FG (diluted in Milli-Q water), and 0.2 wt% Carbopol-0.0032 wt% ciprofloxacin-0.2 wt% Alcalase 2.4 L FG NPs were utilized as treatments to measure their toxicity on biofilm and clusteroids layer. Similar experiments were also carried out using the individual component of the NPs to prove the efficiency brought by the structure. 0.1mL of the prepared solution with exactly the same concentration in the NPs were also added into different well plates contained the biofilm/HaCaT clusteroids co-culture models. After 24 hrs of treatment, the media was discarded and the clusteroids were carefully taken out from the well. The samples were then put into test tubes with 1 mL of new MHB and 2mL of the sterile glass beads. Each example was vortexed for 30 secs to disassociate the biofilm and inoculate the MHB with bacterial cells. The drop plate count technique was utilized to quantify cell CFU/mL. To gauge the suitability of cells inside the biofilms, 10 x dilutions were made in MHB, 10 μL solutions were transferred onto MHA plates and left growing for 24 hours at 37^{o}C. CFUs were checked from the last two droplets which contained a countable number of colonies (3 to 30 states for every 10 μL drop) and calculated as average.

5.3.2.9 Optical microscope observation

The microstructure of the clusteroids and the growth pattern of the clusteroids layer were analyzed under an inverted optical microscope (Zeiss Axio Vert.A1 inverted microscope implemented with Olympus IX 71 inverted microscope for field fluorescence microscopy). Samples were observed under various water immersion objectives at ambient temperature (25 º C).

5.3.2.10 Biofilm staining with Crystal Violet and rhodamine.

A standard 96-well microtiter biofilm formation plate assay was performed using crystal violet and rhodamine dyes. *Crystal Violet staining*: 1 mL of 5×10^5 – 1×10^6 CFU/mL of O/N bacterial culture was pipetted into 48-well TC-treated plates and incubated at 37 ^oC for 24 hrs in static conditions. After incubation, the plates were washed twice by submerging in deionized water to re- move any remaining media and suspended cells. The plate was then shaken dry and left to air dry for 15 mins at room temperature. 1 mL of MHB supplemented with Carbopol-Alcalase synthesized NPs treatment was added to the wells and incubated for 24 hrs at 37 ^oC in static conditions. The plates were then washed vigorously by submersion in de- ionized water to remove excess treated media and sus- pended cells. The plate was then shaken to remove any liquid droplets and left to dry for 15 mins at room temperature. 1 mL of 0.1 wt% Crystal Violet solution was added to each well and incubated at room temperature for 15 mins. The plates were then washed thoroughly by submersion in deionized water and blotted with paper towels to remove excess dye and water. The plate was left to dry for 2 hrs at room temperature. 1 mL of 30 wt% acetic acid was added to each well for 15 min to solubilize to the Crystal Violet. ***Rhodamine staining****;* To visualize the biofilm on the clusteroids, the clusteroids were pre-stained with CFSE and the bacterial was pre-stained with rhodamine prior to the biofilm formation. Generally, 10µl DMSO was added to 50mg of the CFSE to prepare a CFSE solution A. The solution A was diluted with 10ml DMEM medium with FBS to form the CFSE working solution B. The solution B was cultured with HaCaT cells in the incubator for 15min before removal. The cells were then harvest using 0.25wt% trypsin. 10 mL of 5×10^5 – 1×10^6 CFU/mL of O/N bacterial culture was stained by addition of 50µl 1,2-dipalmitoyl-8n-Glyecero-3-phosphoethanollamine-N-(Lissamine Rhodamine B sulfonyl) in the incubator for 15min. The bacterial solution was then centrifugated at 4000g to collect the bacterial pellet. The bacterial pellet was washed with PBS and centrifugated three times to remove the excess dye.

5.3.2.11 TEM images of Alcalase-ciprofloxacin-nanogel and SEM images of the treated biofilms.

Post-treatment the spheroids were gently removed from the plate using sterilized loop and placed onto a 7 mm diameter circular glass slide and adhered using Carbon discs. The biofilm was gently washed with deionized water from remove excess

media and treatment. The biofilms were then fixed in a 1 wt% glutaraldehyde PBS buffer solution for 1 hr at room temperature. After fixation, the biofilms were washed 3 times with deionized water to remove excess glutaraldehyde. The samples were then dehydrated in 50%/75%/90% and absolute ethanol solutions for 30 minutes each. The absolute ethanol was dried using liquid CO_2 at its critical point using an E3000 Critical Point Dryer (Quorum Technologies, UK) and then coated in 10 nm Carbon. Samples were imaged with variable pressure 100-micron aperture at 40 Pa. EHT = 20 kV, probe current 100 pA. Images were captured with Zeiss smart SEM software (Zeiss Evo-60 SEM, Germany). TEM images of bare Carbopol Aqua NPs, free Alcalase 2.4 L FG protease, and Alcalase 2.4 L FG coated Carbopol Aqua SF1 nanogels were obtained by placing a droplet of the suspended sample onto Carbon coated Copper grids (EM Solutions, UK) and allowed to adhere for 2 minutes. The grid was quickly rinsed with deionized water and negatively stained with 1 wt% aqueous uranyl acetate. This was again quickly rinsed with deionized water and allowed to dry in air. The sample was then imaged with a Gatan Ultrascan 4000 digital camera attached to the Jeol 2010 TEM 2010 electron microscope (Jeol, Japan) running at 120kV.

5.3.2.12 Confocal laser scanning microscopy observation (CLSM)

The clusteroids layer was stained using 4′,6-diamidino-2-phenylindole (DAPI) after 7 days of culture. The bacterial was pre-stained before the biofilm formation using CFSE to reach long-term tracking, which could pass through generations. The visualization of biofilm attached on the clusteroids layer was carried out using CLSM (Zeiss LSM710). The samples were imaged using Z-stacking which is composed of 100 slices for each image with 1µm per slice. The channels were set to DAPI (461nm) and FITC (488nm) for the fluorescence signal of the stained cells and biofilm.

5.3.2.13 Cytotoxic of NPs on HaCaT cells clusteroids layer.

The influence of the NPs on the viability of the clusteroids layer was carried out using MTT assay. Generally, the MTT [3-(4,5-dimethylthiazol-2-yl)-2,5-diphenyltetrazolium bromide] assays were carried out using HaCaT cells clusteroids treated with 20µL compound 1, at two distinct incubation times (1h and 24h of incubation). The plates were gently shaken and incubated for 4 hours at 37º C in 5% CO2 incubator. The supernatant was removed, 50 µl of iso-propanol was added, and

the plates were gently shaken to solubilize the formed formazan. The absorbance was measured using a microplate reader at a wavelength of 490 nm.

5.3.2.14 Cryostat sectioning

For measurements, the clusteroids/biofilm co-cultured samples were firstly fixed in Optimal cutting temperature compound and frozen in the fridge overnight. Serial cryostat sections with a thickness of 10 μm through the center region of spheroids were made on Leica CM1950. To visualize the biofilm and clusteroids layer, the sectioned samples were observed under a fluorescence microscope (Olympus BX51).

5.4 Result and discussion

5.4.1 Production of HaCaT clusteroids and HaCaT clusteroids layer

It has been demonstrated that the water-in-water Pickering emulsion template can be used to improve the yield of clusteroids from HaCaT cells. A number of different cell types have been used in previous studies, including Hep-G2, HeK and HaCaT cells, where the clusteroids layer has been observed to grow over time using the Pickering emulsion template.[21, 23] In order to collect clusteroids, the DMEM complete medium was used to break down the emulsion system. From the emulsion droplets, clusteroids of relatively uniform sizes and shapes were successfully obtained, as shown in **Figure 5.2**. According to **Figure 5.3**, this method did not significantly reduce cell viability.

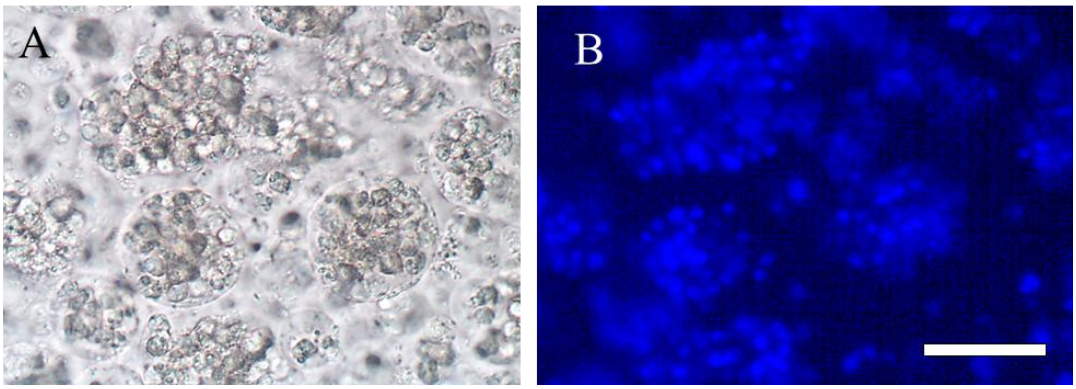

Figure 5.2. Microscopy observation(A) and fluorescence observation (B) of the HaCaT clusteroids in the 5.5wt% DEX-in-PEO emulsion droplet. The bar is 100μM

96-well plates coated with poly-L-lysine were used to collect clusteroids obtained from the emulsion template and to facilitate the formation of the HaCaT clusteroids layer; the layer was designed to mimic skin tissue. A similar growth

pattern was observed for the HaCaT clusteroids layer as previously described by Celik et al.[23] A significant finding of this study is the observation that on day 3, the individual clusteroids had clearly defined structures. The clusteroids formed densely structured tissue after three days in culture. Clusteroids layer showed excellent potential for *in vitro* modeling of biofilm infection after seven days of growth, which is consistent with the literature. Several experiments were conducted using the clusteroids layer that had been formed.

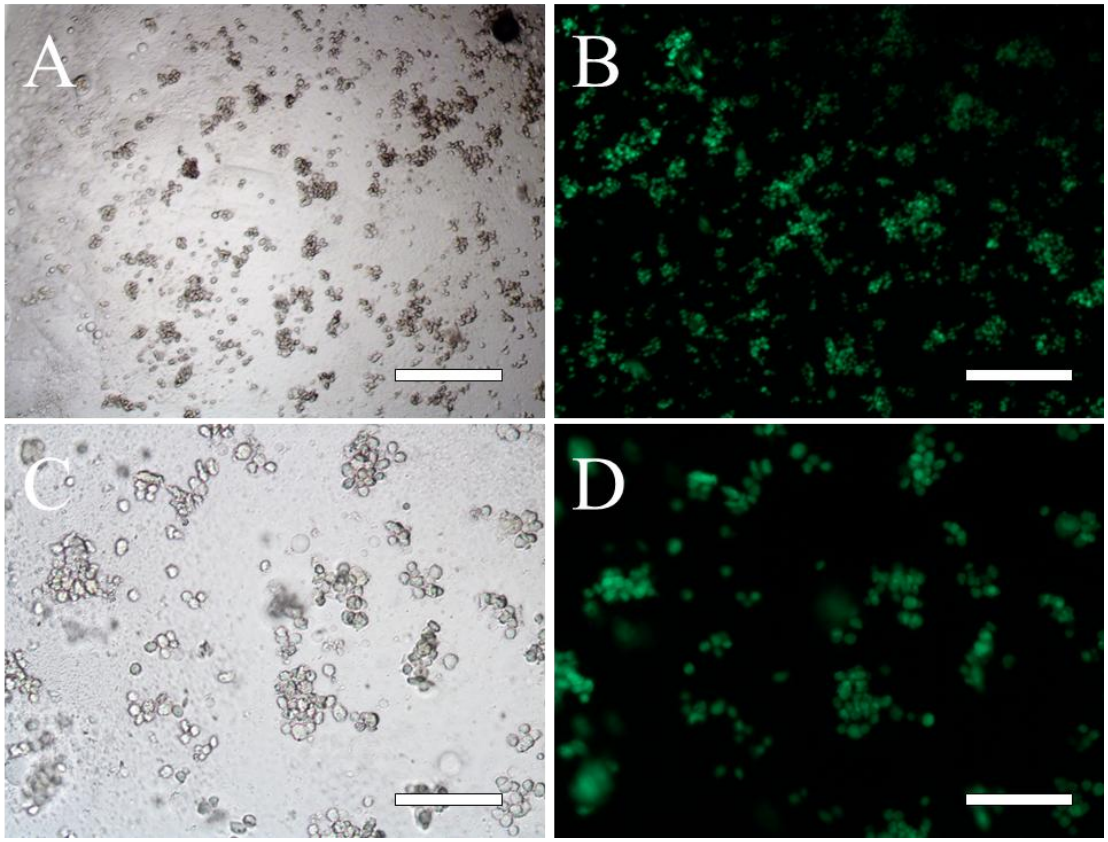

Figure 5.3. Bright field observations (A, C) and fluorescence microscopy observation (B,D) of the collected individual clusteroids from the Water=in-water emulsions. The collected clusteroids were stained using Fluorescence dictate (FDA) to check their viability. 5µL FDA working solution was added to 5mL of the clusteroids culture. The bar is 100 µm

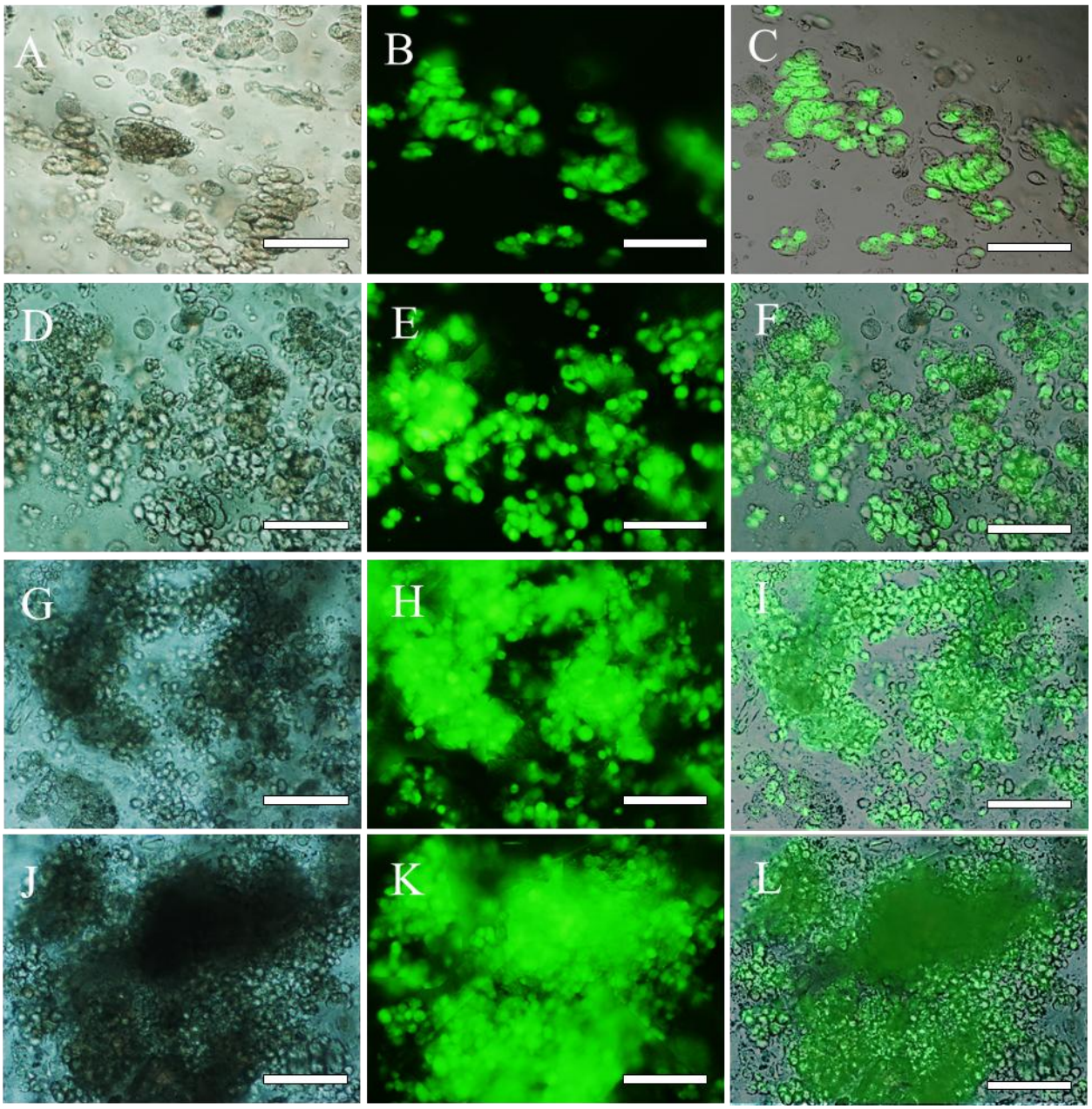

Figure 5.4. Bright filed observations (A,D,G,J), fluorescence observations and merged images of the clusteroids layer after different days of culture: A,B,C:Day1: D,E,F:Day3:.G,H,I:Day5;J,K,L:Day7. The collected clusteroids were normalized to 1 x 10 per mL in DMEM medium. 50µL of the cultures was added to poly-L-lysine coated 96-well plate supplemented with 200µL DMEM medium. Observations were done by inverted Zeiss DP71 fluorescence microscope at different days of culture. The bar is 100µm.

5.4.2 Encapsulation of ciprofloxacin into Carbopol Aqua SF1 nanogel

We developed a colloidal delivery system based on Carbopol nanogel for biofilm clearance in order to improve the efficiency of our clusteroids layer as an alternative to real human skin. This nanoparticle has been reported to be capable of killing biofilms effectively with a low level of toxicity to the cells in several studies. An electrical charge is applied to the carbopol-alcalase nanoparticle at a specific pH value. Since the carboxyl group exists in the carbopol gel, the light cross-linked gel is strongly negatively charged, nearly -30mv at pH 5.5. The alcalase at pH 5.5 exhibited a positive charge, facilitating its immobilization on the carbopol due to ionic interactions. **Figure. 5.4A** illustrates that the NPs were highly negatively charged at low alcalase concentrations (below 0.1 wt%) (-20 mV). A high alcalase concentration in the nanoparticles would lead to a positive charge (+20mV), which would increase the biofilm's killing efficiency.[24, 25] As can be seen in **Figure 5.5B**, the size of the carbopol nanogel is approximately 110nm without the aggregation of alcalase, with the highest size being around 120nm with 0.6wt% concentration (**Figure 5.6C**). Consequently, the results obtained support the idea that alcalase is capable of killing biofilms effectively at relatively high concentrations, without, on the other hand, increasing the size of nanoparticles or affecting the killing efficiency of the biofilm. A time-corresponded zeta-potential test was performed in order to assess the stability of the system further. A stable zeta potential of 16-20 mV was observed over 24 hours over the range of **Figure 5.6D**. This indicates that the alcalase remains electrostatically deposited in the nanogel particles over 24 hrs, indicating that it is a stable carrier for immobilization of the enzyme during treatment.

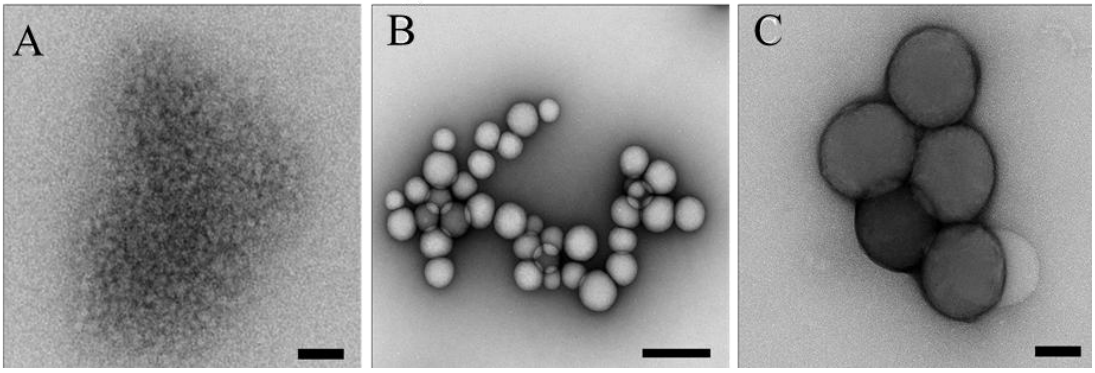

Figure 5.5. TEM images of A: Alclase B: 0.2 wt% Carbopol-0.0032 wt% ciprofloxacin NPs-0.2 wt% Alcalase NPs C: 0.2 wt% Carbopol-0.0032 wt% ciprofloxacin NPs-0.2 wt% Alcalase NPs. The Bar is 50µm (A, C) 100µm(B).

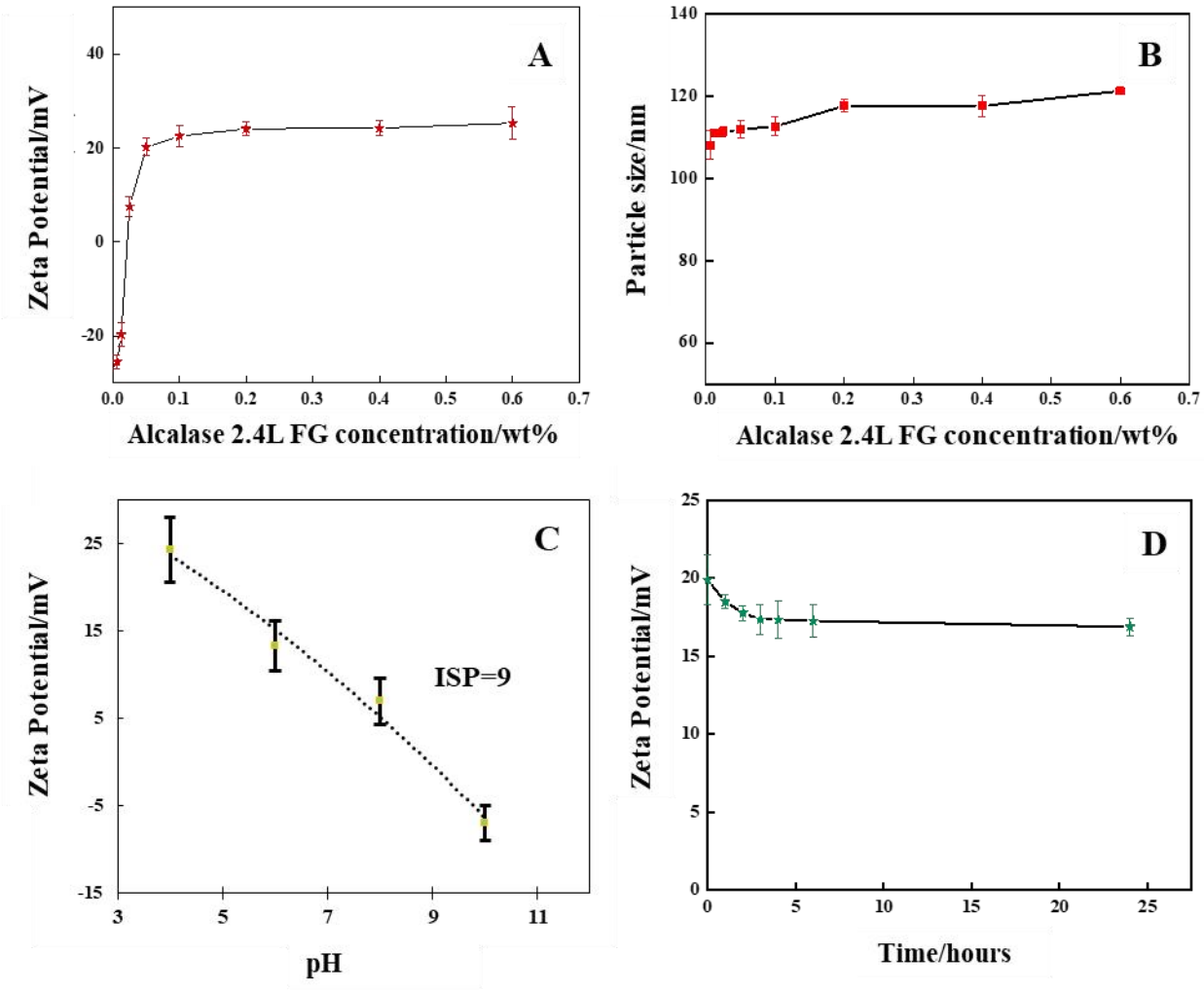

Figure 5.6. (A) mean ζ potential of Alcalase 2.4 L FG-coated Carbopol nanogel particles measured at pH 5.5 (acetate buffered saline) with various concentrations of Alcalase mixed with an equal wt % of Carbopol Aqua SF1 NPs and (B) The mean particle hydrodynamic diameter (C) isoelectric point of 0.6 wt % Alcalase 2.4 L FG measured using a Malvern Zetasizer Nano ZS at 25 °C. Each value represents a triple replicate with ±S.D. (D) The ζ potential of 0.6 wt % Alcalase 2.4 L FG-coated "empty" 0.6 wt % Carbopol nanogel particles at pH 5.5 (adjusted with acetate buffered saline) measured at various time intervals after preparation.

5.4.3 Formation of the *Staphylococcus aureus* biofilm on the HaCaT clusteroids layer.

As part of this study, the first question was to determine if the biofilm had the potential to attach to clusteroids. Biofilm formation in agar, tissues and implants has been investigated in a number of studies.[26-28] The results of the microscopy observation of this study confirmed that *Staphylococcus aureus* is capable of presenting to the clusteroids layer and is anchored there successfully (**Figure 5.6**). It is clear from **Figure 5.6** that the biofilm has formed on the clusteroids layer, despite the use of different dyes. Biofilms formed on agar and clusteroids were also observed by confocal microscopy to compare their morphologies. **Figure 5.7A-D** clearly illustrates that *Staphylococcus aureus* can deposit both on agar plates and on cells. Clusteroids-related biofilms reshaped according to the clusteroids' morphology and formed completely like a planar bacterial layer on agar. According to the results of this study, one of the most evident results is that the biofilm attaches to the clusteroids film, making this bacterial/3D cell co-culture platform an effective antibacterial testing tool. As confirmed by SEM, a biofilm formed on the cell layer was caused by *Staphylococcus aureus.* As shown in **Figure 5.8B**, *staphylococcus aureus* spheres can be found on clusteroids.

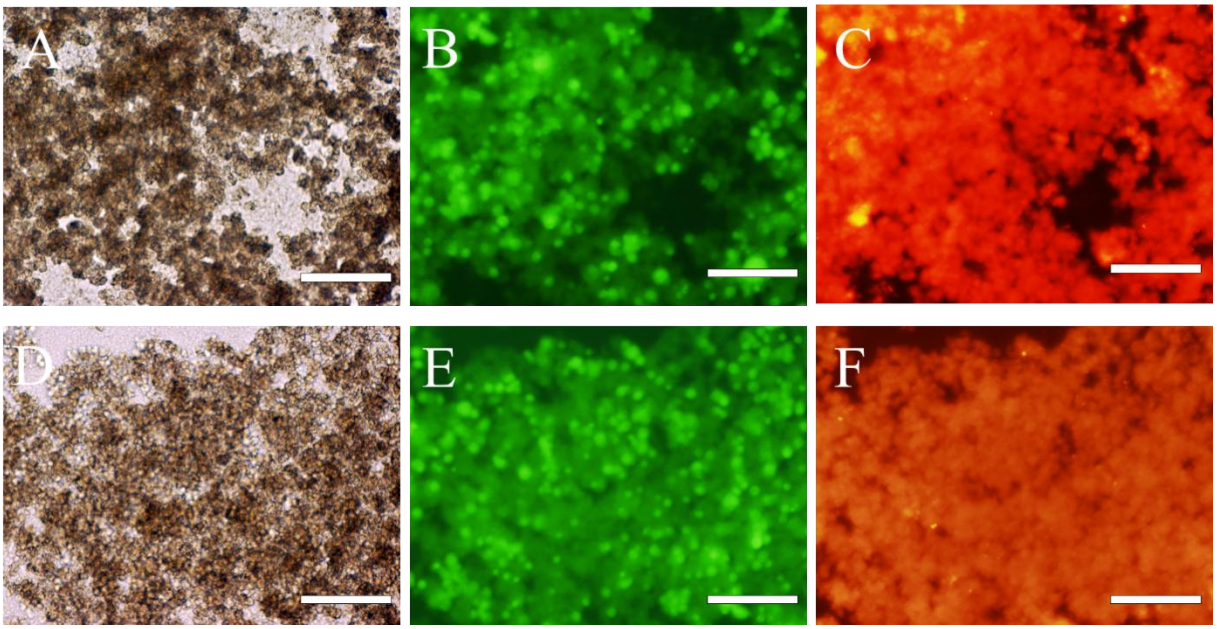

Figure 5.6. Microscopy observation of *S.aureus*/Clusteroids layer co-culture model(A,B,C) and *P.aeruginosa* layer co-culture mode (D,E,F) different filter set: A,D:(Brght field);B,E(CFSE);C,F(Rhodamine). The bar is 100μM

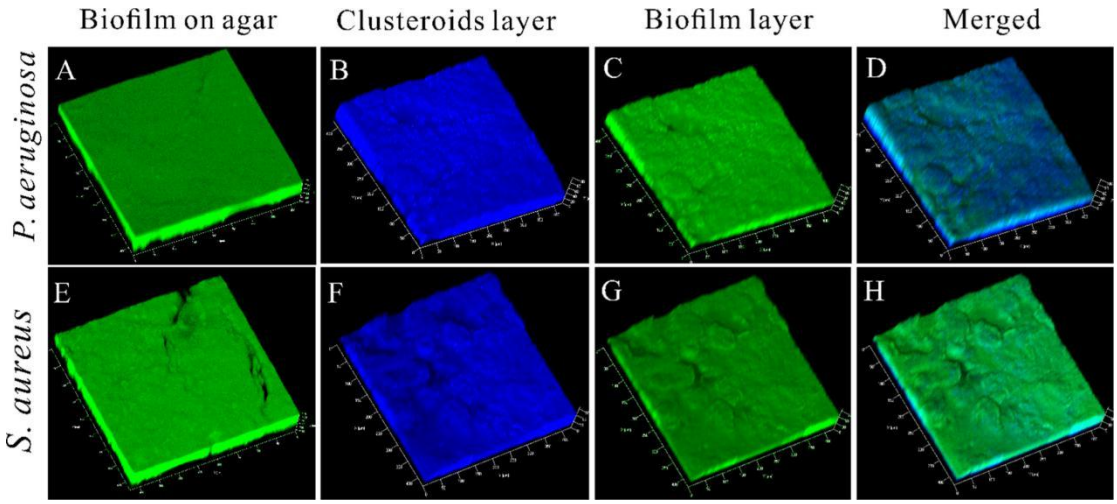

Figure 5.7. Confocal observation of *S.aureus*(A,B,D) and *P.aeruginosa* biofilm(E,F,H) on HaCaT clusteroids layer(B,C,D,F,G,H) or agar(A,E).The observation of the clusteroids layer were stained using DAPI and the biofilms were tracked using CFSE. The x-y axis is 400µm X 400µm.

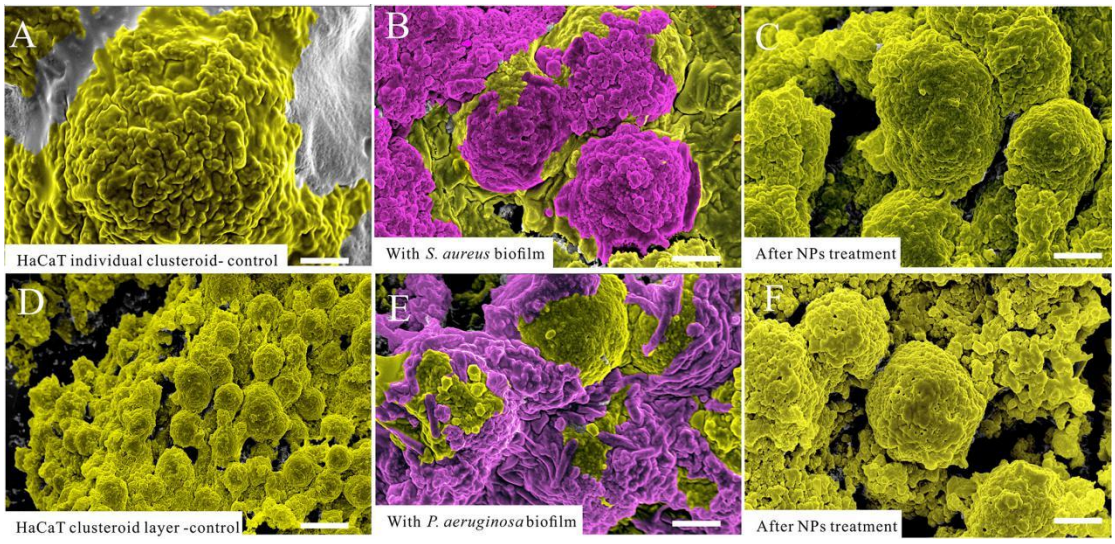

Figure 5.8. SEM observation of A: individual HaCaT cell clusteroid without any bacterial infection or Carbopol-ciprofloxacin NPs treatment. B: *S.aureus* biofilm attached on the HaCaT clusteroid layer C: HaCaT clusteroid layer infected with *S.aureus* biofilm imposed by the treatment of Carbopol-ciprofloxacin NPs. D: HaCaT clusteroid layer without bacterial infection and Carbopol-ciprofloxacin NPs treatment. E: *P.aeruginosa* biofilm attached on the HaCaT clusteroid layer F: HaCaT clusteroid

layer infected with *P.aeruginosa* biofilm imposed by the treatment of Carbopol-ciprofloxacin. The bar is 10µm for (A), 20µm for (B,C,E,F) and 40µm for (D).

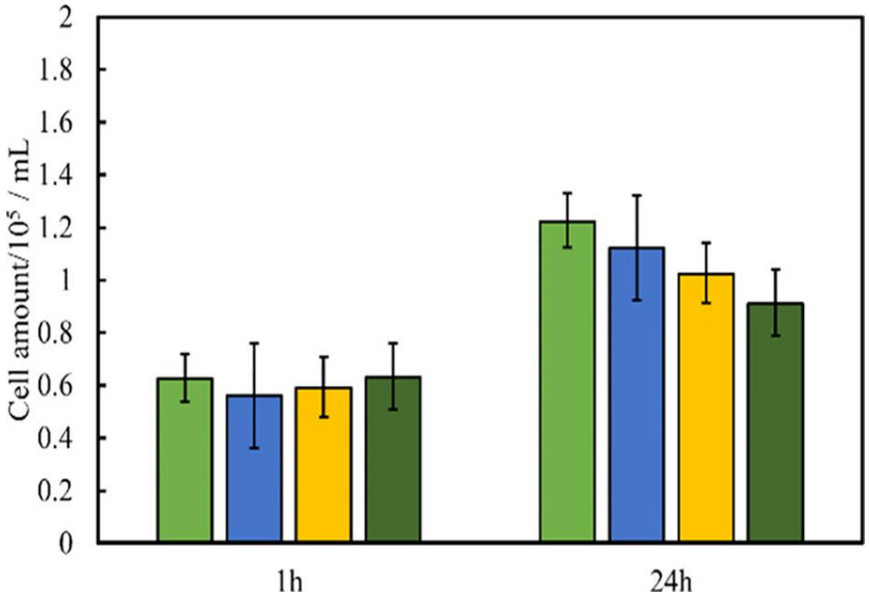

Figure 8. Influence of different concentrations of the Alcalase-coated ciprofloxacin-loaded Carbopol nanogel formulation on the proliferation of the 3D culture of the HaCaT clusteroid layer. The cell numbers in the different cultures taken after 1 and 24 h were normalized by the MTT assay. The concentration of the loaded nanogel particles was normalized based on the concentration of the loaded ciprofloxacin. The concentration of the loaded ciprofloxacin is 0 wt % (control sample-green color), 0.00064, 0.00107, and 0.00137 wt % (from left to right—blue, yellow, and dark green). The cell numbers were normalized by using a standard curve.

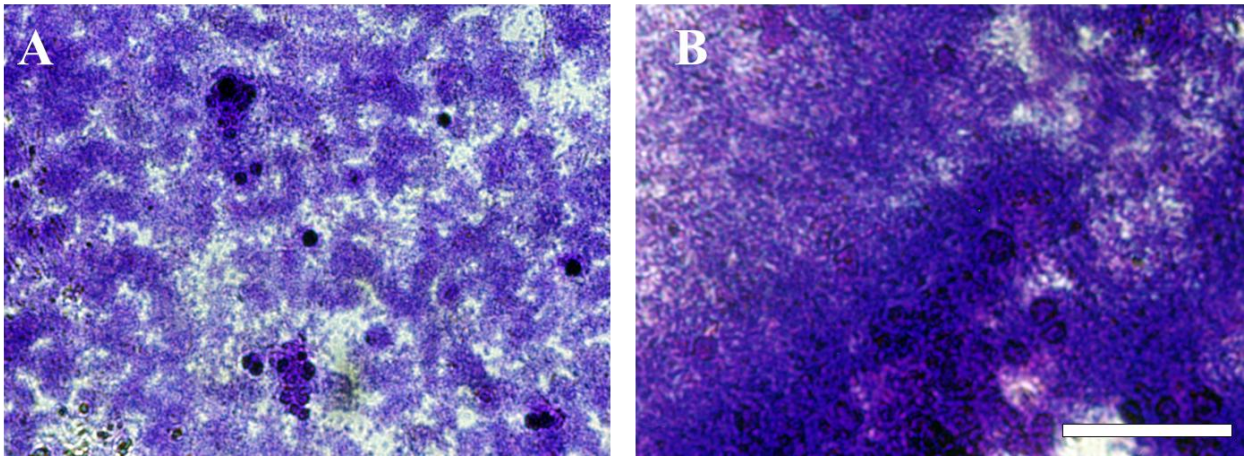

Figure 5.9. Crystal Violet staining images of *S.aureus*(A) and *P.aeruginosa*(B) biofilm attached on the clusteroids layer. The Bar is 100µm.

5.4.4 Formation of the *Pseudomonas aeruginosa* biofilm on the HaCaT clusteroids layer.

Chronic wounds are most commonly infected with *Staphylococcus aureus* and *Pseudomonas aeruginosa*. There is a tendency for *S. aureus* to grow on the surface of wounds, while *P. aeruginosa* tends to be found in the deeper layers of the wound. Therefore, understanding the mechanisms by which *P. aeruginosa* forms biofilms on skin cells would be of great benefit. *P. aeruginosa* biofilms were also observed under bright field and fluorescence microscopes (**Figure5.9**). *P. aeruginosa* biofilms on clusteroids exhibited similar structural characteristics to *S. aureus* biofilms. A rod-like structure was observed in the SEM observations of *P. aeruginosa* (**Figure 5.8E**). This is some remarkable evidence of biofilm clearance efficiency using nanoparticles using 3D cell co-culture.

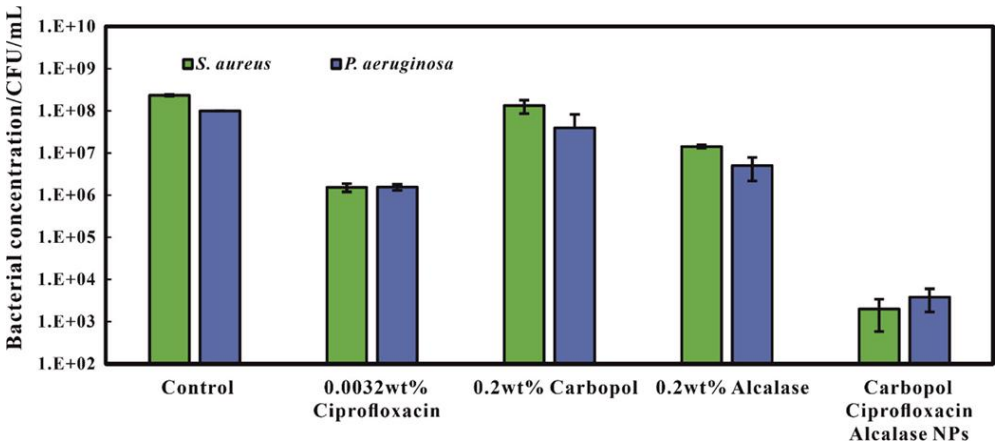

Figure 5.10. Efficiency of the Alcalase-coated ciprofloxacin-loaded Carbopol nanogel formulation and its individual components on the clearance of *S. aureus* and *P. aeruginosa* biofilms attaching on the 3D culture of the HaCaT clusteroid layer. The Alcalase-functionalized ciprofloxacin-loaded Carbopol NPs were compared to equivalent concentrations of the free ciprofloxacin, Carbopol nanogel, and Alcalase 2.4 L FG.

5.4.5 Anti-bacterial action of protease functionalized Carbopol NPs on *Staphylococcus aureus*

Incubation of the co-cultured biofilm/clusteroids layer in the NPs solution of different concentrations for up to 24 hours was used to determine the antibacterial

activity of ciprofloxacin-Carbopol NPs against *Staphylococcus aureus*. **Fig. 5.8B** and C shows SEM images of biofilm and clusteroids layers that were co-cultured with 1% carbopol and 0.0032 % ciprofloxacin NPs, each of which were diluted by 0.2 wt % alcalase NPs, after 24 hours of hydrolysis with 0.2 wt % carbopol. As shown in **Figure5.8A**, the untreated clusteroids and clusteroids layer morphology is shown in the control sample.

There may be an attraction between the protease-functionalized nanogel particle and the anionic surface of the clusteroids for these particles to aggregate and cluster on a clusteroids cell layer. Ciprofloxacin is released into clusteroids via the nanocarrier, resulting in higher antibacterial activity.

The Carbopol coated ciprofloxacin decreases *Staphylococcus aureus* viability when the concentration is increased. Incubations were conducted in DMEM complete medium with multi-dilutions of a stock suspension consisting of 0.2 weight percent carbopol, 0.0032 weight percent ciprofloxacin NPs, and 0.2 weight percent alcalase NPs. Carbopol nanocarrier formulations appear to be more effective at antibacterial effects when ciprofloxacin concentrations are increased. These NPs demonstrate high anti-bacterial efficiency after 24 hours of incubation, demonstrating a five logarithmic decrease in bacteria. A SEM observation demonstrates the removal of the biofilm attached on the clusteroids layer of the co-culture, as well as how the morphology of the model has been altered as a result of this removal of the biofilm. Biofilms formed by *Staphylococcus aureus* coated the clusteroids nearly completely before treatment. A significant reduction in visible bacterial anchoring on clusteroids was observed after the application of NPs. Carbopol, non-coated ciprofloxacin and free alcalase (0.2 wt%) were also tested on their ability to kill the biofilm (attached to the clusteroids) to investigate the key component that kills the biofilm (attached). Incubation with compatible nanoparticles was conducted for up to 24 hours to determine the viability of bacterial cells in all these samples and controls.

There is no doubt the fact that free ciprofloxacin is significantly toxic in comparison to untreated control samples against *Staphylococcus aureus* on its own, and the Carbopol nanocarrier (without ciprofloxacin) does not show obvious toxicity during the course of the experiment when it is compared to the untreated control sample (**Figure 5.10**). Also, the results demonstrated that free alcalase demonstrated similar antibacterial activity as ciprofloxacin of similar strength. It is evident from

these data that ciprofloxacin and alcalase both possess the ability to kill bacteria, and therefore we can conclude that they do not pose a threat to humans (**Figure 5.10**). There was, however, an exponentially stronger effect on removing the biofilm when ciprofloxacin NPs were paired with alcalase NPs with the same amount of each component. This might be explained by the ability of the compounds to penetrate deeply through the 3D bacterial matrix. Ciprofloxacin NPs coated with cationic proteases may further stimulate the release of ciprofloxacin because of their electrostatic attraction to the anionic bacterial biofilms. This may cause the ciprofloxacin to disrupt the cell membrane, resulting in cell death.

Biofilm clearance efficiency using NPs was assessed using confocal observation. After the treatment, the height of the CFSE-labeled film reduced significantly from 50 μm to 10 μm as a result of the decrease in CFSE-labeled film (**Figure 5.11**). Cryostat sectioning was conducted in addition as a means of demonstrating a deeper infection of the biofilm. A type of network of HaCaT clusteroids was observed after cryostat sectioning (**Figure 5.12**). It is possible to test for biofilm clearance or infection using the thickness of HaCaT clusteroids. In **Figure 5.12)**, we can see that before the treatment, the bacteria had largely covered the clusteroids layer before incubation

with NPs, and after incubation with NPs, these bacteria were mostly removed.

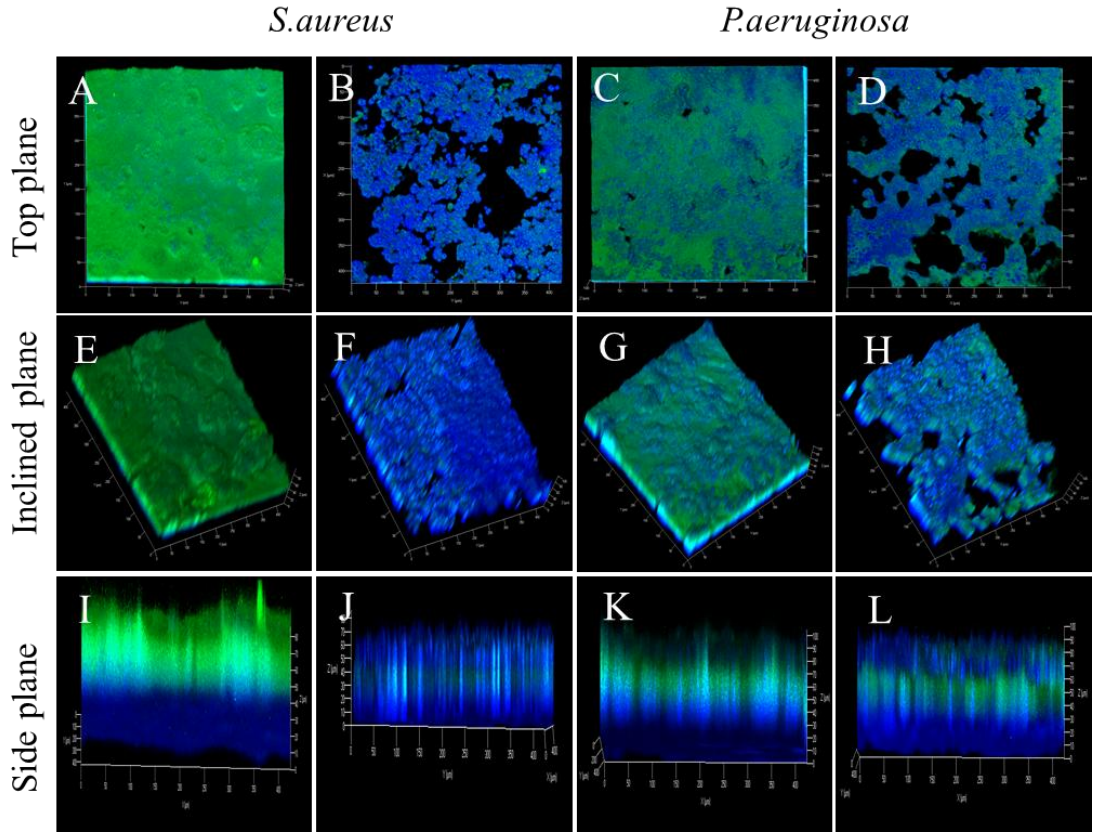

Figure 11. Confocal Z-Stacking image of Clusteroids/Bacterial biofilm (*S. aureus*: A, B, E, F, I, J) (*P. aeruginosa*: C, D, G, H, K, L) before (A, E, I, C, G, K) and after (B, F, J, D, H, L) the treatment of 0.2 wt% Carbopol-0.0032 wt% ciprofloxacin NPs-0.2 wt% Alcalase NPs. The HaCaT cells were stained using DAPI and the bacterium were pre-stained using CFSE before the formation of biofilm. The image stacking was done with 100 slices (1µm per slice). The x-y axis is 400µmX400µm for (A-H) and 60µm X 400µm for(I-L).

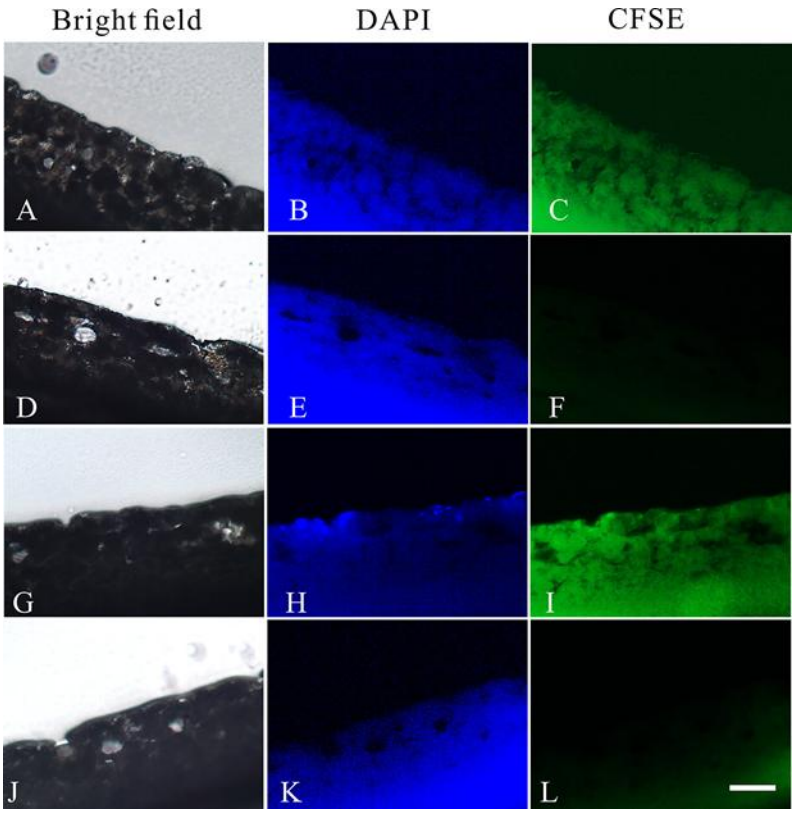

Figure 12. Cryostat sectioning of the co-cultured clusteroids/bacterial biofilm :*S. aureus*(A-F) and *P. aeruginosa*(G-M) biofilm before and after treatment with 0.2 wt% Carbopol-0.0032 wt% ciprofloxacin NPs-0.2 wt% Alcalase NPs. Each slice obtained from cryo-sectioning is 10µm. The bright field and fluorescence observation were carried out on an Olympus DX51 fluorescence microscope. The bar is 100µm.

5.4.6 Anti-bacterial action of protease functionalized Carbopol NPs on *Pseudomonas aeruginosa*

Likewise, carbopol-coated ciprofloxacin was tested for its antibacterial effectiveness against *Pseudomonas aeruginosa* by incubating a fixed amount of *Pseudomonas aeruginosa* suspension for up to 24 hours at room temperature. This figure depicts the SEM images of a control sample of clusteroids that had not been treated with carbopol-coated ciprofloxacin (**Fig. 5.8)E**), compared with the SEM images of clusteroids treated with carbopol-coated ciprofloxacin (**Fig. 5.8F**). This cluster of clusteroids has become heavily coated with *P. Aeruginosa* rods prior to treatment, just as with the biofilm infection (**Fig. 5.8E**). There were only a few bacteria remaining on clusteroids' surfaces after NPs were applied to their layer. Carbopol NPs functionalized with alcalase have a lower threshold of toxicity with

P.Aeruginosa than with normal Carbopol NPs (**Figure 5.13**). In addition, **Figure. 5.10)** illustrates the incubation of *P. Aeruginosa* with NPs as well as solutions containing 0.5 wt% alcalase and non-coated ciprofloxacin. Based on this comparison, we observe a similar trend to what we observed with *S. Aureus*. NPs are capable of performing exponentially better than any other component in terms of antibacterial performance against *P. Aeruginosa* (**Fig 5.10**). Similarly, clusteroids are not adversely affected by the empty alcalases or ciprofloxacin, and the Carbopol coating is not a toxicity to *P. Aeruginosa* (**Fig 5.10**).

The Cryo-stat sectioning and confocal observations were also performed in order to obtain a more comprehensive understanding of the process involved in removing biofilm from the surface of clusteroids as well as the extent to which bacterial penetrated the clusteroids. The infection of *S. Aureus* biofilm formed a thick layer of fungus on the clusteroids that showed higher densities and thicker layers compared to *P. Aeruginosa* biofilm, reaching an overall thickness of about 70 micrometers. Additionally, NPs were found to have clearance effects on *P. Aeruginosa* biofilms. In CFSE-labeled bacteria, weak signals can still be detected using cryostat sectioning. Ciprofloxacin may be more tolerant of *P. aeruginosa*, which may explain this phenomenon.

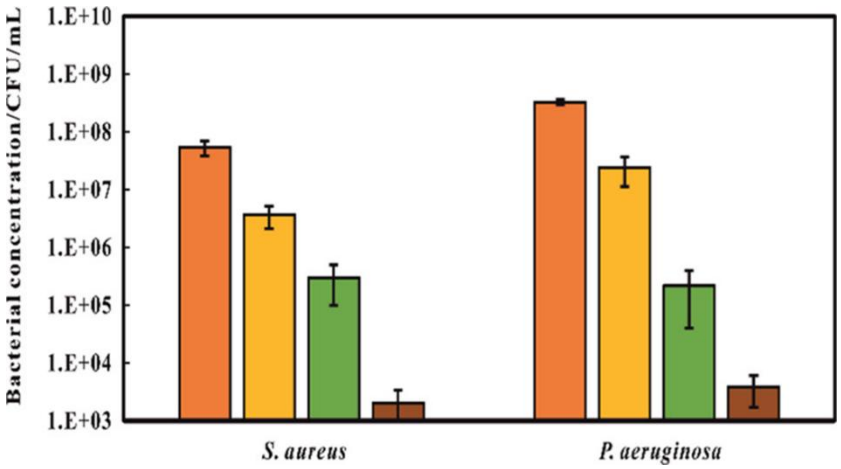

Figure 5.13. Influence of different concentrations of the Alcalase-coated ciprofloxacin-loaded Carbopol nanogel formulation on the clearance efficiency of *S. aureus* and *P. aeruginosa* biofilm attached on 3D culture of the HaCaT cell clusteroid layer. The concentration of the NPs is normalized based on the concentration of the loaded ciprofloxacin. The concentration of the loaded ciprofloxacin is 0 wt % (control

sample-red color), 0.00064, 0.00107 and 0.00137 wt % (from left to right: magenta, yellow, and brown color). The cell numbers were normalized by CFU counting.

5.5 Conclusions

To test the NPs efficiency on biofilm clearance, we developed a novel 3D cell clusteroids/biofilm co-culture platform. Carbopol nanocarrier functionalized with alcalase was the unit of investigation used in previous studies. In comparison with non-coated ciprofloxacin and alcalase, this nanocarrier demonstrated a significant increase in antibacterial activity. In the clusteroids model, such nanoparticles did not pose a significant threat, and the clusteroids could continue to proliferate despite the presence of such nanoparticles. *S. aureus* and *P. aeruginosa* were considered to be two major bacteria related to wound care, and were treated with ciprofloxacin-loaded nanocarriers. As a result of our experiments, we have shown that the nanogel strongly increases the antibacterial action of the ciprofloxacin loaded into it against both of the bacteria species after the incubation period of 24 hours. Our experiment was designed to detect biofilms and clusteroids using confocal, scanning electron microscopy, and cryostat as methods of characterization. Biofilm formation and clearance after treatment with NPs were clearly visible in the Z-stacking image obtained by confocal microscopy. A SEM image of clusteroids treated with nanocarriers revealed that the clusteroids/biofilm co-culture model had a distinct morphology both before and after being treated with nanoparticles. An antibacterial effect of the NPs was also detected through cryo-stat sectioning and the deeper infection of the bacteria was detected using cryo-stat sectioning. NPs and nanocarrier-based therapeutics may be tested for wound healing in this clusteroids/biofilm co-culture model. Moreover, this work shows that 3D cell clusteroids could have the potential to be used in further biomedical applications in the future.

5.6 References

1. Flemming, H. C.; Wingender, J., The biofilm matrix. *Nat Rev Microbiol* **2010,** *8* (9), 623-33.

2. Lewis, K., Riddle of biofilm resistance. *Antimicrob Agents Chemother* **2001,** *45* (4), 999-1007.

3. KOLTER, P. W. A. R., Biofilm, City of Microbes. *JOURNAL OF BACTERIOLOGY* **2000,** *182* (10), 2675–2679.

4. J. W. Costerton, G. G. G. a. K.-J. C., How Bacteria Stick. *Scientific American* **1978,** *238* (1), 86-95.

5. Moreau-Marquis, S.; Stanton, B. A.; O'Toole, G. A., Pseudomonas aeruginosa biofilm formation in the cystic fibrosis airway. *Pulm Pharmacol Ther* **2008,** *21* (4), 595-9.

6. Niels Høiby†1, O. C.; Bjarnsholt, T., Pseudomonas aeruginosa biofilms in cystic fibrosis. *Future Microbiol* **2010,** *5* (11), 1663–1674.

7. C R Kokare*, S. C., A N Khopade and K R Mahadik, Biofilm: Importance and applications. *Indian Journal of Biotechnology* **2009,** *8*.

8. Norsworthy, A. N.; Pearson, M. M., From Catheter to Kidney Stone: The Uropathogenic Lifestyle of Proteus mirabilis. *Trends Microbiol* **2017,** *25* (4), 304-315.

9. Jepson, R. G.; Williams, G.; Craig, J. C., Cranberries for preventing urinary tract infections. *Cochrane Database Syst Rev* **2012,** *10*, CD001321.

10. Davis, S. C.; Ricotti, C.; Cazzaniga, A.; Welsh, E.; Eaglstein, W. H.; Mertz, P. M., Microscopic and physiologic evidence for biofilm-associated wound colonization in vivo. *Wound Repair Regen* **2008,** *16* (1), 23-9.

11. Weldrick, P. J.; Hardman, M. J.; Paunov, V. N., Smart active antibiotic nanocarriers with protease surface functionality can overcome biofilms of resistant bacteria. *Materials Chemistry Frontiers* **2021**.

12. Scotland, K. B.; Lo, J.; Grgic, T.; Lange, D., Ureteral stent-associated infection and sepsis: pathogenesis and prevention: a review. *Biofouling* **2019,** *35* (1), 117-127.

13. Minasyan, H., Sepsis: mechanisms of bacterial injury to the patient. *Scand J Trauma Resusc Emerg Med* **2019,** *27* (1), 19.

14. Klingenberg, C.; Aarag, E.; Ronnestad, A.; Sollid, J. E.; Abrahamsen, T. G.; Kjeldsen, G.; Flaegstad, T., Coagulase-negative staphylococcal sepsis in neonates. Association between antibiotic resistance, biofilm formation and the host inflammatory response. *Pediatr Infect Dis J* **2005,** *24* (9), 817-22.

15. Hoiby, N.; Bjarnsholt, T.; Givskov, M.; Molin, S.; Ciofu, O., Antibiotic resistance of bacterial biofilms. *Int J Antimicrob Agents* **2010,** *35* (4), 322-32.

16. Weldrick, P. J.; Hardman, M. J.; Paunov, V. N., Enhanced Clearing of Wound-Related Pathogenic Bacterial Biofilms Using Protease-Functionalized Antibiotic Nanocarriers. *ACS Appl Mater Interfaces* **2019,** *11* (47), 43902-43919.

17. Gilbertie, J. M.; Schnabel, L. V.; Hickok, N. J.; Jacob, M. E.; Conlon, B. P.; Shapiro, I. M.; Parvizi, J.; Schaer, T. P., Equine or porcine synovial fluid as a novel ex vivo model for the study of bacterial free-floating biofilms that form in human joint infections. *PLoS One* **2019,** *14* (8), e0221012.

18. Salli, K. M.; Ouwehand, A. C., The use of in vitro model systems to study dental biofilms associated with caries: a short review. *J Oral Microbiol* **2015,** *7*, 26149.

19. Gurjala, A. N.; Geringer, M. R.; Seth, A. K.; Hong, S. J.; Smeltzer, M. S.; Galiano, R. D.; Leung, K. P.; Mustoe, T. A., Development of a novel, highly quantitative in vivo model for the study of biofilm-impaired cutaneous wound healing. *Wound Repair Regen* **2011,** *19* (3), 400-10.

20. Coenye, T.; Nelis, H. J., In vitro and in vivo model systems to study microbial biofilm formation. *J Microbiol Methods* **2010,** *83* (2), 89-105.

21. Wang, A.; Madden, L. A.; Paunov, V. N., High-throughput fabrication of hepatic cell clusteroids with enhanced growth and functionality for tissue engineering applications. *Materials Advances* **2020,** *1* (8), 3022-3032.

22. Wang, A.; Madden, L. A.; Paunov, V. N., Advanced biomedical applications based on

emerging 3D cell culturing platforms. *Journal of Materials Chemistry B* **2020,** *8*, 10487--10501.

23. Celik, S. B. G.; Dominici, S. R.; Filby, B. W.; Das, A. A. K.; Madden, L. A.; Paunov, V. N., Fabrication of Human Keratinocyte Cell Clusters for Skin Graft Applications by Templating Water-in-Water Pickering Emulsions. *Biomimetics (Basel)* **2019,** *4* (3).

24. Wang, A., Weldrick, P. J., Madden, L. A., & Paunov, V. N. (2021). Biofilm-infected human clusteroid three-dimensional coculture platform to replace animal

models in testing antimicrobial nanotechnologies. *ACS Applied Materials & Interfaces*, *13*(19), 22182-22194.

25. Paul J. Weldrick, a. S. I., b Matthew J. Hardmanc and Vesselin N. Paunov a,*, Breathing new life into old antibiotics: Overcoming antibacterial resistance by antibiotic-loaded nanogel carriers with cationic surface functionality. *Nanoscale* **2019,** *00*, 1-3.

26. Dusane, D. H.; Lochab, V.; Jones, T.; Peters, C. W.; Sindeldecker, D.; Das, A.; Roy, S.; Sen, C. K.; Subramaniam, V. V.; Wozniak, D. J.; Prakash, S.; Stoodley, P., Electroceutical Treatment of Pseudomonas aeruginosa Biofilms. *Sci Rep* **2019,** *9* (1), 2008.

27. Arciola, C. R.; Campoccia, D.; Montanaro, L., Implant infections: adhesion, biofilm formation and immune evasion. *Nat Rev Microbiol* **2018,** *16* (7), 397-409.

28. Ammann, T. W.; Bostanci, N.; Belibasakis, G. N.; Thurnheer, T., Validation of a quantitative real-time PCR assay and comparison with fluorescence microscopy and selective agar plate counting for species-specific quantification of an in vitro subgingival biofilm model. *J Periodontal Res* **2013,** *48* (4), 517-26.

29. Salgado, J. G. B. C. G., Clinic-epidemiological evaluation of ulcers in patients with leprosy sequelae and the effect of low level laser therapy on wound healing: a randomized clinical trial. *BMC Infectious Diseases* **2010,** *10* (237), 1471-2334.

6. Chapter 6

Enhanced clearing of Candida biofilms on 3D urothelial cell *in-vitro* model by lysozyme-functionalized Fluconazole-loaded shellac nanoparticles

6.1 Abstract:

Due to reduced immunity of patients and the hospital ecosystem, Candida urinary tract biofilms are increasingly observed in nosocomial infections. A significant source of urinary tract biofilm infections is the indwelling devices used to support patients with urethral diseases, which provide a direct connection between the unsterilized environment outside and that in which the patient resides. Recent research has shown that nanoparticles (NPs)-based therapeutics can be effective in fighting bacterial biofilm infections, including antibiotic-resistant bacteria that utilize nanoparticles. There is, however, a lack of precise *in-vitro* and *in-vivo* models for testing the efficacy of nanotherapeutics, so most studies have taken place in the laboratory rather than in clinical trials. In this study, nanoparticle-based antifungal therapeutics are tested on a model of biofilm-infected 3D human urothelial cells. A shellac core and a cationic enzyme lysozyme coating were used to create the nanoparticles. We reported super-enhanced efficiency in removing *Candida albicans* biofilms on a 3D layer of urothelial cell clusteroids using a formulation of lysozyme-coated 0.02 wt% Fluconazole-loaded 0.2 wt% shellac NPs, stabilized by 0.25 wt% Poloxamer 407. Urothelial cells were exposed to a formulation of nanoparticles that displayed a low level of toxicity. There appears to be no reliable *in vitro* model that would be capable of replacing animal testing for antifungal nanotechnologies in the treatment of Candida urinary tract infections in this study. An accurate and reproducible 3D urothelial cell culture model of fungal biofilms could speed up clinical trials of antifungal nanotherapeutics if it can be used in a well-defined biofilm-infected model.

6.2 Introduction

Infections of the urinary tract (UTIs) are among the most common illnesses affecting people of all ages, with medical professionals spending a lot of time and

resources treating them.[1] Women are most likely to suffer from UTIs, with an incidence of more than 40% in their lifetime.[2] Depending on the clinical symptoms and microbiological type, UTIs can be classified as cystitis, pyelonephritis, or prostatitis.[3-5] Lower urinary tracts, upper urinary tracts, and kidneys or prostate are the three main sites of infection in the urinary tract.[6]

Nosocomial infections are more likely to cause Candida urinary tract infections in healthy individuals.[7] There is a strong correlation between this condition and the patient's diminished immunity. The hospital ecosystem also contributes to the increased rate of urinary tract infections among patients. In hospitals, 42 percent of infants with urinary tract infections are infected with *Candida albicans*.[8] The use of indwelling devices to support patients with urethral disease, including catheters and stents, is another major source of nosocomial infection in the urinary tract.[9,10]

Specifically, biofilms serve as a source of infection in catheter-associated urinary tract infections (CAUTI) since they connect a normally sterile, hydrated body site to the outside world by connecting a foreign body - like an indwelling catheter - to the outside world, where they may inevitably become colonized by bacteria. Patients with urinary tract diseases are likely to develop biofilm infections when catheters or other indwelling devices are used to sustain them.[11-13] Oftentimes indwelling medical devices can become colonised by bacteria or fungal cells, which are capable of encapsulating themselves by forming an extracellular polymeric substance (EPS), allowing for the colonization of the device. As a result of this biofilm, the bacteria are able to proliferate and become stronger and more resistant to drugs, increasing their colony size.[14,15] Biofilms are unique ecosystems that promote DNA, RNA, polysaccharides, and protein production through increased cell-to-cell interactions.[16,17] There has been a significant emergence of nanotechnology based approaches and formulations that have been shown to be able to penetrate the EPS of biofilms and kill multidrug-resistant microbial strains, recently. These approaches have started gaining traction and are having a positive impact on antimicrobial formulations and delivery systems.[14,15] EPS absorption properties and the excretion of extracellular enzymes provide colonies with an additional level of antimicrobial resistance.[18-19]

There has been a significant emergence of nanotechnology based approaches and formulations that have been shown to be able to penetrate the EPS of biofilms and kill

multidrug-resistant microbial strains, recently. These approaches have started gaining traction and are having a positive impact on antimicrobial formulations and delivery systems.[20-21] The use of nanoparticles for biofilm prevention traditionally involves inorganic substances, polymers, and various macro and small molecules.[22-25] These nanoparticles are typically manufactured by microfluidics, self-assembly, or mechanical

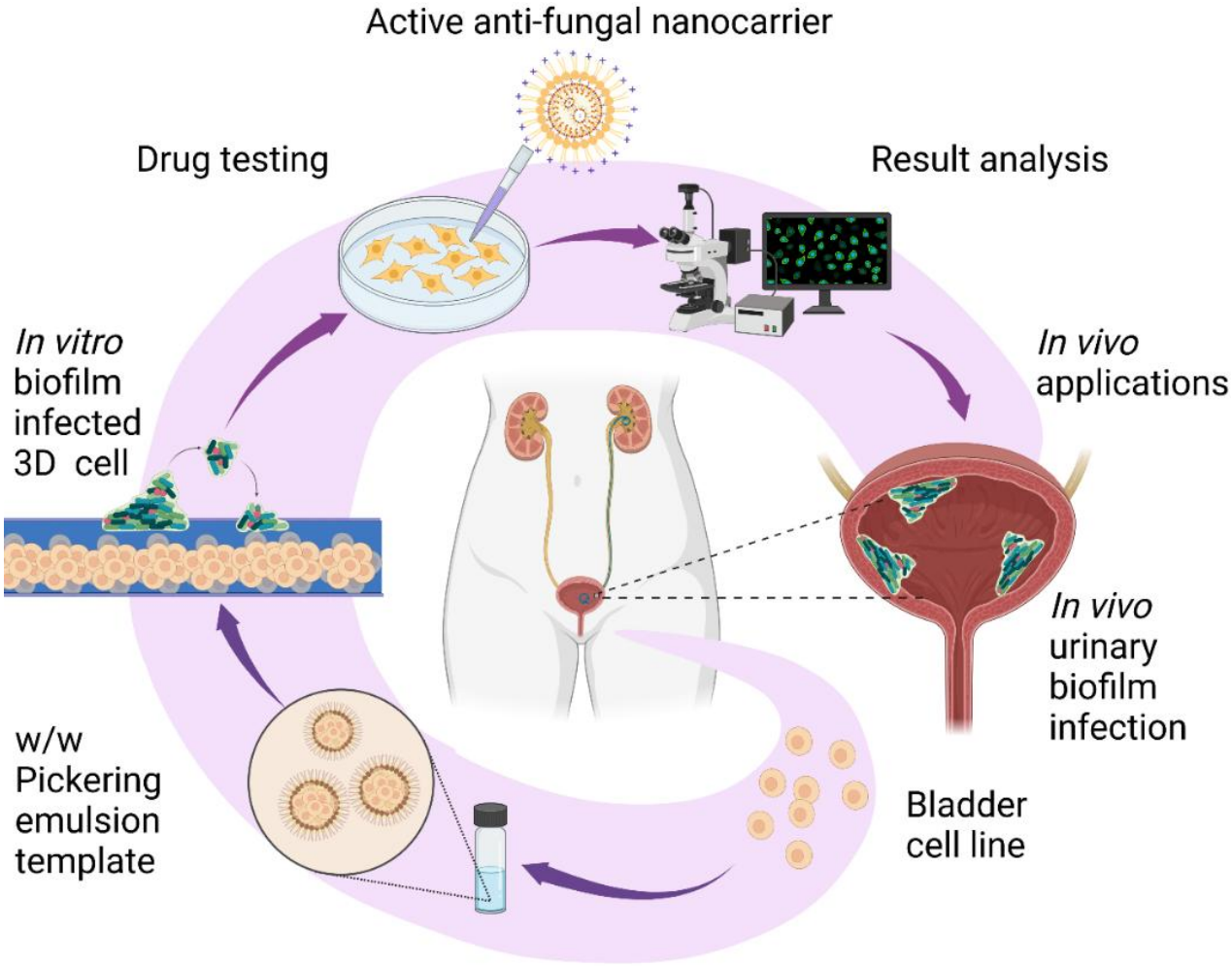

Figure 6.1. Schematic illustration of the *in vitro* 3D urinary cell model for testing anti-fungal nanotechnologies. Created with BioRender.com.

There have been recent developments in the fields of polymeric antimicrobial nanocarriers, metal-based nanocomposites, carbon-based nanomaterials, and dual-functionalized nanoparticles, which have all been developed into important nanotechnologies for enhancing antimicrobial effects and revitalizing old antibacterial compounds. [46-53]

In laboratory conditions, the presence of antibiotic-resistant biofilms is one of the growing threats to the effectiveness of nanotechnology-based antimicrobials.[24-30] As a matter of fact, 99 % of the nanotechnology-based antimicrobials that are currently being developed could not benefit patients as they will never be translated into clinical trials and utilized for medical benefit. In the last few years, there have been some major challenges in the nanotechnology field which have dominated it for many years, including the lack of *in vitro* testing platforms as well as animal models that have been improvised, both of which are crucial before the clinical trials begin. Even though animal models are safe and effective, they are often constrained by ethical and moral issues. A two-dimensional culture of human cells is an inadequate model for simulating biofilms *in vitro*. A long time ago, there was a literature that recommended 3D cell culture as a way to balance real organ complexity with the availability of 3D cultured organs.[31,32] To achieve organoids/spheroids with enhanced cell-to-cell signals and functionality, 3D cell cultures employ microfluidics and extracellular matrix (ECM).[33-35] These models are believed to be more advanced in simulating the *in-vivo* environment, and their cell cluster sizes (200 μm or larger) make it feasible to test the effect of drugs on specific tissue. A majority of research on this topic has concentrated on fabricating spheroids with low yields, which severely limits the use of this technology in biomedical applications.

Recently, the present study described the use of water-in-water Pickering emulsions in an aqueous two-phase system (APTS) for the production of high volumes of spheroids. The unique technology has been reported to produce spheroids rapidly and with significant yield and functionality enhancements by several

researchers.[37,38] *In vitro* simulation of urinary fungal biofilm infection can be achieved by using a 3D urinary cell culture model.

In the present study, we employed the cell line ECV 304 to produce 3D urinary cell clusteroids using the ATPS based template method, which is recognized as a mature bladder cell model with endothelial properties.[36-38] It was first inoculated with a *Candida albicans* biofilm infection in a 3D layer of urothelial cell clusteroids, then a fluconazole-loaded Poloxamer 407 stabilised shellac nanoparticles were tested on their efficiency in clearing the biofilm, before the final formulation, Fishhook-functionalized Lysozyme surface functionalized Poloxamer 407 nanoparticles, was tested on its efficiency in clearing the biofilm. Note that the nanotechnology used here for the treatment of the fungal biofilm could be altered to any existing models. Using as an example here, one of our established shellac nanocarrier systems for antifungal therapy that has lysozyme as the enzymatic component of its surface and Fluconazole as the part of its payload is used.

In this study, two primary goals were addressed: (i) To investigate the feasibility of infecting 3D urinary cells with fungal infection. (ii) To determine whether selected nanotechnology works effectively in clearing fungi from 3D urinary cell layers. Using the current *in vitro* models to simulate urinary track biofilm infection provides an exciting opportunity to advance the state-of-the-art. A variety of nanotechnology applications could be developed using the tested nano formulation.

Future clinical studies could make use of such a nano formulation, which has the potential to clean fungal biofilms from the walls of the bladder and urethra. Using a catheter system to deliver the dual functionalised nano formulation into the bladder through the urethra, biofilms on the urothelium may possibly be clinically targeted, where then, after clearing the infection, the formulation could naturally be excreted through the urinary tract of the patient. By examining its efficacy and examining its biocompatibility with cells of the urothelium in 3D urinary cell models, this nanotechnology could ease the treatment of persistent fungal biofilm infections.

6.3 Materials and Methods

6.3.1 Materials

Shellac aqua solution (25 wt% aqueous suspensions) was sourced from SSB® AquaGold. The fungal species *Candida albicans* (Robin) Berkhout (ATCC MYA-2876) was obtained from ATCC. Poloxamer 407 (P407, analytic grade) and lysozyme powder (from hen egg white), poly-L-lysine, and sodium alginate were obtained from Sigma-Aldrich, UK. Whey protein was a gift from No 1 Supplements, Suffolk, UK. Dulbecco's Modified Eagle Medium, Corning® Transwell® polyester membrane cell culture inserts (96 microwell plates), 0.25 % trypsin-EDTA solutions, and NUNC Cell culture 6-well plates were bought from Thermo Fisher Scientific (UK). The RPMI 1604 medium (BE12-702F) supplemented with L-Glutamine for fungal cell culture was sourced from Lonza, Basel, Switzerland. Dextran (MW 500 kDa) and PEO (MW 200 kDa) were purchased from Alfa Saer, UK. Mueller-Hilton Broth (MHB), Mueller-Hilton Agar (MHA) were sourced from Oxford, UK. 10 %v/v Foetal bovine serum was from Labtech, Heathfield UK MTT kit was bought from Millipore Corp, U.S.A. Deionized water purified by the MilliQ water system (Millipore) was used in all experiments.

6.3.2 Method

6.3.3 ECV 304 monolayer cell culture

The ECV 304 cell line is derived from human urinary bladder carcinoma which also represents many features of endothelial cells. This unique feature made them a valuable model for the study of cellular processes in the urothelium/bladder cells behaviours and the cell-cell interactions. The dual cell characteristics combined with a fast proliferation rate also makes this cell line an ideal *in vitro* model for biofilm infection testing, as described below. The ECV 304 cell line was sourced from ECACC cell collection and was cultured in DMEM mediums supplemented with 10 % Foetal Bovine Serum (FBS) sources from Labtech, UK. The ECV 304 cells were incubated in T75 easYFlask (Fisher, UK) at 37 ^{o}C with 5 % CO_2 before the confluency reached 80 %. The medium was discarded, and the cells were rinsed with

phosphate buffer saline (PBS, Lonza, UK) twice to remove the excessive medium. The cells were passaged 1:8 using 0.25 wt% trypsin solution. The trypsinization was neutralized by adding a complete DMEM medium, and the cells were collected by centrifugation at 400 × g for 4 min.

6.3.3.1 Production of a 3D layer of ECV 304 cell clusteroids

The protocol of producing ECV 304 3D clusteroids was retouched from the method introduced by Das et. al.[36] Briefly, the protocol is based on an ATPS, water-in-water Pickering emulsion. 22 g PEO and 11 g dextran powders were suspended in 50 mL deionized water followed by autoclaving (121 ^{o}C , 15 min) to obtain 22 wt% PEO and 11 wt% DEX sterile solution. The 11 wt% PEO was blended with an equal volume of heat-treated whey protein particle (WPP) suspenion[36,37] before mixing with DMEM complete medium at a ratio of 1:1 to obtain 5.5 wt% PEO/DMEM/WPP solution. Similarly, a 5.5 wt% DEX solution was obtained in DMEM. The dextran phase (DEX) was used as the dispersed phase where the ECV 304 cells were initially affiliated to and altered to a fixed cell concentration (1×10^{6}/mL). The DEX and PEO phases were gently emulsified using a BD Plastipak™ syringe fitted with a BD Microlance™ 12 needle (21G 12, internal diameter 0.512 mm, BD biosciences, Wokingham, UK) by 6 pumps. After the DEX/PEO w/w Pickering emulsion was fabricated, the affiliation of the cells to the DEX phase would facilitate their encapsulation in the DEX droplets. The cells were compressed to form cell clusteroids by adding PEO/DMEM solution with a higher concentration (11 wt%) to a final PEO concentration of 8 wt%. This causes a transfer of water from the DEX drops to the continuous PEO phase which shrinks the DEX drops along with the encapsulated cells. The w/w Pickering emulsions were incubated overnight to generate clusteroids by increased cell-cell interactions. The emulsions were diluted tenfold with a DMEM complete medium to enable the emulsion to break down and to allow sedimentation of the clusteroids by gravity. The clusteroids were then taken out and transferred to poly-L-lysine coated 6 well plates to produce a 3D layer of ECV 304 cell clusteroids. The culture was incubated with complete media at 37^{o}C with 5% CO_2.

6.3.3.2 Preparation of *C. albicans* biofilm infected ECV 304 3D cell platform

A single colony of *C. albicans* was collected with a plastic loop and seeded in a 10 mL Yeast Extract–Peptone–Dextrose (YPD) medium (Sigma-Aldrich, UK). The *C. albicans*-YPD suspension was incubated at 37^{o}C for 12 h with stirring at 150 RPM. The overnight culture (O/N) was centrifugated at 1000×g for 5 min. The cells pellet was rinsed twice with sterile PBS solution to remove excess YPD medium before the *C. albicans* were reseeded in RPMI medium supplemented with 1 % L-glutamine. The fungal cell concentration was adjusted to 1×10^{5}/mL by series of dilutions using RPMI medium since this is the optimal condition for the formation of *C. albicans* biofilm. To monitor the spread of fungal infection, the *C. albicans* cells were stained using carboxyfluorescein succinimidyl ester (CFSE), which is a multi-generational dye that binds to lysine residues and other amine sources.[55] The CFSE has been employed to generationally track the bacterial proliferation over discrete cycles.[56] Extended research has demonstrate that the CFSE was capable to monitor the bacterial/human cell interaction.[57]CFSE shows green signals under confocal microscopy or fluorescence microscopy set at the FITC channel (494 nm). The protocol for staining the fungal cells is given below. Briefly, a 10 mL aliquot of the *C. albicans* suspension with a fixed cell concentration of 1 x 10^{5}/mL was pelleted by centrifugation at 4000 x g.

The sediment was rinsed twice with sterilized PBS solution and resuspended in 2 × CFSE working solution (20 μg CFSE in 10 ml PBS). The working suspension of *C. albicans* (labelled with CFSE or unlabeled) with optimal cell density was seeded to the formed 3D ECV304 cell clusteroids layer growing on the bottom of six well plates. Briefly, 20 μL of the *C. albicans* working suspension was added to each well. To allow the proliferating of the clusteroids, 200 μL DMEM complete medium was also

pipetted into the wells. The plates were incubated *at* 37ºC for 12 h to generate biofilm on the clusteroids layer. After the allotted time, the medium was discarded by gentle pipetting, and the clusteroids infected by biofilm adhered to the wells were rinsed two times with sterilized PBS solution. DMEM medium was used for the cell culture and RPMI medium for fungal cell culture.

6.3.3.3 Preparation of Fluconazole-loaded P407-stabilised shellac NPs

To prepare the NPs suspension, 200 µL of 25 wt% ammonium shellac solution (Aqua Gold) was diluted to 50 mL using deionized water to get 0.2 wt% ammonium shellac solution. Then 0.125 g of P407 and 0.01 g Fluconazole were added to the 0.2 wt% shellac solution followed by dropwise addition of 0.25M NaOH to change the pH to 10. This was followed by 30 min sonication using an ultrasonic bath (Ultrawave, U.K.) at 40 % of the maximum power of 200 at 25ºC and 30 min of magnetic stirring were conducted to solubilize the p407 and Fluconazole. The pH was then adjusted to 5.5 using 0.25M HCl solution to precipitate the individual components to shellac NPs. The final concentration of the 1 × stock NPs formulation is 0.02 wt% Fluconazole-loaded 0.2 wt% Shellac NP sterically stabilized with 0.25 wt% P407.

6.3.3.4 Coating of the Fluconazole-Loaded Shellac NPs with Lysozyme.

To functionalize the shellac nanoparticles with a cationic surface functionality, 0.125 g of lysozyme powder was added to the 0.02 wt% Fluconazole-loaded 0.2 wt% Shellac NPs stabilized with 0.25 wt% P407 with agitation. The solution was sonicated for 15 min to avoid aggregation. The Lysozyme exhibits a very high positive charge at pH 5.5 and charge-reverse the originally anionic shellac NPs into cationic surface functionality by electrostatic binding. The Lysozyme-coated shellac NPs were collected by centrifugation at 8000×g for 30 min. The pelleted NPs were then resuspended in 50 mL deionized water to reach a final concentration of 0.02 wt% Fluconazole-loaded 0.2 wt% Shellac NPs stabilized by 0.25 wt% P407 and coated with 0.2 wt% Lysozyme.

6.3.3.5 Bright field, fluorescence, and Confocal microscopy observations

The micro-structure of the individual clusteroids and the proliferation of the clusteroids collected from the DEX/PEO emulsion template were imaged with bright field optical microscopy supplemented with fluorescence microscopy (Olympus BX-51). 20 μL of the sample was carefully pipetted onto a concave slide at room temperature under various immersion objectives. To visualize the clusteroids, 4′,6-diamidino-2-phenylindole (DAPI) was used as the fluorescence dye on the clusteroids before the clusteroids were observed. For tracking of the long-term proliferation of the clusteroids or the *C. albicans,* CFSE was used which would permeate into cells and bind to their interior by the succinimidyl group. The fungal and ECV 304 cells were pre-stained prior to the biofilm formation. For selective experiments, the clusteroids was stained by CellTracker Green CMFDA (5-chloromethylfluorescein diacetate) and the *C. albicans* were stained with CFSE to allow monitoring over longer periods by fluorescence microscopy. The observation of the *C. albicans* biofilms and the 3D clusteroids co-culture model was carried out using Confocal Laser canning microscope (CLSM, Zeiss LSM710). Z-stacking images were taken to generate a 3D view of the biofilms on the clusteroids model, which composed 100 slices with 2 μm per slice. Two channels, 461 nm (DAPI) and 488 nm (FITC) were set at precise mode to avoid signal interference of the fluorescence signal within the stained ECV 304 cell clusteroids and *C. albicans biofilm*.

6.3.3.6 Biofilm clearance efficiency after the NPs treatment

After the biofilm-infected ECV 304 *in vitro* 3D model was obtained by the method mentioned above, the culture was firstly rinsed with PBS twice to remove any remaining planktonic fungal cells. The 1 × standard stock solution was 0.02 wt% Fluconazole-loaded 0.2 wt% Shellac NP sterically-stabilized with 0.25 wt% P407. 100 μL of 1 ×, 2 ×, 3 × and 4 × stock suspensions were added separately to clusteroids/biofilm co-cultures and 100 μL of DMEM complete medium was

supplemented to keep the cells proliferating. 0.1 mL of PBS with 0.2 mL DMEM complete medium was added to a well as control. The antibiofilm properties of the individual components of the NPs were also tested to prove the efficiency of the nanostructure. 100 µL of the prepared solutions of different individual components with an equal concentration in the NPs were also added into different well plates contained the biofilm/ECV 304 clusteroids co-cultures.

After 24 hrs of treatment, the media was discarded, and the cultures were collected and shaken for 30 secs with glass beads to release the fungal cells from the biofilm. The samples were then transferred to test tubes with 100 µL of fresh Mueller Hinton broth (MHB). Each example was vortexed for 30 secs to disassociate the biofilm and inoculate the MHB with fungal cells. The drop plate count technique was utilized to quantify cell colony-forming unit (CFU)/mL. To enumerate the fungal cell viability inside the biofilms, 10 × dilutions were made in MHB, 10 µL solutions were transferred onto MHA plates and left growing for 24 hours at 37^{o}C. CFUs were checked from the last two droplets, which contained a countable number of C.F.U. (3 to 30 counts for every 10 µL drop) and calculated as average. Compared to the conventional CFU assay, the drop plate count technique (10 ul drop) allows us to more accurately and faster count the visible colony by distributing the samples in drops.[54]

6.3.3.7 Characterization of Free Lysozyme, Lysozyme-coated shellac NPs, and Lysozyme-Coated Fluconazole-Loaded shellac NPs

Malvern Zetasizer Nano ZS was used to measure the zeta potential and particle size of the modified shellac NPs. The refractive index (RI) was set to 1.512, which is the RI of shellac. 1 mL of the samples was added to a quartz cuvette and tested three times at 25^{o}C. The data was collected as a mean of three separate tests.

6.3.3.8 Preparation of the Fluconazole-loaded Shellac NPs and encapsulation efficiency test

The encapsulation of the antifungal agent, Fluconazole, was achieved by pH drop. The mixture of 0.2 wt% shellac, 0.25 wt% P407, and 0.02 wt% Fluconazole was fully soluble at pH 10 after sonication. The NPs precipitated after the pH was lowered to 4, which intercalated the Fluconazole inside their shellac cores. The NPs were collected by centrifugation and used as 1 × stock nanosuspension. The encapsulation efficiency of the NPs was detected by a UV-visible spectrometer at 260 nm as a function of time and pH. The pH of the stock 1 × nanosuspension was changed by dropwise addition of 0.25M HCl and 0.25M NaOH, and then the solution was pelletized to collect the supernatant for encapsulation test. The remaining Fluconazole in the supernatant was regarded as nonencapsulated.

6.3.3.9 Cytotoxicity test of the NPs treatment using MTT assay

The cytotoxicity of the NPs treatment on the ECV 304 cell clusteroids is a key feature in evaluating their potential to be used in clinical applications. An MTT assay was used to test the ECV 304 cell viability after the clusteroids were exposed to the NPs treatment. The MTT is a colorimetric assay for evaluating the cell metabolic activity. Nicotinamide adenine dinucleotide phosphate (NADPH)-dependent cellular oxidoreductase enzymes may, under defined conditions, reflect the number of viable cells present. These enzymes can reduce the tetrazolium dye 3-(4,5-dimethylthiazol-2-yl)-2,5-diphenyltetrazolium bromide to its insoluble formazan, which has a purple colour. 20 μL of Compound 1 was added to each microwell contained ECV 304 cells clusteroids with an initial cell number of about 5×10^5 supplemented with 100 μL DMEM complete medium, after 1 h and 24 h of cell incubation at 37^o C with 5% CO_2, respectively. The Compound 1 was incubated with the cells for 30 min before removing the medium and adding 50 μL isopropanol. The microwell plates were then incubated for another 30 min and the then their absorbance at a wavelength of 490 nm was read into a microplate reader (BioTek Synergy HT).

6.3.3.10 SEM Imaging of shellac NPs, ECV 304 cells, and *C. albicans* biofilms on the ECV 304 3D clusteroirds layer

A sample of the stock formulation of 0.02 wt% Fluconazole-loaded 0.2 wt% Shellac NPs stabilized by 0.25 wt% P407 and coated with 0.2 wt% Lysozyme was left to air dry before they were coated with gold for imaging. ECV 304 cells, *C. albicans* biofilm infected clusteroids, and NPs treated clusteroids/biofilm co-culture were gently collected from the well plate using a sterilized loop and shifted to glass slides. The cultures were fixed with 1 wt% glutaraldehyde in PBS buffer solution for 1 h at 25^{o}C. The cultures were then rinsed three times with deionized water to wash away the excess of glutaraldehyde. Post-treatment, the 3D clusteroids were gently removed from the plate using a sterilised loop and placed onto a 7 mm diameter circular glass slide and adhered to carbon discs.

The biofilm was gently washed with deionized water to remove excess media and treatment. The biofilms were then fixed in a 1 wt% glutaraldehyde in PBS buffer solution for 1 h at room temperature. After fixation, the biofilms were washed 3 times with deionized water to remove excess glutaraldehyde. Samples were imaged with Zeiss smart SEM software (Zeiss Evo-60 S.E.M., Germany). The SEM images were processed with psuedo colour to distinguish cells from biofilms (yellow colour for cells, green for *C. albicans* biofilm).

6.3.3.11 Cryostat sectioning

For the characterisation of the fungal infection inside the clusteroids layer, the *C. albicans* infected layer of ECV 304 clusteroids culture was detached from the microwell plate by a sterilized loop and placed on a filter paper. The culture was then frozen in optimal cutting temperature compound overnight before cryostat sectioning. A Leica CM1950 was used to create slices with a thickness of 10 μm, and the slice in the central region was collected and moved on to the glass slide. An Olympus BX51 fluorescence microscope was used to visualize the sectioned slice.

6.4 Results and discussion

6.4.1 Preparation of ECV304 clusteroids and 3D clusteroids layer

After the ECV 304 cells had been grown in the 2D monolayer culture for 80% confluency, they were harvested and then moved to the Pickering emulsion template of DEX/PEO w/w whey protein particles stabilized by 2 weight percent whey protein. A PEO solution at a higher concentration was added to the droplets in order to compact the cells. As the cells shrink, the adhesion between them increases, resulting in clusteroids being formed (**Figure 6.2**). A significant fact that we have discussed in our previous work is the importance of the concentration of PEO/DEX and the shrinking process to the formation of clusteroids. As shown in **Figure 6.3**, clusteroids were diluted with 10 folds PBS to allow cellular interaction and adhesion for 12 h, and then collected by dilution with Pickering emulsion. As can be seen in **Figure 6.4**, a typical ECV 304 clusteroids are collected from a w/w emulsion that contains ECV 304 particles. In order to examine the microstructure of ECV 304 cells within clusteroids, SEM images were compared between individual ECV 304 cells and clusteroids of ECV 304 cells (**Figure 6.4**A, B). Clusteroids were preliminarily assessed for their integrity and viability using DAPI and FDA stainings. **Figure 6.5** shows that the ATPS-based production process had no detrimental effect on the viability of the cells in clusteroids. Clusteroids were collected as a fixed quantity of cells (1×10^5 per mL) and were then placed into poly-L-lysine-coated 96-well microwell plates. A clusteroids layer forms on the bottom of the wells upon the application of this substrate. By using FDA cell labeling, which is a generational dye used to identify living cells, the clusteroids' growth was continuously monitored. **Figure 6.6** shows an example of a 3D clusteroids layer which has developed within the bladder inner urothelium over the course of seven days. From these observations, it can be concluded that the clusteroids would proliferate rapidly and fuse into a dense 3D clusteroids layer within seven days, thus functioning as a proxy for the bladder inner urothelium. As the clusteroids grew, they eventually filled the space between themselves, and then they began to fuse together into a tissue-like layer of cells that was compacted into a 3D structure. The fusion of the clusteroids was shown in **Figure**

6.7. The results of these experiments indicate that our sheet-form Pickering emulsion template, w/w, would be an ideal platform for preparing a realistic *in-vitro* environment that can be tested more extensively after treatment with biofilms and after infection with biofilms, as its process could be very fast and easy.

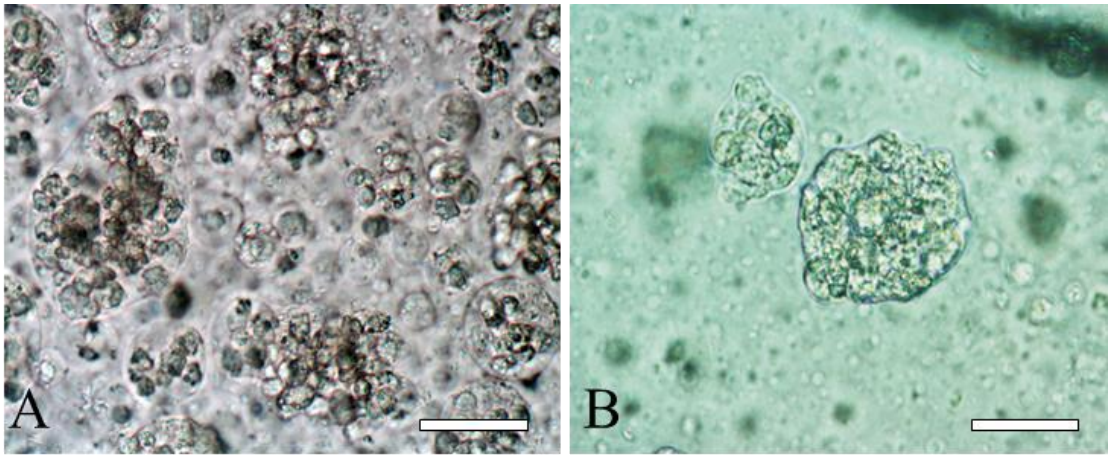

Figure 6.2. Microscopy observation of the clusteroids encapsulated in the 5.5 wt% DEX/5.5 wt% PEO w/w Pickering emulsion before (A) and after (B) shrinking with more concentrated (11 wt%) PEO solution. The bar is 50 μm.

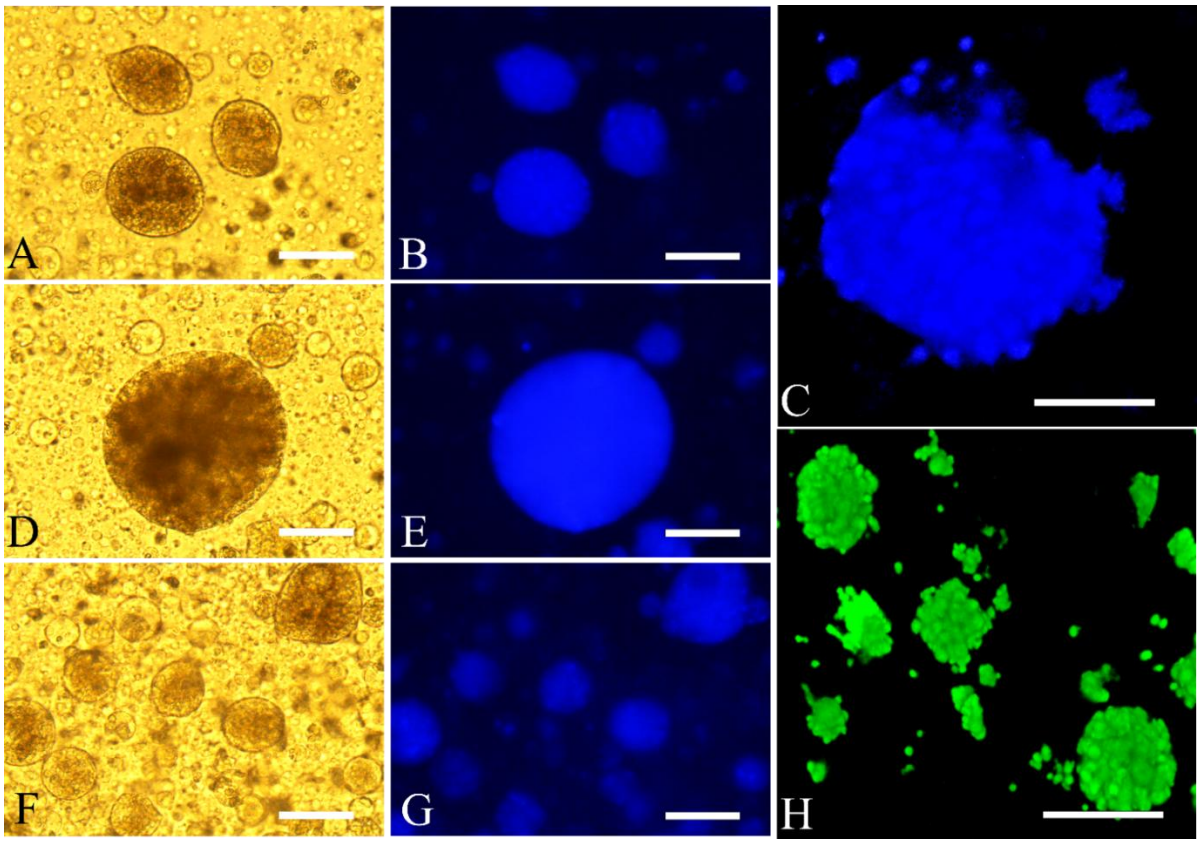

Figure 6.3 Optical brightfield microscopy images (A, D, F), fluorescence microscopy images (B, E, G, C), and confocal laser scanning microscope observation (E) of the individual ECV 304 cell clusteroids encapsulated in the w/w Pickering emulsions (5.5 wt % DEX,5.5 wt% PEO).[36,37] The clusteroids were stained with DAPI (B, E, G, C) or FDA live/dead assay (H). The bar is 50 μm for (A, B, D, E), 100 μm for (F, G), 50 μm for (C) and 200 μm for (H). The fluorescence intensity was measure by ZEN software (Blue edition).

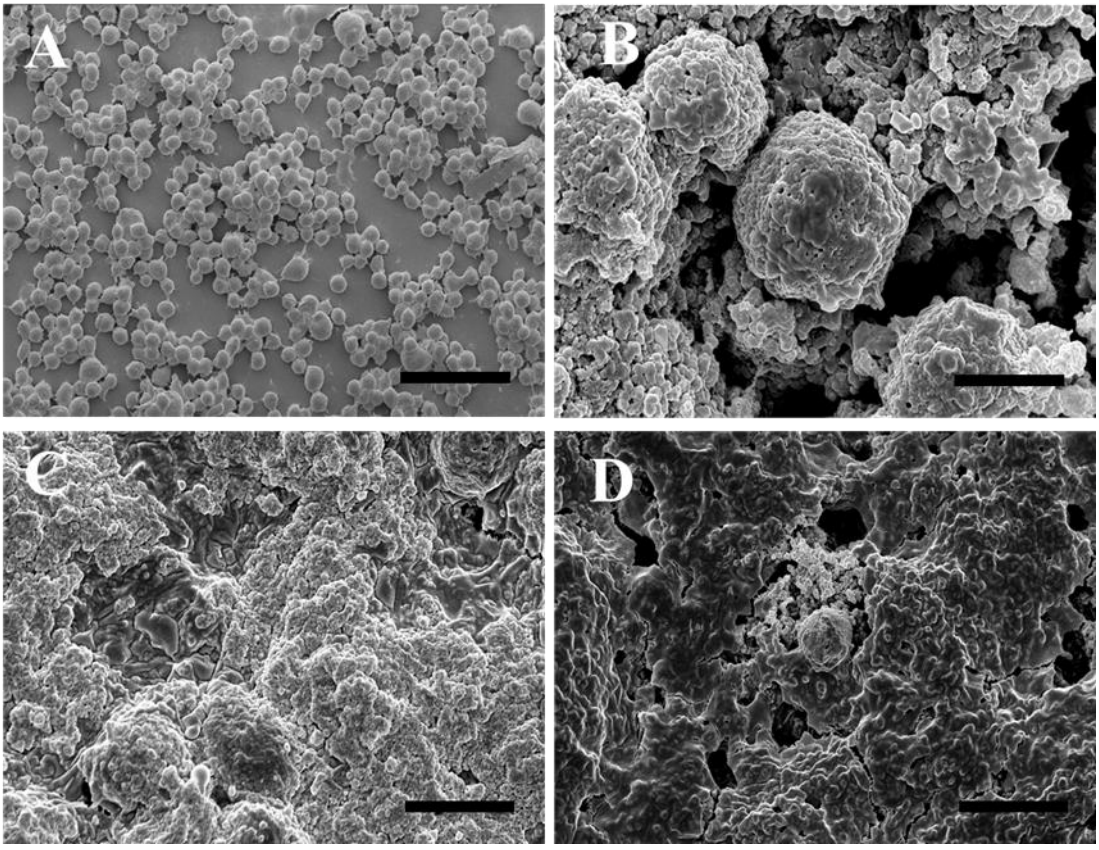

Figure 6.4. Original SEM observation of (A) individual ECV 304 cell layer without any fungal infection or treatment by 4 × Shellac-Fluconazole-Lysozyme NPs stock solution. (B) Individual ECV 304 clusteroids layer without any fungal infection or Shellac-Fluconazole NPs treatment. (C) ECV 304 clusteroid layer infected with a *C. albicans* biofilm. D: ECV 304 clusteroid layer infected with *C. albicans* biofilm imposed by the treatment of 4 × Shellac-Fluconazole NPs stock solution. The bar is 100 μm for (A, B, C,) and 200 μm for (D). The 1 × stock suspension of the Shellac-Fluconazole-Lysozyme NPs is 0.2 wt% Shellac, 0.25 wt% P407, 0.2 wt% Lysozyme

and 0.02 wt% Fluconazole. The cell concentration used in the experiments was 1×10^5/mL.

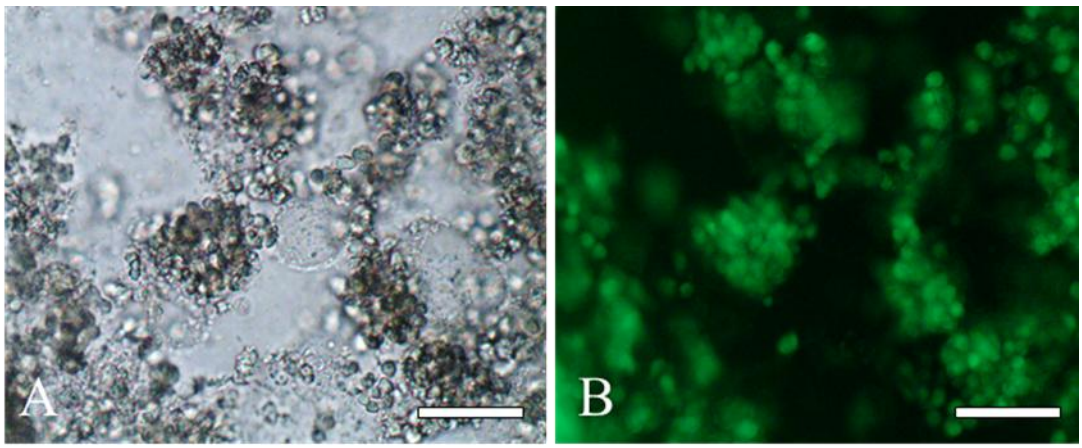

Figure 6.5. Collected clusteroids (A) by diluting the w/w Pickering emulsion template with FDA staining (B) showing the viability of the clusteroids. The bar is 50 μm.

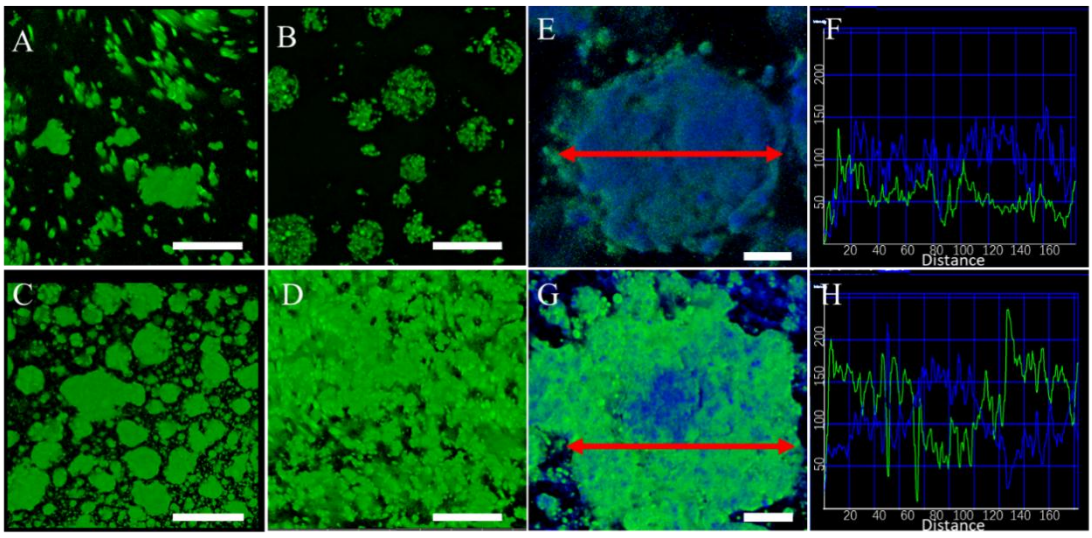

Figure 6.6 CLSM images of the proliferation of clusteroids layer at different days of culture: (A): day 1: (B): day 3; (C): day 5; (D): day 7. The initial cell number was normalized to 1 × 10^6 cells/mL. Zeiss LSM750 fluorescence microscope was employed to capture the images. The bar is 100 μm Confocal laser scanning

microscope observation of individual ECV 304 clusteroids infected by *C. albicans* after E:1 h and G:24 h. TheF and H show the fluorescence intensity of A and C, respectively. The bar is 50 μm. The red arrows indicate where the fluorescence intensity was measured. This concentration is treated as 1×stock suspension. To get more concentrated 2 ×, 3 × or 4 × suspension, the pelletized NPs were diluted in 25 mL, 16.7 mL, and 12.5 mL of deionized water, respectively.

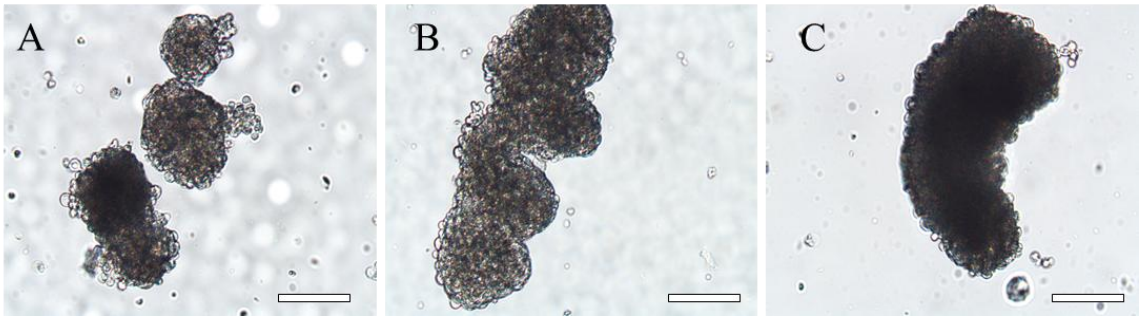

Figure 6.7. Microscopy observation showing the ECV304 clusteroids fusion progress on day 3 (A),5 (B),7 (C). The bar is 100 μm

6.4.2 Fluconazole-loaded Shellac NPs' encapsulation efficiency

A shellac core and P407 NP design is used in the present study. It has been reported that Al-Obaidy et al. and Weldrick et al. investigated the fabrication of the current NPs. [46,47],[29]

We determined that pH 5.5 is the ideal precipitation condition for shellac nanoparticles, which was used in our subsequent experiments. In this paper, the primary purpose of the research is to determine whether or not it is possible to test antimicrobial nanotherapeutics on biofilm-infected 3D urothelial cells, which were tested for their ability to act as nanocarriers for antifungal agents, using the current work as a platform for pre-clinical screenings. It is suitable for the use of these antifungal nanotherapeutics with a range of antimicrobial agents.

Fig 6.8 shows the average hydrodynamic diameter and zeta-potential analysis of the shellac nanoparticles which were produced as a result of using fluconazole as a nitrate at pH 5.5 and benthic acid as a reducing agent. Nanoparticle hydrodynamic

diameter was only marginally affected by fluconazole concentration increases, ranging from 68 nm to 79 nm.

An acidic pH drop was used to encapsulate Fluconazole, the antifungal agent. After sonication, a mixture containing 0.2 weight percent shellac, 0.25 weight percent P407, and 0.02 weight percent fluconazole was completely soluble at pH 10. Fluconazole was intercalated inside the shellac cores of the NPs after the pH was lowered to 4. By centrifuging the NPs, we were able to collect 1 x stock nanosuspension of the NPs. NP encapsulation efficiency was determined using a UV-visible spectrophotometer at 260 nm in response to pH and time. For the encapsulation test, the pH of the stock nanosuspension was changed by the addition of 0.25M HCl and 0.25M NaOH dropwise. The supernatant collection was then performed using a pelletizer to collect the supernatant. It was determined that Fluconazole that was not encapsulated remained in the supernatant.

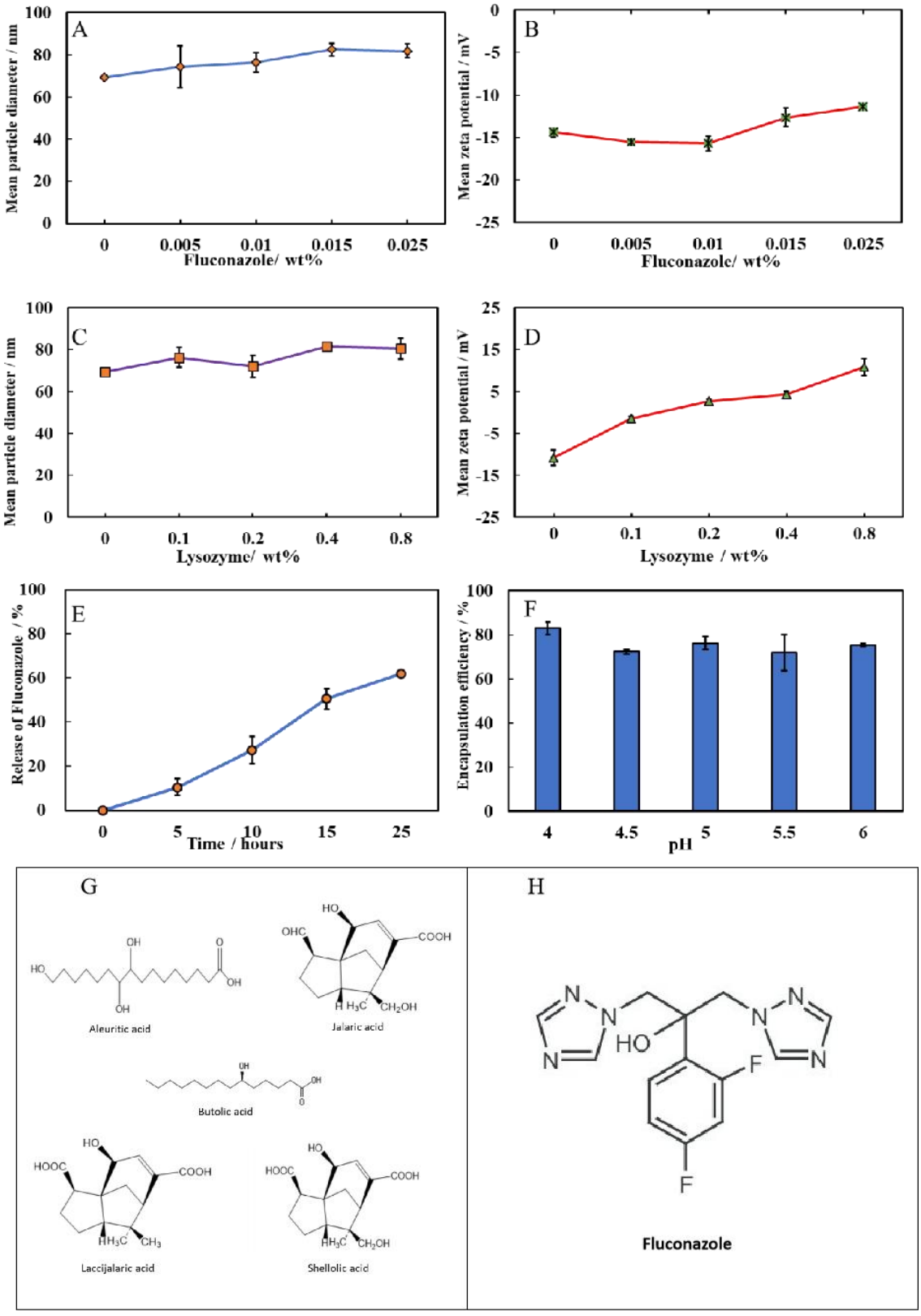

Figure 6.8. (A) Mean particle diameter of 0.2 wt% Shellac-0.25 wt% P407-Fluconazole nanoparticles measured at pH 5.5 (acetate buffered saline) with various concentrations of Fluconazole. (B) Mean particle zeta potential of 0.2 wt% Shellac-

0.25 wt% P407-Fluconazole nanoparticles versus the Fluconazole concentration. (C) Mean particle diameter vs. Lysozyme concentration of the 0.2 wt% Shellac-0.25 wt% P407-0.02 wt% Fluconazole-Lysozyme nanoparticles measured using a Malvern Zetasizer Nano ZS at 25 °C. Each value represents a triple replicate with ±S.D. (D) ζ-potential of 0.2 wt% Shella-0.25 wt% P407-0.02 wt% Fluconazole-Lysozyme nanoparticles immobilized with different concentrations of the Lysozyme at pH 5.5 (adjusted with acetate buffered saline) measured immediately after preparation. (E) Release of Fluconazole from 0.02 wt% Fluconazole-loaded 0.2 wt% Shellac NPs stabilized by 0.25 wt% P407 and coated with 0.2 wt% Lysozyme at different time points. (F) Encapsulation efficiency of 0.02 wt% Fluconazole-loaded 0.2 wt% Shellac NPs stabilized by 0.25 wt% P407 and coated with 0.2 wt% Lysozyme nanoparticles. The encapsulation efficiency was tested immediately after the NPs were prepared using a UV-Vis spectrum. (G)The chemical structures of the main components of shellac (59). Aleuritic acid, Jalaric acid, Butolic acid, Laccijalaric acid and Shellolic acid.(H)The chmical structure of fluoconazole.

Figure 6.8F illustrates that the pH of the aqueous solution had only a marginal effect on the encapsulation efficiency of Fluconazole, as can be seen here. The encapsulation efficiency for all set groups exceeded 70%. In order to determine the release kinetics of Fluconazole from NPs 1 x stock suspension at pH 5.5 as time progressed, it was measured how fast the NPs discharged the drug. Fluconazole released approximately 50 percent of its active ingredient after 15 hours, and approximately 70 percent after 25 hours. It is ideal to treat biofilms using these release kinetics. The formation of the nanoparticles were observed using TEM**(Figure 6.4(9))**

As shown in **Figure 6. 8B**, the hydrodynamic diameters and zeta-potentials of the shellac nanoparticles produced by fluconazole at pH 5.5 as a function of Fluconazole concentration showed a good correlation with the fluconazole concentrations. **Figure 6. 8A** shows that the concentration of Fluconazole had only a

very minor effect on the average diameter of the nanoparticle, which ranged from 68 nm to 79 nm as a result of the increase in concentration of Fluconazole.

Shellac consists of polyesters of mainly aleuritic acid, shellolic acid, and a small amount of free aliphatic acids (Figure 6.8G).[59] The composition varies depending on the insect species as well as the host tree from which the raw material is obtained. The main composition of shellac gives it an acidic nature. Fluconazole is an antifungal agent that is efficacious in the treatment of fungal peritonitis. Fluconazole has an excessive carboxyl group, which gives him a basic alkaline nature (Figure 6.8H). The difference in chemical structure between shellac and fluconazaole would cause them to bind electrostatically since they would be reversibly charged at a neutral pH. As Fluconazole encapsulation efficiency was only slightly affected by pH, as shown in **Figure 6.8E**. Encapsulation efficiency was greater than 70% for all set groups. This study was conducted at pH 5.5 to determine the release kinetics of the fluconazole from the stock suspension of 1 x NPs and to measure it as a function of time. Based on **Figure 6.8F**, Fluconazole released approximately 50 percent after 15 hours and approximately 70 percent after 25 hours. It is ideal to treat biofilms using these release kinetics. The results from the Malvern Zetasizer were correlated with those from the SEM on size of the nanoparticles (**Figure 6.9**). It is estimated that the nanoparticles had a spherical shape and measured 60-90 nm in size. It was found that fluconazole had a moderate effect on the zeta potential, with variations of less than 30%. All the groups of the set were found to be negatively charged due to the residual amounts of -COOH groups that were present in the shellac components (shelloic acids).

6.4.3 *C. albicans* infection and formation of biofilm on top of the ECV 304 3D clusteroids layer

We simulated bladder inner urothelial wall to determine the formation of biofilm. Implanted devices and substrate surfaces, including tissues and implanted devices, have been well studied and know how biofilms are formed.[39-45] As demonstrated in

our previous studies, *S. aureus* and *P. aeruginosa* forms biofilms on keratinocyte clusteroids.[27] To the best of our knowledge, no research has been done on the formation of biofilms in an *in-vitro* bladder wall model. Confocal microscopy observations were carried out to ascertain whether *C. albicans* was capable of embedding on the 3D clusteroids layer model after being infected with a biofilm (**Figure 6.6E-H**). After one hour of incubation, the fungal cells proliferated and encompassed the ECV 304 clusteroids. **Figure 6.6E,G** illustrates clearly the infiltration of the fungal cells into individual cell clusteroids.

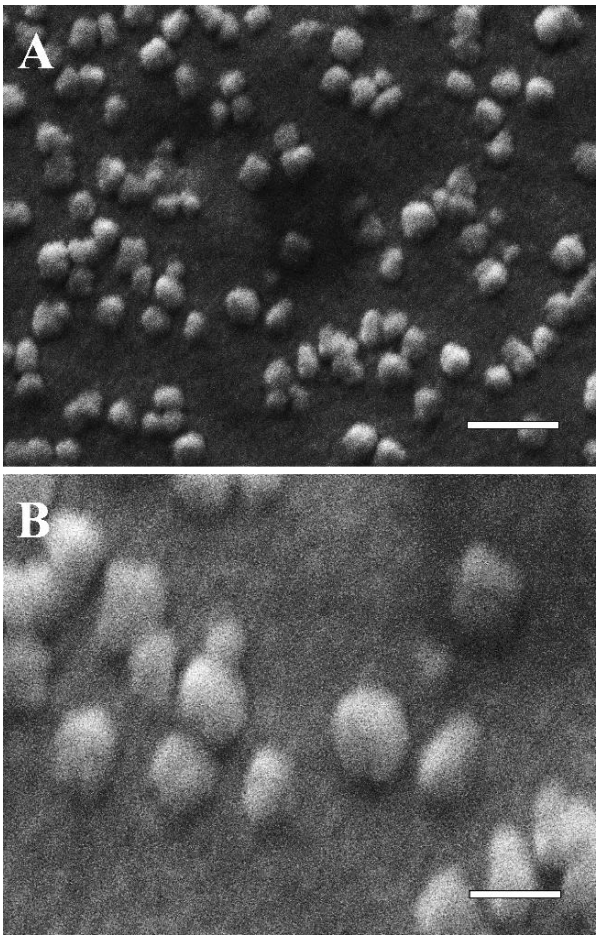

Figure 6.9. SEM observation of 0.25 wt% P407-stabilized 0.02 wt% Fluconazole-loaded 0.2 wt% Lysozyme coated 0.2 wt% shellac nanoparticles. The bar is 500 nm for (A) and 100 nm for (B).

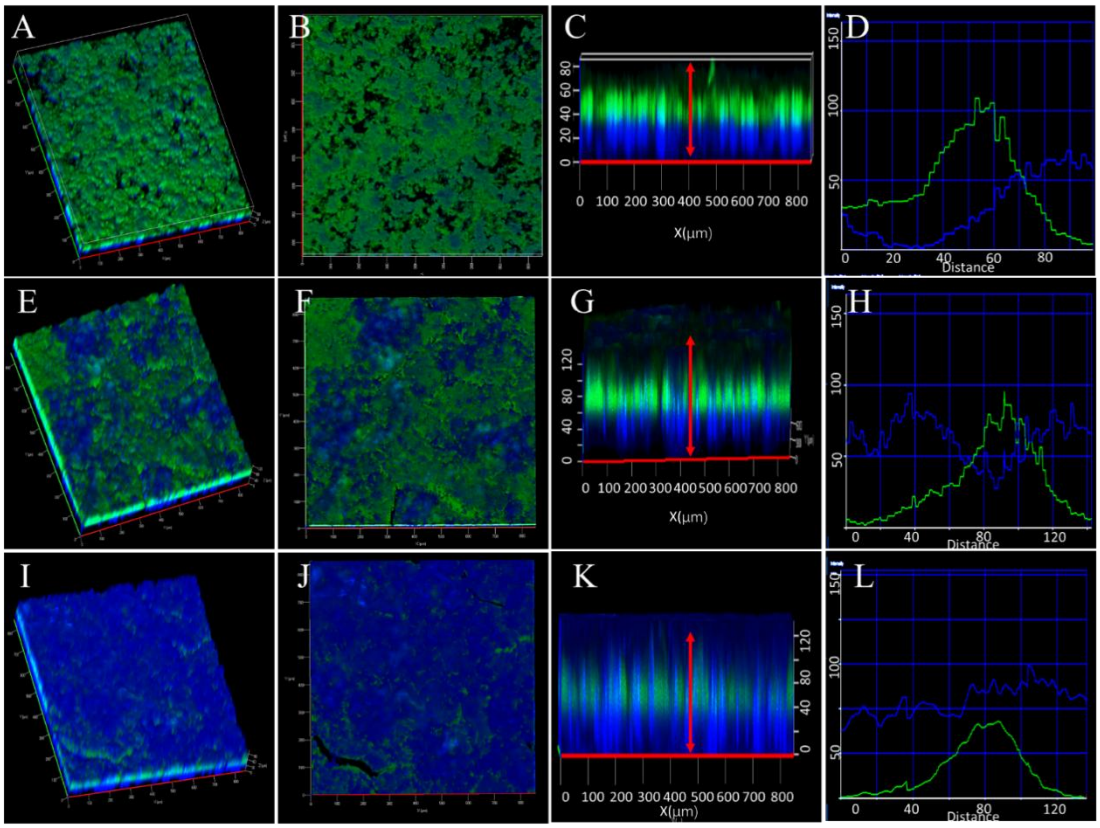

Figure 6.10. Confocal laser scanning microscope observation of biofilm/ECV 304 clusteroids co-cultures before (A, B, C), after 12 h (E, F, G) and 24 h (I, J, K) the treatment of 4 × stock solution of the NPs. 50 μm for D-J. The fluorescence intensity of **Figures C, G, K** is displayed in **Figures D, H, L**, respectively. The size of the box is 800 μm×800 μm×80 μm (X, Y, Z). The concentration of the 1 × stock solution of NPs is 0.2 wt% Shellac, 0.25 wt% P407, 0.2 wt% Lysozyme and 0.02 wt% Fluconazole. The fluorescence intensity was measure by ZEN software (Blue edition). The red arrows indicate where the fluorescence intensity was measured.

The fluorescence signals were dominated by green FITC channel in the "1 h" and "24 h" groups, indicating that fungal cells had covered the layer of clusteroids and a biofilm had formed. A similar investigation was conducted using CLSM to determine whether *C. albicans* biofilms developed above the 3D clusteroids layer (**Figure 6.10**). As the fluorescence microscopy results indicate, a biofilm has also developed on the clusteroids layer after 24 hours. A SEM examination was conducted on the ECV 304

cells clusteroids in addition to the 3D clusteroids layer to examine the specific morphology of the *C. albicans* biofilm. *C. albicans* cells are normally oval in shape, as stated in **Figures 6.11C and 6.11D**, and they form an aggregated layer on top of the clusteroids on ECV 304, resulting in an oval shape. Cell clusteroids are not disintegrated by the formation of the biofilm, despite being contaminated and floating off the surface when the biofilm forms.

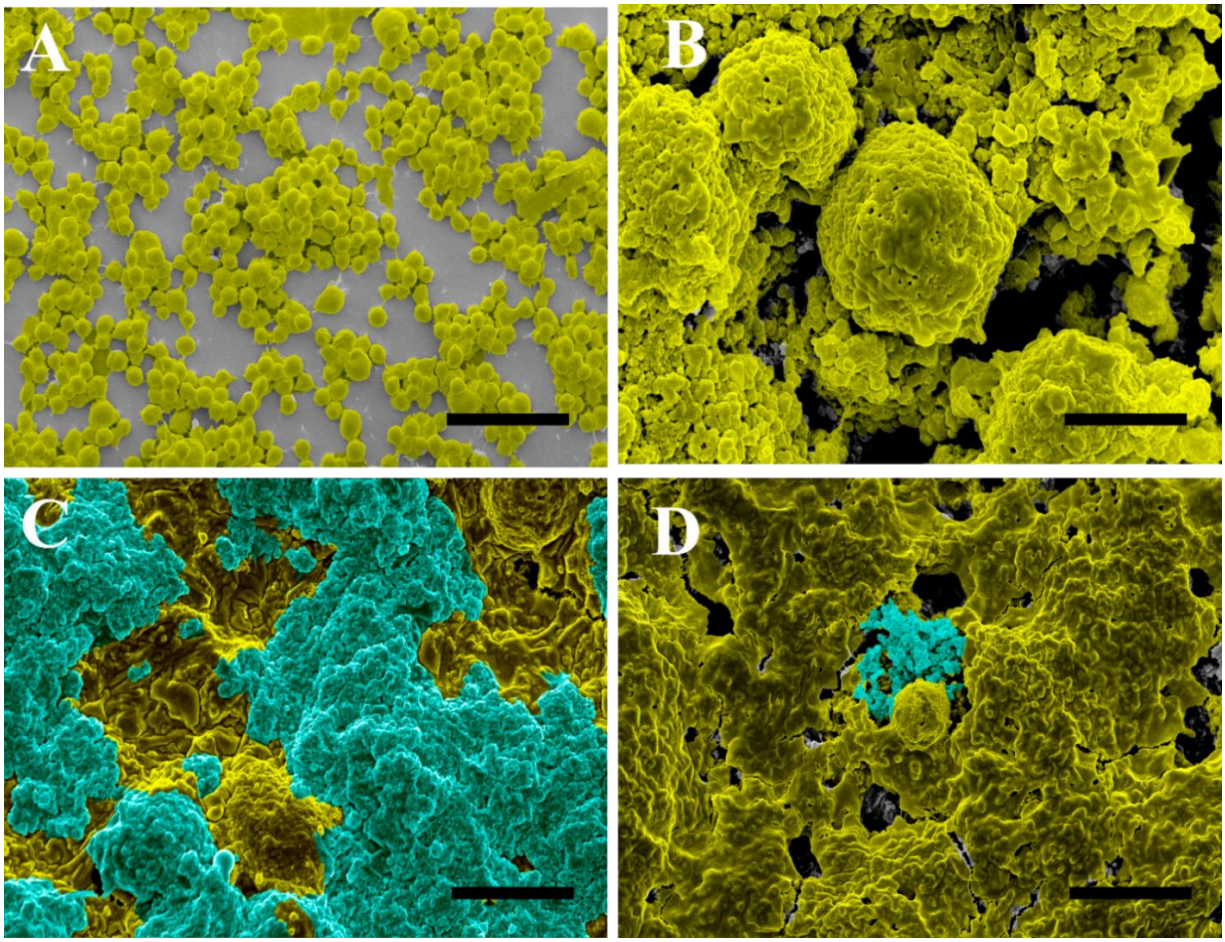

Figure 6. 11. Pseudo colour SEM images of A: a layer of individual ECV 304 cells without any fungal infection or treatment by 4× Lysozyme-coated Fluconazole-loaded Shellac NPs stock solution. B: Individual ECV 304 clusteroids layer without fungal infection or Lysozyme-coated Fluconazole-loaded Shellac NPs treatment. C: ECV 304 clusteroid layer infected with *Candida. albicans* biofilm. D: ECV 304 clusteroid layer infected with *C. albicans* biofilm imposed by the treatment of Lysozyme-coated Fluconazole-loaded Shellac NPs stock formulation. The bar is 100 µm for (A, B, C,) and 200 µm for (D). The 1× stock suspension of the Lysozyme-

coated Fluconazole-loaded Shellac NPs is 0.2 wt% Shellac, 0.25 wt% P407, 0.2 wt% Lysozyme and 0.02 wt% Fluconazole. The cell concentration used in the experiments was 1×10^5/mL. Yellow colour represents the ECV 304 cell clusteroids while green colour represents the *C. albicans* biofilm. The original images of the SEM were provided in **Figure 6.4**.

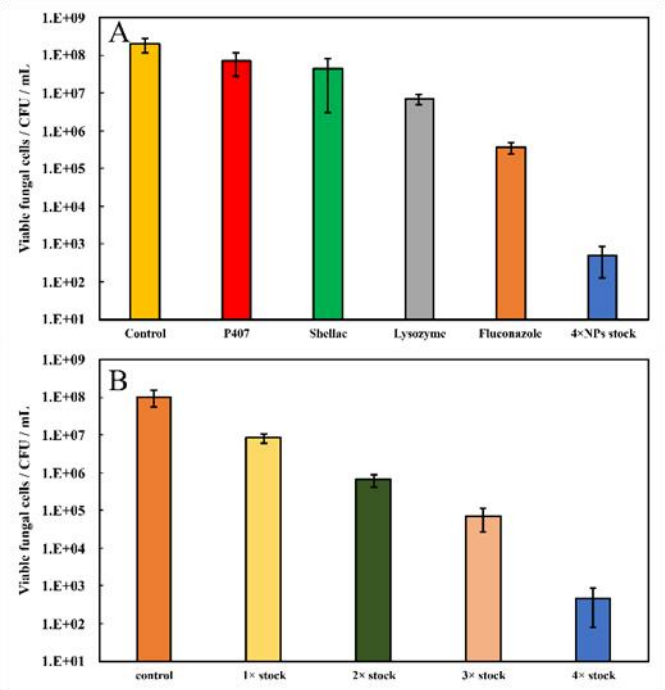

Figure 6.12. A: Efficiency of equivalent Individual components of the 4×stock NPs solution on of the clearance of *C. albicans* biofilm infected on the 3D culture of ECV 304 cell clusteroid layer. The fungal cell numbers were normalized by CFU B: Influence of different concentrations of the Lysozyme-coated Fluconazole-loaded Shellac NPs the on the proliferation of the 3D culture of ECV304 clusteroid layer after 1 h and 48 h culture. The concentration of the 1×standard stock solution is 0.2 wt% Shellac, 0.25 wt% P407, 0.2 wt% Lysozyme and 0.02 wt% Fluconazole.

6.4.4 The efficiency of the lysozyme-coated Fluconazole-loaded NPs treatment for clearance the Candida biofilm on 3D layer of Clusteroids

Here we examined with the antifungal activity of the Lysozyme-coated Shellac nanocarriers of Fluconazole on the biofilm anchored on the 3D layer of urothelial

clusteroids. To determine the efficiency of the biofilm clearance of the NPs, different concentrations of stock solutions were applied on the *C. albicans* biofilm infected 3D layer of ECV 304 cell clusteroids.

The purpose of this study was to determine whether the Lysozyme-coated Shellac nanocarriers of Fluconazole have antifungal activity in the biofilm that is embedded on the 3D layer of urothelial clusteroids that are coated with fluconazole. We applied different concentrations of stock solutions on a 3D layer of ECV 304 cell clusteroids infected with *C. albicans* biofilm to determine the efficiency of the biofilm clearance of the NPs.

As **Figure 6.12A** shows that when the concentration of the nanoparticles was increased to a 4 x stock solution, the high concentrations produced a greater effect on the clearance of the fungus biofilm, achieving a 5 log reduction in viable fungal cells when combined with the 4 x stock solution of the nanoparticles. Low concentrations of nanoparticles were not sufficient to eliminate the entire fungal biofilm. *C. albicans* is intrinsically highly resistant to fluconazole. Separate tests were also conducted on the performance of the individual components of the NPs when used at equivalent concentrations to those in the formulations. The illustration in **Figure 6.12B** demonstrates that Fluconazole is primarily responsible for the antifungal effect. It was also reported that the Lysozyme has contributed to the kill of fungi, as it is capable of catalyzing the hydrolysis of N-acetylmuramic acid and N-acetyl-D-glucosamine residues in peptidoglycans, which are linked by beta-linkages. There was a limited positive effect on the clearance of biofilms from the other components of the NPs.

SEM imaging was employed to examine the microstructure of the fungal biofilm infection on the 3D layer of clusteroids (**Figure 6.11**). The biofilm was manually adjusted to green colour, and the cells were painted yellow. The SEM images clearly shows the morphology of the biofilm stuck on the cell clusteroids layer (**Figure 11C, D**). After the treatment of the NPs, only a few planktonic fungal cells could be observed. The original images of the SEM were provided in **Figure 6.4**.

It All the individual components of the nanocarriers failed to achieve the same level of biofilm clearance compared to the composite nanoparticles, which dominated the individual components' performance. Hence, the nano formulation appears to have a synergistic effect in killing the *C.albicans* cells and removing the fungal biofilm. A CLSM observation was used in order to visualize the biofilm clearing process of the 4 x stock NPs solution in order to illustrate its removal. In order to visualize the interesting characteristics of clusteroids, the 3D layer was incubated in DAPI dye before infection with fungal biofilm, which was contrast-stained using CFSE dye (generation dye). Incubation for 1 hour partially removed the biofilm, starting with its outer layer (**Figure 6.10A-D**). It was noted that the signal of CFSE fluorescence had been slightly reduced. The biofilm deposited on the surface of the clusteroids peeled off after twelve hours of incubation with the NPs treatment (**Figure6.10 E-H**). Upon incubation with the 3D clusteroids layer for 24 hours, the biofilm initially attached to its surface was largely removed, leaving only a very small number of fungal cells inside (**Figure 6.10 H-K**). A peak of fluorescence intensity was detected at the center of the sample, which could be verified by the fluorescence intensity. In order to completely remove a biofilm, it is necessary to remove its thick EPS, which increases its intractability. It has been demonstrated that the release of nanoparticles over a long period of time, as well as their electrostatic absorbancy, had a positive synergistic effect towards removing biofilms. Although the images collected from CLSM observations suggested that fungal biofilm removal may be less efficient than expected due to the partly rough morphology of the 3D layer of clusteroids, this is unlikely to be the case. The fungal cell infection was examined in the core of the clusteroids using cryostat sectioning in order to clarify this point. Based on the bright field observations of **Figure 6.13**, one can clearly see the junction between the clusteroids. A similar reduction of over 60% was noticed in the green fluorescence signal from the fungal cells at the same time. In the sectioning slice, a residue of fungal cells was still detectable after treatment with 4 x stock solution.

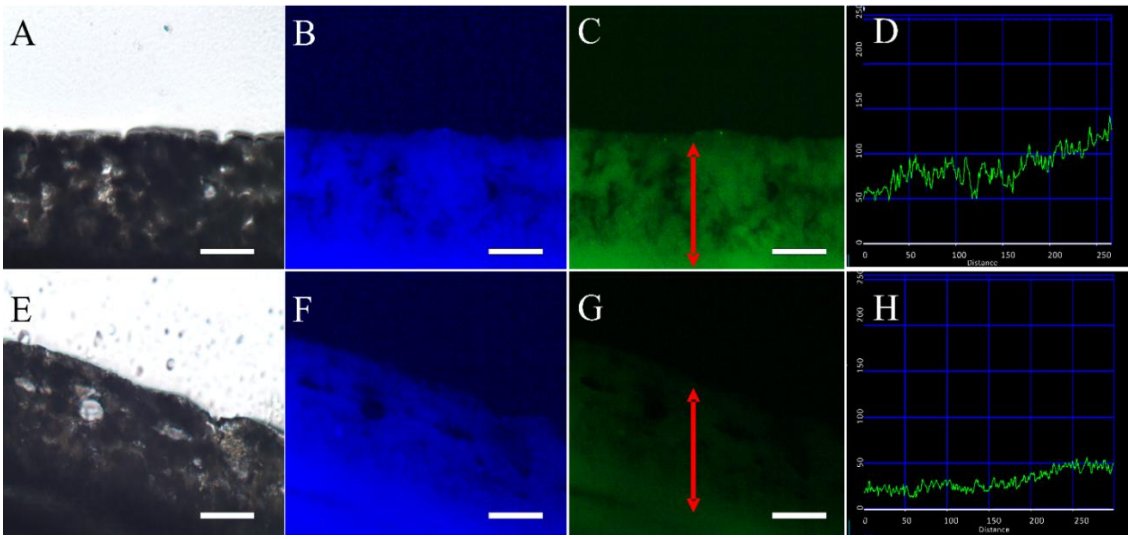

Figure 6.13. Microscopy observation of cryostat sectioning slices of the 3D co-cultured fungal biofilm infected clusteroids layer: before (A, B, C) and after (E, F, G) treatment with 4 × stock solution. Each slice produced by the cryo-sectioning is 10 μm. Olympus BX51 fluorescence microscope was used for the series observations. The fluorescence intensity of C and G was measure by ZEN software (Blue edition) and is shown in D and H. The bar is 100 μm (same for all images). The concentration of 1 × stock solution is 0.2 wt% Shellac, 0.25 wt% P407-0.2 wt% Lysozyme and 0.02 wt% Fluconazole. The red arrows indicate where the fluorescence intensity was measured.

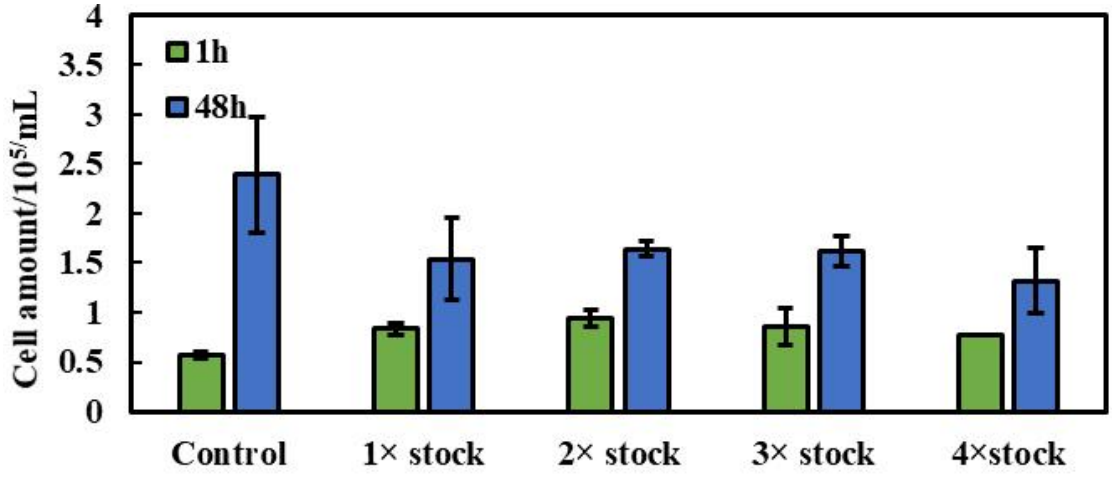

Figure 6.14. Cytotoxicity of different concentrations of Lysozyme-coated Fluconazole-loaded shellac NPs solutions on the proliferation of the 3D layers of ECV304 clusteroids after 1 h and 48 h culture. The cell numbers in the different cultures taken after 1 h and 48 h were calculated by standard curve.

6.4.5 Cytotoxicity of the NPs treatment on the ECV 304 clusteroids

In order to investigate the cytotoxicity of the NPs on the ECV 304 cells, NPs at different concentrations of the suspension stock were injected into the microwell plate containing the 3D cluster oids layer in order to assess the cytotoxicity of the NPs. It is likely that the use of NPs in clinical practice would have a detrimental effect on uninfected cells surrounding the treated area. As a means of evaluating and potentially reducing the influence of these factors, an MTT assay was used to assess cytotoxicity. A reduction of 40% in the overall number of cells was shown in **Figure 6.9(14)** after 48 hours by using 1 x stock solution. A high concentration of the NPs (4 x stock) did not affect the proliferation of the cells, which indicates that the NPs have been saturated. The viability of ECV 304 cells was only marginally affected by the 4 x stock solution. Despite treatment with different concentrations of the stock solution for 1 hour, no significant differences were observed in the amount of ECV 304 cells. It is evident that only a 40% inhibition in ECV 304 cell proliferation after 24 hours of treatment is comparable to the 5-log reduction in *C. albicans* cells after 24 hours of treatment, thus demonstrating the effective nature of this formulation for the cleaning of biofilms.

6.5 Conclusions

The aim of this study was to develop a 3D urothelial cell clusteroids model that mimicked the inner cell wall of the bladder infected with *C. albicans* biofilm. Using Fluconazole-loaded shellac nanotherapeutics in conjunction with a cationic enzyme Lysozyme to functionalize the Fluconazole nanocarriers, we have made it possible to remove fungal biofilms from 3D urothelial clusteroids. By coating the negatively charged Shellac nanoparticles with cationic Lysozyme, the negatively charged Shellac nanoparticles were converted into positively charged nanocarriers that targeted the negatively charged *C. albicans* biofilm on the surface. A Lysozyme-coated nanocarrier is fortified with peptidoglycans that are rich in peptides which can be

partially digested by lysozyme, thus expediting delivery of Fluconazole to the encased *C .albicans* cells and as a result increasing their resistance to the antifungal drug.

C. albicans biofilm-infected 3D urothelial clusteroids were characterized before and after the nano therapy treatment with CLSM and SEM imaging, bright field microscopy, CFU counts, and MTT assays. A significant improvement in biofilm clearance was observed using these antifungal NPs, as compared to using any individual component (Shellac, P407, or Fluconazole). As a result of the strong antifungal effects of this treatment, the 3D clusteroid model showed no significantly increased cytotoxicity; treatment of the clusteroids had a minor effect on the proliferation of the clusteroids. This work involves the culture of urothelial cells, the formation of clusteroids, the infection of biofilms, and the treatment of NPs. An extensive array of fungal biofilm infections, or bacterial infections, could be mimicked using a protocol such as this by changing the species of cellular type and pathogen type of the organism, so that a wide range of fungal biofilm infections or bacterial infections could be mimicked. All in all, the 3D urothelial cell clusteroids platform introduced here is a good model for simulating urinary tract infections because it comprises biofilm-infected urothelial cells. A straightforward testing platform for nanocarrier-based therapeutics, specifically for biofilm clearance, is provided by this platform. Using this method, we can fill in the gaps in *in vitro* urinary models for biofilm infection and could provide useful information for relevant biofilm *in vitro* simulations, which could assist in the development of antimicrobial therapeutics based on nanotechnology.

6.6 References

1 J. Kaufman, M. Temple-Smith and L. Sanci, *BMJ Paediatr. Open*,. 2019, **3**, e000487.

2 P. Yousefi, A. Cyrus, Z. Moghaddasi, F. Dorreh and A. Aravand, *J. Adv. Med. and Biomed*. Res., 2011, **19**, 66-76.

3 K. Gupta, L. Grigoryan and B. Trautner, *Ann. Intern. Med.*, 2017, **167**, ITC49-ITC64.

4 T. M. Hooton, J. *Antimicrob. Chemother*., 2000, **46** Suppl 1, 1-7; discussion 63-5.

5 K. Gupta, T. M. Hooton, K. G. Naber, B. Wullt, R. Colgan, L. G. Miller, G. J. Moran, L. E. Nicolle, R. Raz, A. J. Schaeffer, D. E. Soper, *Clin. Infect. Dis*., 2011, **52**, e103-20.

6 C. W. Tan and M. P. Chlebicki, *Singapore Med. J*., 2016, **57**, 485-490.

7 F. Wagenlehner and K. Naber, *J. Hosp. Infect*., 2000, **46**, 171-181.

8 J. R. Phillips and M. G. Karlowicz, *Pediatr. Infect. Dis. J*., 1997, **16**, 190-194.

9 E. H. Elpern, K. Killeen, A. Ketchem, A. Wiley, G. Patel and O. Lateef, *Am. J. Crit. Care.*, 2009, **18**, 535-41; quiz 542.

10 S. Niveditha, S. Pramodhini, S. Umadevi, S. Kumar and S. Stephen, *J. Clin. Diagn. Res*., 2012, **6**, 1478-1482.

11 H. Pelling, J. Nzakizwanayo, S. Milo, E. L. Denham, W. M. MacFarlane, L. J. Bock, J. M. Sutton and B. V. Jones, *Lett. Appl. Microbiol*., 2019, **68**, 277-293.

12 N. S. Morris, D. J. Stickler and R. J. McLean, *World J. Urol*., 1999, **17**, 345-350.

13 S. P. Hawser and L. J. Douglas, *Infect. Immun*., 1994, **62**, 915-921.

14 J. Chandra, D. M. Kuhn, P. K. Mukherjee, L. L. Hoyer, T. McCormick and M. A. Ghannoum, *J. Bacteriol.*, 2001, **183**, 5385-5394.

15 D. Davies, *Nat. Rev. Drug Discov*., 2003, **2**, 114-122.

16 G. O'Toole, H. B. Kaplan and R. Kolter, *Annu. Rev. Microbiol*., 2000, **54**, 49-79.

17 M. G. Trulear and W. G. Characklis, *J. Water Pollut. Control Fed*., 1982, 54, 1288-1301.

18 K. Lewis, *Antimicrob. Agents Chemother*., 2001, 45, 999-1007.

19 H.-C. Flemming and J. Wingender, *Nat. Rev. Microbiol*., 2010, **8**, 623-633.

20 L. Robino and P. Scavone, *Future Microbiol*., 2020, **15**, 377-379.

21 Y. Liu, L. Shi, L. Su, H. C. van der Mei, P. C. Jutte, Y. Ren and H. J. Busscher, *Chem. Soc. Rev.*, 2019, **48**, 428-446.

22 E. N. Taylor, K. M. Kummer, D. Dyondi, T. J. Webster and R. Banerjee, *Nanoscale*, 2014, **6**, 825-832.

23 F. Haghighi, S. R. Mohammadi, P. Mohammadi, M. Eskandari and S. Hosseinkhani, *Bratisl. Lek. Listy*, 2012, **113**, 707-711.

24 S. M. Abdelghany, D. J. Quinn, R. J. Ingram, B. F. Gilmore, R. F. Donnelly, C. C. Taggart and C. J. Scott, *Int. J. Nanomedicine*, 2012, **7**, 4053-4063.

25 K. Qvortrup, L. D. Hultqvist, M. Nilsson, T. H. Jakobsen, C. U. Jansen, J. Uhd, J. B. Andersen, T. E. Nielsen, M. Givskov and T. Tolker-Nielsen*, Front. Chem*., 2019, **7**, 742.

26 P.J. Weldrick, M.J. Hardman and V.N. Paunov, *Mater. Chem. Front.*, 2021, **5**, 961-972.

27 A. Wang, P. J. Weldrick, L.A. Madden and V.N. Paunov, *ACS Appl. Mater. Interf*., 2021, **13**, 22182–22194.

28 P. J. Weldrick, M. J. Hardman and V. N. Paunov, *ACS Appl. Mater. Interf*., 2019, **11**, 43902-43919.

29 A. F. Halbus, T. S. Horozov and V. N. Paunov, *ACS Appl. Mater. Interf*., 2019, **11**, 12232-12243.

30 P. J. Weldrick, S. Iveson, M. J. Hardman and V. N. Paunov, Nanoscale, 2019, **11**, 10472-10485.

31 D. Huh, G. A. Hamilton and D. E. Ingber, *Trends Cell Biol*., 2011, **21**, 745-754.

32 M. Ravi, V. Paramesh, S. R. Kaviya, E. Anuradha and F. D. P. Solomon, *J. Cell. Physiol*., 2015, **230**, 16-26.

33 O. Chaudhuri, *Biomater. Sci*., 2017, **5**, 1480-1490.

34 V. van Duinen, S. J. Trietsch, J. Joore, P. Vulto and T. Hankemeier*, Curr. Opin. Biotechnol*., 2015, **35**, 118-126.

35 A. Wang, L. A. Madden and V. N. Paunov, *J. Mater. Chem. B*., 2020, **8**, 10487-10501.

36 A. A. K. Das, B. W. Filby, D. A. Geddes, D. Legrande and V. N. Paunov, *Mater. Horiz*., 2017, **4**, 1196-1200.

37 S. B. G. Celik, S. R. Dominici, B. W. Filby, A. A. K. Das, L. A. Madden and V. N. Paunov, *Biomimetics*, 2019, **4**, 50.

38 A. Wang, L. A. Madden and V. N. Paunov, *Mater. Adv*., 2020, **1**, 3022-3032.

39 Z. Khatoon, C. D. McTiernan, E. J. Suuronen, T.-F. Mah and E. I. Alarcon, *Heliyon*, 2018, **4**, e01067.

40 S. Veerachamy, T. Yarlagadda, G. Manivasagam and P. K. Yarlagadda, *Proc. Inst. Mech. Eng. H*, 2014, **228**, 1083-1099.

41 W. Fu, T. Forster, O. Mayer, J. J. Curtin, S. M. Lehman and R. M. Donlan, *Antimicrob. Agents Chemother*., 2010, **54**, 397-404.

42 A. E. Hodgson, S. M. Nelson, M. R. W. Brown and P. Gilbert, J. *Appl. Bacteriol*., 1995, **79**, 87-93.

43 K. Marion-Ferey, M. Pasmore, P. Stoodley, S. Wilson, G. P. Husson and J. W. Costerton, *J. Hosp. Infect*., 2003, **53**, 64-71.

44 C. Badet, A. Furiga and N. Thébaud, *Oral Health Prev. Dent*., 2008, **6**, 337-341.

45 K. E. Hill, S. Malic, R. McKee, T. Rennison, K. G. Harding, D. W. Williams and D. W. Thomas, *J. Antimicrob. Chemother*., 2010, **65**, 1195-1206.

46 S.S.M, Al-Obaidy, G.M. Greenway and V.N. Paunov, *Nanoscale Adv*., 2019, **1**, 858–872.

47 S.S.M. Al-Obaidy, A.F Halbus, G.M. Greenway and V.N. Paunov, J. *Mater. Chem. B*, 2019, **7**, 3119-3133.

48 A.P. Richter, J.S. Brown, B. Bharti, A. Wang, S. Gangwal, K. Houck, E.A. Cohen Hubal, V.N. Paunov, S.D. Stoyanov, O.D. Velev., *Nat. Nanotechnol.*, 2015, **10**, 817−823.

49 M.J. Al-Awady, A. Fauchet, G.M. Greenway, V.N. Paunov, *J. Mater. Chem. B*, 2017, **5**, 7885-7897.

50 M. Al-Awady, P. J. Weldrick, M.J. Hardman, G. M. Greenway and V.N. Paunov, *Mater. Chem. Front.*, 2018, **2**, 2032-2044.

51 A.F. Halbus, T.S. Horozov and V.N. Paunov, *Biomimetics*, 2019, **4**, 1-20.

52 A.F. Halbus, T.S. Horozov and V.N. Paunov, *Nanoscale Adv.*, 2019, **1**, 2323-2336.

53 M.J. Al-Awady, G.M. Greenway, V.N. Paunov. *RSC Adv*., 2015, **5**, 37044–37059.

54B. Herigstad, M. Hamilton and J. Heersink, *J. Microbiol. Methods*, 2001, **44**, 121–129.

55.C. R. Parish, Immunol. *Cell Biol*., 1999, 77, 499–508.

56.H. Tuominen-Gustafsson, M. Penttinen, J. Hytönen and M. K. Viljanen, *BMC Microbiol*., 2006, 6, 92.

57.D. Hoefel, W. L. Grooby, P. T. Monis, S. Andrews and C. P. Saint, *J. Microbiol. Method*s, 2003, 52, 379–388.

58.Wang A, Weldrick P J, Madden L A, et al.. *Biomaterials Science.*, 2021, 9(20): 6927-6939.

59 Wang, L, Ishida, Y, Ohtani, H, Tsuge, S., and Nakayama, T. *Analytical chemistry*., 1999,**71**, 1316-1322.

7. Chapter 7

7.1 Summary of thesis and outlook

3D culture system is advancing the research in drug testing, tissue engineering and regenerative medicine. The basic understanding on the 3D culture systems have been well established. The development of a novel 3D cell culture method with high yield and boosted cell functionality is in urgent need. A confounding factor that limited the utilization of the 3D cell culture models are the relatively low-yield rate. The cell spheroids or organoids are commonly generated using polymeric hydrogel or microfluidic devices, which would restrict the proliferation of the 3d cell models in limited area, thus, multi-generation of the spheroids are hard to achieve. Widening the downstream applications of the generated cell spheroids or organoids is also essential for the further development of the models. The research presented in this thesis explores the possibility of using a novel method based on water-in-water Pickering emulsion to generated massive amount of 3D cell clusteroids with high viability and functionality. The 3D cell clusteroids were used as urinary track and skin models to simulate the biofilm infection *in vitro* and the removal process of the biofilm using Nano therapeutics.

Chapter 2 shows the design and optimisation of using water-in-water Pickering emulsion to encapsulate and generate the Hep-G2 cell clusteroids. The biocompatible PEO and DEX were selected as continuous and separated phase, the food-grade whey protein particles were chosen as the stabilizer. The spontaneous partition behaviour to the DEX phase of the cells enabled an easy seizure of the cells within the DEX droplets. It is shown that by varying the cell numbers and DEX/PEO ratio, the cells could be successfully encapsulated and generated into cell clusteroids. The cell clusteroids were collected by diluting the emulsion with complete medium. A large amount of individual cell clusteroids was shown to be generate using our method. Crucially, the collected clusteroids were assessed using FDA assay to show that they remain highly viable after the preparation procedures. The cell clusteroids were seeded into a sodium alginate hydrogel to facilitate their long-term growth over 7

days. The constant tracking of the cell growth within the hydrogel proved that the cell clusteroids would fuss into denser tissue with higher growth speed. A systematic evaluation on the hepatic specified factors including Urea and Albumin comparing the 2D and 3D cell clusteroids revealed that our method would greatly enhance the cell functionality. The SEM results also show that the collected cell clusteroids were uniform in size. This novel approach for the generation of 3D cell clusteroids opens window to the produce massive amount of cell clusteroids, which could ideally be used for tissue regeneration applications. In Chapter 2, we learned how to effectively prepare the hepatic 3D cell clusteroids with increased functionality. The basic preparation and characterization protocols were introduced here. Any other fibroblast cell type, either from patient biopsy or commercial cell lines, could also be adapted in this model to rapidly generate clusteroids for tissue engineering applications, or in some cases, drug testing. The limitation of the necrotic core formation was also observed in these experiments, and we tried to vascularize these necrotic clusteroids with endothelial cell type to widen their downstream applications.

Chapter 3 advances our ATPS based 3D cell culture method into Co-culture level. Chapter 3 follows on from the research reported in chapter 2. The aim was to prove that the water-in-water Pickering emulsion could encapsulate two cells in on droplets to generate co-culture cell clusteroids. These results the two types of cell could co-exist in a single droplets and could be compacted into a co-cultured clusteroids. The collected co-cultured Hep-G2/ECV 304 cells were both carcinoma cells, which would require the existence of blood vessel when the clusteroids grow into bigger size. The formation and proliferation of the co-cultured clusteroids were confirmed using fluorescence, bright field, and confocal scaning microscopy. Additionally, the cell ratio of two types of cells within the co-cultured clusteroids were proved to be variable by simply change the initial cell ratio added to the DEX phase. The ECV 304 cells are bladder carcinoma with endothelial cell features which were shown to be able to vascularize the co-cultured clusteroids in our results. The co-cultured cell clusteroids were seeded into hydrogel to support the angiogenesis

process. The microscopy tracking showed that the clusteroids could sprout into the hydrogel, which is the key feature of angiogenesis *in vitro*. The angiogenesis proteome array kit proved a series of vascularization-related proteins were triggered in the co-culture model. Several markers were only detectable in the co-culture pattern. When Hep-G2 cells were co-cultured with ECV304 cells, there was a very significant boost to the Hep-G2 cell functionality in producing urea and albumin. These results suggested that our method could provide a facile tool for producing vascularized co-culture clusteroids using carcinoma cell lines *in vitro*. The method could be ideally suitable for all cell types and could provide an advantageous platform for tracking the neo-angiogenesis and various biomedical applications, especially in anti-vascularization drugs. On completion of the work reported in Chapter 3, we had developed sufficient knowledge about angiogenesis-related biology to offer significant scientific advance. We had solved the problem that occurred in traditional spheroid culture--the necrotic core. Our clusteroids could break the limitation of nutrients and oxygen delivery and grow to a bigger size. After we tackled this problem with carcinoma endothelial cell lines, we would be more confident in handling the primary cell culture for the purpose of more in-depth mimicry of in vitro tumour vascularization process. Achieving vascularization of hepatic cell clusteroids using endothelial carcinoma would enable the drug testing applications to be more precise. Anti-vascularization drugs could be tested on this platform. More importantly, the drug penetration process through blood vessels could be easily tracked and traced in vitro.

Chapter 4 aimed to further examine the feasibility of utilising w/w Pickering emulsion to co-culture Hepatic cells with primary endothelial lines with angiogenesis potential. The primary endothelial cells line would mimic the *in vivo* environment and could better simulate the process of angiogenesis. Similarly, the two cells types were firstly tested at different cell ratio to see if they could co-exist in a droplet. The pripary cells show no repulsion to the carcinoma cell lines. Co-cultured clusteroids could be generated after condensing the continuous PEO phase. The clusteroids were

collected and examined using bright filed microscopy, fluorescence microscopy and confocal observations. These observations revealed the integrity of the co-cultured clusteroids and high viability. Co-cultured clusteroids produced from ATPS could sprout into Matrigel when the cell ratio was adjusted to 1:2 (Hep-G2 : HUVEC), which approximated the real *in vivo* environment. The length of the sprouts could be analyzed using wimasprouts software. The co-culture clusteroids produced a greater amount of angiogenesis proteins than the individual types of cells. The HUVEC produce less angiogenesis proteins comparing to the ECV cells (Chapter 3). The Hep-G2 cells served as a VEGF pump to stimulate the angiogenesis of HUVEC cells in the co-culture model. It is possible to handle this approach without the use of expensive instruments or consumables. Ideally, cells could be substituted for any two kinds of cells except those used for 3D cell vascularization. Additionally, this model could be used to investigate drug toxicology as well as other applications related to tissue engineering. The research reported in Chapter 2 proved our cells could be vascularized using primary endothelial cell lines. We understood the difference between carcinoma cells and primary cell cultures. The primary cell cultures usually consist of fewer cell markers and could mimic the in vivo environment more realistically. The handling of these primary cell lines might be an issue but they are definitely of huge value in biomedical research. The completion in vascularizing hepatic clusteroids with HUVECs enables us to use these vascularized spheroids for various applications including tissue regeneration and precise drug testing.

Chapter 5 aimed to find a suitable application for the massive amount of the clusteroids collected from w/w Pickering emulsion. The advantage of our method is the ultra-high yiled rate. Using this point, we generated a dense layer of 3D keratinocytes clusteroids to simulate skin *in vitro*. The HaCaT clusteroids layer was co-cultured with pathogens, *Staphylococcus aureus* and *Pseudomonas. Aeruginosa* to track the biofilm formation on the clusteroids. The *S. aureus* and *P. aeruginosa* could form biofilm on the clusteroids layer without breaking the structure of the 3D cell interactions. The SEM images and CLSM images proved the successful formation of

the biofilm on top of the clusteroids. We further designed a nanotherapeutics based on antibiotic encapsulated Carbopol NPs, surface functionalised with a protease- alcalase. In comparison with non-coated ciprofloxacin and alcalase, this nanocarrier demonstrated a significant increase in antibacterial activity. In the clusteroids model, such nanoparticles did not pose a significant threat, and the clusteroids could continue to proliferate despite the presence of such nanoparticles. *S. aureus* and *P. aeruginosa* were considered to be two major bacteria related to wound care, and were treated with ciprofloxacin-loaded nanocarriers. As a result of our experiments, we have shown that the nanogel strongly increases the antibacterial action of the ciprofloxacin loaded into it against both of the bacteria species after the incubation period of 24 hours. Our experiment was designed to detect biofilms and clusteroids using confocal, scanning electron microscopy, and cryostat as methods of characterization. Biofilm formation and clearance after treatment with NPs were clearly visible in the Z-stacking image obtained by confocal microscopy. A SEM image of clusteroids treated with nanocarriers revealed that the clusteroids/biofilm co-culture model had a distinct morphology both before and after being treated with nanoparticles. An antibacterial effect of the NPs was also detected through cryo-stat sectioning and the deeper infection of the bacteria was detected using cryo-stat sectioning. NPs and nanocarrier-based therapeutics may be tested for wound healing in this clusteroids/biofilm co-culture model. Moreover, this work shows that 3D cell clusteroids could have the potential to be used in further biomedical applications in the future. On finishing the resesrch reported in chapter 4, we started thinking about the proper applications of our cell clusteroids. The high yield rate of our clusteroids firstly motivated us to use them for skin tissue regeneration. We shifted our research to test the in vitro microbial-host interaction using our model to potentially replace the animal models. Maintaining bacteria, keratinocytes, and nanoparticles were major components of Chapter 5. We learned the whole process of bacterial culture, nanoparticle preparation, and characterization in order to perform these epxeriments. The success of Chapter 5

greatly broadened the application of 3D spheroids as researchers could try to use this concept to test microbial-host interaction using donor cells from other organs.

Chapter 6 aim to broaden the application of the clusteroids layer to simulate the urinary track infection, which is commonly seen and tricky to solve in nosocomial infection. The aim of this study was to develop a 3D urothelial cell clusteroids model that mimicked the inner cell wall of the bladder infected with *C.albicans* biofilm. Using Fluconazole-loaded shellac nanotherapeutics in conjunction with a cationic enzyme Lysozyme to functionalize the Fluconazole nanocarriers, we have made it possible to remove fungal biofilms from 3D urothelial clusteroids. By coating the negatively charged Shellac nanoparticles with cationic Lysozyme, the negatively charged Shellac nanoparticles were converted into positively charged nanocarriers that targeted the negatively charged *C.albicans* biofilm on the surface. A Lysozyme-coated nanocarrier is fortified with peptidoglycans that are rich in peptides which can be partially digested by lysozyme, thus expediting delivery of Fluconazole to the encased *C.albicans* cells and as a result increasing their resistance to the antifungal drug. *C.albicans* biofilm-infected 3D urothelial clusteroids were characterized before and after the nano therapy treatment with CLSM and SEM imaging, bright field microscopy, CFU counts, and MTT assays. A significant improvement in biofilm clearance was observed using these antifungal NPs, as compared to using any individual component (Shellac, P407, or Fluconazole). As a result of the strong antifungal effects of this treatment, the 3D clusteroid model showed no significantly increased cytotoxicity; treatment of the clusteroids had a minor effect on the proliferation of the clusteroids. This work involves the culture of urothelial cells, the formation of clusteroids, the infection of biofilms, and the treatment of NPs. An extensive array of fungal biofilm infections, or bacterial infections, could be mimicked using a protocol such as this by changing the species of cellular type and pathogen type of the organism, so that a wide range of fungal biofilm infections or bacterial infections could be mimicked. All in all, the 3D urothelial cell clusteroids

platform introduced here is a good model for simulating urinary tract infections because it comprises biofilm-infected urothelial cells. A straightforward testing platform for nanocarrier-based therapeutics, specifically for biofilm clearance, is provided by this platform. Using this method, we can fill in the gaps in *in vitro* urinary models for biofilm infection and could provide useful information for relevant biofilm *in vitro* simulations, which could assist in the development of antimicrobial therapeutics based on nanotechnology. In Chapter 6, we applied our bacterial-host interaction models using urinary cells and fungi. Fungi are considered tricky problems in any infection. We try to prove that our bacterial-host interaction models could be used to test more than one specified type of bacterial or organ. We also employed other nanotherapeutics based on shellac and lysozyme. We learned the full details about electrostatic absorbance and the importance of electricity in nanoparticle preparation. We proved our previously developed proof-of-concept could be validated and applied to other types of cells.

I learned how to scientifically design and carry out research through my Ph.D. and thesis writing. It is of great importance to be consistent in my research rather than spreading my interests. I was also taught to be precise and careful in scientific investigations. The importance of evaluating the value of my research is also a great step before carrying out any laboratory work.

Future work

For future work, the w/w Pickering emulsion template-based 3D cell clusteroids could be utilized to test various drug, pharmaceutic formulations and nano therapeutics. The 3D cell clusteroids could be co-cultured with the drug components to monitor the kinetics and efficiency of various therapy. Testing the possibility of generating various types of mono-cellular spheroids of multi-cellular organoids maybe also feasible. The vascularization of the tumour clusteroids or healthy cell types can be used for either in vitro drug testing or in vivo implantation. By employing our vascularized tumour spheroids model, the anti-vascularization drugs

could be easily accessed. The ATPS system could also be expanded to use other polymers such as poly acrylic acid or methylcellulose.

In addition by using the clusteroids to test drugs *in vitro,* the introduction of organoid has widen the usage of traditional 3D cell models including spheroids. Our generated 3D cell clusteroids could be possibly used as a pre-organoids to facilitate the fabrication of organoids in hydrogel.The limitation of organoids for use as pre-clinical drug testing platforms is that they require a long time in matrigel before they show proper cell function. Our model could be used to facilitate the formation of organoids on a large scale. The in-detail functionality of the spheroids or organoids generated from our model maybe also be interesting.

Another promising approach to utilising the ATPS-based 3D cell clusteroids is by adapting the Dextran phase as bio-ink. The PEO solution could be modified to cross-linkable polymers that could be used as bio-paper. The ATPS system would be a fascinating platform for 3D bioprinting to generate micro-tissues. This method would enable materials-free printing by simply using bio-compatible polymers and the cells needed.

Our host-microbial interaction model could be used to test different types of bacterial infection on different organs. The promising application would be testing the intestinal microbial community. The bacteria can be micro-injected into our organoids to study the bulk RNA-seq or single RNA-seq about intestinal organoids or bacteria. By understanding the biological mechanism of biofilm formation on the intestinal organoids, researchers should be able to develop anti-biofilm formation or biofilm-targeting drugs. The study of how bacteria attached to the surface of contractile cardiac cells may also be able to push forward the research into fatal bacterial endocarditis.